11-14-2014 12:00 AM

Impact of Local Bed Hydrodynamics on Jet-Bed Interaction

Maryam Mohagheghi Dar Ranji, *The University of Western Ontario*

Supervisor: Dr. Franco Berruti, *The University of Western Ontario*
Joint Supervisor: Dr. Cedric Briens, *The University of Western Ontario*
A thesis submitted in partial fulfillment of the requirements for the Doctor of Philosophy degree in Chemical and Biochemical Engineering

IMPACT OF LOCAL FLUIDIZED BED HYDRODYNAMICS ON JET-BED INTERACTION

(Thesis format: Integrated Article)

by

Maryam Mohagheghi Dar Ranji

Graduate Program in Engineering Science
Department of Chemical and Biochemical Engineering

A thesis submitted in partial fulfillment
of the requirements for the degree of
Doctor of Philosophy

The School of Graduate and Postdoctoral Studies
The University of Western Ontario
London, Ontario, Canada

Abstract

In Fluid Coking™ or Fluid Catalytic Cracking liquid feedstocks are injected into a bed of fluidized particles. Uniform distribution of liquid feed on fluidized particles increases the yield of valuable products and improves operability in these processes. Contact between the injected liquid and the bed particles can be greatly affected by the liquid properties and local bed hydrodynamics.

The impact of parameters such as liquid properties, fluidization velocity, nozzle atomization gas flowrate, nozzle location and inclination were investigated on the distribution of liquid sprayed into a fluidized bed with a reliable and fast response capacitance meter. This method was also extended to monitor the agglomerate breakup kinetics.

The research showed that a liquid whose viscosity and contact angle on the surface of solid particles are similar to the liquid used in the high temperature commercial reactors provides a good simulation of liquid distribution into a fluidized bed with room temperature experiments. Varsol™ was selected for a cold simulation of Fluid Cokers™.

The research also presents an innovative design of a cold model fluidized bed to investigate the impact of the velocity of particles, relative to the spray nozzle, on solid-liquid contact since it varies greatly with location in actual Fluid Cokers. This design provided an inexpensive and accessible means to study the effect of the relative velocity between the spray jet and particles independently of other bed hydrodynamic characteristics.

The investigation found that distribution of the injected liquid in the bed can be improved by either increasing the atomization gas flowrate or, preferably, the fluidization velocity. Study of nozzles at different locations and inclinations identified the dominant effects of bed hydrodynamics at the nozzle and jet tips on the distribution of liquid on solid particles.

A model for the interactions between sprayed liquid and fluidized particles was developed for two cases: a) a stationary spray nozzle and no net motion of the fluidized solids and b) a moving nozzle with a relative velocity between spray nozzle and particles. The model results were compared with experimental results and were found to provide consistent information on the liquid concentration of the agglomerates.

Keywords

- gas-solid fluidized bed
- Fluid Coking™
- liquid distribution

- hydrodynamics
- capacitance method
- spray nozzle
- liquid injection
- agglomerate formation

Dedication

This thesis is dedicated to the memory of my mother, Fatemeh Jan Kazemi Ranjbar. I miss her every day, and I thank her for her love and support. She was a really special person, and never gave up supporting me. She always encouraged me to pursue my graduate studies, and taught me plenty of life lessons. It is also dedicated to my dear father, Mohammad Hossein Mohagheghi Dar Ranji.

Co-Authorship Statement

The journal articles written from the thesis work are listed below. The individual contributions of all members are also indicated.

Chapter 2

Article Title: Study of the effect of local hydrodynamics on liquid distribution in a gas-solid fluidized bed using a capacitance method
Authors: Maryam Mohagheghi, Majid Hamidi, Franco Berruti, Cedric Briens and Jennifer McMillan
Status: Published in The Fuel Journal (2013)
Individual Contributions: Maryam Mohagheghi conducted all experimental work, analyzed the data and wrote the manuscript. Majid Hamidi designed and made the measuring sensors. Cedric Briens and Franco Berruti provided guidance, supervision, and reviewed several drafts of the work. Jennifer McMillan provided useful advice throughout the project and reviewed the final draft of the manuscript.

Chapter 3

Article Title: The Effects of Liquid Properties and Bed Hydrodynamics on the Distribution of Liquid on Solid Fluidized Particles in a Cold-Model Fluidized Bed
Authors: Maryam Mohagheghi, Majid Hamidi, Franco Berruti, Cedric Briens and Jennifer McMillan
Status: Published in The Powder Technology Journal (2014)
Individual Contributions: Maryam Mohagheghi conducted all experimental work, analyzed the data and wrote the manuscript. Majid Hamidi designed and made the measuring sensors. Cedric Briens and Franco Berruti provided guidance, supervision, and reviewed several drafts of the work. Jennifer McMillan provided useful advice throughout the project and reviewed the final draft of the manuscript.

Chapter 4

Article Title: The effects of injection nozzle location and inclination on the interaction between a gas-liquid jet and a gas solid fluidized bed
Authors: Maryam Mohagheghi, Majid Hamidi, Franco Berruti, Cedric Briens and Jennifer McMillan
Status:

In preparation for Powder Technology Journal
Individual Contributions: Maryam Mohagheghi conducted all experimental work, analyzed the data and wrote the manuscript. Majid Hamidi designed and made the measuring sensors. Cedric Briens and Franco Berruti provided guidance, supervision, and reviewed several drafts of the work. Jennifer McMillan provided useful advice throughout the project and reviewed the final draft of the manuscript.

Chapter 5

Article Title: The effects of relative velocity between nozzle and particles on the distribution of injected liquid in a fluidized bed
Authors: Maryam Mohagheghi, Majid Hamidi, Franco Berruti, Cedric Briens and Jennifer McMillan
Status: In preparation for Powder Technology
Individual Contributions: Maryam Mohagheghi conducted all experimental work, analyzed the data and wrote the manuscript. Majid Hamidi designed and made the measuring sensors. Cedric Briens and Franco Berruti provided guidance, supervision, and reviewed several drafts of the work. Jennifer McMillan provided useful advice throughout the project and reviewed the final draft of the manuscript.

Chapter 6

Article Title: Modelling of interactions between liquid-gas spray jet and fluidized particles in a gas-solid fluidized bed (Part I: stationary nozzle)
Authors: Maryam Mohagheghi, Franco Berruti, Cedric Briens and Jennifer McMillan
Status: In preparation for AICHE Journal
Individual Contributions: Maryam Mohagheghi conducted all experimental work, analyzed the data and wrote the manuscript. Cedric Briens and Franco Berruti provided guidance, supervision, and reviewed several drafts of the work. Jennifer McMillan provided useful advice throughout the project and reviewed the final draft of the manuscript.

Chapter 7

Article Title: Modelling of interactions between liquid-gas spray jet and fluidized particles in a gas-solid fluidized bed (part II : Moving spray nozzle)
Authors: Maryam Mohagheghi, Franco Berruti, Cedric Briens and Jennifer McMillan
Status: In preparation for AICHE Journal

Individual Contributions:
Maryam Mohagheghi conducted all experimental work, analyzed the data and wrote the manuscript. Cedric Briens and Franco Berruti provided guidance, supervision, and reviewed several drafts of the work. Jennifer McMillan provided useful advice throughout the project and reviewed the final draft of the manuscript.

Acknowledgments

Many people supported me during the completion of this thesis with insightful criticism, assistance, and expertise. This thesis would have never been possible without them.

I am very thankful to both my supervisors Dr. Cedric Briens and Dr. Franco Berruti, from the Institute for Chemicals and Fuels from Alternative Resources (ICFAR) at Western University, for their excellent guidance, continuous support, and valuable feedback during the course of this research project.

I would like to express my sincere thanks to Dr. Jennifer McMillan and the research teams at Syncrude Canada Limited and ExxonMobil for their valuable feedback, guidance and help in the transition and completion of this research.

I would like to thank Syncrude Canada Limited for their financial support as well as the Natural Science and Engineering Research Council (NSERC) of Canada.

Special thanks to my dear husband, Majid Hamidi, who is doing his PhD in chemical engineering at ICFAR, Western University, for his contribution to this research. Your invaluable knowledge of Electrical Engineering and advice in that field is greatly appreciated. I would like to thank Rob Taylor who helped me in the construction of my setup. In addition, I would like to express my appreciation to my friends, colleagues, secretaries and personnel in the Institute for Chemicals & Fuels from Alternative Resources (ICFAR), the Department of Chemical and Biochemical Engineering and the University of Western Ontario; without them, this work would not have been possible.

Finally, my deepest gratitude goes to my parents Mr. Mohammad Hossein Mohagheghi Dar Ranji and Mrs. Fatemeh Jan Kazemi Ranjbar for their endless love and support. I hope I have made them proud. I would like to thank my sisters and brothers, especially my younger sister, Mohadeseh Mohagheghi Dar Ranji, for their love, encouragement and help. Finally, I would like to express my deepest thanks to my husband for his love and persistent support.

Table of Contents

List of Tables

List of Figures

Nomenclature

A_c	the area of control volume, m^2	F_{Sa}	mass flowrate of solids carried by detached bubble from the jet due to atomization gas flowrate, kg/s
C	Capacitance, F	F_{SE}	mass flowrate of solids entrained into the jet cavity, kg/s
c_i	average concentration of liquid in agglomerates at jet tip at the end of ith jet expansion	F_{SB}	flux of solids carried by gas bubbles into the jet cavity, kg/m^2 . s
$C_{predicted}$	average concentration of liquid in agglomerates at the end of injection, mass ratio of liquid to dry solids, wt/wt	$F_{S_{out}}$	mass flowrate of solids carrying out of control volume by detached bubbles from jet cavity, kg/s
C_{last}	average concentration of liquid in agglomerates at jet tip at the end of injection, mass ratio of liquid to dry solids, wt/wt	F_L	mass flowrate of liquid into the jet through spray nozzle, kg/
dr	distance between center of two adjacent electrodes, m	GLR	Gas-to-Liquid ratio, wt%
d_b	bubble diameter, m	I	current, A
$\bar{d}_b$	mean bubble diameter, m	k	the ratio of volume of wake to volume of bubble
d_d	diameter of detached bubble from jet, m	L_{jet}	jet penetration length, m
d_N	nozzle diameter, m	L_{tip}	length of jet tip region, m
F	frequency, Hz	M	total mass, kg
F_a	mass flowrate of atomization gas into the jet through spray nozzle, kg/s	m_{tip}	total mass of solid at the jet tip that interacts with the jet, kg

m_w	mass of solid entrained in the wake of the bubble detaching from the jet tip, kg	t_b	bed thickness, m
m_r	mass of solid at the jet tip replaced by the volume of the released bubble, kg	Δt_B	average time between successive bubbles hitting the jet cavity, s
m_{last}	m_r plus the mass of entrained solids into the jet during the partial jet expansion, kg	U_f	fluidization velocity (superficial gas velocity), m/s
M_S	total mass of solid, kg	U_b	local bubble velocity, m/s
M_L	total mass of liquid, kg	$\overline{U}_b$	mean bubble velocity, m/s
n	number of released bubbles during total time of injection	$U_{expansion}$	velocity of jet expansion, m/s
Δp	Bed pressure drop, Pa	V	fluidization velocity, m/s
q_b	volumetric local bubble gas flux, m^3/ m^2s	V_I	fluidization velocity during injection, m/s
Q_a	volumetric atomization gas flowrate, m^3/s	V_r	fluidization velocity during refluidization, m/s
Q_g	volumetric gas flowrate in the bed, m^3/s	V_{tip}	total volume of solids at jet tip that interacts with the jet, m^3
Q_{mf}	volumetric gas flowrate at minimum fluidization velocity, m3/s	V_d	volume of detached bubble from jet, m^3
Q_b	bubble gas flowrate, m3/s	V_r	volume of replaced solid near the jet tip region because of jet expansion, m^3
R	resistance, Ω	W_{tip}	width of jet tip region, m
t	duration of injection, s	W_c	width of bubble capture area, m
t_d	time delay between two local minimums of measured capacitance, s	w	bed width, m

t_r	time required for a full jet expansion, s	X	mass concentration of free liquid on a dry solid basis, wt%
$\bar{x}$	average free moisture of 6 electrodes, %	x_c	length of control volume, m
x_L	lateral distance, m	Z	nozzle height, m

Greek Letters

δ_{in}	lateral penetration of nozzle tip from the bed wall, m	ε_b	bubble volume fraction in the bed, i.e. (bubble volume) / (bed volume)
τ	time constant of agglomerate breakage, s	ε_d	dense phase void fraction
θ	contact angle, degree	$\bar{\varepsilon}_b$	mean bubble volume fraction, -
θ_j	jet expansion angle, degrees	ε_{bj}	bubble volume fraction at jet tip location, -
σ	surface tension, mN/m	ε_{bN}	bubble volume fraction at nozzle tip location, -
ρ_p	particle density, kg/m^3	ρ_{mf}	density of bed at minimum fluidization velocity, kg/m^3
ε	void fraction	μ	liquid viscosity, mPa·s

Preface

The thesis was written in an integrated article format, with six articles in total, and two extra sections were added:

1. Introduction (Chapter 1): Literature review of oil sands bitumen; commercial technologies for upgrading bitumen; Fluid Coking process and the importance of uniform distribution of the liquid feed on solid particles in this process; the gas-liquid jets in a gas-solid fluidized bed; measurement techniques to assess the interaction between a gas-liquid jet and a gas-solid fluidized bed; and finally the motivation and the specific objectives of this dissertation
2. Conclusion and Recommendations (Chapter 8): General conclusions of the research and recommendations for future work for interaction between a gas-liquid jet and a gas-solid fluidized bed

The order of the Chapters 2 to 7 reflects when the experiment or the construction was made; i.e. the experimental work described in Chapter 2 was performed with the first version of the capacitance meter. Then, the capacitance meter was modified and adapted to the setup and liquid-solid system of experiments. Therefore, for the rest chapters of thesis the new capacitance meter was used. The six integrated articles are:

1. Study of the effect of local hydrodynamics on liquid distribution in a gas-solid fluidized bed using a capacitance method (Chapter 2)
2. The effects of liquid properties and bed hydrodynamics on the distribution of liquid on solid fluidized particles in a cold-model fluidized bed (Chapter 3)
3. The effects of injection nozzle location and inclination on the interaction between a gas-liquid jet and a gas solid fluidized bed (Chapter 4)
4. The effects of relative velocity between nozzle and particles on the distribution of injected liquid in a fluidized bed (Chapter 5)
5. Modelling of interactions between liquid-gas spray jet and fluidized particles in a gas-solid fluidized bed (Part I: stationary nozzle) (Chapter 6)
6. Modelling of interactions between liquid-gas spray jet and fluidized particles in a gas-solid fluidized bed (part II : Moving spray nozzle) (Chapter 7)

Chapter 1

1. INTRODUCTION

The research work presented in this thesis investigates how bed hydrodynamics affect the distribution of liquid droplets on solid particles in a cold model gas-solid fluidized bed. Although this work can be applied to other processes, it focuses on the Fluid Coking™ process. The format used in this thesis is the "integrated article" format.

This chapter provides some information about oil sands bitumen as well as commercial technologies for upgrading bitumen followed by more detail about the Fluid Coking process and the importance of uniform distribution of the liquid feed on solid particles in this process. The next section of this chapter reviews previous studies on the gas-liquid jets in a gas-solid fluidized bed and on measurement techniques to assess the interaction between a gas-liquid jet and a gas-solid fluidized bed. Finally, the motivation and the specific objectives of this dissertation are presented.

1.1 Introduction

Canada has the third largest oil reserves in the world with 173 billion barrels that can be recovered economically with today's technologies. About 97% of Canadian oil reserves, 168 billion barrels, are in the form of oil sands (Oil & Gas Journal Dec 2012 and ERCB). Canada's oil sands are extracted from three deposits- the Athabasca, Peace River and Cold Lake areas in Alberta and part of Saskatchewan. Oil sand is a mixture of sand, clay, water and bitumen. Bitumen is a heavy and high viscous oil with a density over 1000 kg/m^3 and a viscosity about 1000 times that of light crude oil: it cannot flow or be pumped without being diluted or heated. Bitumen needs upgrading to, at a minimum, reduce its viscosity to allow for pipeline transportation and, at best, to yield a synthetic crude oil that can be processed in conventional refineries. The most commonly used thermal cracking processes for bitumen upgrading are Delayed Coking and Fluid Coking™ .

For both these processes, pressure is slightly higher than atmospheric and temperature is greater than 482 ^{0}C in which the feedstock cracks thermally into products such as naphtha and distillate. Petroleum coke is a by-product of these processes. Based on the coking operating temperature and its residence time, there are two types of petroleum coke: fuel-grade petroleum coke and anode-grade petroleum coke that needs additional heating or calcining.

In the delayed coking process, the heated feedstock thermally cracks in two or more large reactors, called coke drums. Coke is deposited in the coke drums as a solid where it builds up. The deposited coke is removed using high pressure water. To facilitate coke removal, the hot feed is rotated between several drums so that continuous production can be maintained while some drums are being cleaned.

With Fluid Coking, bitumen is injected on fluidized coke particles where thermal cracking occurs. In Fluid Cokers, coke particles at 510-530 ^{0}C are fluidized by steam. Preheated bitumen is injected with steam through several rings ("banks") of convergence-divergence-convergence nozzles (Base et al., 1999). Steam exits the spray nozzle with a cloud of bitumen droplets into the bed of hot fluidized coke particles. The cracking products that are lighter hydrocarbons rise up and exit the top of the bed to produce "synthetic crude" with further processing. The remaining heavy hydrocarbons and the solid coke by-product of cracking reactions collect on the surface of the hot coke particles and flow down to the stripper. In the stripper, the remaining heavy hydrocarbons are displaced with rising steam and the coke particles exit the bottom of the bed and are transported to the burner. The burner provides the required energy for the re-heating of coke particles by burning a portion of them and the heated particles are conveyed back to the reactor (Ariyapadi 2004 and Hammond et al. 2003). Figure 1.1 shows a schematic diagram of the Fluid Coking process (Ariyapadi 2004).

In the Fluid Coking process, contact between liquid droplets and solid particles results in two forms of liquid: liquid forming a thin layer around individual particles, or "free liquid", and liquid trapped within "agglomerates" (Ariyapadi et al. 2003; Bruhns and Werther 2005; Knapper et al. 2003). In Fluid Cokers, the thickness of bitumen layer on

hot coke particles depends on the bitumen droplet size (Gray 2002). According to Gray et al. 2004, the bitumen thickness continuously decreases with reaction time due to cracking and coking reactions. Both bitumen viscosity and thickness affect the agglomeration of particles in Fluid Cokers. As cracking reactions proceed, the bitumen thickness on hot coke particles reduces and the viscosity of bitumen increases due to coke formation. The increase in bitumen viscosity enhances the agglomeration tendency while the reduction in bitumen thickness counteracts (Darabi et al. 2010). Gray (2002) showed the agglomeration tendency would be maximum in an intermediate time during coking reaction.

Several experimental studies have shown that a gas-liquid spray injected into a gas-solid fluidized bed forms a jet cavity. They have shown that particles enter the jet and agglomerates form near the tip of the jet cavity of the spray (Bruhns and Werther 2005; Knapper et al. 2003).The strength of the formed agglomerates depends upon the material properties and the bed hydrodynamics (McDougall et al. 2005; Weber et al. 2006). Depending on the strength of agglomerates, they can quickly break up into smaller agglomerates and individual wet particles or survive for a longer time. Morales (2013) assumed that agglomeration occurs in three stages: 1) initial distribution of the liquid on entrained solid particles to the jet cavity, 2) wetting and spreading of the liquid among solid particles in the jet cavity and 3) breakup of agglomerates in the fluidized bed (Figure 1.2).

In the Fluid Coking^{TM} process, it is essential to increase the free liquid, i.e. the proportion of injected liquid that is not trapped within liquid-solid agglomerates (House et al. 2004), because the trapped liquid cannot easily react and vaporize, and the slower reaction reduces the yield of valuable products in Fluid Cokers. It is also preferable that the liquid trapped within agglomerates be freed rapidly through agglomerate breakup, before it can have a detrimental effect on the process: for example, if wet agglomerates reach the stripper, this promotes fouling of the stripper shed through coke deposits and may lead to unscheduled shutdowns.

The local bed hydrodynamics have a strong impact on the contact between the injected liquid and the bed solids, and the formation of agglomerates. By adjusting the local bed hydrodynamics or locating the injection nozzle in the appropriate region of the bed, the contact between the injected liquid and the bed solids may be optimized to minimize agglomerate formation, which is detrimental to the Fluid Coking process.

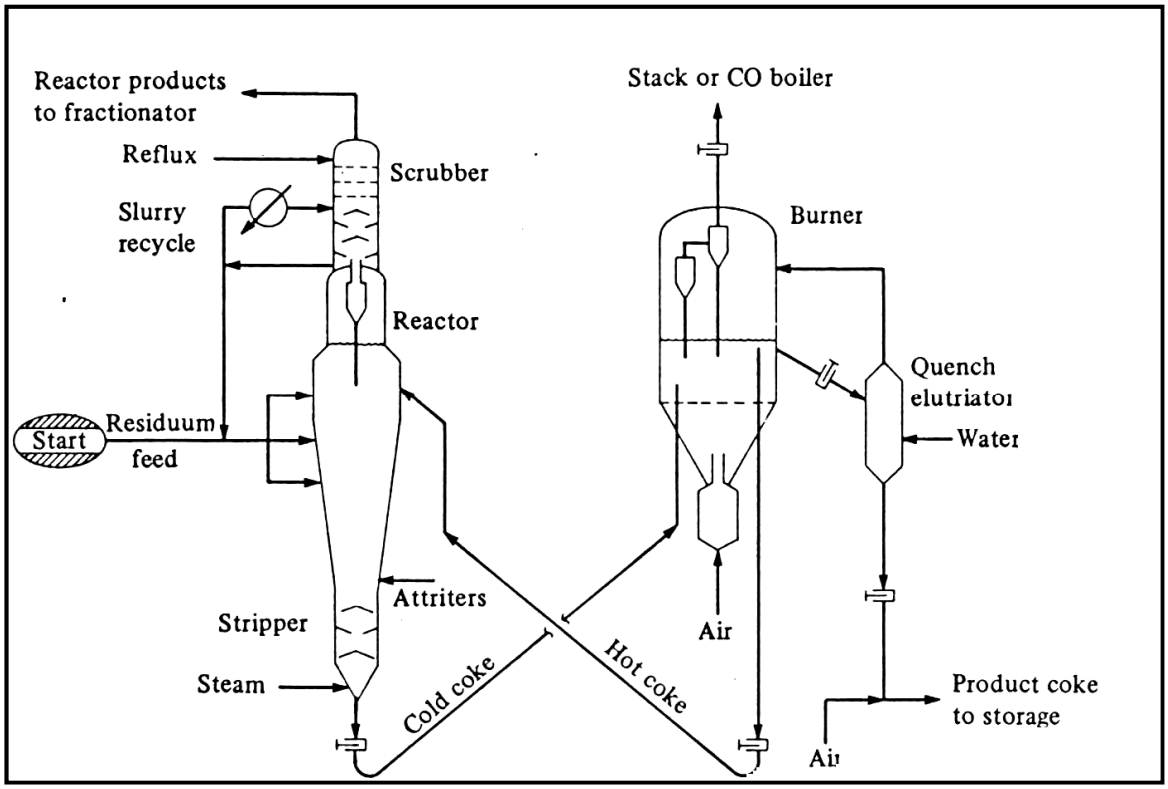

Figure 1.1. Schematic diagram of Fluid Coking process from (Ariyapadi 2004)

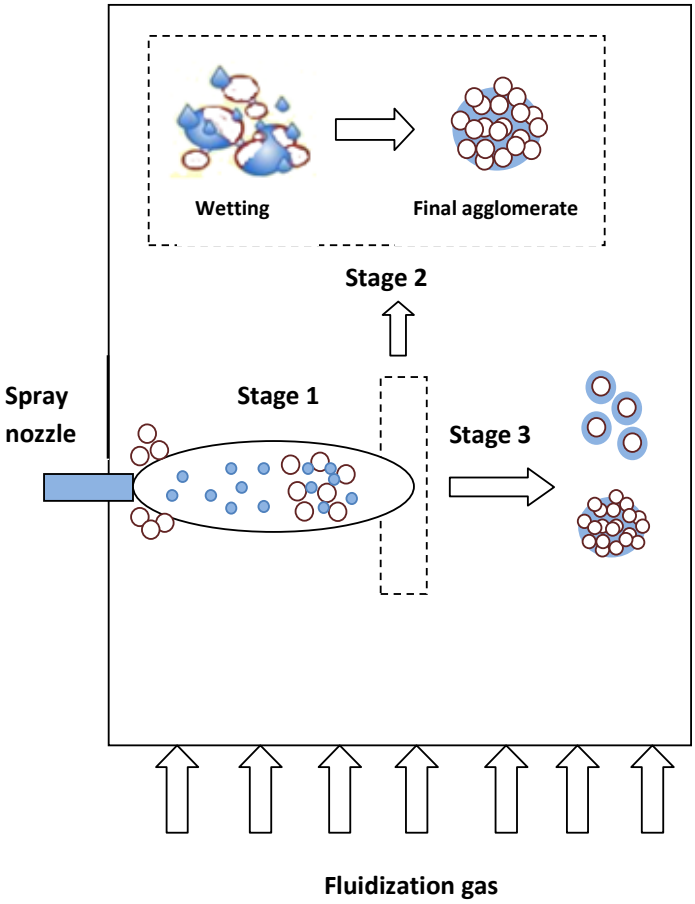

Figure 1.2. Agglomeration and break up process (Morales 2013)

1.2 Previous studies on the distribution of the liquid in a gas-solid fluidized bed and previously used measurement techniques: a review

The previous studies on the distribution of injected liquid in a gas-solid fluidized bed can be considered in two categories: a) injection in a hot fluidized bed b) injection in a cold model fluidized bed. The present review focuses on the experimental studies that have investigated the impact of different parameters on the distribution of the injected liquid in a gas-solid fluidized bed. This review also covers the previously used measuring techniques to assess the interaction between injected liquid and solid particles in a gas-solid fluidized bed. These studies are relevant to the Fluid Coking process since the cracking reactions of heavy hydrocarbon feedstock in Fluid Cokers take place in the liquid phase.

1.2.1 Previously used measurement techniques to assess the distribution of the injected liquid on fluidized particles

Van Ommen and Mudde (2007) reviewed all the measurement techniques for measuring the gas-solid distribution in a fluidized bed. Some of these techniques have been also used for measuring the liquid distribution in a gas-solid fluidized bed. Table 1.1 shows all these measurement methods and their advantage and disadvantages.

Table 1.1. Measurement techniques in fluidized beds

Methods		**Used in measurement of:**	**advantages**	**Disadvantages**	**limitations**
Direct visualization	Photographic and video techniques	Solid concentration (voidage distribution), particle velocity	Non-invasive, easy to use	Data analysis tedious and difficult	Very dilute systems, transparent walls of fluidized bed
Tomography	X-ray or γ-ray tomography	Solid concentration, gas-liquid jets	Non-invasive, Spatial resolution is good	High cost, temporal resolution is low	Column dimension
	Electric capacitance tomography	Solid and liquid concentration	Non-invasive, fast	Spatial resolution is low	Only differentiate materials with dielectric difference, small measurement volume
Probes-	Capacitance	Solid and liquid	Non-invasive	Spatial resolution	Only differentiate

electrodes	probe-electrode	concentration	(using electrodes)	is low	materials with dielectric difference, small measurement volume
	Conductive probe-electrode	Solid and liquid concentration	Non-invasive (using electrodes)	Spatial resolution is low	only differentiate an electrical conducting phase from a non-conducting one
	Optical fiber probe	Solid concentration, particle velocity	Well-developed method	Invasive method, lack of a properly defined measuring volume	Small measurement volume
Pressure measurements	Pressure transducers	Bed density and height, voidage	Non-invasive	Obtaining good measurements is related to the dimension and placement of the probe	Obtaining quantitative voidage data is a difficult task
Acoustic measurements	Microphones	Voidage	Non-invasive	Signals are complicated	Only used to obtain qualitative information about the state of fluidization

Ariyapadi et al. (2003) employed an X-ray imaging system to study the jet expansion angle and its penetration distance into a fluidized bed. The authors also studied the formation of liquid-solid agglomerates using radio opaque tracers mixed with the feed liquid.

Some studies used a conductance method to assess the distribution of injected liquid on solid particles. Portoghese et al. (2007) used a triboelectric probe to evaluate the spray nozzle performance, since wet solids give completely different triboelectric charging then dry solids. Because the triboelectric method is very sensitive to the local bed hydrodynamics, Leach et al. 2008; and Portoghese et al. (2008) developed another method that is much less sensitive to the local hydrodynamics. They measured the electric conductance of the bed solids after the liquid injection and defluidization of the wetted particles. Ali Zirgachian et al. (2013) used an electrical conductance method in a large scale bubbling pie-shape fluidized bed to measure the liquid distribution on solid particles. The author studied the effect of Gas to Liquid ratio in the nozzle on the distribution of the liquid on solid particles.

Fan et al. (2001) developed an electric capacitance tomography method for real time imaging of a gas-solid fluidized bed with an evaporative liquid jet, and used this method to study the distribution of bubbles in gas-solid fluidized bed with and without an evaporative liquid jet. Gehrke and Wirth (2008) implemented temperature and capacitance measurement methods to identify the spray zone with injecting liquid feed in a high density circulating fluidized bed.

1.2.2 Previous studies on the distribution of injected liquid in a hot gas-solid fluidized bed

Several authors injected cold liquids into hot fluidized beds and evaluated the liquid distribution from local temperature measurements. McMillan et al. (2005) studied the injection of cold ethanol into a fluidized bed of coke particles in order to develop a quick method to determine the quality of the solid-liquid mixing on a short time scale from temperature measurements. Bruhns and Werther (2005) investigated the mechanism of the liquid injection into a pilot plant bubbling fluidized bed using water and ethanol and a bed temperature between 120 to 180 ^{0}C. They found that particles enter the jet cavity and immediately form agglomerates. Saha (2012) studied the simultaneous agglomeration and attrition process in a hot fluidized bed by injecting a sugar solution into a bed of coke particles at a temperature high enough to promote caramelization. Saha (2012) found that increasing the flowrate of atomization gas in a spray nozzle always decreased the formation of large agglomerates or macro agglomerates, which have a detrimental effect on the process.

1.2.3 Study the distribution of the injected liquid in a cold gas-solid fluidized bed

There are different studies on the optimization of the operating conditions in a gas-solid fluidized bed to provide quick and uniform liquid-solid contact at room temperature, which is easier and more convenient than performing experiments at high temperature.

Portoghese et al. (2010) characterized the effect of nozzle geometry on the liquid-solid contact efficiency using electric conductance measurements. Chan et al. (2004) found that placing a cylindrical tube downstream of a gas-liquid jet can enhance the liquid-solid

contact efficiency by increasing the turbulence within the jet cavity that is formed within the bed by the spray jet. Ariyapadi et al. (2005) developed a model to evaluate the liquid-solid mixing in such a tube. Briens et al. (2009) showed the impact of the draft tube on the expansion angle and the jet penetration of a liquid jet in a fluidized bed. Briens et al. (2008) developed a novel technique to measure the entrainment of the solid to the horizontal liquid jet flowing through a draft tube which is intended to increase solid-liquid mixing. House et al. (2008) studied the effect of the spray nozzle design on the distribution of the liquid on solid particles. Leach et al. (2009) investigated the impact on the jet-bed interactions of several spray nozzle geometries, under different operating conditions, using a conductance probe. Pougatch et al. (2012) investigated the impact of a conical nozzle attachment on the liquid distribution using numerical simulation. The authors found that a 40^0 attachment provides the best spray dispersion because this attachment destabilizes the boundaries of the jet in a fluidized bed.

Some studies used a commercial scale nozzle to study the impact of parameters such as Gas to Liquid ratio in the nozzle and liquid-solid mixing on the efficiency of Fluid Cokers. Tafreshi et al. (2002) studied the impact of two phase feed characteristics such as the Gas to Liquid ratio in a commercial scale injector on the efficiency of Fluid Cokers by measuring the droplet size and spray dispersion in open air. House et al. (2004) investigated the impact of liquid-solid mixing on Fluid Coker yield. The author developed an empirical technique to determine the liquid-solid mixing using an industrial nozzle and a new enhanced solid entrainment (ESE) device. They concluded that enhancing liquid-solid mixing can improve the liquid yield by up to 0.6 wt% and decrease the coke yield by up to 2 wt%.

Ejim et al. (2010) studied the effect of liquid properties such as viscosity and surface tension on the atomization quality in gas-liquid Fluid Coker nozzles spraying into open air. Bi et al. (2005) studied the impact of bed hydrodynamics in a scaled down cold model Fluid Coker, without liquid injection, using pressure fluctuations measurements, and showed that the bed hydrodynamics are mainly affected by the superficial gas velocity and the solid circulation rate.

The review of previous studies shows that most of the published works have focused on the impact of the nozzle geometry, nozzle design, nozzle attachments and nozzle operating conditions such as Gas to Liquid ratio on the distribution of the liquid on solid particles. It shows that there is a less focus on the impact of the bed hydrodynamics such as superficial gas velocity, spray nozzle position and relative velocity of solid particles in a fluidized bed which this study tends to cover.

1.3 Research Objectives

The main objectives of this thesis are:

- investigation of the effects of local hydrodynamics on the liquid distribution in a gas-solid fluidized bed, using a capacitance method, by changing the fluidization velocity, Gas to Liquid ratio of the spray nozzle, nozzle inclination angle, location of the spray nozzle, and relative velocities of solid particles. A major advantage of the bed capacitance system used in this study is that capacitance can be measured without invasive probes, which would interfere with the bed hydrodynamics and the liquid distribution. The designed capacitance meter in this study can also detect local liquid concentration in a gas-solid fluidized bed with good accuracy.

- development of an experimental method that makes it possible to separate the effects of the local hydrodynamics on the initial liquid-solid agglomerate formation during liquid injection from the effects on the agglomerate breakup subsequent to the liquid injection.

- investigation of the effect of the relative velocity of particles on the liquid-solid contact efficiency in a fluidized bed, since there is a relative velocity range of 0.5 to 1 m/s between particles and the gas-liquid jet in actual Fluid Cokers (Song et al. 2004).

- development of a model that provides information on the liquid concentration of the initial agglomerates formed from the contact between the gas-liquid spray jet and fluidized particles, exploring the impacts of the spray quality and bed

hydrodynamics such as the atomization gas flowrate, fluidization velocity during injection, and nozzle location and inclination with the model, and related to experimental results.

References

Ali Zirgachian, M., M. Soleimani, C. Briens and F. Berruti. 2013. "Electric Conductance Method for the Assessment of Liquid-Gas Injection into a Large Gas-Solid Fluidized Bed." *Measurement: Journal of the International Measurement Confederation* 46(2):893-903.

Ariyapadi, S. 2004. "Interaction between Horizontal Gas-Liquid Jets and Gas-Solid Fluidized Beds." Western University,.

Ariyapadi, S., D. Holdsworth, C. Norley, F. Berruti and C. Briens. 2003. "Digital X-Ray Imaging Technique to Study the Horizontal Injection of Gas-Liquid Jets into Fluidized Beds." *International Journal of Chemical Reactor Engineering* 1 (A56).

Ariyapadi, S., F. Berruti, C. Briens, B. Knapper, R. Skwarok and E. Chan. 2005. "Stability of Horizontal Gas-Liquid Sprays in Open-Air and in a Gas-Solid Fluidized Bed." *Powder Technology* 155(3):161-174.

Base, T. B., E. W. Chan, R. D. Kennett and D. A. Emberley. 1999. "Nozzle for Atomizing Liquid in Two Phase Flow.".

Bi, H. T., J. R. Grace, C. J. Lim, D. Rusnell, D. Bulbuc and C. A. McKnight. 2005. "Hydrodynamics of the Stripper Section of Fluid Cokers." *The Canadian Journal of Chemical Engineering* 83(2):161-168.

Briens, C., F. Berruti, V. Felli and E. Chan. 2008. "Solids Entrainment into Gas, Liquid, and Gas-Liquid Spray Jets in Fluidized Beds." *Powder Technology* 184(1):52-57.

Briens, C., M. Dawe and F. Berruti. 2009. "Effect of a Draft Tube on Gas-Liquid Jet Boundaries in a Gas-Solid Fluidized Bed." *Chemical Engineering and Processing: Process Intensification* 48(4):871-877.

Bruhns, S. and J. Werther. 2005. "An Investigation of the Mechanism of Liquid Injection into Fluidized Beds." *AICHE Journal* 51(3):766-775.

Chan, E. W., S. McDougall and B. Knapper. 2004. "Fluid Coking Reactor with Mixing of Bitumens with Steam Carrier Gas and Spray Atomization Nozzle for Coking of Bitumens and Heavy Oils.".

Darabi, P., Pougatch, K., Salcudean, M., Grecov, D. 2010. "Agglomeration of Bitumen-Coated coke particles in fluid cokers", *International Journal of Chemical Reactor Engineering,* 8 (A122).

Ejim, C. E., M. A. Rahman, A. Amirfazli and B. A. Fleck. 2010. "Effects of Liquid Viscosity and Surface Tension on Atomization in Two-Phase, gas/liquid Fluid Coker Nozzles." *Fuel* 89(8):1872-1882.

Fan, L., R. Lau, C. Zhu, K. Vuong, W. Warsito, X. Wang and G. Liu. 2001. "Evaporative Liquid Jets in Gas-Liquid-Solid Flow System." *Chemical Engineering Science* 56(21-22):5871-5891.

Gehrke, S. and K. Wirth. 2008. "Liquid Feed Injection in a High-Density Riser." 31(11):1701.

Gray, M. R. 2002. "Fundamentals of Bitumen Coking Processes Analogous to Granulations: A Critical Review." *The Canadian Journal of Chemical Engineering,* 80 (3):393-401.

Gray, M. R., W. C. McCaffrey, I. Huq and T. Le. 2004. "Kinetics of Cracking and Devolatilization during Coking of Athabasca Residues." *Industrial & Engineering Chemistry Research, 43 (18):5438-5445.*

Hammond, D. G., L. F. Lampert, C. J. Mart, S. F. Massenzio, G. E. Phillips, D. L. Sellards and A. C. Woerner. 2003. "Refining: Review of Fluid Bed Coking Technologies." *Petroleum Technology Quarterly* 8(5):27-31, 33.

House, P. K., C. L. Briens, F. Berruti and E. Chan. 2008. "Effect of Spray Nozzle Design on Liquid-Solid Contact in Fluidized Beds." *Powder Technology* 186(1):89-98.

House, P. K., M. Saberian, C. L. Briens, F. Berruti and E. Chan. 2004. "Injection of a Liquid Spray into a Fluidized Bed: Particle-Liquid Mixing and Impact on Fluid Coker Yields." *Industrial and Engineering Chemistry Research* 43(18):5663-5669.

Knapper, B. A., M. R. Gray, E. W. Chan and R. Mikula. 2003. "Measurement of Efficiency of Distribution of Liquid Feed in a Gas-Solid Fluidized Bed Reactor." *International Journal of Chemical Reactor Engineering* 1 (A35).

Leach, A., F. Portoghese, C. Briens and F. Berruti. 2008. "A New and Rapid Method for the Evaluation of the Liquid-Solid Contact Resulting from Liquid Injection into a Fluidized Bed." 184(1):44.

Leach, A., G. Chaplin, C. Briens and F. Berruti. 2009. "Comparison of the Performance of Liquid-Gas Injection Nozzles in a Gas-Solid Fluidized Bed." *Chemical Engineering and Processing: Process Intensification* 48(3):780-788.

McDougall, S., M. Saberian, C. Briens, F. Berruti and E. Chan. 2005. "Effect of Liquid Properties on the Agglomerating Tendency of a Wet gas–solid Fluidized Bed." *Powder Technology* 149(2–3):61-67.

McMillan, J., D. Zhou, S. Ariyapadi, C. Briens, F. Berruti and E. Chan. 2005. "Characterization of the Contact between Liquid Spray Droplets and Particles in a Fluidized Bed." *Industrial and Engineering Chemistry Research* 44(14):4931-4939.

Morales M, C. B. 2013. " Development and Application of an Experimental Model for the Fluid Coking™ Process " Western University, .

Portoghese, F., F. Berruti, C. Briens and E. Chan. 2007. "Novel Triboelectric Method for Characterizing the Performance of Nozzles Injecting Gas-Atomized Liquid into a Fluidized Bed." *Chemical Engineering and Processing: Process Intensification* 46(10):924-934.

Portoghese, F., L. Ferrante, F. Berruti, C. Briens and E. Chan. 2010. "Effect of the Injection-Nozzle Geometry on the Interaction between a Gas-Liquid Jet and a Gas-Solid Fluidized Bed." *Chemical Engineering and Processing: Process Intensification* 49(6):605-615.

Portoghese, F., L. Ferrante, F. Berruti, C. Briens and E. Chan. 2008. "Effect of Injection-Nozzle Operating Parameters on the Interaction between a Gas-Liquid Jet and a Gas-Solid Fluidized Bed." *Powder Technology* 184(1):1-10.

Pougatch, K., M. Salcudean and J. McMillan. 2012. "Influence of Conical Nozzle Attachments on Horizontal Spray Dispersion in a Fluidized Bed." *Chemical Engineering Research and Design* 90(10):1506-1516.

Saha, M. 2012. "Simultaneous Particle Agglomeration and Attrition in a High Temperature Fluidized Bed." Western University,.

Song, X., H. Bi, C. J. Lim, J. R. Grace, E. Chan, B. Knapper and C. McKnight. 2004. " Hydrodynamics of the Reactor Section in Fluid Cokers." *Powder Technology* 147:126.

Tafreshi, Z. M., D. Kirpalani, A. Bennett and T. W. McCracken. 2002. "Improving the Efficiency of Fluid Cokers by Altering Two-Phase Feed Characteristics." *Powder Technology* 125(2–3):234-241.

Van Ommen, J. R. and R. F. Mudde. 2007. "Measuring the Gas-Solids Distribution in Fluidized Beds – a Review.".

Weber, S., C. Briens, F. Berruti, E. Chan and M. Gray. 2006. "Agglomerate Stability in Fluidized Beds of Glass Beads and Silica Sand." *Powder Technology* 165(3):115-127.

Chapter 2

2. STUDY OF THE EFFECT OF LOCAL HYDRODYNAMICS ON LIQUID DISTRIBUTION IN A GAS-SOLID FLUIDIZED BED USING A CAPACITANCE METHOD

2.1 Abstract

Injection of liquid feed into fluidized beds is widely applied in the petrochemical, chemical, food and pharmaceutical industries. The local bed hydrodynamics have a strong impact on the contact between the injected liquid and the bed solids. By adjusting the local bed hydrodynamics or locating the injection nozzle in the appropriate region of the bed, the contact between the injected liquid and the bed solids may be optimized to minimize agglomerate formation, which is detrimental to many industrial operations such as Fluid Coking. The effect of bed hydrodynamics on liquid distribution was investigated with a new, reliable and sensitive capacitance method. Results show that the fluidized bed hydrodynamics have a considerable impact on the contact efficiency between injected liquid and fluidized solids.

2.2 Introduction

Many industrial processes, such as Fluid Coking, Fluid Catalytic Cracking (FCC) and gas-phase polymerization, utilize the process of liquid injection into a fluidized bed. The liquid distribution on the fluidized particles has been found to have a considerable impact on the performance of these processes. Bruhns and Werther (2005) showed that particles enter the jet cavity formed by the injected liquid and immediately form agglomerates. Agglomeration is a problem in Fluid Coker units as it reduces the yield of valuable products by increasing mass and heat transfer resistances and influencing the thermal cracking reactions (House et al. 2008). Therefore, identifying the operating conditions that enhance the liquid distribution over individual free flowing solid particles is essential to minimize the agglomerate formation.

Several publications address the characteristics of liquid jets in a fluidized bed. Ariyapadi et al. (2003) employed an X-ray imaging system to study the jet expansion angle and its

penetration distance into a fluidized bed. These authors also studied the formation of liquid-solid agglomerates using radio opaque tracers mixed with the feed liquid. Knapper et al. (2003) used a tracer to measure the liquid-solid contact in a pilot plant Fluid Coker, and showed that the liquid distribution on the bed solids strongly depends on the nozzle geometry. Gehrke and Wirth (2008) implemented temperature and capacitance measurement methods to identify the spray zone with injecting liquid feed in a high density circulating fluidized bed. House et al. (2004) used a simple model to show that liquid distribution has a major impact on the yield of valuable products in Fluid Cokers. Darabi et al. (2010) proposed a simplified mathematical method to determine the agglomeration tendency of bitumen-coated coke particles in Fluid Cokers, showing that liquid distribution has a significant impact on agglomerate formation, which is detrimental to Coker operation.

Several authors injected cold liquids into hot fluidized beds and inferred the liquid distribution from local temperature measurements. McMillan et al. (2005) studied the injection of cold ethanol into a fluidized bed of coke particles in order to develop a quick method to determine the quality of solid-liquid mixing on a short time scale from temperature measurements. Bruhns and Werther (2005) investigated the mechanism of liquid injection into a pilot plant bubbling fluidized bed using water and ethanol and a bed temperature between 120 to 180 ^{0}C. They found that the agglomerates formed at the exit tip of the nozzle.

Methods were developed to evaluate the liquid distribution at room temperature, which is easier and more convenient than performing experiments at high temperature. Portoghese et al. (2007) used a triboelectric probe to evaluate spray nozzle performance, since wet solids give completely different triboelectric charging then dry solids. Because the triboelectric method is very sensitive to the local bed hydrodynamics, Portoghese et al. (2008b) and Leach et al. (2008) developed another method that is much less sensitive to the local hydrodynamics. They measured the electric conductance of the bed solids after liquid injection and defluidization of the wetted particles. Fan et al. (2001) developed electrical capacitance tomography as an imaging technique to study gas-solid flow systems with evaporative liquid jets. Leach et al. (2009) showed that the performance of

various spray nozzles could be ranked with a Nozzle Performance Index (NPI), obtained from bed conductivity measurements. Leach et al. (2009) and Portoghese et al. (2008a) found that increasing the mass ratio of atomization gas to injected liquid (GLR) improves the spray nozzle performance. However, in industrial units increasing the GLR is associated with significant costs and flow constraints. Therefore, it is necessary to accurately assess the effect of atomized gas to injected liquid on the performance of the nozzle.

The objective of this study was to investigate the effects of local hydrodynamics on liquid distribution in a gas-solid fluidized bed, using a capacitance method, by changing the fluidization velocity. Another objective was to develop experimental methods that make it possible to separate the effects of the local hydrodynamics on the initial liquid-solid agglomerate formation during liquid injection from the effects on the agglomerate breakup subsequent to the liquid injection.

2.3 Experimental

2.3.1 Experimental setup

The experiments were performed in a fluidized bed 1.97 m high with a 1.54 m by 0.288 m rectangular cross sectional area, as shown in Figure 1a. Two banks of calibrated sonic orifices and pressure regulators were used to adjust the fluidization velocity. Three rectangular wooden windows were mounted on each side of the unit walls.

For most of the experiments, the liquid injection was carried out with a scaled-down version of a proprietary industrial convergent-divergent-convergent spray nozzle, with a 3 mm tip diameter as shown in Figure 2.1b (Base et al. 1999). Nitrogen as atomization gas was mixed with water in a pre-mixer (Item 12 in Figure 1a) upstream of the spray nozzle (McCracken et al. 2006). The flow rate of the atomization gas was set with a calibrated sonic orifice and a pressure regulator (Item 1 and Item 9 in Figure 2.1a). For the regular experiments, the fluidization velocity was set at a specified value and the liquid was injected for 10 s. The liquid flowrate for these experiments was about 20 g/s.

The bed temperature was measured with 2 thermocouples (Item 13 in Figure 2.1a). The thermocouple at the top of bed measured the freeboard temperature. The bed height and bed mass were calculated from pressure measurements performed with transducers located at different positions on the side of the unit wall.

a)

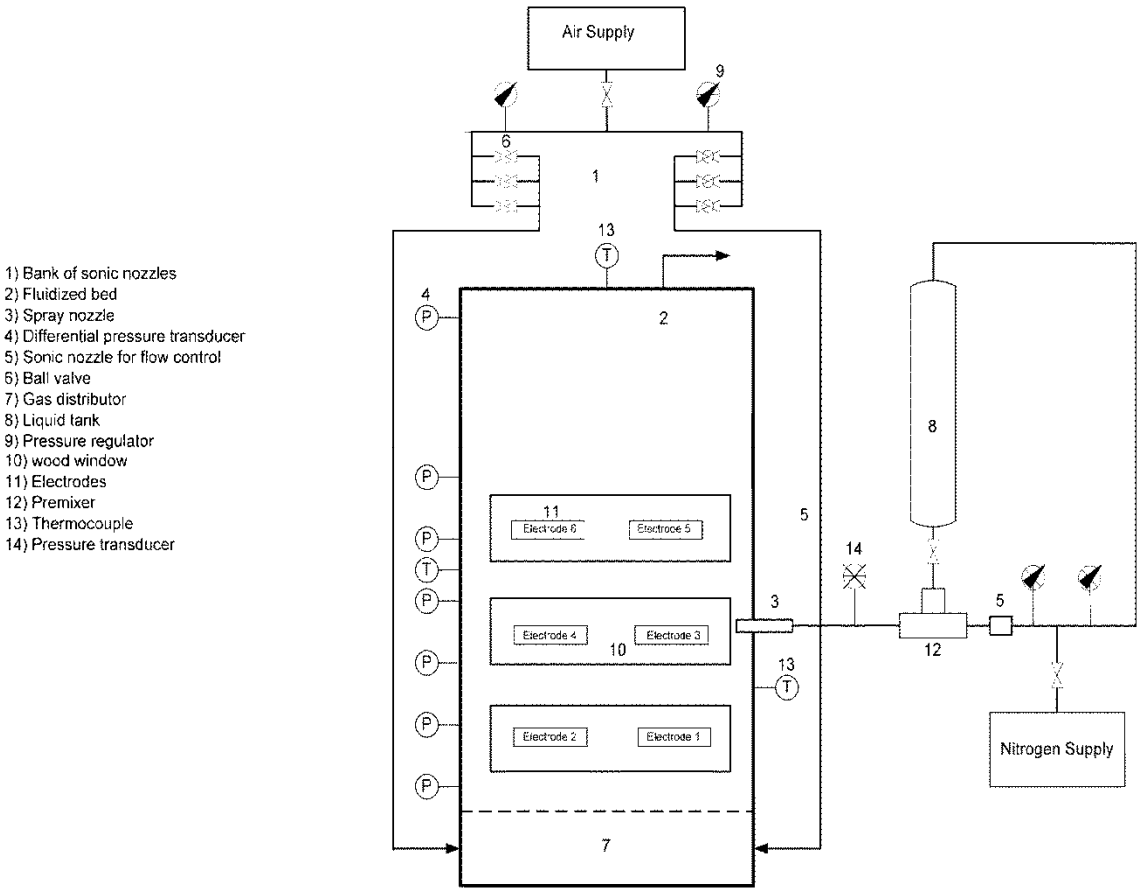

b)

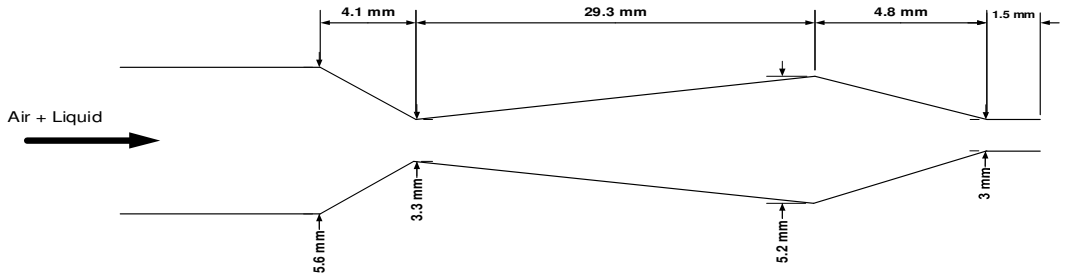

Figure 2.1. a) Schematic diagram of experimental setup; b) Injection nozzle

2.3.2 Measuring system

In preliminary experiments, bed solids were sampled just after the liquid injection. The injected liquid was found in three forms: liquid forming a thin layer around individual free-flowing particles that is called “free moisture”; liquid trapped within “micro-agglomerates” that were small enough to remain fluidized; and liquid trapped within “macro-agglomerates”, which defluidized and settled to the bottom of the bed just above the gas distributor plate.

Initial experiments were conducted in a small test cell equipped with 2 electrodes to measure the capacitance of the bed solids. These tests indicated that the liquid trapped in the agglomerates has a negligible effect on the capacitance of defluidized solids. They also showed that the defluidized bed capacitance is a function of the free moisture and that it is not affected by the presence of agglomerates. This is due to the large difference between the dielectric constant of water (80.4) and that of sand (2.5-3.5) and air (1) (Department of Physics and Astronomy, Georgia State University).

An AC-based capacitance meter was used to measure the bed capacitance between electrodes. It used a sine-wave voltage as the excitation source to produce an AC input current, and an amplifier to convert this current into an AC voltage (Yang 1996). The output signal from the capacitance meter was then sent to a data acquisition card

(National Instruments model number USB-6259 BNC) and recorded by a computer. Figure 2.2 shows a block diagram of the capacitance meter.

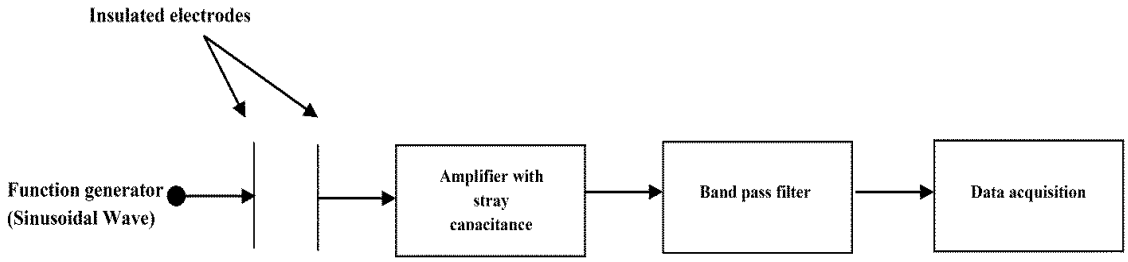

Figure 2.2. Block diagram of capacitance meter

Electrodes are electrically insulated to block the conduction current and to ensure that only the capacitance current passes through the electrodes. The amplifier rejects stray capacitance through appropriate grounding of the electrodes on one side of the column. Figure 2.3 shows a schematic diagram of the measuring system which has been used in this study. Each set of electrodes was supplied with current at a different frequency to prevent interference between the various electrodes.

For the regular experiments, the fluidization velocity was set at a specified value and the liquid was injected for 10 s. The bed continued to be fluidized at the same velocity for 5 s after the injection and then was defluidized. After this process, the bed capacitance was measured. In some experiments, the bed was refluidized and the evolution of the bed capacitance with time was recorded.

A major advantage of the bed capacitance system used in this study is that capacitance can be measured without invasive probes, which would interfere with the bed hydrodynamics and the liquid distribution. Electrodes were located on the outside of the wooden windows and the local bed capacitance was measured through the windows seen in Figure 2.1a. Six sets of electrodes were used, as shown in Figure 2.3. Each set constituted of 2 opposing electrodes, placed at the same location on opposing walls.

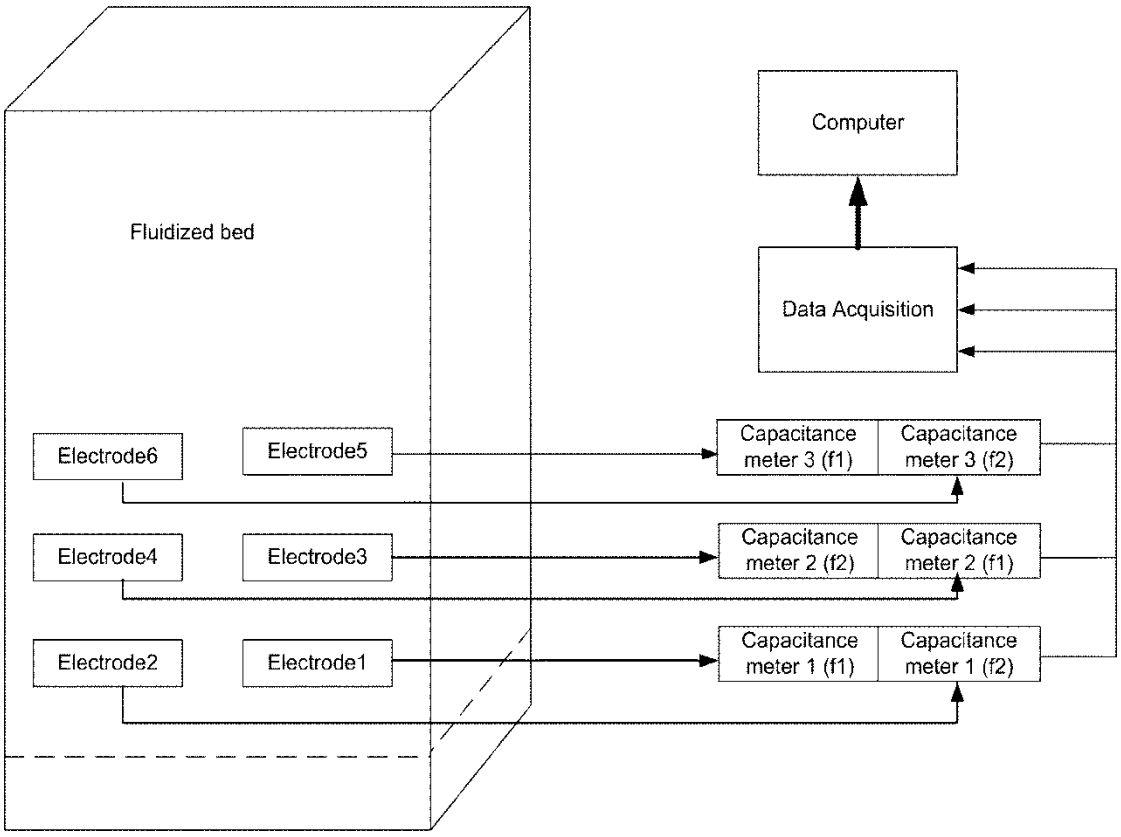

Figure 2.3. Schematic diagram of measuring system

2.3.3 Calibration experiments

This study used the capacitance method to measure the distribution of injected liquid on fluidized solid particles. This method, which can be used at room temperature, is non-invasive, and it does not use probes that would interfere with bed hydrodynamics. This method was used to evaluate the liquid distribution both after injection and after refluidization, which was achieved through appropriate calibration experiments.

2.3.3.1 Calibration for free moisture measurements after injection

Preliminary experiments had shown that the capacitance of a defluidized bed depends only on its free moisture. To determine the relationship between bed capacitance and free moisture, a special spray nozzle was used for the calibration experiments. It was operated with a large flowrate of atomization gas and a relatively small flowrate of liquid of 1.7 g/s to ensure close to ideal distribution of the injected liquid on the fluidized particles (Farkhondehkavaki 2012). The nozzle was a straight cylindrical tube, 3.6 mm in

diameter. The ratio of the mass flowrate of atomization gas to the mass flowrate of injected liquid was higher than 50%. Using such a high gas-to-liquid mass ratio is impractical from an industrial standpoint because of high costs and flow restrictions. Other experiments utilized a scaled down version of an industrial nozzle with more realistic atomization gas flowrates. The fluidization gas velocity was 0.3 m/s during injection for calibration experiments.

For all the experiments, 680 kg of sand particles with a Sauter mean diameter of 185 μm and a particle density of 2600 kg/m^3 were used. The expanded bed height was approximately 1.17 m when the fluidization velocity was 0.3 m/s.

Because of the relatively longer liquid injection time, there was significant evaporation of some of the liquid into the fluidization gas: the liquid concentration of the bed was, therefore, directly measured by taking samples from the bed and measuring their moisture content with the Karl Fischer titration method. The samples were taken with a dipper equipped with an extra-long handle dipper from the top of the bed when it was defluidized. As will be shown later, the bed was well mixed and the sample from the top of the bed is representative of the whole bed. Pure ethanol was used as a solvent to dissolve the water of the sample and the resulting solution was then injected in an automated Karl Fisher apparatus. For each experiment, five samples were tested with the Karl Fischer method.

After the injection, the bed was defluidized for about 4 minutes and capacitance measurements were performed. Figure 2.4 shows how the bed capacitance varied with time during one of the calibration experiments. Bed capacitance measurements were less accurate when the bed was fluidized, as the passage of gas bubbles in the measurement zone caused strong fluctuations in the measured capacitance signal. Therefore, the free moisture after injection was obtained from capacitance measurements that were performed while the bed was defluidized.

Figure 2.4 also shows that there was a negligible increase of the defluidized bed capacitance with time, which confirmed that the amount of liquid diffusing out of the agglomerates was negligible. This proves that there were no agglomerates formed during

the calibration experiments; if there had been wet agglomerates, water would have slowly diffused from the agglomerates throughout the bed material, increasing the measured capacitance.

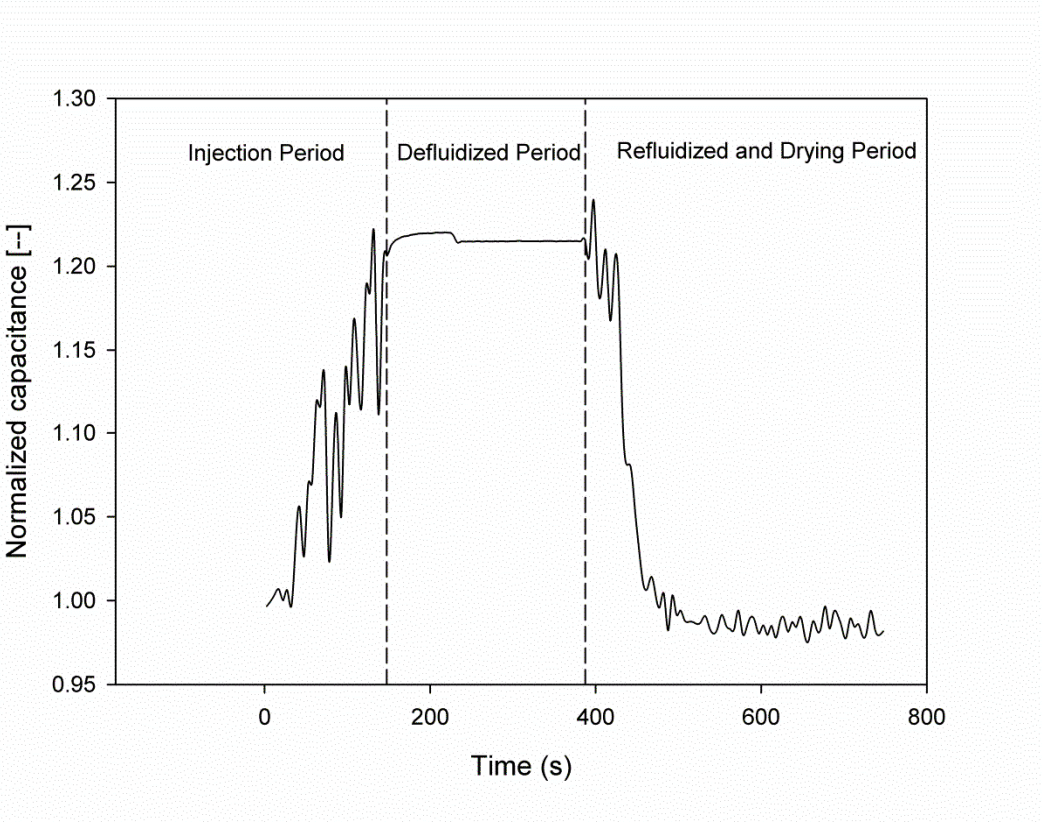

Figure 2.4. Normalized capacitance of electrode 1 versus time for one of the calibration experiments

The free moisture level was varied by changing the amount of injected liquid. The calibration experiments measured the capacitance of the bed for each electrode and for specific free moisture levels. For instance, Figure 2.5 and 2.6 show the calibration curves for electrodes 1 and 2. These figures show the dry-basis free moisture, x_i where subscript i refers to the electrode number. For each calibration experiment, the results obtained from the Karl Fischer analysis of the five samples are shown against the measured, normalized capacitance. The normalized capacitance is the ratio of the capacitance for the wet defluidized bed to the capacitance for the dry defluidized bed. In addition, each Figure shows a regression line with its 95% confidence interval.

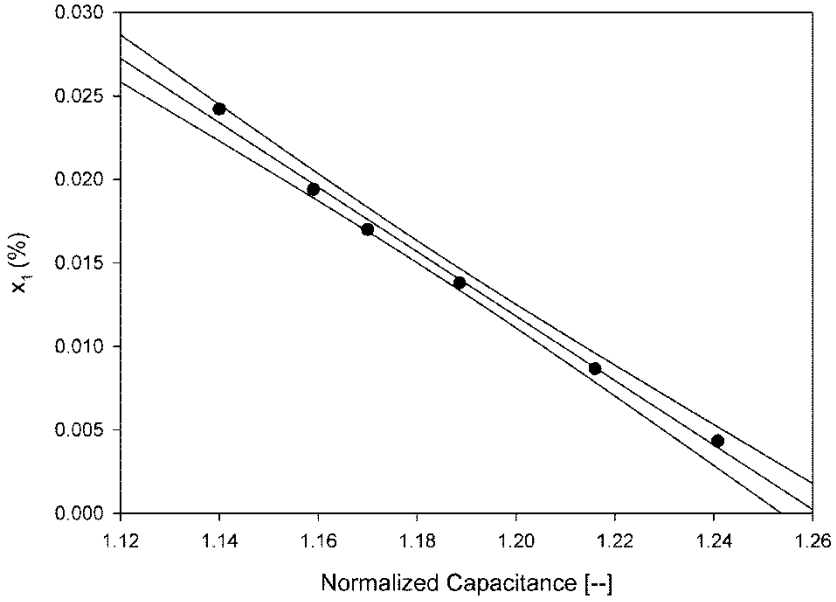

Figure 2.5. Calibration curve for defluidized period after injection for Electrode 1

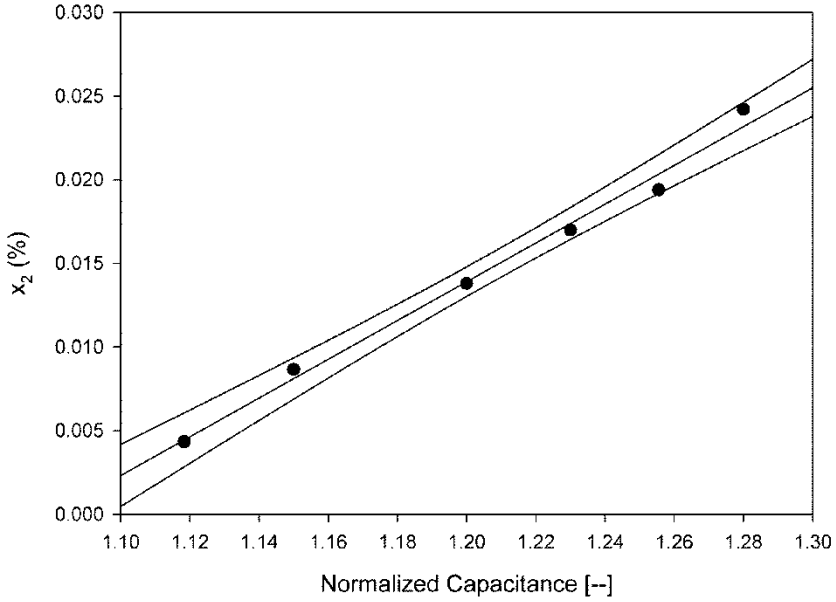

Figure 2.6. Calibration curve for defluidized period after injection for Electrode 2

Theoretically, injecting water should increase the capacitance, because the dielectric coefficient is 80 for water, 3 for sand and 1 for air. However, the calibration results show that the capacitances of Electrodes 1, 3 and 5, which are close to the nozzle, decrease with increasing moisture as seen in Figure 2.5 for electrode 1.

Figure 2.7 shows the bed structure from the electrical point of view. The electrode on the right side is virtually grounded to avoid stray capacitance. Also, the nozzle and the metallic frame are grounded. When the moisture in the bed increases, the electrical contact between the nozzle and the sand becomes stronger because the nozzle has a metallic frame and the water injected through the nozzle provides a path for the current that goes to ground through the nozzle. Figure 2.8a and 2.8b show the schematic and equivalent circuit that accounts for this effect at electrodes 1, 3 and 5. Other electrodes were not affected due to the considerable distance from the nozzle. In Figure 2.8a and 2.8b, R represents the contact resistance between the nozzle and sand, C_w is the capacitance of the wooden frame, and C_b is the capacitance of the bed. R decreases with increasing moisture. When the resistance R decreases, the voltage across C_b also decreases, and the current passing through the bed, the measured current (I_m) and the measured bed capacitance also decrease. The bed capacitance decreases linearly with increasing moisture because R decreases linearly with increasing moisture.

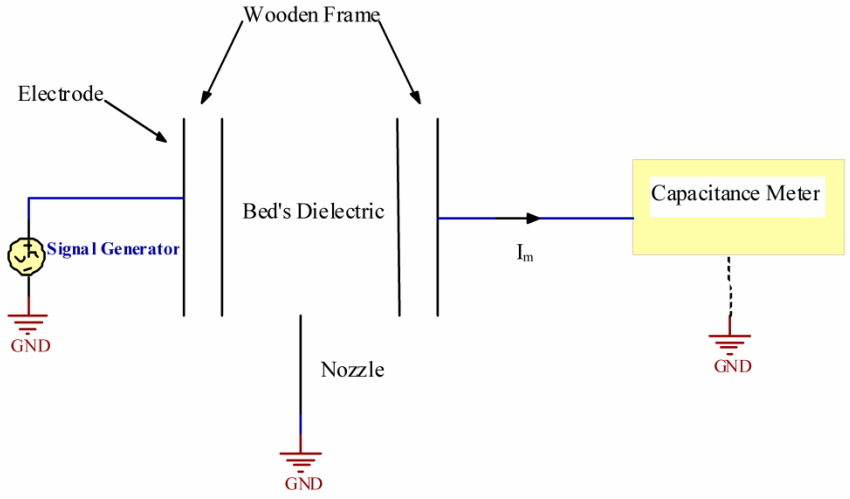

Figure 2.7. Schematic diagram of the fluidized bed from electrical point of view

a)

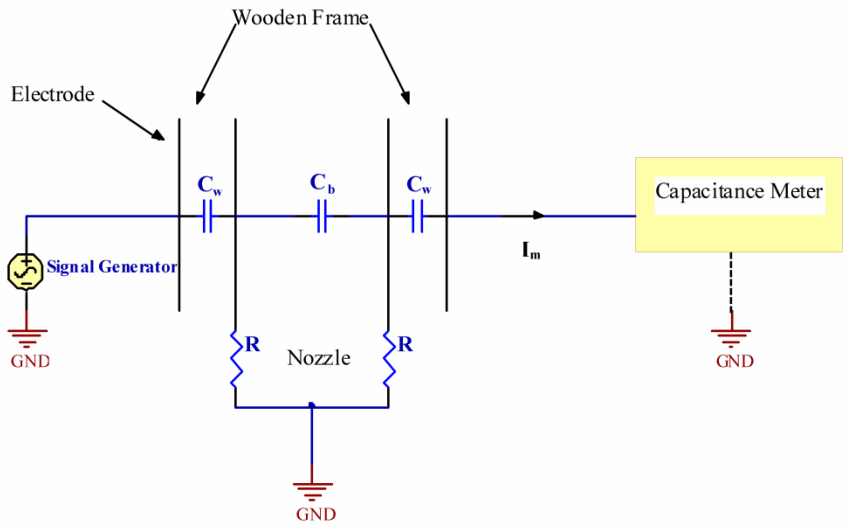

b)

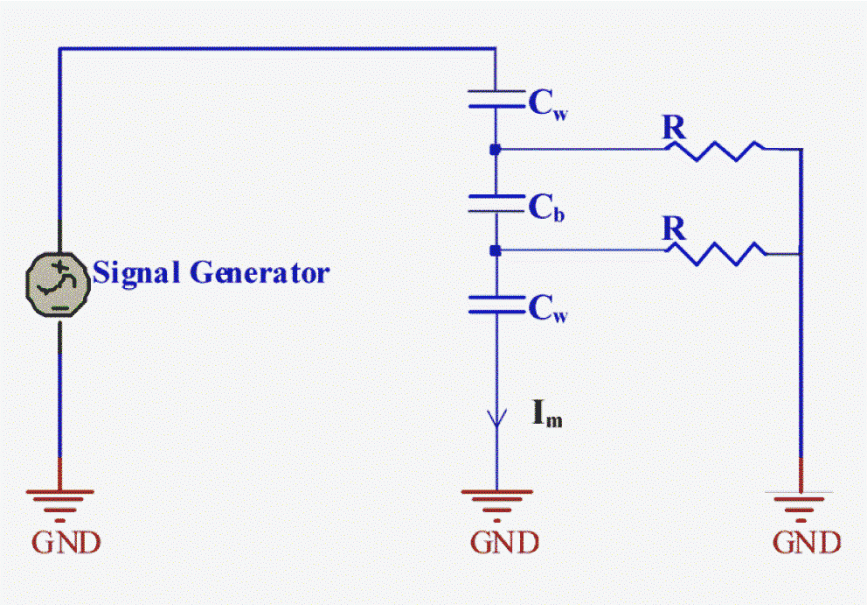

Figure 2.8. a) The schematic of bed from electrical point of view after injection of water; b) Equivalent circuit of the bed after injection of water

The conduction currents to the spray nozzle explains why the measured capacitance either decreases or increases with increasing free moisture, depending of the location of the electrodes relative to the nozzle. This is why it is important to determine the local free

moisture from individual electrode sets and then average them to get the average bed free moisture, rather than using an average bed capacitance to estimate the average bed free moisture.

To validate the assumption that the bed is well mixed, the method described in Figure 2.9 was used. Each electrode was calibrated assuming ideal mixing conditions. For each calibration experiment, the free moisture was calculated from the calibration equations based on the capacitance measured for each electrode, and the coefficient of variation of the moisture obtained for the various electrodes was calculated. For all the calibration experiments, the calculated coefficient of variation c_v ranged between 0.05 and 0.1, indicating that the bed was well mixed.

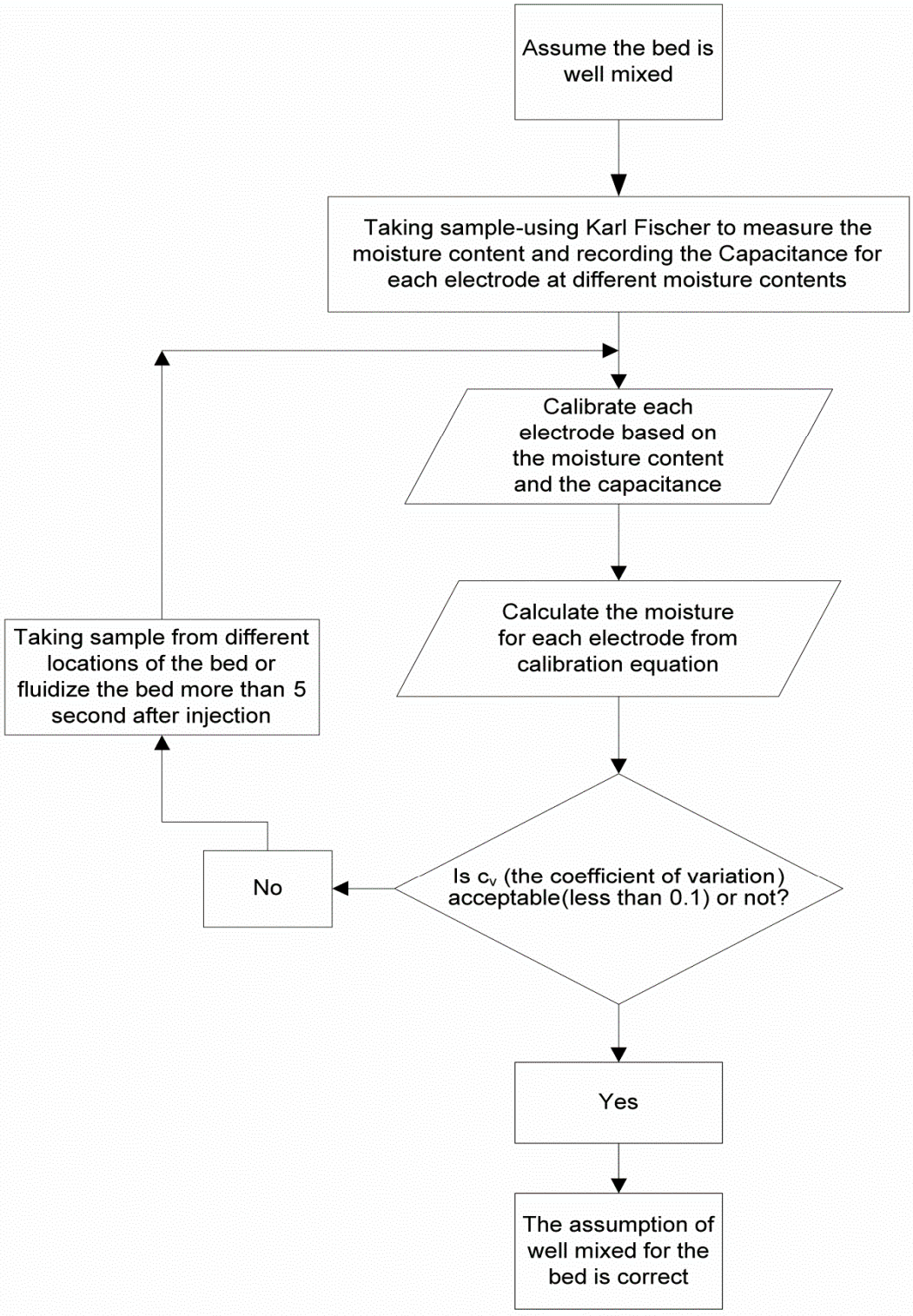

Figure 2.9. Algorithm for checking the assumption of well mixed bed during calibration experiments

2.3.3.2 Calibration for free moisture measurements during refluidization

The rate of evaporation of water from the fluidized bed depends on the air velocity and on the free moisture of the bed, which can be obtained from the bed capacitance. During the calibration experiments, all the moisture was indicated as free moisture, i.e. no agglomerates were present. In experiments with practical spray nozzles, a large fraction of the bed moisture is trapped in agglomerates, but these agglomerates do not contribute significantly to the evaporation of water from the bed. Hence, the evaporation rate can be considered to be the same as for calibration experiments with the same free moisture, gas velocity and bed temperature, since the evaporation rate from agglomerates is negligible when compared to the evaporation rate of the free moisture. This section, therefore, shows how to obtain the evaporation rate at various gas velocities and free moistures.

For these experiments, after defluidization and measurement of the defluidized bed capacitance, the bed was refluidized at 0.2, 0.3, and 0.4 m/s and the variation of the bed capacitance with time was recorded for each electrode. Because of the fluctuations in the measured capacitance while the bed is fluidized, the bed was defluidized every 15 s for 30 s and then the capacitance was measured. Using the calibration curves from the previous section, the moisture at each point of the defluidized period during refluidization was calculated. The total free moisture was then calculated from the average of the free moistures given by all electrodes at each time until the bed was dried, for several fluidization velocities.

Figure 2.10 shows how the average free moisture ($\bar{x}$) varied with time. These curves were fitted with smoothing software ("Table Curve") and the slope, $\left(\frac{d\bar{x}}{dt}\right)_{calibration}$, at each point for these curves was calculated, which provides the evaporation rate.

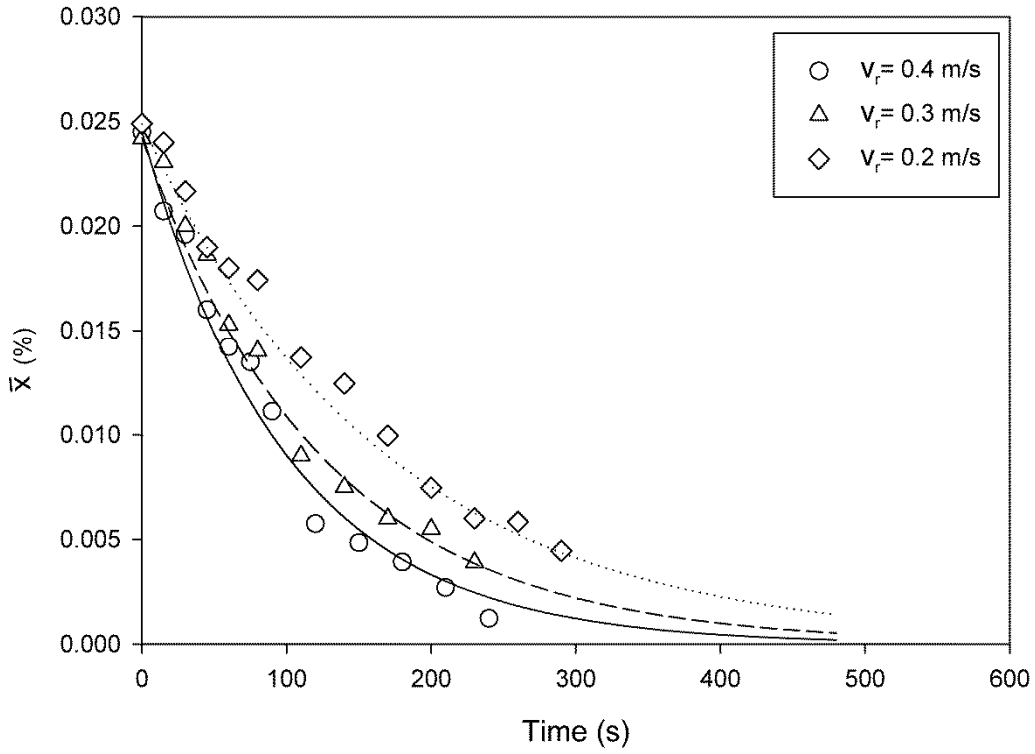

Figure 2.10. Average free moisture versus time during refluidization at several refluidization velocities

2.4 Results and discussion

2.4.1 Effect of fluidization velocity during injection

Some experiments were performed with a regular nozzle at different fluidization velocities during injection and at the same velocity during refluidization. Table 2.1 shows the experimental conditions. For these experiments the mass ratio of the atomization gas to injected liquid (GLR) was varied over the range between 1 and 3.5%. The experiments were repeated for the same conditions two times. For all experiments, the injection time was kept constant at 10 s and then the bed was defluidized for 1 minute. The capacitance was measured during defluidization for each electrode by the capacitance meter and the free moisture was calculated based on the capacitance signal for the calibration experiments.

Table 2.1. Experimental Conditions for experiments with different fluidization velocities during injection

Experiment	Velocity During Injection (m/s)	Velocity During Refluidization (m/s)	Total Water Injected (g)	Atomization Gas Flowrate (g/s)	Gas-to-Liquid Mass Ratio (GLR %)
Experiment-1	0.2	0.3	197.5	0.68	3.5
Experiment-2	0.2	0.3	209.7	0.55	2.6
Experiment-3	0.2	0.3	222.8	0.41	1.9
Experiment-4	0.3	0.3	204.6	0.55	2.7
Experiment-5	0.3	0.3	206	0.41	2
Experiment-6	0.3	0.3	205	0.28	1.3
Experiment-7	0.4	0.3	198.5	0.68	3.4
Experiment-8	0.4	0.3	168	0.41	2.4
Experiment-9	0.4	0.3	188.4	0.28	1.5

Figures 2.11, 2.12 and 2.13 show the dry-basis free moisture at different GLRs measured by each electrode after fluidization at 0.2 m/s, 0.3 m/s and 0.4 m/s during injection, respectively. The injection time for all experiments was 10 s and the bed was defluidized 5 s after injection. For all the experiments, the results show that the second, fourth and sixth electrodes, which are far from the spray nozzle, detected the smallest amount of free moisture. This is because the bed did not have time to mix well over the short injection time.

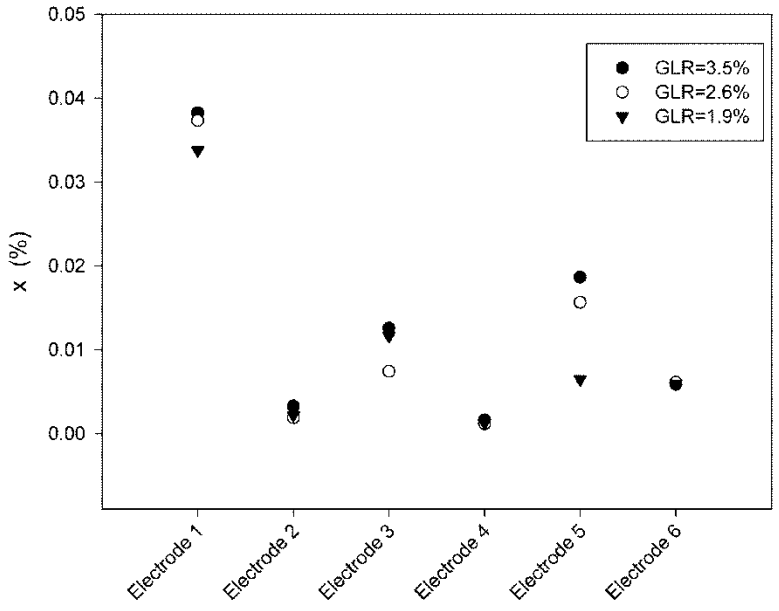

Figure 2.11. Dry-basis free moisture during defluidization at different GLRs (%) for each electrode at V_I= 0.2 m/s

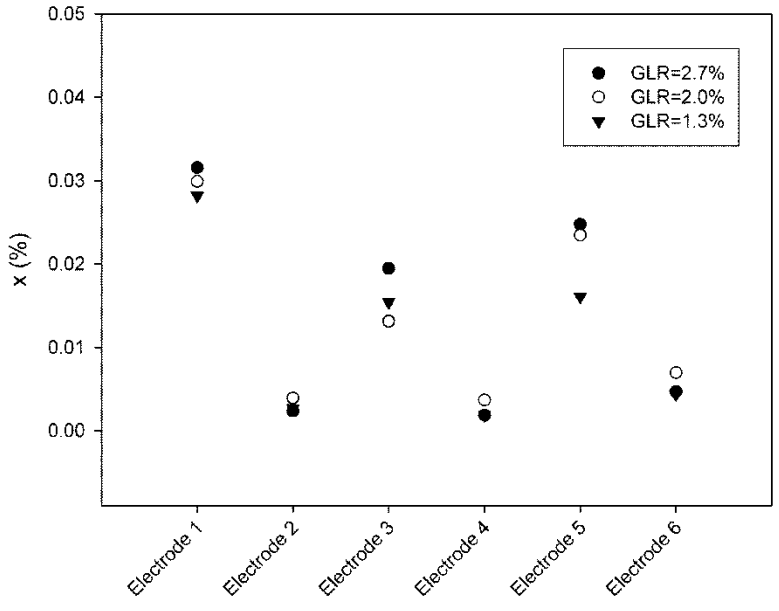

Figure 2.12. Dry-basis free moisture during defluidization at different GLRs (%) for each electrode at V_I= 0.3 m/s

Figure 2.13 shows that the effect of the GLR on the local free moisture measured by each electrode is not very clear, due to relatively poor mixing of the bed. To get a clearer picture, one must use the bed averaged free moisture, obtained from the average of x values given by the 6 electrodes during defluidization. The fraction of the total bed moisture that is free moisture is given by:

$$(M_s\bar{x})/M_L \qquad (2.1)$$

Where M_s is total mass of dry sand, $\bar{x}$ is the average of $x_i$values given by 6 electrodes and M_L is the total injected liquid.

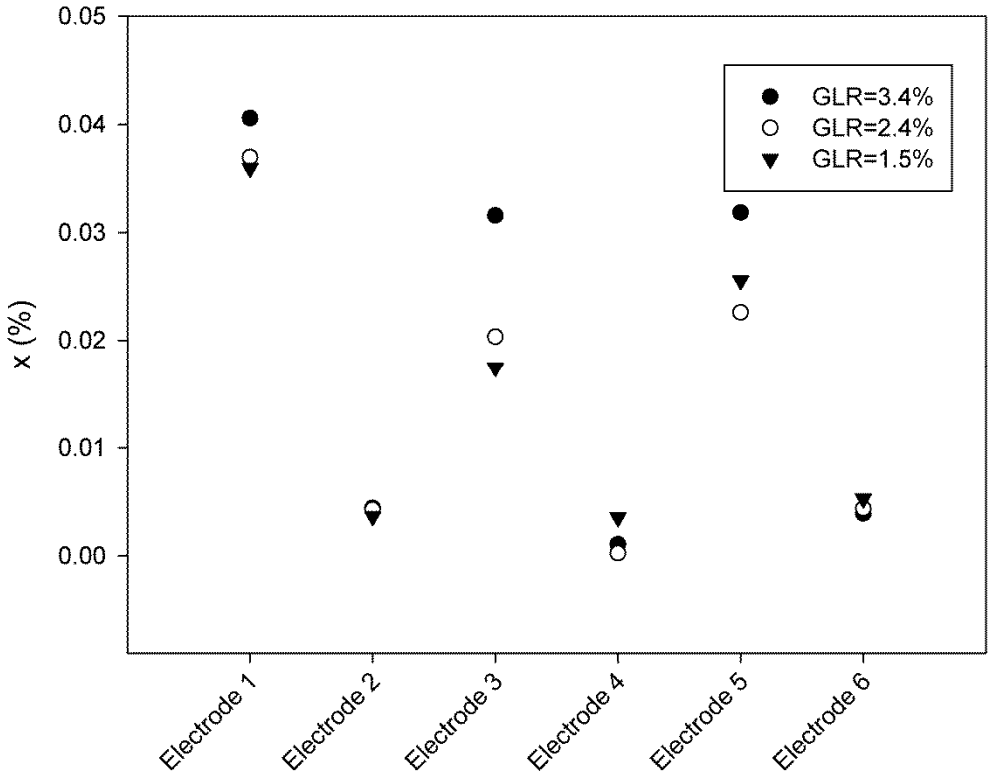

Figure 2.13. Dry-basis free moisture during defluidization at different GLRs (%) for each electrode at V_I= 0.4 m/s

Figure 2.14 shows the fraction of the total bed moisture that is free moisture when the bed is defluidized as a function of the spray GLR. According to this Figure, the highest GLR gives the highest free moisture because it results in finer droplets and a better distribution

of water throughout the fluidized bed, for all the fluidization velocities during injection. This corresponds to what was found by other researchers (Leach et al. 2008). Figure 2.14 also shows that increasing the fluidization velocity during injection increases the free moisture by improving the distribution of the injected liquid on the fluidized particles.

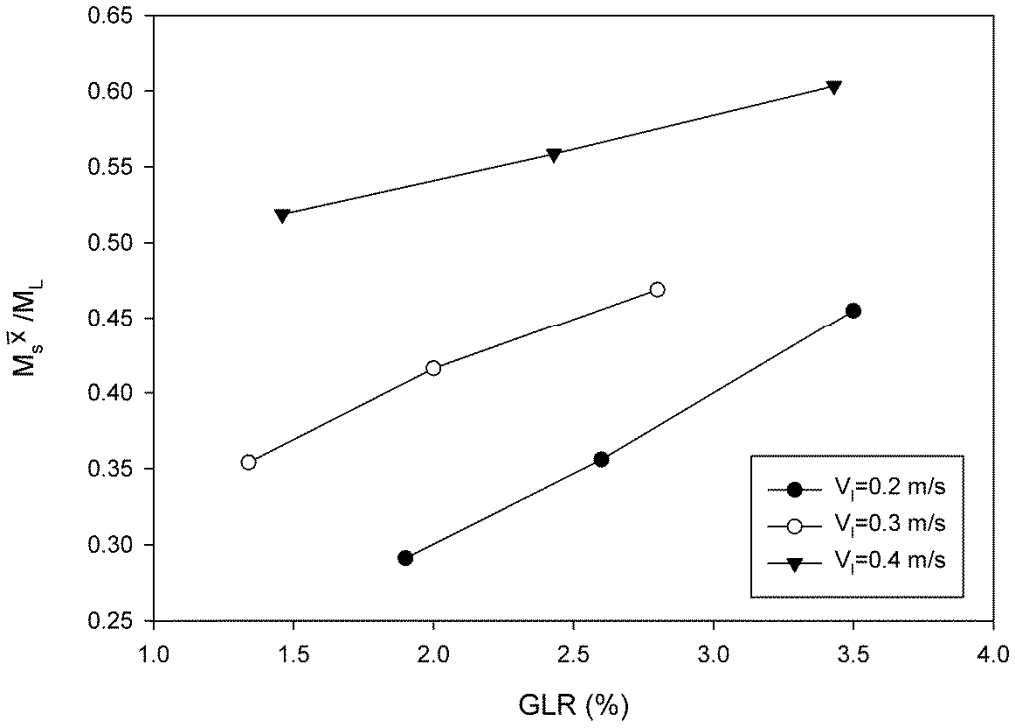

Figure 2.14. Fraction of total bed moisture that is free moisture during defluidization at different GLRs and different V_I

To confirm this result, two long period experiments were performed. The GLR was 2.6% and the fluidization velocity during injection was either 0.2 or 0.4 m/s. A short time after injection, the bed was defluidized for a long time and the capacitance was converted to free moisture using the calibration curves. Figure 2.15 shows the fraction of moisture that is free moisture during defluidization versus time for these two experiments. The free moisture is increasing over time in both experiments because of the diffusion of water out of the agglomerates and through the bed solids. It shows that at the higher fluidization velocity (0.4 m/s) and after about 10 hours the fraction of total bed moisture which is free moisture reached its steady state value which is about 0.69. However, at 0.2 m/s, it took about 32 hours to reach a nearly steady value of about 0.47. This indicates that a lower

fluidization velocity during injection not only reduces the initial free moisture but also produces larger agglomerates from which water diffuses more slowly when the bed is defluidized.

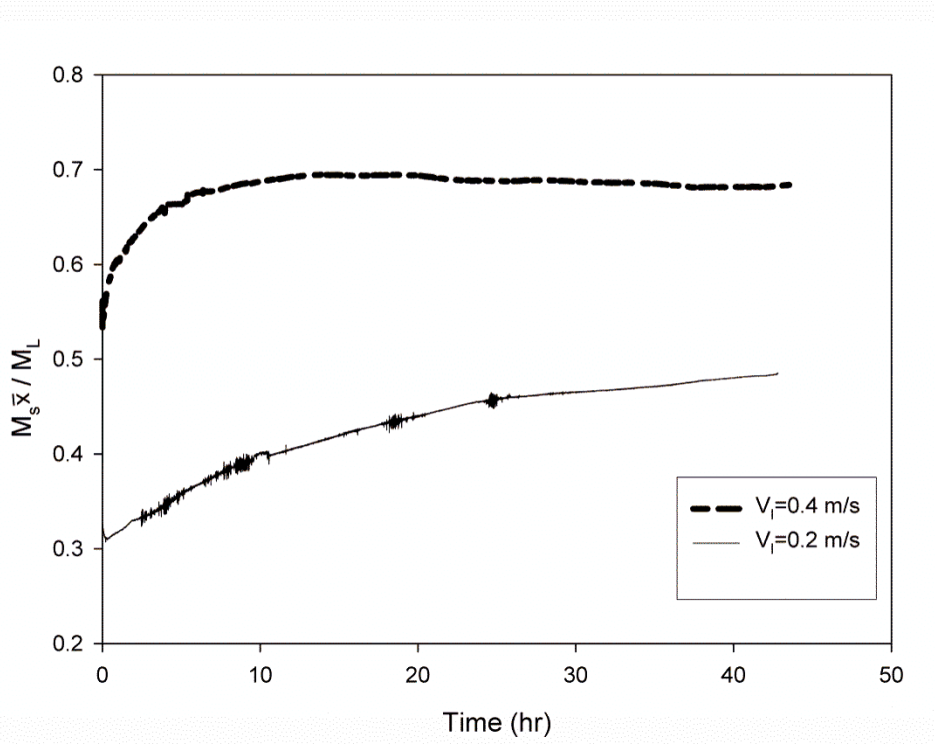

Figure 2.15. Fraction of total bed moisture that is free moisture versus time during defluidization for different fluidization velocities during injection

2.4.2 Effect of fluidization velocity during refluidization

In order to study the effect of the fluidization velocity when the bed is refluidized, some experiments were done at the same fluidization velocity during injection and at different fluidization velocities during refluidization. Table 2.2 shows the operating conditions for these experiments. The experiments were repeated for the same conditions two times.

Table 2.2. Experimental Conditions for experiments with different fluidization velocities during refluidization

Experiment	Velocity During Injection (m/s)	Velocity During Refluidization (m/s)	Total Water Injected (g)	Atomization Gas Flowrate (g/s)	GLR (%)
Experiment-1	0.3	0.2	205	0.55	2.7
Experiment-2	0.3	0.2	183	0.28	1.5
Experiment-3	0.3	0.3	205	0.55	2.7
Experiment-4	0.3	0.3	183	0.28	1.5
Experiment-5	0.3	0.4	205	0.55	2.7
Experiment-6	0.3	0.4	183	0.28	1.5

To analyze the results of these experiments, the fraction of total bed moisture which is distributed as free moisture was plotted versus time during refluidization using the calibration curves. Figure 16 shows the results for several refluidization velocities at a constant GLR of 2.7%. The effect of refluidization velocity on the breakage of agglomerates was calculated from the total free liquid which is corrected by removing the impact of vaporization during refluidization.

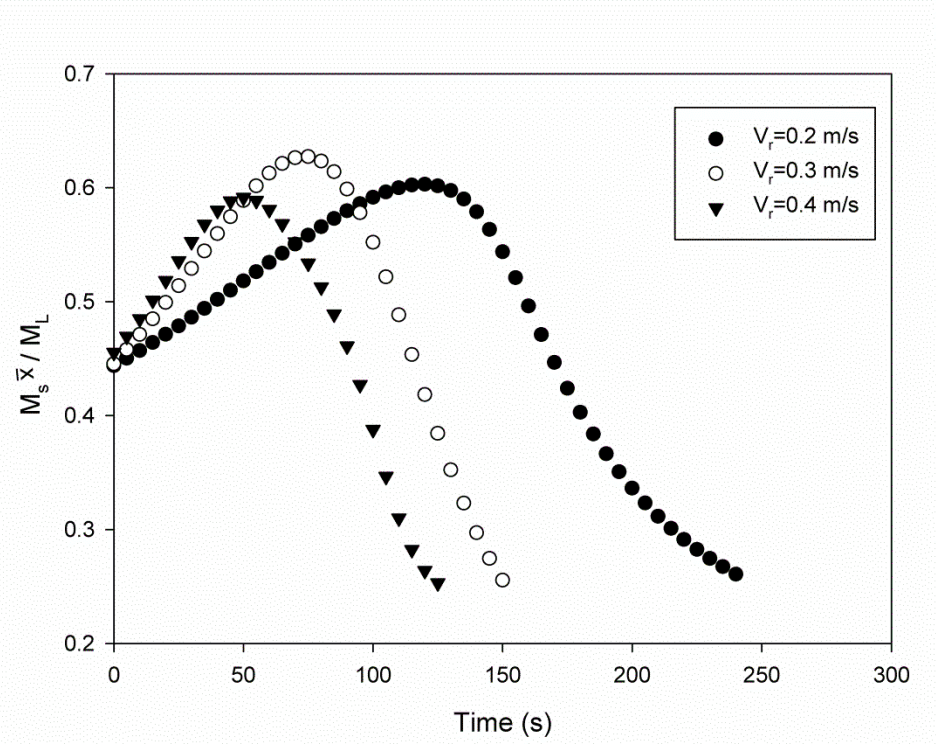

Figure 2.16. Fraction of total bed moisture that is free moisture during refluidization versus time at GLR=2.7% for several refluidization velocities

For experiments with agglomerates, the breakage rate is defined as additional free liquid resulting from agglomerate breakage.

$$(\text{breakage rate}) = \left[\frac{d(M_s\bar{x})}{dt}\right]_{br} = M_s\left(\frac{d\bar{x}}{dt}\right)_{br} \tag{2.2}$$

With regular experiments, free liquid continuously disappears through evaporation and is continuously generated from agglomerate breakage:

$$\frac{d(M_s\bar{x})}{dt} = \left[\frac{d(M_s\bar{x})}{dt}\right]_{br} + \left[\frac{d(M_s\bar{x})}{dt}\right]_{e} \tag{2.3}$$

With calibration experiments for free liquid during refluidization, there are no agglomerates and the Equation 2.2 simplifies to:

$$\left[\frac{d(M_s\bar{x})}{dt}\right]_{calibration} = \left[\frac{d(M_s\bar{x})}{dt}\right]_{e} \tag{2.4}$$

Evaporation rate is a function of gas velocity (V_g) and total mass of free liquid ($M_s\,\bar{x}$). In all the experiments in this study, Vg and Ms were kept constant, so the evaporation rate depends only on free moisture, $\bar{x}$. It can be obtained from the calibration experiments, using Equation 2.3.

$$f_e(\bar{x}) = \left[\frac{d(M_s\bar{x})}{dt}\right]_e = \left[\frac{d(M_s\bar{x})}{dt}\right]_{calibration} \tag{2.5}$$

$$f_e(\bar{x}) = M_s\left[\frac{d\bar{x}}{dt}\right]_e = M_s\left[\frac{d\bar{x}}{dt}\right]_{calibration} \tag{2.6}$$

By substituting Equation 2.5 into Equation 2.2:

$$M_s\left[\frac{d\bar{x}}{dt}\right] = M_s\left[\frac{d\bar{x}}{dt}\right]_{br} + f_e(\bar{x})$$

$$M_s\left[\frac{d\bar{x}}{dt}\right]_{br} = M_s\left[\frac{d\bar{x}}{dt}\right] - f_e(\bar{x}) \tag{2.7}$$

The total liquid freed from agglomerates is the sum of the liquid freed during the injection, i.e. the free liquid at the end of the injection period, and the cumulative liquid that has been freed from the agglomerates since the start of refluidization (t=0):

$$F(t) = M_s\bar{x}|_{t=0} + \int_0^t \left[M_s\left(\frac{d\bar{x}}{dt}\right) - f_e(\bar{x})\right] dt \tag{2.8}$$

The total liquid freed from agglomerates can also be expressed as a ratio to the total mass M_L of injected liquid:

$$G(t) = \frac{F(t)}{M_L} = \frac{M_s}{M_L}\left[\bar{x}|_{t=0} + \int_0^t \left[\left(\frac{d\bar{x}}{dt}\right) - \frac{f_e(\bar{x})}{M_s}\right] dt\right] \tag{2.9}$$

Figure 2.17 shows G(t) versus time during refluidization for several refluidization velocities, and for different GLRs. Because the effect of vaporization was eliminated, only the effect of agglomerate breakage remains. For example, Figure 2.17 indicates that, for a GLR of 2.7% and a refluidization velocity of 0.4 m/s, about 46% of the injected

liquid is free liquid and 54% is trapped within agglomerates just after the liquid injection. As the refluidization proceeds, agglomerates break up, gradually freeing more liquid until, at a time of about 75 s, all the injected liquid has been freed and there are no agglomerates left.

Figure 2.17 illustrates that agglomerates break up more quickly as the refluidization velocity is increased. Moreover, agglomerates break up more quickly, at the same refluidization velocity, when the spray nozzle GLR is increased.

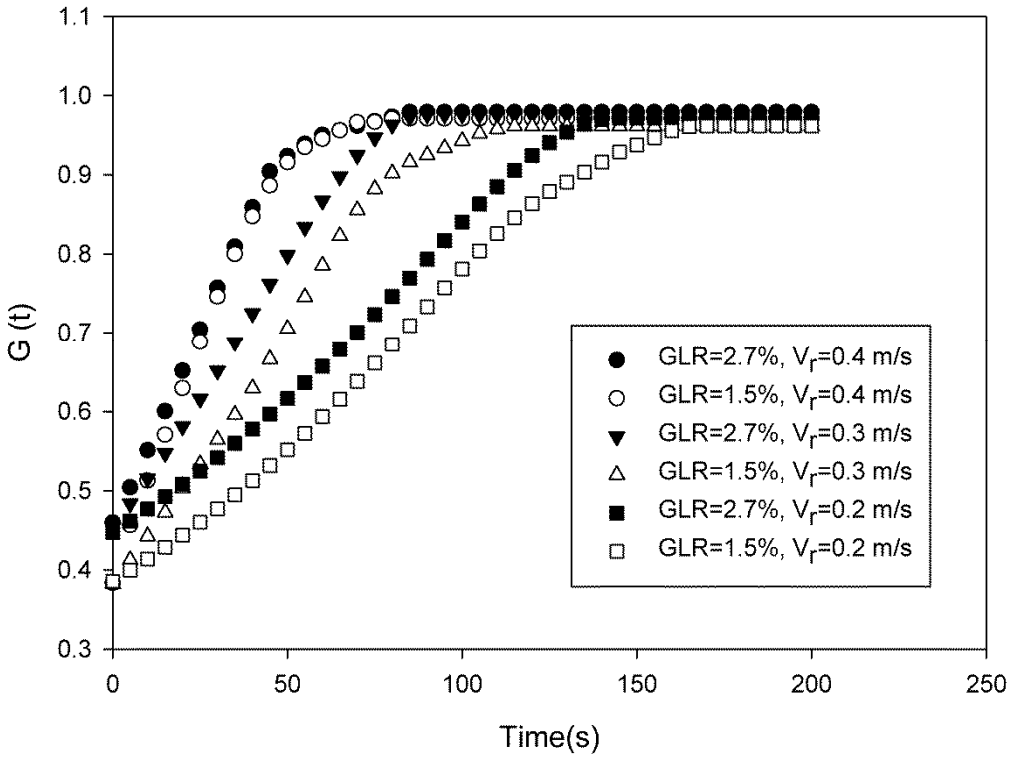

Figure 2.17. The ratio of total liquid freed from agglomerates to total mass of injected water during refluidization for several refluidization velocities and GLRs

2.5 Conclusions

A capacitance method has been developed to determine how liquid injected in a fluidized bed is distributed on particles. It is accurate, rapid, non-invasive, low cost and provides fundamental information.

In this study, the capacitance of a gas-solid fluidized bed was measured at different locations during liquid injection, defluidization and refluidization. With appropriate calibration experiments, provided free moisture, i.e. the liquid distributed on individual particles, could be obtained from capacitance measurements. The evolution of the free moisture with time, during refluidization, provided information on the break-up rate of the liquid-solid agglomerates that were formed during the injection.

The contact between atomized liquid and fluidized particles can be improved by increasing the Gas-to-Liquid Mass Ratio of the spray nozzle or the fluidization velocity during liquid injection. Increasing the fluidization velocity after the liquid injection enhances the break-up rate of the agglomerates.

References

Ariyapadi, S., D. Holdsworth, C. Norley, F. Berruti and C. Briens. 2003. "Digital X-Ray Imaging Technique to Study the Horizontal Injection of Gas-Liquid Jets into Fluidized Beds." *International Journal of Chemical Reactor Engineering* 1 (A56).

Base, T. B., E. W. Chan, R. D. Kennett and D. A. Emberley. 1999. "Nozzle for Atomizing Liquid in Two Phase Flow.".

Bruhns, S. and J. Werther. 2005. "An Investigation of the Mechanism of Liquid Injection into Fluidized Beds." *AICHE Journal* 51(3):766-775.

Darabi, P., K. Pougatch, M. Salcudean and D. Grecov. 2010. "Agglomeration of Bitumen-Coated Coke Particles in Fluid Cokers." *International Journal of Chemical Reactor Engineering* 8.

Department of Physics and Astronomy. "Dielectric Constant at 20 ^{o}C. Department of Physics and Astronomy, Georgia State University.". (http://hyperphysics.phy-astr.gsu.edu.).

Fan, L. -., R. Lau, C. Zhu, K. Vuong, W. Warsito, X. Wang and G. Liu. 2001. "Evaporative Liquid Jets in Gas-Liquid-Solid Flow System." *Chemical Engineering Science* 56(21-22):5871-5891.

Farkhondehkavaki, M. 2012. "Developing Novel Methods to Characterize Liquid Dispersion [Dissertation]." Western University, London (ON), .

Gehrke, S. and K. Wirth. 2008. "Liquid Feed Injection in a High-Density Riser." 31(11):1701.

House, P. K., C. L. Briens, F. Berruti and E. Chan. 2008. "Effect of Spray Nozzle Design on Liquid-Solid Contact in Fluidized Beds." *Powder Technology* 186(1):89-98.

House, P. K., M. Saberian, C. L. Briens, F. Berruti and E. Chan. 2004. "Injection of a Liquid Spray into a Fluidized Bed: Particle-Liquid Mixing and Impact on Fluid Coker Yields." *Industrial and Engineering Chemistry Research* 43(18):5663-5669.

Knapper, B. A., M. R. Gray, E. W. Chan and R. Mikula. 2003. "Measurement of Efficiency of Distribution of Liquid Feed in a Gas-Solid Fluidized Bed Reactor." *International Journal of Chemical Reactor Engineering* 1 (A35).

Leach, A., F. Portoghese, C. Briens and F. Berruti. 2008. "A New and Rapid Method for the Evaluation of the Liquid-Solid Contact Resulting from Liquid Injection into a Fluidized Bed." 184(1):44.

Leach, A., G. Chaplin, C. Briens and F. Berruti. 2009. "Comparison of the Performance of Liquid-Gas Injection Nozzles in a Gas-Solid Fluidized Bed." *Chemical Engineering and Processing: Process Intensification* 48(3):780-788.

McMillan, J., D. Zhou, S. Ariyapadi, C. Briens, F. Berruti and E. Chan. 2005. "Characterization of the Contact between Liquid Spray Droplets and Particles in a Fluidized Bed." *Industrial and Engineering Chemistry Research* 44(14):4931-4939.

McCracken, T., A. Bennett, K. Jonasson, D. Kirpalani, Z. Tafreshi, T. Base, I. Base, D. Emberley, R. Kennett, D. Bulbuc and E. Chan. 2006. "*Mixing Arrangement for Atomizing Nozzle in Multi-Phase Flow*.".

Portoghese, F., F. Berruti, C. Briens and E. Chan. 2007. "Novel Triboelectric Method for Characterizing the Performance of Nozzles Injecting Gas-Atomized Liquid into a Fluidized Bed." *Chemical Engineering and Processing: Process Intensification* 46(10):924-934.

Portoghese, F., L. Ferrante, F. Berruti, C. Briens and E. Chan. 2008a. "Effect of Injection-Nozzle Operating Parameters on the Interaction between a Gas-Liquid Jet and a Gas-Solid Fluidized Bed." *Powder Technology* 184(1):1-10.

Portoghese, F., L. Ferrante, F. Berruti, C. Briens and E. Chan. 2008b. "Effect of Injection-Nozzle Operating Parameters on the Interaction between a Gas-Liquid Jet and a Gas-Solid Fluidized Bed." *Powder Technology* 184(1):1-10.

Yang, WQ. 1996. "Hardware Design of Electrical Capacitance Tomography Systems." 7:225.

Chapter 3

3. THE EFFECTS OF LIQUID PROPERTIES AND BED HYDRODYNAMICS ON THE DISTRIBUTION OF LIQUID ON SOLID FLUIDIZED PARTICLES IN A COLD-MODEL FLUIDIZED BED

3.1 Abstract

Uniform distribution of liquid feed on fluidized particles increases the yield of valuable products and improves operability in processes such as Fluid Coking™ and Fluid Catalytic Cracking. Contact between the injected liquid and the bed particles can be greatly affected by the liquid properties and local bed hydrodynamics. In this study, the effect of liquid viscosity, liquid surface tension, liquid contact angle with solid particles, fluidization velocity and atomization gas flowrate on the distribution of liquid sprayed into a fluidized bed was investigated with a reliable and fast response capacitance meter. This method was also extended to monitor the agglomerate breakup kinetics.

3.2 Introduction

In Fluid Coking™, heavy oil is injected with gas-atomization nozzles into solid-gas fluidized beds of hot coke particles, where it thermally cracks. Improving the contact between injected liquid and fluidized particles boosts the yields of valuable liquid products in these reactors by minimizing the formation of agglomerates (House et al. 2004; Mohagheghi et al. 2013a) that cause detrimental heat and mass transfer limitations. Several publications reported that liquid injected into a gas-solid fluidized bed with spray nozzles is present in 2 forms: liquid forming a thin layer around individual particles, or "free liquid", and liquid trapped within "agglomerates" (Ariyapadi et al. 2003; Bruhns and Werther 2005; Knapper et al. 2003). In the Fluid Coking™ process, it is essential to increase the free liquid, i.e. the proportion of injected liquid that is not trapped within liquid-solid agglomerates. It is also preferable that the liquid trapped within agglomerates be freed rapidly through agglomerate breakup, before it can have a detrimental effect on the process. Bruhns and Werther (2005) and Knapper et al. (2003) showed that agglomerates form near the tip of jet cavity of the spray. Knapper et al. (2003) also

studied the impact of spray nozzle performance on the quality of interaction between the gas-liquid jet and fluidized bed particles. Portoghese et al. (2008) found that the distribution of liquid injected into a fluidized bed can be improved by increasing the atomization gas flowrate, decreasing the liquid mass flow rate, and reducing the size of the gas-atomization nozzle. Leach et al. (2009) showed that the liquid distribution greatly depends on the nozzle type and geometry.

Literature studies have identified the liquid properties that affect the distribution of liquid on solid particles, and agglomerate formation in the granulation process: viscosity, surface tension, and contact angle. Tardos et al. (1997) showed that to agglomerate particles through granulation requires a minimum amount of binder that is a key characteristic of the particles/binder combination. The author presented a special procedure to select an adequate binder for granulation based on binder surface wetting and spreading, binder strengthening and bridge strength. Simons and Fairbrother (2000) showed that the energy needed to rupture a liquid bridge increases when binder surface tension increases or contact angle is decreased. Iveson et al. (1998) found that, with porous particles, although decreasing the contact angle of the binder results in better wetting, successful granulation growth then requires higher degrees of liquid saturation due to the increased flow of binder liquid into pores. Iveson et al. (1998) found that the impact of the viscosity and surface tension of the binder on the strength of partially saturated powder compacts depends on the range of strain rates to which they are exposed in the granulator bed; this implies that any experimental study should be performed at realistic fluidization velocities. In granulation studies, however, the objective is to incorporate most of the bed solids into agglomerates while, in the Fluid Coking™ process, the goal is to eliminate agglomerates.

Three studies focused on conditions that are more relevant to the Fluid Coking™ process. McLaughlin and Rhodes (2001) studied the effect of liquid viscosity and surface tension on the fluidized bed behavior and presented a map which shows the transition in Geldart's powder group behavior for different liquid concentrations and viscosities. McDougall et al. (2005) showed that the impact of the injected liquid on bed fluidity and agglomeration depends on the liquid viscosity and the particle-liquid contact angle. These

authors presented a map that shows the combined effects of viscosity of the liquid and contact angle on whether various wetted particles will agglomerate in a fluidized bed. Morales (2013) assumed that agglomeration occurs in three stages: 1) initial distribution of liquid on entrained solid particles to the jet cavity, 2) wetting and spreading of liquid among solid particles in the jet cavity and 3) breakup of agglomerates in the fluidized bed. According to Morales (2013), lowering the liquid viscosity or using a more effective spray nozzle provides a spray with smaller liquid droplets, which improves the initial distribution of liquid on solid particles (stage 1), resulting in fewer agglomerates. Stage 2, the wetting and spreading stage, could be improved by decreasing the contact angle to spread the liquid over a larger particle surface, which results in more agglomerates (Morales 2013). Stage 3, the agglomerates breakup, could be enhanced by increasing the fluidization velocity as higher shear forces act on agglomerates (Morales 2013).

An earlier study showed that both the initial amount of free liquid and the breakup rate of wet agglomerates could be accurately determined in a fluidized bed with capacitance probes (Mohagheghi et al. 2013b). These experiments were, however, conducted with water and sand, and their relevance to the Fluid Coking™ process may be questioned.

The first objective of this study was to determine how liquid properties affect the distribution of a liquid on fluidized particles and, thus, identify an appropriate experimental model for the Fluid Coking™ process. The second objective was to use this experimental model to study the impact of atomization and fluidization gas flowrates on the distribution of liquid injected into a fluidized bed.

3.3 Experimental

3.3.1 Experimental Setup

The experiments were carried out in a fluidized bed with a height of 1.97 m and a rectangular cross section of 1.54 m by 0.288 m (Figure 3.1a). The fluidization velocity was set and controlled with two banks of calibrated sonic orifices and pressure regulators. Three rectangular wooden windows were mounted on each side of the bed walls, to allow for capacitance measurements (Figure 3.1a).

For most of the experiments, a scaled-down version of an industrial spray nozzle (Base et al. 1999) with an internal diameter of 2.2 mm was used for the liquid injection. Liquid was mixed with atomization nitrogen gas in a pre-mixer upstream of the spray nozzle (McCracken et al. 2006). The flow rate of the atomization gas was set and controlled with a calibrated sonic orifice and a pressure regulator (Figure 3.1a). The mass ratio of atomization gas to liquid (also defined as Gas-to-Liquid Ratio, or GLR) ranged from 0 to 3 wt%. The injection time was 10 s with a liquid flowrate of 55 g/s.

A different spray nozzle called "ideal nozzle" in this study was used for calibration experiments (Mohagheghi et al. 2013b). It was operated at a mass ratio of atomization gas to liquid of over 50 wt%. This ratio was much higher than for regular experiments (1 to 3 wt%) and provided an excellent liquid distribution on the fluidized particles, thus preventing agglomerate formation. A large GLR (e.g. 50 wt%) gives a very fine droplet size distribution, which results in the formation of thin liquid films on particles, whereas a low ratio (e.g. 1 to 3 wt%) produces a smaller number of relatively large droplets, which poorly distributes the liquid between particles, thus leading to localized coalescence and agglomeration of the over-wet particles, and leaving the rest relatively dry. This "ideal nozzle" consisted of a straight cylindrical tube, 3.6 mm in diameter.

To ensure relevant results, the bed particles were fluid coke extracted from an industrial Fluid Coker with negligible porosity (Furmisky 2000). For all the experiments, 430 kg of coke particles with a Sauter mean diameter of 140 μm that was measured by a HELOS particle size analyzer and a particle density of 1470 kg/m^3 were used. The density was measured by the liquid pycnometry technique. The bed height was approximately 1.2 m when the fluidization superficial velocity was 0.3 m/s. The bed pressure was measured with transducers installed at different locations on the bed wall. The bed height and mass were calculated from pressure measurements. Two thermocouples were used to measure the temperature in the bed and in the freeboard.

a)

1) Bank of sonic nozzles
2) Fluidized bed
3) Spray nozzle
4) Differential pressure transducer
5) Sonic nozzle for flow control
6) Ball valve
7) Gas distributor
8) Liquid tank
9) Pressure regulator
10) wood window
11) Electrodes
12) Premixer
13) Thermocouple
14) Pressure transducer

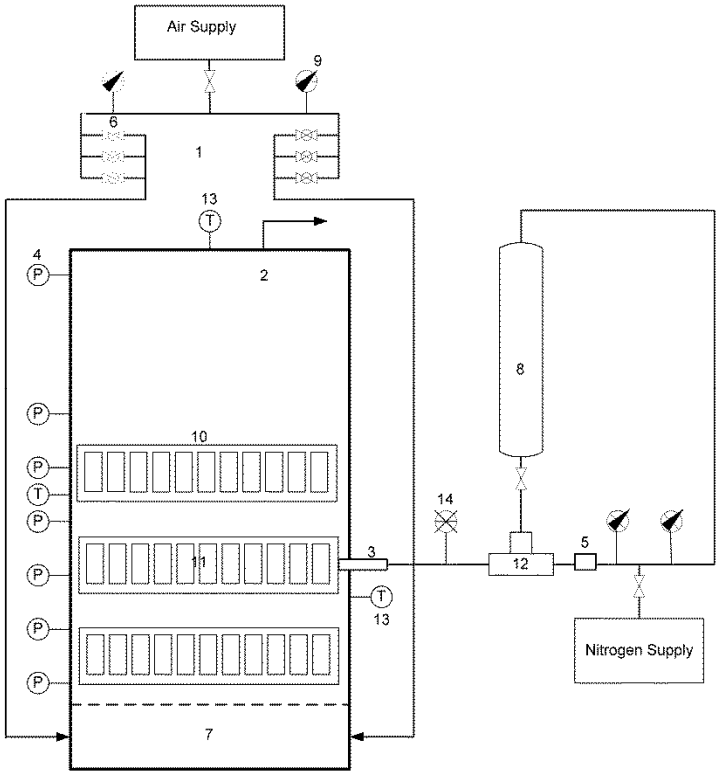

b)

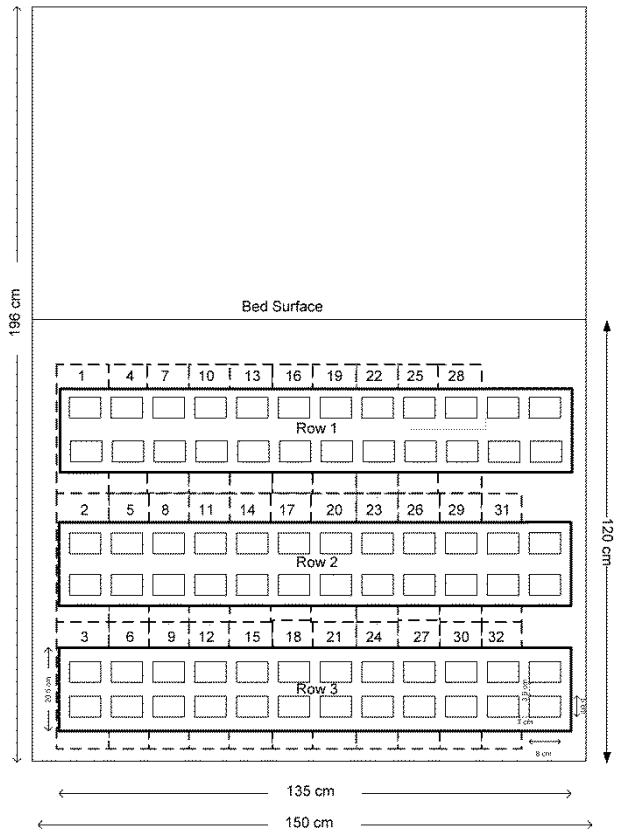

Figure 3.1. a) Schematic diagram of the experimental setup; b) Position of electrodes on the wooden windows of fluidized bed setup

3.3.2 Measuring methods

In this study, the properties of liquid mixtures were measured experimentally. An Ubbelohde capillary viscometer, the Washburn method (Galet, Patry, and Dodds 2010) and the Pendant Drop test (Stauffer 1965) were used to measure viscosity, contact angle and surface tension, respectively. Varsol^{TM} was considered as the reference liquid for the Washburn method for the coke particles as it wets coke perfectly (McDougall et al. 2005). The density and vapor pressure of Varsol^{TM} at room temperature are 0.785 g/cm^3 and 0.2 kPa respectively (U.S. National Library of Medicine). Table 3.1 shows the other properties of Varsol^{TM}.

The distribution of liquid on coke particles was measured using capacitance sensors. To find the sensitivity of capacitance sensors to liquid trapped in agglomerates, some

experiments were carried out in a small box of coke particles, with flat metal electrodes on two opposing walls (Mohagheghi et al. 2013b). In these experiments, liquid could either be spread evenly on the solid particles with intense mechanical agitation or dripped as large drops at various locations on the powder surface, forming large agglomerates. The results of these experiments confirmed that the normalized capacitance of a wet bed is a linear function of the free liquid volume fraction and is not affected significantly by the presence of liquid trapped within agglomerates.

Varsol^{TM} was used as liquid feed for the injections in the fluidized bed. The key advantage of using Varsol^{TM} as the liquid is that its relative permittivity (dielectric constant) of 3 can be detected with high contrast when mixed with coke particles, which have a relative permittivity of 7 (U.S. National Library of Medicine). The relative permittivity of coke that was used in this study was calculated based on comparing the measured capacitance of air and coke in a small box (the relative permittivity of air is 1 (Department of Physics and Astronomy, Georgia State University).

Thirty-two 8 cm × 10 cm electrodes were installed on the inside of three wooden windows to measure the local bed capacitance (Figure 3.1b). Three 135 cm × 20 cm electrodes were also located on the opposing wall of each window. The measuring circuit was an AC based capacitance meter with a differential noise cancelling system and a sampling frequency of 11.5 Hz for each electrode. Figure 3.2 shows a general diagram of the capacitance circuit and more details are provided in (Yang 1996).

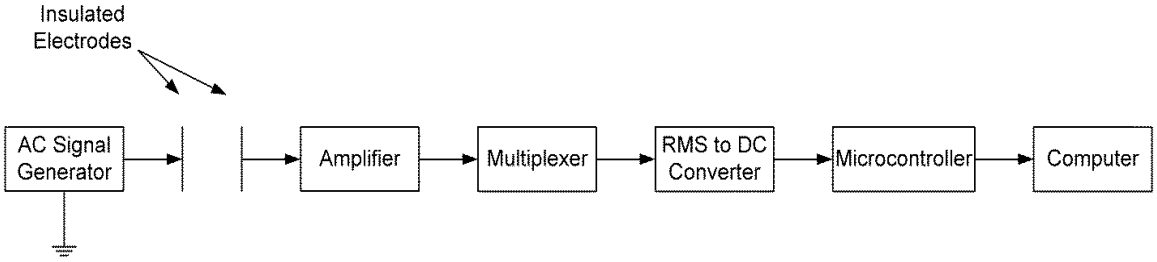

Figure 3.2. Block diagram of capacitance circuit

3.3.3 Calibration Experiments

In the calibration experiments, the amount of free liquid was varied by changing the amount of liquid injected with the "ideal nozzle", which did not form any agglomerates (Mohagheghi et al. 2013b). The calibration experiments allowed for the measurement of the capacitance with each electrode for various amounts of free liquid. Figures 3.3a and 3.3b show examples of the calibrations curves for two electrodes. Each electrode had a different calibration curve because of the non-uniform distribution of the electric field at different locations that results from the metallic structure of the bed. All electrodes gave linear calibration curves similar to the examples of Figures 3.3a and 3.3b. The experiments were repeated for the same conditions three times. The reproducibility of calibration experiments is shown in Appendix A for two electrodes.

For the actual experiments with the regular spray nozzle, the local free liquid content was calculated from the capacitance measured by each electrode using calibration curves, and then these values averaged to get the bed-averaged free liquid.

a)

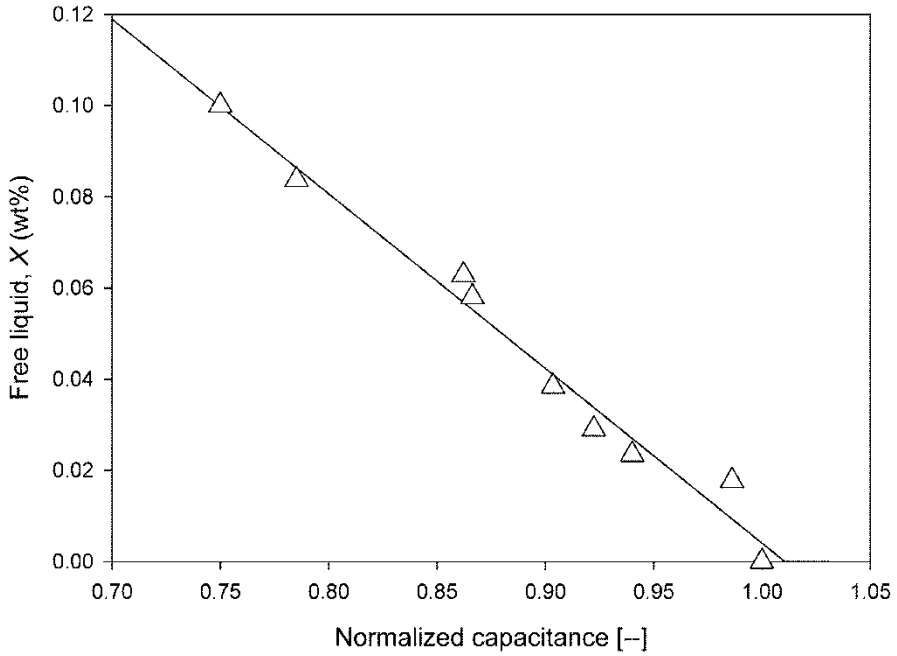

b)

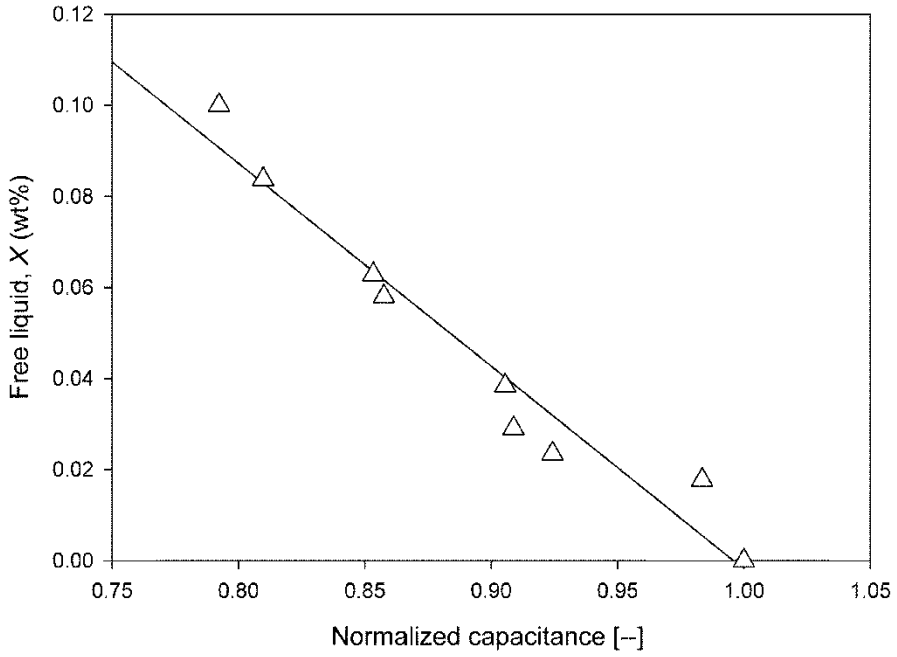

Figure 3.3. a) Calibration curve for electrode 15 (with Varsol^{TM} liquid); b) Calibration curve for electrode 2 (with Varsol^{TM} liquid)

3.4 Results and Discussion

3.4.1 Liquid Properties

To investigate the effect of liquid properties, binary mixtures of alcohol and water classified as Group A, binary mixtures of alcohol (e.g. tert-Butanol and isobutanol) classified as Group B, and pure components classified as Group C were prepared as shown in Table 3.1. The properties of these mixtures were determined experimentally using methods described in Section 3.3.2. McDougall et al. (2005) showed how to predict whether particles initially wetted with well-distributed liquid will agglomerate in a fluidized bed. According to McDougall et al. (2005), Varsol^{TM} does not promote agglomeration and all the other mixtures promote agglomeration in a fluidized bed. McDougall et al. (2005) also predicted that bitumen, under Fluid Coking conditions, would not promote agglomeration in a fluidized bed of coke particles. Experiments were performed to determine the minimum liquid content required to create a sufficient change

in powder cohesivity that can be detected by the capacitance sensor which has been used in this study. The detectable change in powder cohesivity was measured with an avalanche machine (Rev 2007 Revolution Powder Analyzer). This machine characterizes the cohesivity of a powder from its avalanche characteristics, such as avalanche time or avalanche energy. It can also determine the bulk density of the aerated powder in the avalanche machine. Coke particles were thoroughly mechanically mixed with each liquid before they were introduced in the avalanche machine to ensure that all the liquid was in the form of free liquid. A moisture balance was used to determine the liquid content in each sample. The evolution of avalanche parameters during the avalanche measurements also showed that for the presented mixtures, except Varsol™, the wetted particles form agglomerates in the fluidized bed, as predicted (McDougall et al. 2005). Preliminarily tests demonstrated that the sensitivity of the avalanche machine and capacitance sensors to the change in powder cohesivity is qualitatively similar in all cases as illustrated, as an example, for the case of liquid mixture B1 in Figure 3.4. This figure shows that the capacitance and avalanche time gave about the same minimum detectable liquid content.

Table 3.1. Binary mixtures of liquid feed and their properties

Mixture	Liquid Mixtures	Mass fraction (wt%)	Viscosity (mPa·s)	Contact angle (^{0})	Surface Tension (mN/m)
A1	Water	75	2.8	64	24.7
	Tert-Butanol	25			
A2	Water	50	4.6	70	22.9
	Tert-Butanol	50			
A3	Water	25	5.2	70	22.9
	Tert-Butanol	75			
A4	Water	95	1.09	67	42
	Tert-Butanol	5			
B1	Tert-Butanol	25	4.9	44	20.8
	Isobutanol	75			
B2	Tert-Butanol	50	3.9	54	22.8
	Isobutanol	50			
B3	Tert-Butanol	75	4.6	43	23.4
	Isobutanol	25			
C1	Water	100	1	75	68.0
C2	Isobutanol	100	4.2	46	23
C3	Varsol™	100	1.2	0	24.7

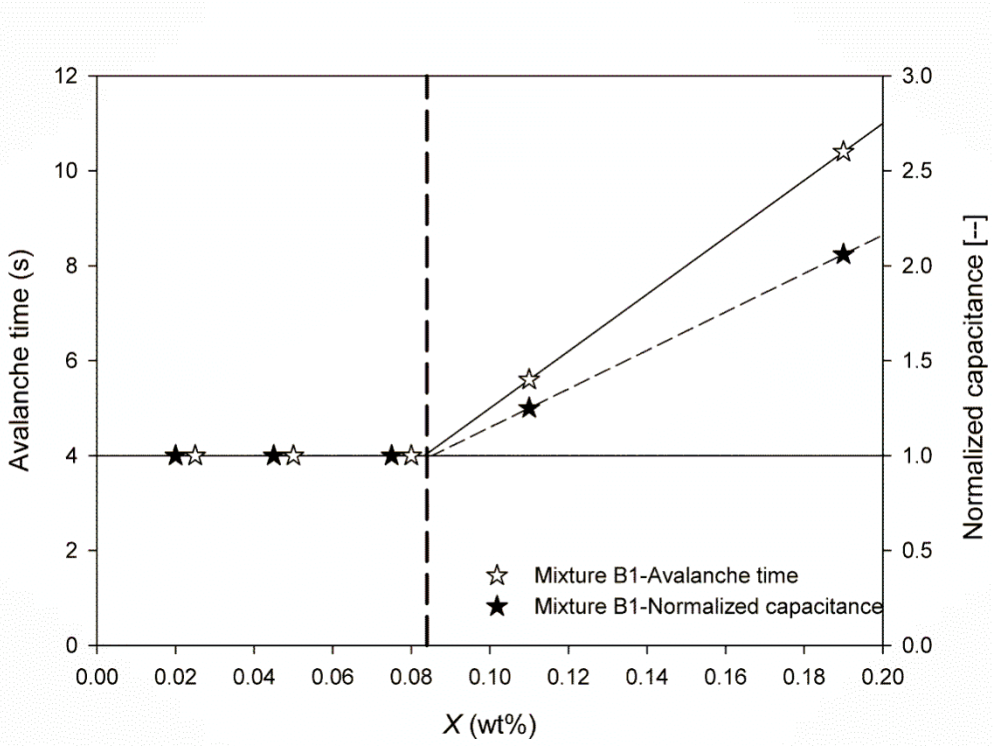

Figure 3.4. Avalanche time and normalized capacitance as functions of the liquid content for liquid mixtures B1

Figure 3.5 shows that the minimum liquid contents detectable from avalanche time, avalanche energy or bulk density (determined by the avalanche machine) are in very good agreement. It shows that the minimum detectable liquid content is related to a significant change in powder cohesivity. To find the minimum detectable liquid content for the mixtures, values obtained from the avalanche time, avalanche energy and bulk density of the powder-liquid mixture were averaged for all tested powders (Table 3.2). Note that for Varsol^{TM} (mixture C3), avalanche measurements could not be performed as particles stuck to the wall of the drum; in this case, the minimum detectable liquid content was obtained from capacitance measurements.

Table 3.2. Minimum detectable liquid content for all powder-liquid mixtures

Mixture	Liquid Mixtures	Mass fraction (wt%)	X_{min} (wt%)
A1	Water	75	0.564
	Tert-Butanol	25	
A2	Water	50	0.158
	Tert-Butanol	50	
A3	Water	25	0.244
	Tert-Butanol	75	
A4	Water	95	1.50
	Tert-Butanol	5	
B1	Tert-Butanol	25	0.084
	Isobutanol	75	
B2	Tert-Butanol	50	0.133
	Isobutanol	50	
B3	Tert-Butanol	75	0.127
	Isobutanol	25	
C1	Water	100	1.65
C2	Isobutanol	100	0.11
C3	Varsol™	100	0.018

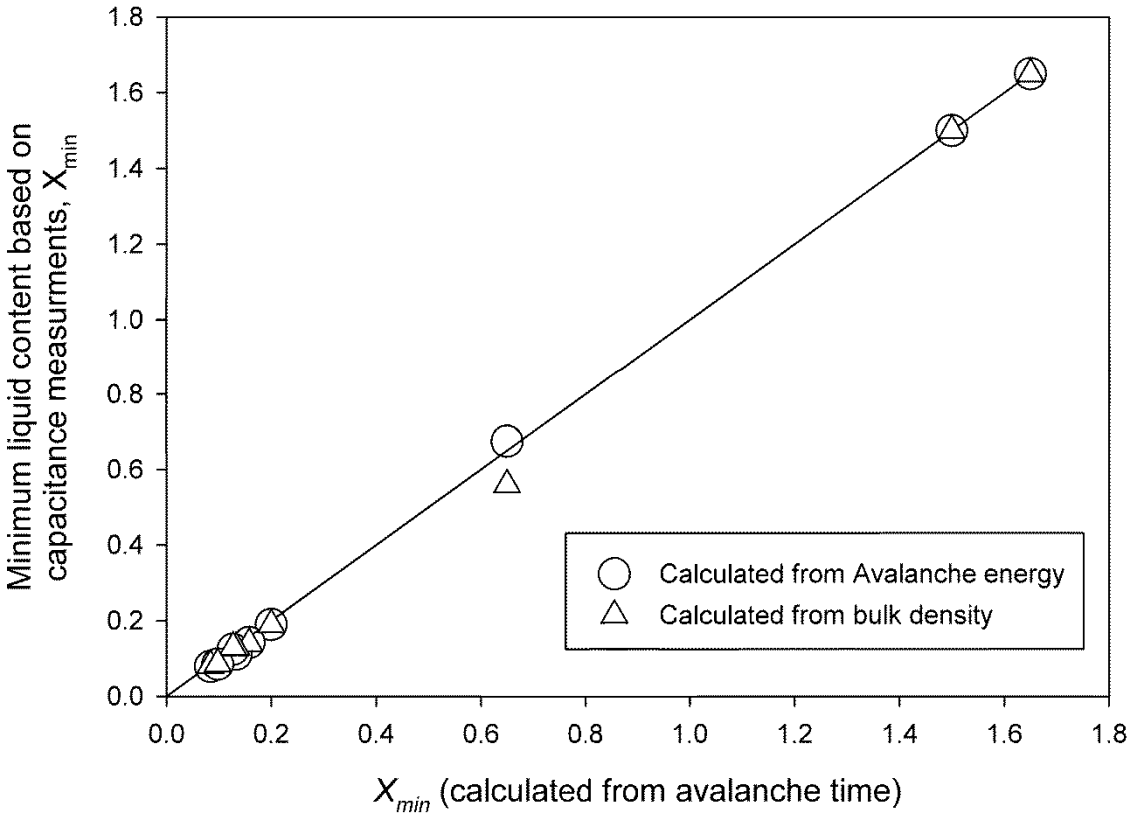

Figure 3.5. Minimum liquid contents detectable from avalanche energy and bulk density measurements vs. minimum liquid content detectable from avalanche time, for the liquid mixtures of Table 3.1

An empirical correlation between liquid properties and the minimum liquid content that causes a change in cohesivity of coke particles has been derived as:

$$X_{min} = 0.0976 \frac{(1 + sin\,\theta)^{6.88}}{\mu^{1.54}\sigma^{0.43}} \tag{3.1}$$

where μ is the viscosity in mPa·s, θ is the contact angle in degree and σ is the surface tension in unit of mN/m.

The experimental results and Equation 1 show that the contact angle of the liquid with the coke particles has the most significant impact on the minimum liquid content. Decreasing the contact angle decreases the minimum liquid content. The viscosity has also a considerable impact on the cohesiveness of solid particles as the minimum liquid content

decreases with increasing viscosity. The surface tension is the parameter which has the least impact on powder cohesivity. The statistical t-test results of the parameters used in Equation 1 also demonstrate that viscosity and contact angle are the most statistically significant parameters for the prediction of the minimum liquid content as their p-value is less than 0.05.

Therefore, Equation 3.2 shows the simplified correlation accounting only for the effects of viscosity and contact angle:

$$X_{min} = 0.0235 \frac{(1 + sin\,\theta)^{6.47}}{\mu^{1.31}} \tag{3.2}$$

Figure 3.6 compares, for all of the liquid mixtures of Table 3.1, the measured minimum liquid content with the predicted values from Equation 3.2.

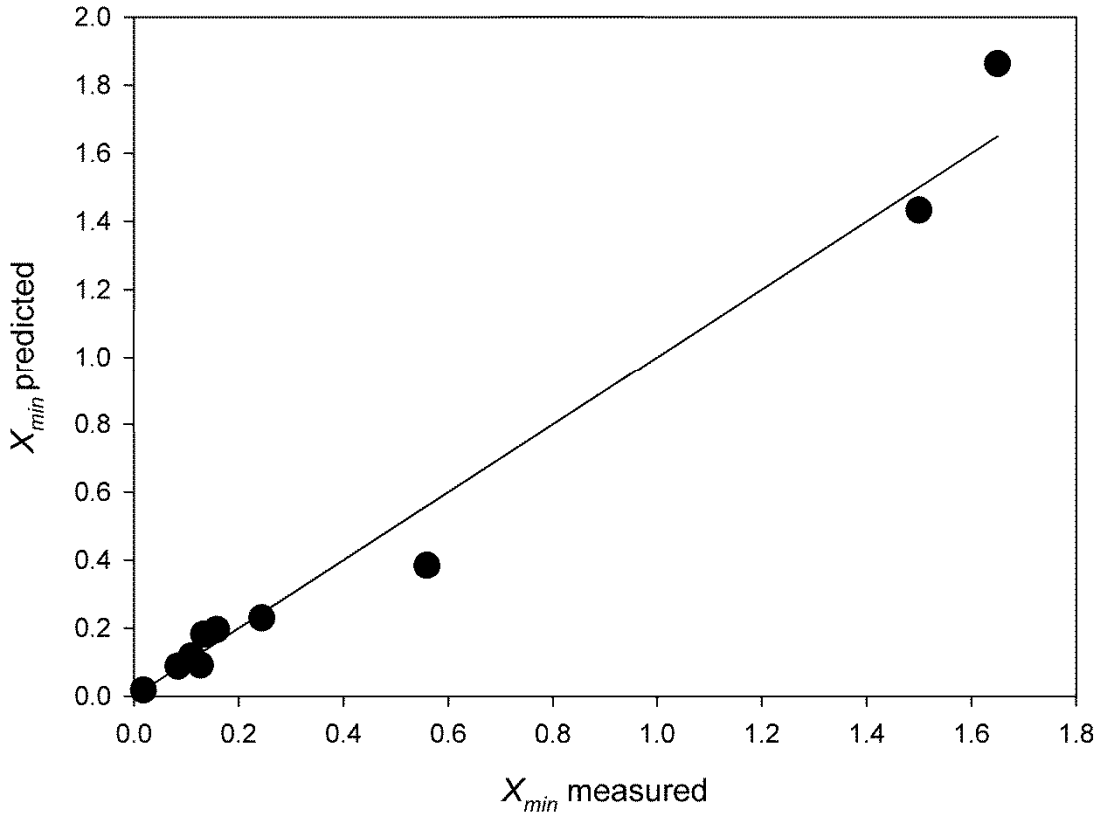

Figure 3.6. Measured minimum liquid content versus predicted value from Equation 3.2, for all the liquid mixtures of Table 3.1

To confirm the significant impact of contact angle on the cohesiveness of a mixture of solid particles and liquid, a non-wettable system (water and coke) was compared with a perfectly wettable system (Varsol^{TM} and coke) in the fluidized bed. With a ratio of injected liquid to bed solids of 0.13 wt%, no free liquid was detected for the non-wettable system under a variety of operating conditions, while a significant amount of free liquid was always detected with the wettable system. For example, Figure 3.7 shows the normalized capacitance after injection with either Varsol^{TM} or water in a cold fluidized bed of coke particles at a fluidization superficial velocity of 0.1 m/s. The "ideal nozzle" was used for injection with a Gas-to-Liquid Ratio (GLR) higher than 50 wt%. Under fluidized conditions, water or Varsol evaporated and the free liquid content therefore gradually decreased with time until the bed became completely dry. This figure illustrates no change in normalized capacitance after injecting 500 g of water, while there is a considerable change after injecting 250 g of Varsol^{TM}. Because of the high dielectric constant of water, when compared to coke and Varsol^{TM}, it should have been much easier to detect water than Varsol^{TM} with the capacitance measurement system. Therefore, it appears that water behaves completely differently from Varsol^{TM}; with water, although the fine injected liquid droplets were initially well-distributed on the bed particles, the liquid content was less than the minimum value required to create a change in powder cohesivity.

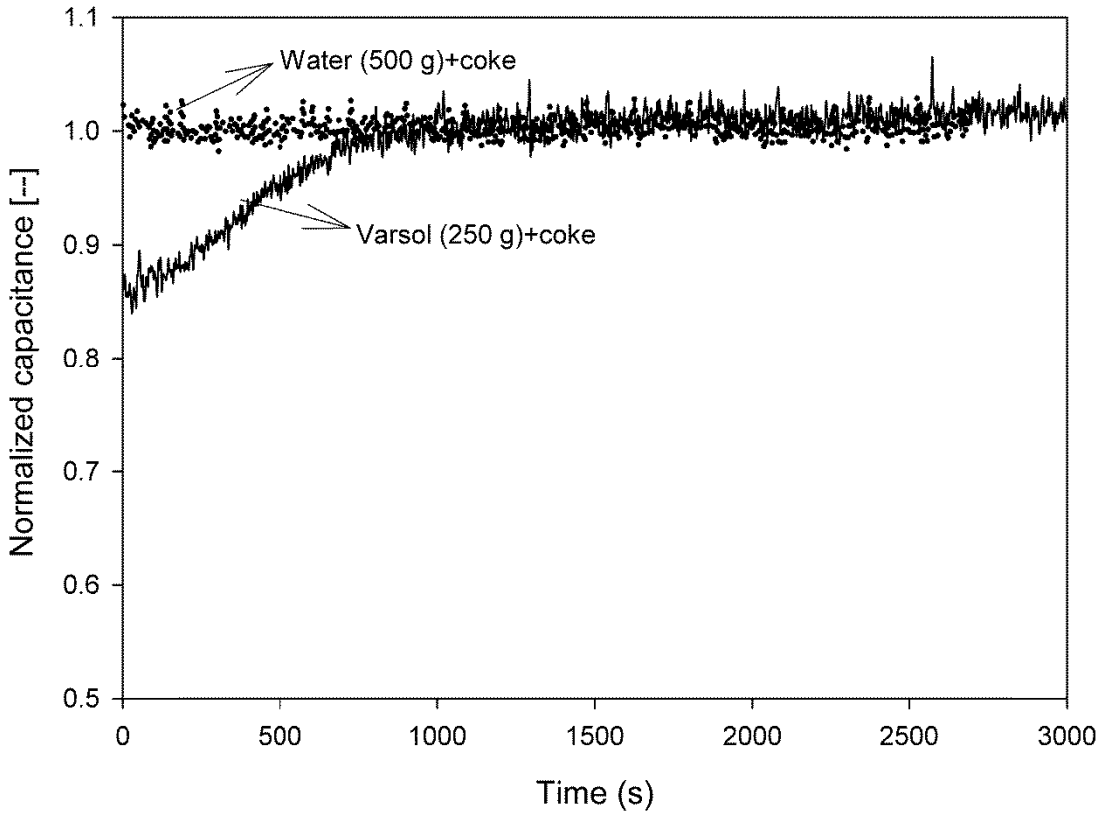

Figure 3.7. Normalized capacitance after injection for a non-wettable system (water and coke) and a perfectly wettable system (Varsol^{TM} and coke)

Based on the minimum liquid content results, mixtures B1 and B2 with viscosities of 4.9 and 3.9 mPa·s and wettabilities of 44^0 and 54^0 were selected for the injection experiments in the fluidized bed of coke particles. The 1 mPa·s difference between the viscosities of these two mixtures, within a reasonable range of liquid to solid ratios for both of them, and the similar contact angle values make them suitable for testing in the bed in order to investigate the effect of viscosity on agglomerate formation. A scaled-down version of an industrial spray nozzle (Base et al. 1999) was used for injection of liquid mixtures. The results indicate that a liquid with a higher viscosity forms more agglomerates and, consequently, result in a lower free liquid content: for example, at a fluidization superficial velocity of 0.1 m/s, a liquid to solid ratio of 0.63 wt% and GLR of 2 wt%, the free liquid after injection was 22.5 % of the injected liquid for the mixture with a viscosity of 4.9 mPa·s and 30 % for the mixture with a viscosity of 3.9 mPa·s. Since the fluidization superficial velocity and GLR is the same for both experiments and also the

contact angle on the surface of coke particles is close, the only parameter that has an effect on the agglomeration mechanism is viscosity. Viscosity affects the spray droplet size and, thus, the initial distribution of liquid on solid particles entrained into the jet cavity (Morales 2013).

3.4.2 Bed Hydrodynamics

Varsol^{TM} and coke were, therefore, selected to study the impact of the atomization gas to liquid ratio (GLR) and of the fluidization velocity on the distribution of liquid injected into a fluidized bed of coke particles. Varsol^{TM} perfectly wets the coke particles, as does the bitumen in the commercial Fluid Cokers (McDougall et al. 2005). In addition, Varsol^{TM} has a viscosity of 1.2 mPa·s at room temperature; according to Aminu et al. (2004), the initial viscosity of the heavy oil used in commercial Fluid Cokers is between 1 and 2 mPa·s. Therefore, the model system at room temperature provides a good match to the industrial conditions.

Figure 3.8a shows that the mass ratio of free liquid immediately generated after the injection increases with increasing GLR, for a fluidization superficial velocity of 0.3 m/s and liquid flowrate of 55 g/s, with a change in slope between about 1.1 and 1.7 wt% GLR. This change in slope has been shown in other studies (Farkhondehkavaki 2012). Figure 3.8b shows that the pressure measured just downstream of the premixer follows a similar trend with the GLR. This suggests that the change in slope of the variation of the free liquid mass ratio with the GLR is likely the result of a change in hydrodynamics within the nozzle, which then affects the initial liquid distribution (stage 1).

The impact of fluidization velocity during the injection (V_l) on the initial liquid distribution, and of the fluidization velocity after the injection (V_R) on the agglomerate breakup, were investigated separately for various GLRs. Table 3.3 shows the experimental conditions selected for these tests: the first series of experiments (1 to 12) was carried out by varying the fluidization velocity during the injection, while keeping a constant fluidization superficial velocity after the injection of 0.3 m/s; in the second series of experiments (13 to 20), the fluidization velocity was varied after the injection, while keeping a constant fluidization superficial velocity during the injection of 0.3 m/s.

The experiments were repeated for the same conditions three times. The reproducibility of these experiments is shown in Appendix A.

Table 3.3. Experimental conditions for different fluidization velocities during the injection (Varsol^{TM} –coke system)

Experiment No.	Fluidization velocity during injection (m/s)	Fluidization velocity after injection (m/s)	GLR (wt%)	Liquid injection rate (g/s)
1	0.2	0.3	1	55
2	0.2	0.3	1.5	55
3	0.2	0.3	2	55
4	0.2	0.3	2.5	55
5	0.3	0.3	1	55
6	0.3	0.3	1.5	55
7	0.3	0.3	2	55
8	0.3	0.3	2.5	55
9	0.4	0.3	1	55
10	0.4	0.3	1.5	55
11	0.4	0.3	2	55
12	0.4	0.3	2.5	55
13	0.3	0.2	1	55
14	0.3	0.2	1.5	55
15	0.3	0.2	2	55
16	0.3	0.2	2.5	55
17	0.3	0.4	1	55
18	0.3	0.4	1.5	55
19	0.3	0.4	2	55
20	0.3	0.4	2.5	55

a)

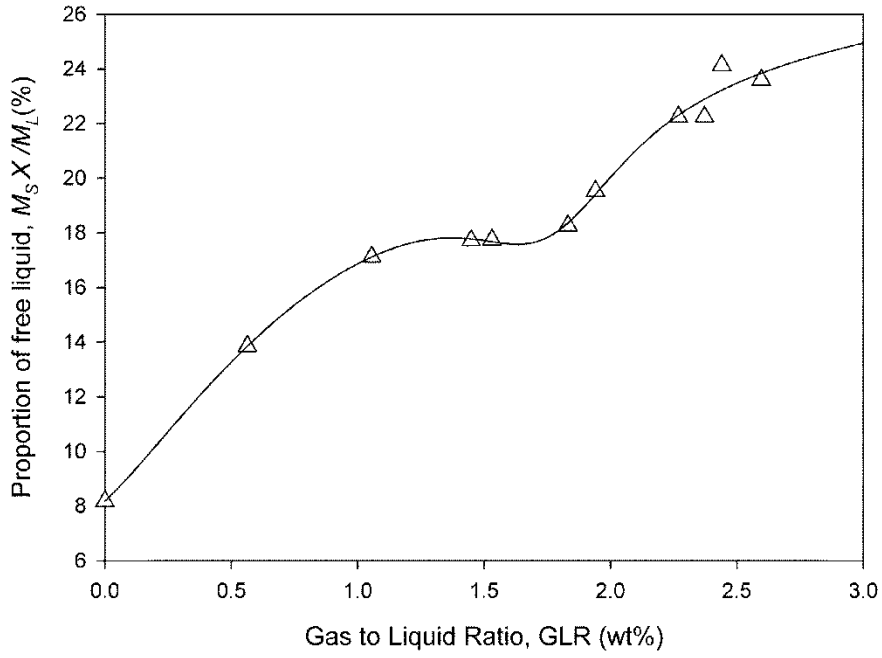
Proportion of free liquid, $M_S X / M_L$ (%)
26
24
22
20
18
16
14
12
10
8
6
0.0
0.5
1.0
1.5
2.0
2.5
3.0
Gas to Liquid Ratio, GLR (wt%)

b)

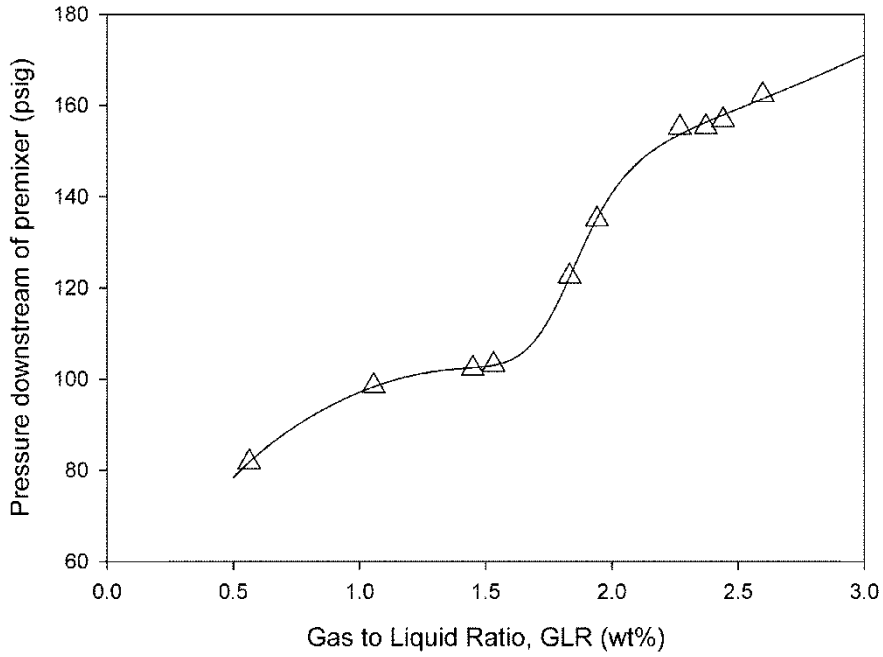

Figure 3.8. a) Percentage of total injected liquid which is free liquid after injection versus GLR for a fluidization superficial velocity of 0.3 m/s and liquid flowrate of 55 g/s; b) Pressure downstream of the premixer versus GLR for liquid flowrate of 55 g/s

Figure 3.9 shows that increasing the fluidization velocity during the injection increases substantially the amount of free liquid. Doubling the fluidization velocity during the injection roughly triples the amount of free liquid, while doubling the GLR, at best, only increases the free liquid by 50%.

To determine the effect of fluidization velocity on the breakage of agglomerates, the total amount of liquid freed from agglomerates after injection was calculated by accounting for liquid vaporization (Mohagheghi et al. 2013b). The breakage rate is the rate of liquid freed from agglomerates as they break up. The breakage and evaporation phenomena occur simultaneously. The rate of change in free liquid in the bed is the sum of the rate of liquid freed from agglomerates and of the rate of evaporation of the free liquid, as shown in Equation 3.3.

$$\frac{d(M_S X)}{dt} = \left[\frac{d(M_S X)}{dt}\right]_{br} + \left[\frac{d(M_S X)}{dt}\right]_{e} \tag{3.3}$$

In each experiment in this study, both the fluidization velocity (V_R) and mass of solid (M_S) were kept constant after injection. Under these conditions, the evaporation rate can be considered to be only a function of the free liquid. Therefore, to find the evaporation rate, the results of calibration experiments could be used, as there were no agglomerates formed in those experiments. Substituting the calibration results for the evaporation rate in Equation 3.3, we obtain:

$$M_S\left[\frac{dX}{dt}\right]_{br} = M_S\left[\frac{dX}{dt}\right] - M_S\left[\frac{dX}{dt}\right]_{cal} \tag{3.4}$$

The total free liquid is the sum of the free liquid during injection and the cumulative liquid freed from agglomerates after injection. The ratio of the total free liquid to the total mass of injected liquid (M_L) can be calculated from:

$$g(t) = \frac{f(t)}{M_L} = \frac{M_S}{M_L}\left[X|_{t=0} + \int_0^t \left[\left(\frac{dX}{dt}\right) - \left(\frac{dX}{dt}\right)_{cal}\right] dt\right] \tag{3.5}$$

$g(t)$ has been plotted as a function of time after injection for several fluidization velocities and for different GLRs. For instance, Figure 3.10 shows $g(t)$ as a function of time after injection for GLR=1 wt% and fluidization superficial velocities of 0.2 and 0.4 m/s during injection. The time constant for the agglomerate breakage (τ) was calculated based on the exponential curve fitted to these data:

$$g(t) = 1 + (g(0) - 1)e^{-t/\tau} \tag{3.6}$$

where $g(0)$ represents the value of $g(t)$ at the end of injection.

Figure 3.11 shows the time constants for agglomerate breakage at different GLRs and fluidization velocities during injection. Increasing the fluidization velocity during injection greatly reduces the time constant. The effect of the GLR on agglomerate breakage is much weaker than the effect of the fluidization velocity. Doubling the fluidization velocity during injection about halves the agglomerate breakage time constant, while doubling the GLR, at best, only reduces the time constant by 20%.

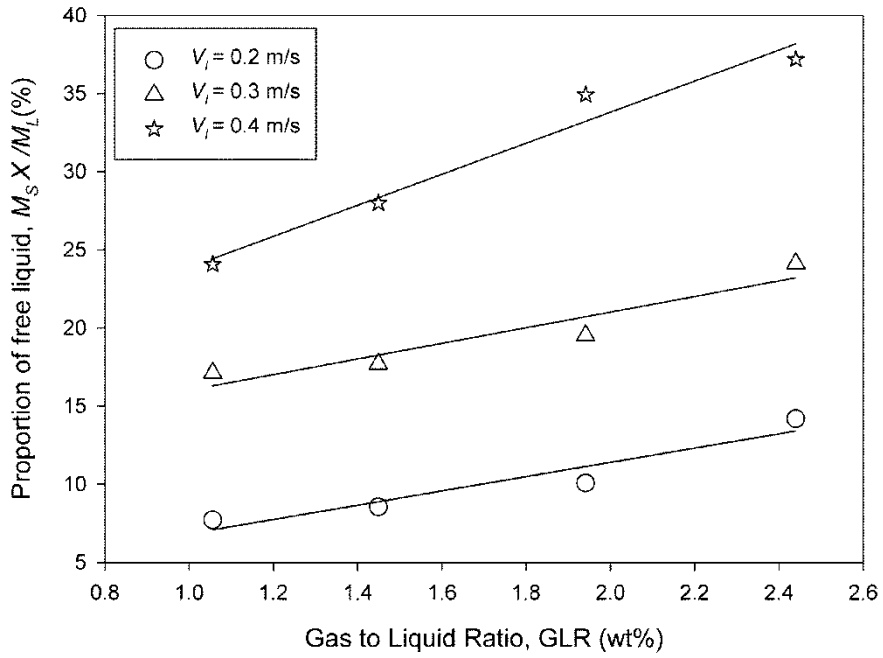

Figure 3.9. Percentage of total injected liquid which is free liquid after injection versus GLR for 3 different fluidization velocities during injection

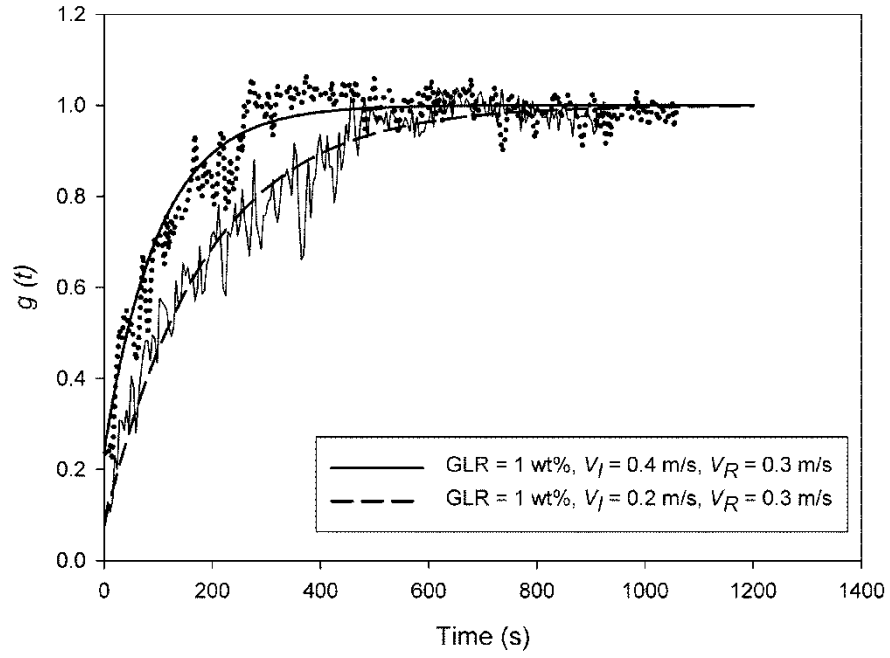

Figure 3.10. The ratio of total liquid freed from agglomerates to total mass of injected liquid after injection for several fluidization velocities during injection

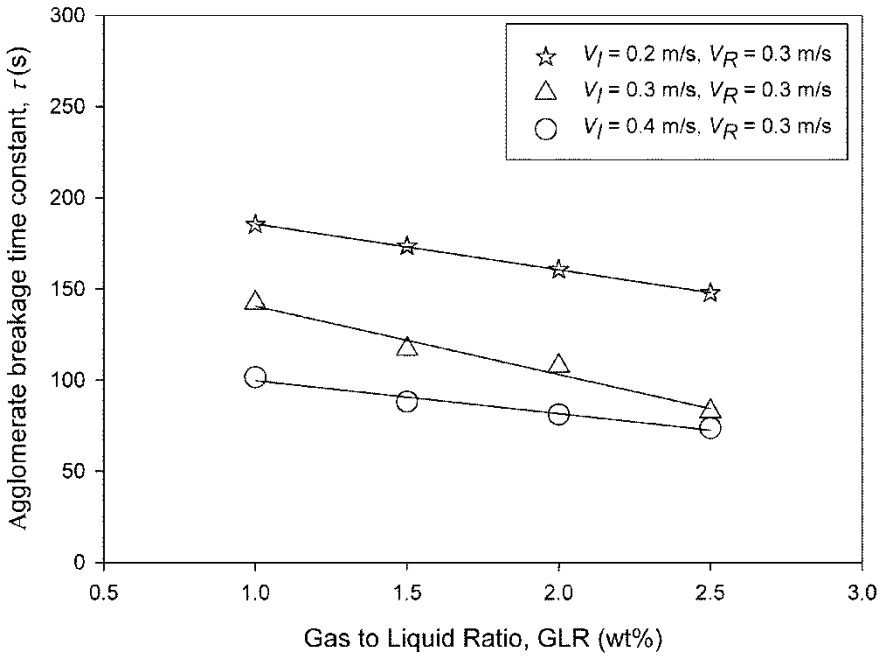

Figure 3.11. Time constant of agglomerate breakage versus GLR for three different fluidization velocities during injection

Figure 3.12 shows that the breakage rate increases with increasing fluidization velocity after injection. The fluidization velocity after injection (Figure 3.12) has a stronger impact on agglomerate breakage than the fluidization velocity during injection (Figure 3.11).

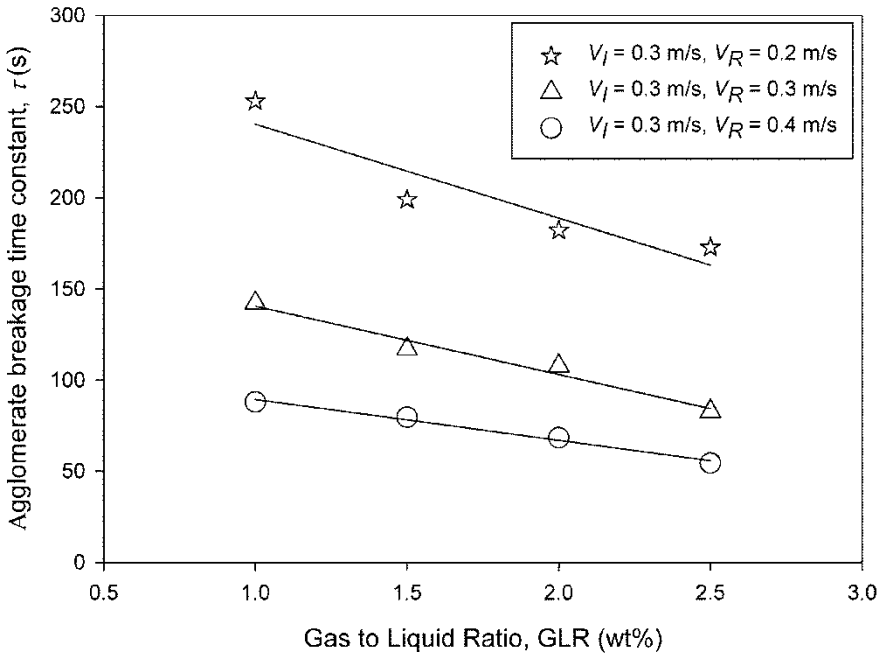

Figure 3.12. Time constant of agglomerate breakage versus GLR for three different fluidization velocities after injection

3.5 Conclusions

This study demonstrated that properties such as liquid viscosity and liquid-particle contact angle have a significant impact on the cohesiveness of wet solid particles and agglomerate formation.

This study also showed that a good simulation of liquid distribution into a fluidized bed with room temperature experiments must use a liquid whose viscosity and contact angle on the surface of solid particles are similar to the liquid used in the high temperature commercial reactors. Varsol^{TM} was selected for a cold simulation of Fluid Cokers.

Distribution of the injected liquid on the bed particles is strongly affected by bed hydrodynamics and can be improved in two manners:

- By improving the initial distribution of the liquid during injection. This can be achieved by either increasing the atomization gas flowrate or, preferably, the fluidization velocity near the spray nozzle.

- By increasing the rate of agglomerate breakage after injection. This can be achieved by increasing the fluidization velocity in the bed regions where the agglomerates move just after being formed in the spray region.

References

"U.S. National Library of Medicine.". *(http://www.webwiser.nlm.nih.gov).*

Aminu, M. O., J. A. W. Elliott, W. C. McCaffrey and M. R. Gray. 2004. "Fluid Properties at Coking Process Conditions." *Industrial and Engineering Chemistry Research* 43(12):2929-2935.

Ariyapadi, S., D. Holdsworth, C. Norley, F. Berruti and C. Briens. 2003. "Digital X-Ray Imaging Technique to Study the Horizontal Injection of Gas-Liquid Jets into Fluidized Beds." *International Journal of Chemical Reactor Engineering* 1 (A56).

Base, T., E. Chan, R. Kennett and D. Emberley. 1999. " Nozzle for Atomizing Liquid in Two Phase Flow.".

Bruhns, S. and J. Werther. 2005. "An Investigation of the Mechanism of Liquid Injection into Fluidized Beds." *AICHE Journal* 51(3):766-775.

Department of Physics and Astronomy. "Dielectric Constant at 20 ^{o}C. Department of Physics and Astronomy, Georgia State University.". (http://hyperphysics.phy-astr.gsu.edu.).

Farkhondehkavaki, M. 2012. "Developing Novel Methods to Characterize Liquid Dispersion [Dissertation]." Western University, London (ON), .

Furmisky, E. 2000. "*Charactrization of Cokes from fluid/flexi-Coking of Heavy Feeds*." 67:205.

Galet, L., S. Patry and J. Dodds. 2010. " *Determination of the Wettability of Powders by Washburn Capillary Rise Method with Bed Preparation by a Centrifugal Packing Technique*." 346(2):470.

House, P. K., M. Saberian, C. L. Briens, F. Berruti and E. Chan. 2004. "Injection of a Liquid Spray into a Fluidized Bed: Particle-Liquid Mixing and Impact on Fluid Coker Yields." *Industrial and Engineering Chemistry Research* 43(18):5663-5669.

Iveson, S. M., S. Holt, C. E. Loo Rapmond and S. R. Biggs. 1998. "The Effect of Solid Contact Angle on the Granulation of Porous Materials." 1:127.

Knapper, B. A., M. R. Gray, E. W. Chan and R. Mikula. 2003. "Measurement of Efficiency of Distribution of Liquid Feed in a Gas-Solid Fluidized Bed Reactor." *International Journal of Chemical Reactor Engineering* 1 (A35).

Leach, A., G. Chaplin, C. Briens and F. Berruti. 2009. "Comparison of the Performance of Liquid-Gas Injection Nozzles in a Gas-Solid Fluidized Bed." *Chemical Engineering and Processing: Process Intensification* 48(3):780-788.

McCracken, T., A. Bennett, K. Jonasson, D. Kirpalani, Z. Tafreshi, T. Base, I. Base, D. Emberley, R. Kennett, D. Bulbuc and E. Chan. 2006. "*Mixing Arrangement for Atomizing Nozzle in Multi-Phase Flow*.".

McDougall, S., M. Saberian, C. Briens, F. Berruti and E. Chan. 2005. "Effect of Liquid Properties on the Agglomerating Tendency of a Wet gas–solid Fluidized Bed." *Powder Technology* 149(2–3):61-67.

McLaughlin, Loretta J. and Martin J. Rhodes. 2001. "Prediction of Fluidized Bed Behaviour in the Presence of Liquid Bridges." *Powder Technology* 114(1–3):213-223.

Mohagheghi, M., M. Hamidi , F. Berruti , C. Briens and J. McMillan. 2013a. "The Effects of Liquid Properties and Bed Hydrodynamics on the Distribution of Liquid on Solid Fluidized Particles in a Cold-Model Fluidized Bed.".

Mohagheghi, M., M. Hamidi, F. Berruti, C. Briens and J. McMillan. 2013b. "Study of the Effect of Local Hydrodynamics on Liquid Distribution in a Gas-Solid Fluidized Bed using a Capacitance Method." *Fuel*.

Morales M, C. B. 2013. " Development and Application of an Experimental Model for the Fluid Coking^{TM} Process " Western University, .

Portoghese, F., L. Ferrante, F. Berruti, C. Briens and E. Chan. 2008. "Effect of Injection-Nozzle Operating Parameters on the Interaction between a Gas-Liquid Jet and a Gas-Solid Fluidized Bed." *Powder Technology* 184(1):1-10.

Simons, S. J. R. and R. J. Fairbrother. 2000. "Direct Observations of Liquid Binder-Particle Interactions: The Role of Wetting Behavior in Agglomerate Growth." 110:44.

Stauffer, C. 1965. "*the Measurement of Surface Tension by the Pendant Drop Technique*." 69(6):1933.

Tardos, G., M. Irfan Khan and P. R. Mort. 1997. "Critical Parameters and Limiting Conditions in Binder Granulation of Fine Powders." 94:245.

Yang, WQ. 1996. "Hardware Design of Electrical Capacitance Tomography Systems." 7:225.

Chapter 4

4. THE EFFECTS OF INJECTION NOZZLE LOCATION AND INCLINATION ON THE INTERACTION BETWEEN A GAS-LIQUID JET AND A GAS SOLID FLUIDIZED BED

4.1 Abstract

Injecting liquid feed is a crucial step in Fluid Coking™ and Fluid Catalytic Cracking processes. In such processes, heavy oil is sprayed using spray nozzles on hot fluidized particles, where cracking take places. There are several arrangements for spray nozzles to introduce liquid feed into fluidized beds. They could be inclined, directed upward, downward, or horizontally as in current Fluid Coker™ commercial units. The injected liquid feed interacts with fluidized solid particles. The yield of these processes is strongly affected by the distribution of liquid feed on solid particles. Non-uniform distribution of liquid causes the formation of wet agglomerates. Heat and mass transfer limitations within agglomerates decrease the yield of cracking reactions. To increase the yield and reduce the formation of such agglomerates, uniform and rapid distribution of injected liquid feed on the surface of coke particles is required. Some parameters involving bed hydrodynamics, spray nozzle geometry and arrangement affect the interaction between liquid and particles in a fluidized bed. In the present study, the effect of nozzle location and inclination on the interaction between a liquid jet and fluidized particles has been investigated using non-intrusive capacitance sensors. Experiments provided information on not only the initial liquid-particles contact, but also on the strength of the resulting wet agglomerates.

4.2 Introduction

Gas-assisted feed nozzles are generally used in chemical and petrochemical processes such as Fluid Coking™ and Fluid Catalytic Cracking. In Fluid Cokers™, bitumen at 300-350 ^{0}C is injected through steam atomized feed nozzles into a fluidized bed of coke particles at 500-550 ^{0}C (Darabi et al. 2010; McMillan et al. 2005). The hot coke particles provide the required heat for the highly endothermic cracking and coking reactions. Coke

is a by-product in this process, which forms on the surface of fluidized coke particles. The vapour products from the cracking reactions rise through the bed and coke particles flow downward to a stripper where the trapped hydrocarbon products are removed using steam before being transported to a burner where a portion of the coke is burned to provide re-heating. Uniform distribution of bitumen feed on solid particles increases the yield of cracked products and minimizes the amount of coke formation (McMillan et al. 2005). Non-uniform distribution results in liquid that is trapped in wet agglomerates. Heat and mass transfer limitations within agglomerates decrease the operating yield of cracking reactions in Fluid Cokers^{TM} (Darabi et al. 2010; McMillan et al. 2005).

There are different studies on the optimization of the operating conditions in Fluid Cokers^{TM} to provide quick and uniform liquid-solid contact. A number of studies have investigated the effect of nozzle geometry on the quality of liquid-solid contact in a gas-solid fluidized bed. Portoghese et al. (2010) characterized the effect of nozzle geometry on the liquid-solid contact efficiency using electric conductance measurements. Chan et al. (2004) found that placing a cylindrical tube downstream of a gas-liquid jet can enhance the liquid-solid contact efficiency by increasing the turbulence within the jet cavity that is formed within the bed by the spray jet. Ariyapadi et al. (2005) developed a model to evaluate the liquid-solid mixing in such a tube. Briens et al. (2009) showed the impact of the draft tube on the expansion angle and jet penetration of a liquid jet in a fluidized bed. Briens et al. (2008) developed a novel technique to measure the entrainment of solids into the horizontal liquid jet flowing through a draft tube which is intended to increase solid-liquid mixing. House et al. (2008) studied the effect of spray nozzle design on the distribution of liquid on solid particles. Leach et al. (2009) investigated the impact on jet-bed interactions of several spray nozzle geometries, under different operating conditions, using a conductance probe. Pougatch et al. (2012) investigated the impact of a conical nozzle attachment on the liquid distribution using numerical simulation. The author found that an attachment with a full included angle of 40^{o} provides the best spray dispersion. This attachment destabilizes the boundaries of the jet in the fluidized bed, causing solids to periodically enter and, then, be expelled out of the jet cavity, which results in better liquid distribution.

Nozzles with different geometries, operating conditions and arrangements create spray jets of different lengths. Several techniques have been proposed to evaluate horizontal and inclined gas and gas-liquid jet penetration. Ariyapadi et al. (2004) developed a technique to predict the horizontal gas-liquid jet penetration into a gas-solid fluidized bed, and proposed a correlation that predicts the jet penetration for a wide range of nozzle geometries. Hong et al. (2005) used numerical simulation to predict the inclined jet penetration length, considering the effect of jet velocity, nozzle diameter, nozzle inclination angle and position and they validated the simulation results with experimental data. Vaccaro et al. (1997) assessed the impact of jet velocity, fluidization velocity and nozzle diameter on the jet length in a gas-solid fluidized bed using pressure signals. They found that increasing jet velocity and nozzle size increases the length of the jet region, while the effect of fluidization velocity is more complex and cannot be separated from the effect of nozzle size.

The objective of this study is the investigation of the impact of nozzle location and inclination on the distribution of liquid droplets on fluidized coke particles in a cold model fluidized bed. It uses accurate non-intrusive capacitance sensors to measure the performance of the spray nozzle.

4.3 Experimental setup

The fluidized bed that has been used in this study is a rectangular fluidized bed with a 1.5 m by 0.28 m cross-section and 2 m high. The windbox is partitioned in two equal sections and two banks of sonic nozzles are used to separately adjust the fluidization velocity for each half of the fluidized bed. Air and nitrogen were used as fluidization and atomization gas, respectively.

Figure 4.1a shows the schematic diagram of the setup. Pressure transducers on the bed wall measure the pressure at different heights to determine the bed pressure drop and the bed height. The bed and freeboard temperature were measured using thermocouples as shown in Figure 1a.

A scaled down version of an industrial nozzle, which is a convergent-divergent-convergent type with a throat diameter of 2.2 mm, was used as the spray nozzle for regular experiments as shown in Figure 4.1b (Base et al. 1999). Varsol^{TM} as liquid feed was mixed with atomization gas in a premixer and sprayed by the spray nozzle on the fluidized coke particles (McCracken et al. 2006). The flowrate of atomization gas was set with a calibrated sonic nozzle and pressure regulator ahead of the premixer where liquid and gas met. For regular experiments, the liquid flowrate was 55 g/s and the injection time was 10 s. There are five ports on the side wall of the fluidized bed at different heights for changing the vertical position of the nozzle. Figure 4.1a shows the position of these ports. A plastic ball joint was used to adjust the nozzle inclination.

a)

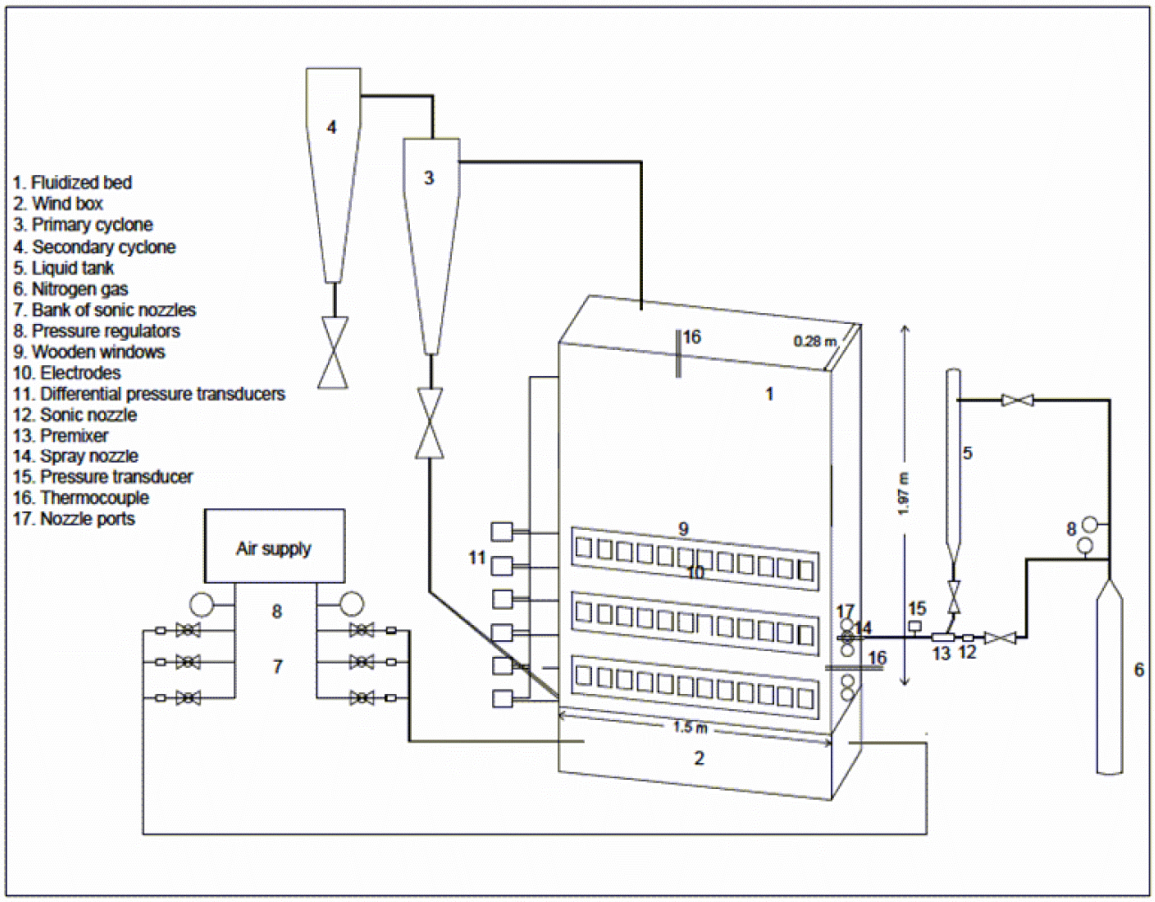

b)

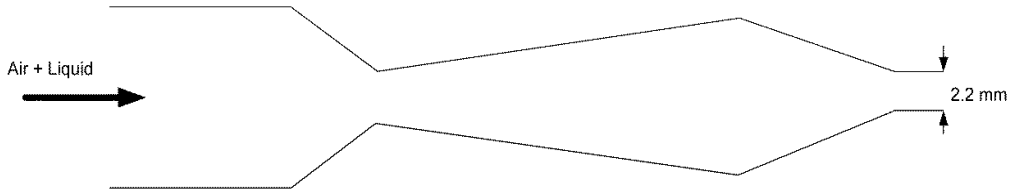

Figure 4.1. a) Schematic diagram of experimental setup; b) Schematic diagram of spray nozzle

4.4 Measuring system

When liquid is injected into a gas-solid fluidized bed with a spray nozzle, a "free liquid" fraction forms a thin layer around individual particles, while the remainder is trapped within wet agglomerates (Ariyapadi et al. 2003; Bruhns and Werther 2005; Knapper et al. 2003). To determine the local free liquid concentration, the local capacitance was measured by placing electrodes at different locations of the fluidized bed. To find the sensitivity of capacitance sensors to liquid trapped in agglomerates, some experiments were carried out in a small box of coke particles, with flat metal electrodes on two opposing walls. In these experiments, liquid could either be spread evenly on the solid particles with intense mechanical agitation or dripped as large drops at various locations on the powder surface, forming large agglomerates. The results of these experiments have shown that the normalized capacitance of a wet bed is a linear function of the free liquid volume fraction and is not affected significantly by the presence of liquid trapped within agglomerates. A dedicated electrical circuit measures the capacitance of the material between each set of electrodes based on their relative permittivity. The relative permittivity of Varsol^{TM} is 3 which compares with a permittivity of 7 for coke (U.S. National Library of Medicine). The relative permittivity of coke that was used in this study was calculated based on comparing the measured capacitance of air and coke in a small box (the relative permittivity of air is 1 (Department of Physics and Astronomy, Georgia State University).

Thirty-two rectangular 8 by 10 cm copper electrodes were placed at different lateral and vertical positions on three wooden windows positioned on one side of the fluid bed.

Three rectangular 135 by 20 cm copper electrodes were also located on the opposing wall of each window. Figure 4.2 shows the electrodes arrangement on one side of the fluid bed.

The capacitance meter used in this study is an AC based circuit with a differential noise cancelling system. The circuit consists of (a) an amplifier which is connected to the 32 electrodes through its virtual ground, (b) a multiplexer switches between electrodes every 3 ms, (c) a RMS to DC converter which takes the RMS of the signal every 3 ms, and (d) a microcontroller to record data and transmit it to a computer. Figure 4.3 shows a schematic diagram of the capacitance meter.

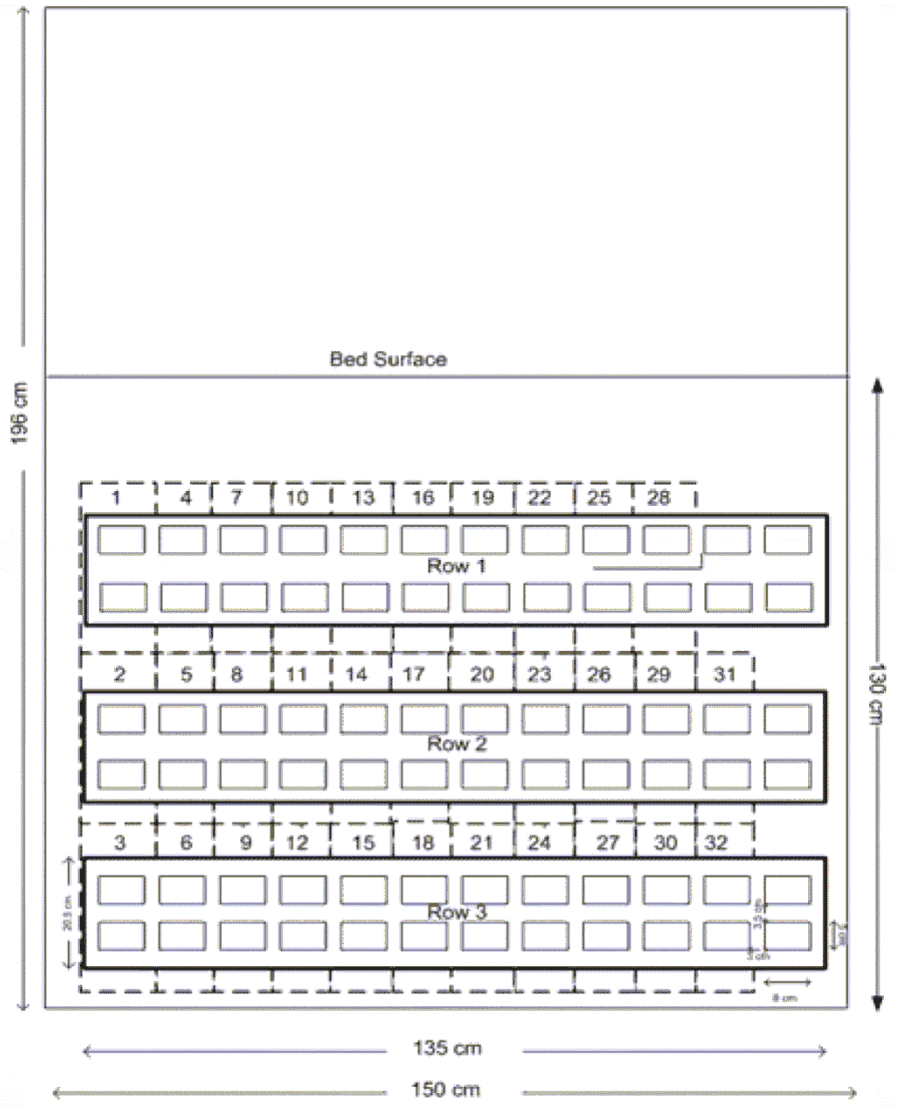

Figure 4.2. Position of electrodes on wooden windows of fluidized bed setup

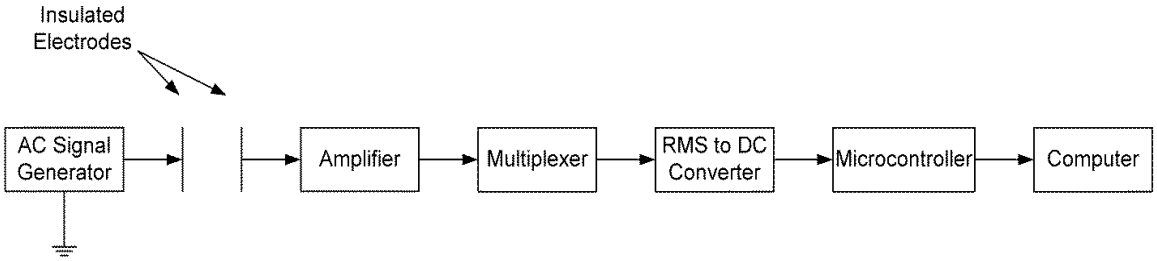

Figure 4.3. Schematic diagram of capacitance meter

4.4.1 Calibration experiments

Calibration experiments were carried out using a special nozzle consisting of a straight cylindrical tube with a diameter of 3.6 mm. This special nozzle provides a low liquid flow rate (1.5 g/s) and is operated with a very high atomization gas-to-liquid mass ratio (GLR = 85 wt%) to ensure the formation of a very diluted spray resulting in a nearly perfect distribution of liquid on fluidized particles. This nozzle required a very high GLR that is not practical for industrial operation.

To obtain the calibration curves, some experiments were performed with different amounts of free liquid. To change the amount of free liquid, the amount of injected liquid was changed as no agglomerate was formed during the calibration experiments. Calibration curves provide the normalized capacitance, calculated by dividing the measured capacitance after liquid injection by that obtained before the injection. For example, Figure 4a and 4b show the calibration curves for electrodes 15 and 2 (see Figure 4.2 for the electrode location).

a)

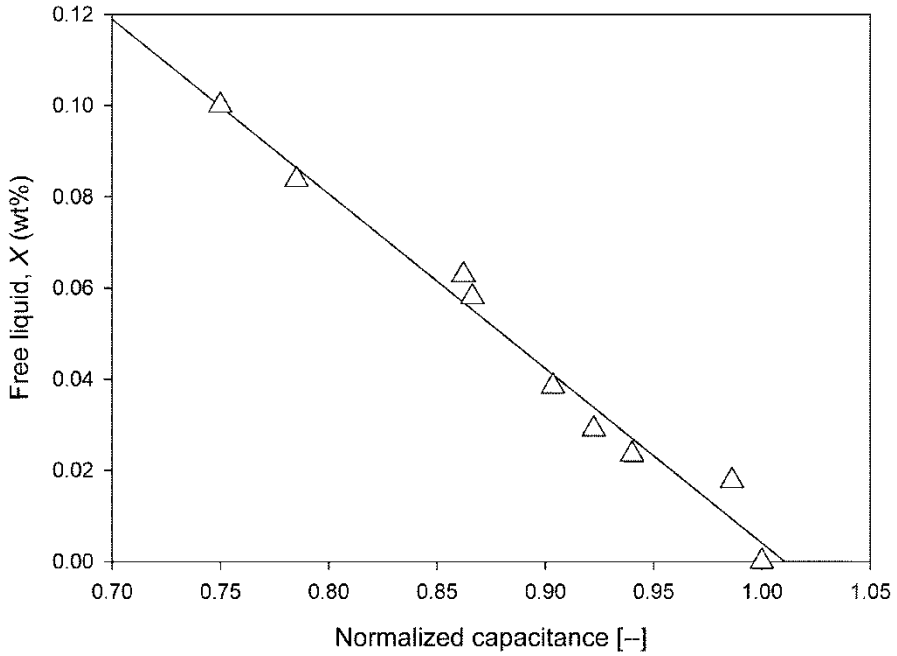

b)

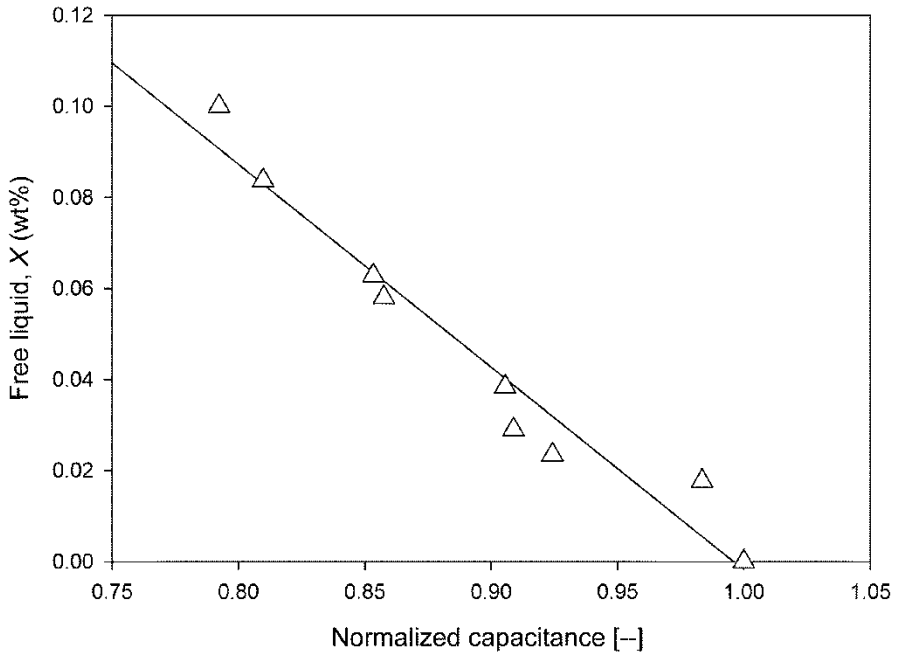

Figure 4.4. a) Calibration curve for electrode 15 (with Varsol^{TM} liquid); b) Calibration curve for electrode 2 (with Varsol^{TM} liquid)

4.4.2 Measurement of local bubble volume fraction

The local bubble volume fraction, ε_b, was calculated from local capacitance measurements in the dry bed, before liquid injection. The average void fraction of the dry bed at different fluidization velocities was first calculated from the measured bed pressure drop using Equation 4.1:

$$\frac{\Delta p}{\Delta z} = \rho_p(1-\varepsilon)g \qquad (4.1)$$

To find the correlation between the bed capacitance and bed voidage, the capacitance of each electrode at different fluidization velocities was normalized by the capacitance of that electrode for the defluidized bed. Then, the average of local normalized capacitances was calculated to obtain the normalized capacitance of the bed at each fluidization

velocity. Figure 4.5 provides the calibration curve between the average normalized capacitance and the average bed voidage. This calibration curve could be used to easily calculate the local void fraction in the bed from local capacitance measurements as the correlation between the average void fraction and the average normalized bed capacitance is linear.

The local bubble volume fraction was calculated from local void fractions using equation 4.2 (Gogolek 1998).

$$\varepsilon_b = \frac{\varepsilon - \varepsilon_d}{1 - \varepsilon_d} \tag{4.2}$$

where ε_b is bubble volume fraction, ε is void fraction and ε_d is the uniform void fraction of the dense phase.

ε_d was calculated from the aerated density of coke particles measured by the avalanche machine, which is $875\ \frac{\mathrm{kg}}{\mathrm{m}^3}$, and the particle density measured by the particle size analyzer, $1450\ \frac{kg}{m^3}$. Therefore, the calculated value for ε_d is 0.4.

Figure 4.6 shows the local void fraction versus different lateral positions of the bed for two different vertical positions and a fluidization velocity of 0.2 m/s. Figure 4.7 shows the local bubble volume fraction that was calculated from the local void fraction provided in Figure 4.6. The average bubble volume fraction is lower at the higher location due to larger and faster bubbles. There is also a maximum bubble volume fraction in a central location.

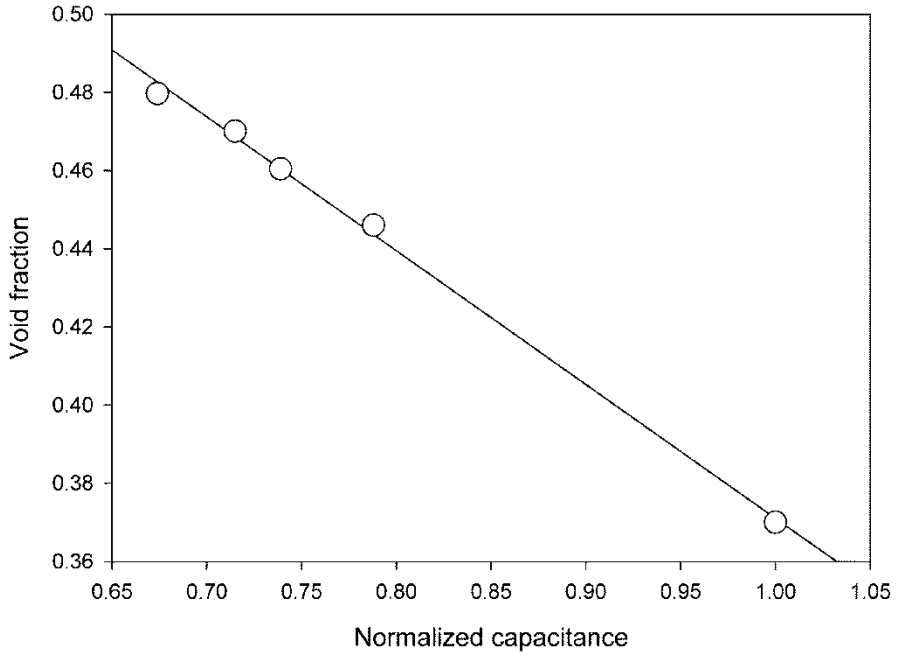

Figure 4.5. Average normalized capacitance of the bed at different fluidization velocities versus average void fraction of the bed

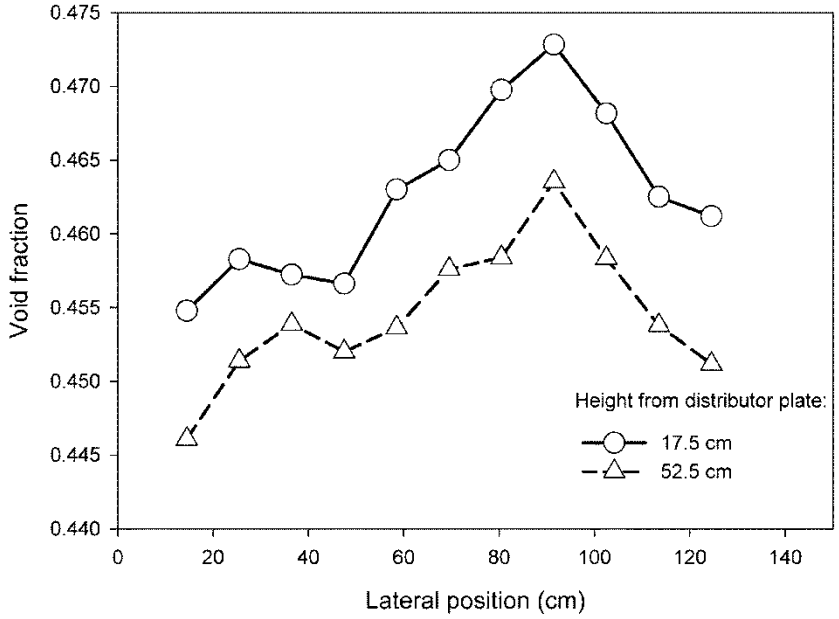

Figure 4.6. Void fraction versus lateral distance relative to inner left-hand side wall for two different vertical positions in the bed and a fluidization velocity of 0.2 m/s

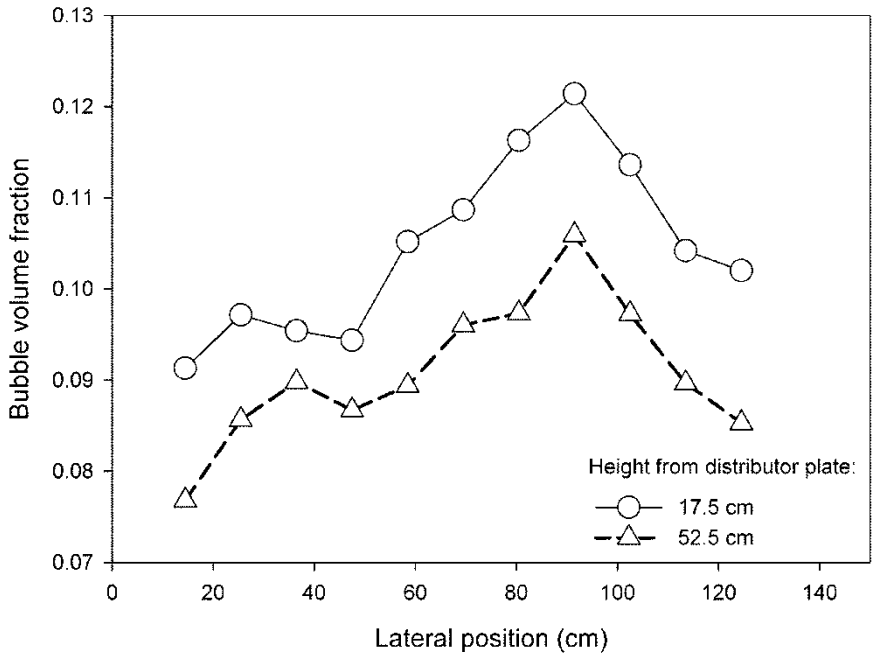

Figure 4.7. Bubble volume fraction versus lateral distance relative to inner left-hand side wall for two different vertical positions in the bed and a fluidization velocity of 0.2 m/s

4.4.3 Measurement of the time constant for agglomerate breakup

To determine the time constant of the agglomerates breakup, the total amount of liquid freed from the agglomerates was calculated by accounting for vaporization (Mohagheghi et al. 2013a; Mohagheghi et al. 2013b). For regular experiments, evaporation happens as agglomerates break and generate free liquid. The rate of liquid freed from agglomerates was calculated using Equation 4.3.

$$M_S\left[\frac{dX}{dt}\right]_{br} = M_S\left[\frac{dX}{dt}\right] - M_S\left[\frac{dX}{dt}\right]_e \tag{4.3}$$

where X is mass concentration of free liquid on a dry solids basis, wt% and M_S is total mass of dry solid in kg.

The evaporation rate was calculated from the calibration experiments, as there were no agglomerates formed during those tests.

The total free liquid is the sum of the free liquid during injection and the cumulative liquid freed from agglomerates after injection. The ratio of the total free liquid to the total mass of injected liquid, $g(t)$, was calculated from Equation 4.

$$g(t) = \frac{M_S}{M_L}\left[X|_{t=0} + \int_0^t \left[\left(\frac{dX}{dt}\right) - \left(\frac{dX}{dt}\right)_{cal}\right] dt\right] \quad (4.4)$$

where X is mass concentration of free liquid on a dry solids basis, wt%, M_S is total mass of solids and M_L is total mass of liquid in kg.

$g(t)$ was plotted versus time after injection for the experiments. The time constant of agglomerate breakage (τ) was then calculated based on an exponential curve fit to $g(t)$:

$$g(t) = 1 + (g(0) - 1)e^{-t/\tau} \quad (4.5)$$

where $g(0)$ represents the value of $g(t)$ at the end of injection.

4.5 Effects of nozzle location on liquid-solid contact

4.5.1 Experimental conditions

4.5.1.1 Experiments without additional gas injection

To study the impact of nozzle position on the initial distribution of liquid on the solid particles and on the formation of agglomerates, some experiments were performed with the horizontal nozzle placed at different vertical and lateral positions at a fluidization velocity of 0.2 m/s and an atomization gas to liquid ratio (GLR) of 1.5 wt%. Table 4.1 shows the experimental conditions of these experiments. The tests were repeated for the same conditions two times. For all these experiments, 550 g of Varsol™ was injected on about 420 kg of dry coke particles for 10 s through a scaled-down version of an industrial nozzle (Figure 4.1b).

Table 4.1. Experimental conditions for experiments with different vertical and lateral positions of spray nozzle

Run #	Lateral position relative to inner left-hand side wall (m)	Height relative to top of distributor plate (m)	GLR (wt %)	Fluidization velocity (m/s)
1	0.08	0.525	1.5	0.2
2	0.3	0.525	1.5	0.2
3	0.6	0.525	1.5	0.2
4	0.08	0.175	1.5	0.2
5	0.3	0.175	1.5	0.2
6	0.6	0.175	1.5	0.2

The bubble volume fraction was evaluated both at the nozzle and at the jet tips for each experiment using the data illustrated in Figure 4.7, since all the experiments in this study have been performed at a fluidization velocity of 0.2 m/s. To estimate the bubble volume fraction just below the tip of the jet, the jet penetration must be known. The standard deviation of the capacitance measurements during the injection was used to obtain the jet penetration. The lateral location displaying the maximum standard deviation of the capacitance was considered as the position of the jet tip, because of the typical local instability at that location. For instance, Figure 4.8 shows the standard deviation of the capacitance measured by the row of electrodes located 52.5 cm above the distributor plate (middle row) for the horizontal nozzle located at the same height. The experimental values show that there is a point where the standard deviation peaks and then drops sharply: this location can be considered to correspond to the jet penetration depth. The jet penetration was also calculated from the correlation developed by Ariyapadi et al. (2004) for gas-liquid spray jets. The calculated value from this correlation is consistent with the results from the capacitance measurements which is about 52 cm.

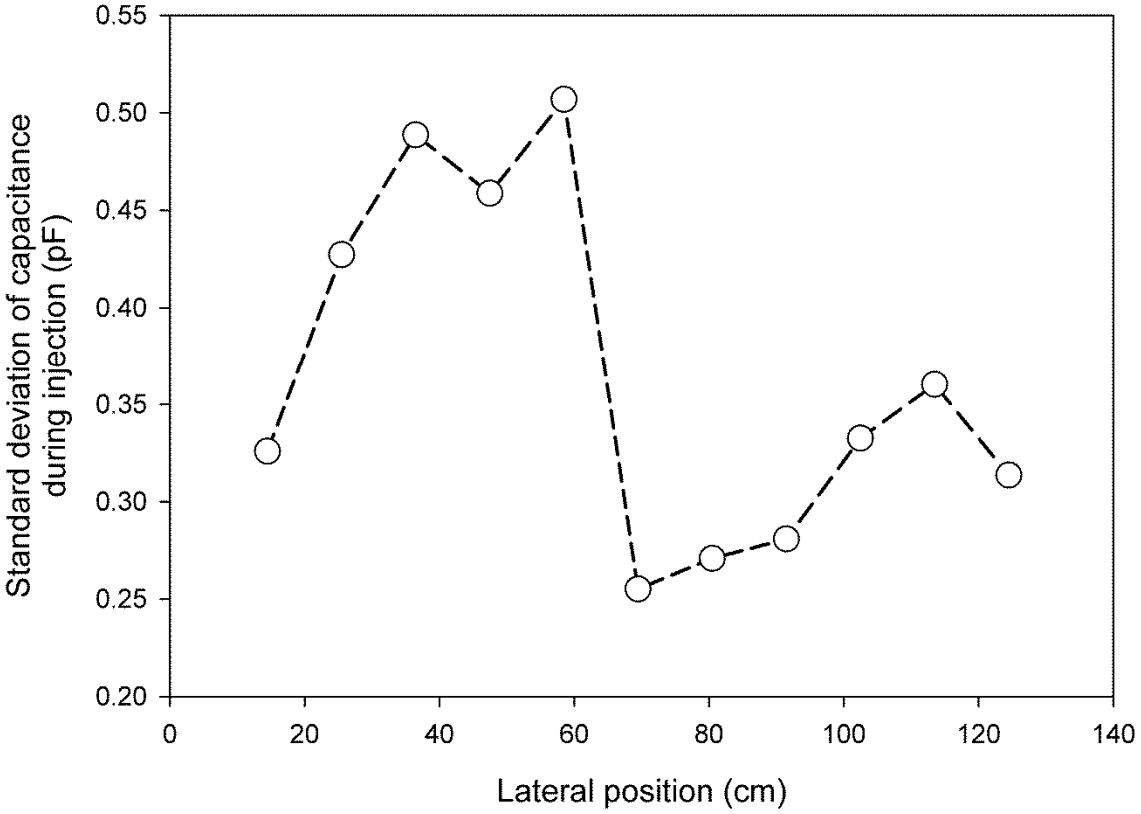

Figure 4.8. Standard deviation of the capacitance for the electrodes located 52.5 cm above the distributor plate during injection versus lateral distance relative to inner left-hand side wall for a horizontal nozzle located at the same height, GLR = 1.5 wt%, fluidization velocity = 0.2 m/s and nozzle penetration depth = 6 cm

4.5.1.2 Experiments with additional gas injection

Some experiments were performed at the same nozzle location but using extra gas to change the local bubble volume fraction near either the nozzle tip or the jet tip. To add extra gas locally, a moving tube with an inner diameter of 3.8 mm was placed 27 cm below the horizontal spray nozzle level. To change the bubble volume fraction near the tip of the nozzle, the tube was adjusted so that its tip was 27 cm below the nozzle tip. The local bubble volume fraction was obtained from capacitance measurements. Table 4.2 shows the experimental conditions and calculated bubble volume fractions for these experiments. Similarly, to change the bubble volume fraction near the jet tip, the tube was adjusted so that its tip was 27 cm below the jet tip. The experimental conditions of these

experiments were shown in Table 4.3. The experiments were repeated for the same conditions two times.

Table 4.2. Experimental conditions of experiments with additional gas injection to change the bubble volume fraction at the nozzle tip

Run #	Lateral position relative to inner left-hand side wall (m)		Height relative to top of distributor plate (m)		Bubble volume fraction near the nozzle tip location	GLR (wt %)	Fluidization velocity (m/s)
	nozzle tip	additional injection tube tip	nozzle tip	additional injection tube tip			
1	0.08	0	0.525	0	0.0768	1.5	0.2
1en	0.08	0.08	0.525	0.25	0.0897	1.5	0.2
2	0.3	0	0.525	0	0.0867	1.5	0.2
2en	0.3	0.3	0.525	0.25	0.0944	1.5	0.2

Table 4.3. Experimental conditions of experiments with additional gas injection to change the bubble volume fraction at the jet tip

Run #	Lateral position relative to inner left-hand side wall (m)		Height relative to top of distributor plate (m)		Bubble volume fraction near the jet tip location	GLR (wt %)	Fluidization velocity (m/s)
	nozzle tip	additional injection tube tip	Nozzle tip	additional injection tube tip			
1	0.08	0	0.525	0	0.0894	1.5	0.2
1ej	0.08	0.60	0.525	0.25	0.098	1.5	0.2
2	0.3	0	0.525	0	0.0973	1.5	0.2
2ej	0.3	0.92	0.525	0.25	0.1113	1.5	0.2

4.5.2 Results and discussion

4.5.2.1 Results of experiments without additional gas injection

The free liquid right after the injection was calculated from the capacitance measurements using the calibration experiments for each electrode. The ratio of total injected liquid which is free liquid right after injection, *g(0)*, which corresponds to the average of the free liquid given by the thirty-two electrodes, was plotted as a function of bubble volume fractions near nozzle and jet tips, as shown in Figure 4.9. This figure shows that the initial distribution of liquid on solid particles is a strong function of the bubble volume fraction near the tip of the nozzle. This figure also illustrates that a higher bubble volume fraction near the nozzle tip decreases the formation of agglomerates due to higher solids entrainment and mixing within the jet cavity. Figure 4.9 also shows a weaker correlation between the initial free liquid and the bubble volume fraction near the jet tip. The statistical t-test results of the multilinear regression between the initial free liquid and the bubble volume fractions near the nozzle and jet tips show that the bubble volume fraction near the jet tip is not the significant parameter as its p-value is higher than 0.05 (p-value=0.254), whereas the p-value of the bubble volume fraction near the nozzle tip is 0.024.

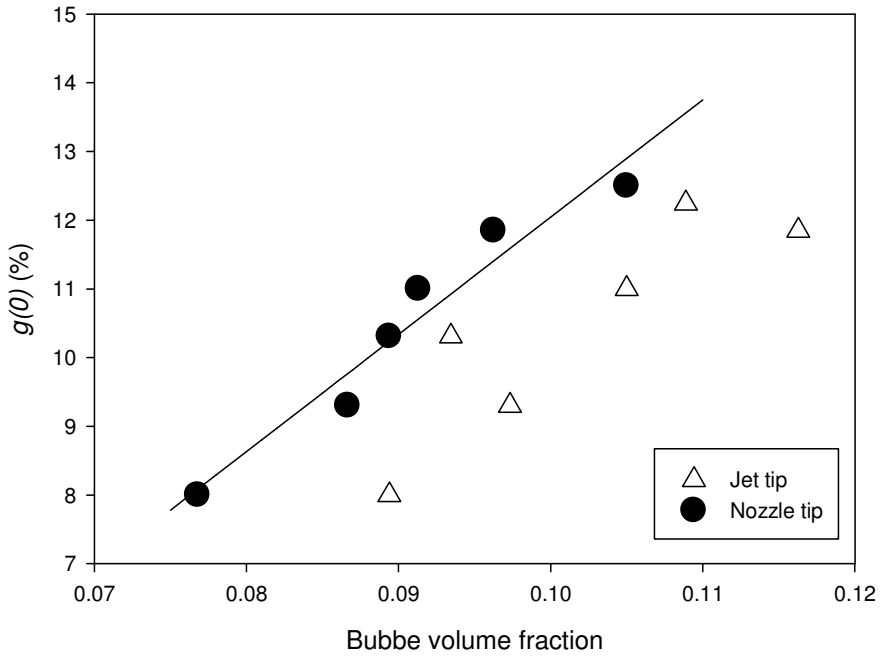

Figure 4.9. Percentage of injected liquid which is free liquid right after injection versus bubble volume fraction at the nozzle and jet tip for a horizontal nozzle and a fluidization velocity = 0.2 m/s (no additional injection of gas) (line is from linear regression of nozzle tip results)

The following equation shows the simplified correlation accounting only for the effect of bubble volume fraction near the nozzle tip:

$$X = -5.027 + 170.73\ \varepsilon_{bN} \qquad (4.6)$$

where X is the percentage of injected liquid which is free liquid just after injection, and ε_{bN} is the bubble volume fraction near the tip of the nozzle.

To determine the effect of nozzle location on the breakage of agglomerates, the time constant of agglomerate breakup (τ) was calculated from Equation 4.5. Figure 4.10 shows τ as a function of bubble volume fraction at the nozzle and jet tips. This figure shows that the breakage rate of the agglomerates is a strong function of the bubble volume fraction near the jet tip. The bubble volume fraction near the jet tip is important because the gas bubbles interact with the agglomerates where most of them are formed, i.e. near the tip of the jet cavity (Bruhns and Werther 2005). There is a weaker correlation between the time

constant of agglomerate breakage and the bubble volume fraction near the nozzle tip. The statistical t-test results of the multilinear regression between the time constant of agglomerate breakage and the bubble volume fractions near the nozzle and jet tips show that the bubble volume fraction near the nozzle tip is not the significant parameter as its p-value is higher than 0.05 (p-value=0.332). On the other hand, the p-value of the bubble volume fraction near the jet tip is 0.027, which indicates a strong correlation between the bubble volume fraction near the jet tip and the time constant of agglomerate breakage.

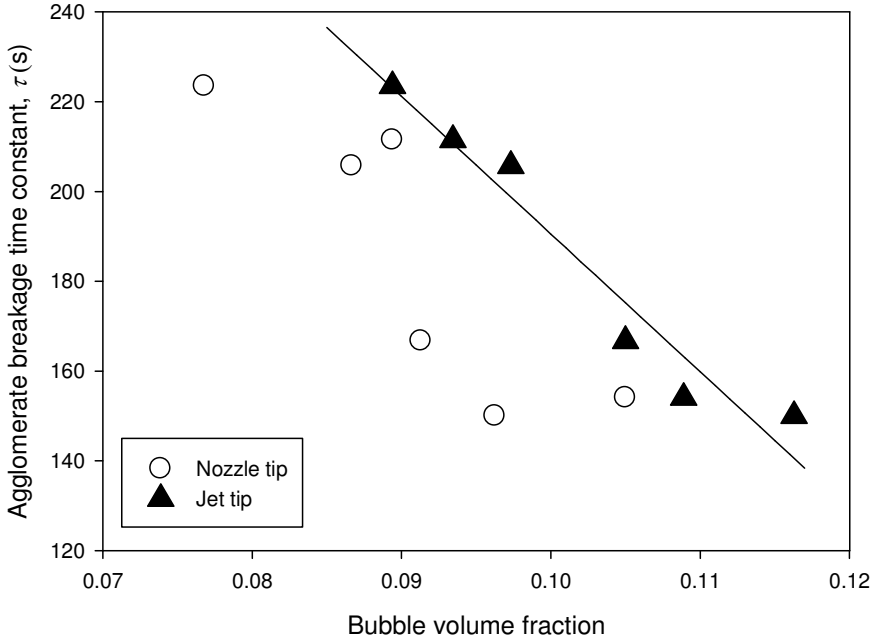

Figure 4.10. Time constant of the agglomerate breakage versus bubble volume fraction at the nozzle and jet tips for a horizontal nozzle and a fluidization velocity = 0.2 m/s (no additional injection of gas) (line is from linear regression of jet tip results)

The following equation shows the simplified correlation accounting only for the effect of bubble volume fraction near the jet tip:

$$\tau = 497.14 - 3066.24\ \varepsilon_{bj} \tag{4.7}$$

where τ is the time constant of agglomerate breakage and ε_{bj} is the bubble volume fraction at the jet tip.

4.5.2.2 Results of experiments with additional gas injection

The results of the nozzle location experiments without additional gas suggest that there is not a clear correlation between the bubble volume fraction near the jet tip and initial free liquid (*g(0)*) and none between the bubble volume fraction near the nozzle tip and the time constant of agglomerate breakage. To find whether there is a correlation, some experiments with additional gas injection were performed. Figure 4.11a shows the percentage of injected liquid which is free liquid immediately after injection before and after the local addition of extra gas to change bubble volume fraction at the tip of the nozzle at the same nozzle location. The conditions of each run have been provided in Table 4.2. The local addition of extra gas confirms that increasing the bubble volume fraction at the tip of the nozzle increases the free liquid by decreasing the formation of agglomerates. Figure 4.11b shows the time constant of agglomerate breakage before and after the local addition of extra gas to change the bubble volume fraction at the tip of the nozzle. This figure shows adding extra gas near the nozzle tip does not affect the agglomerate breakage time constant.

a)

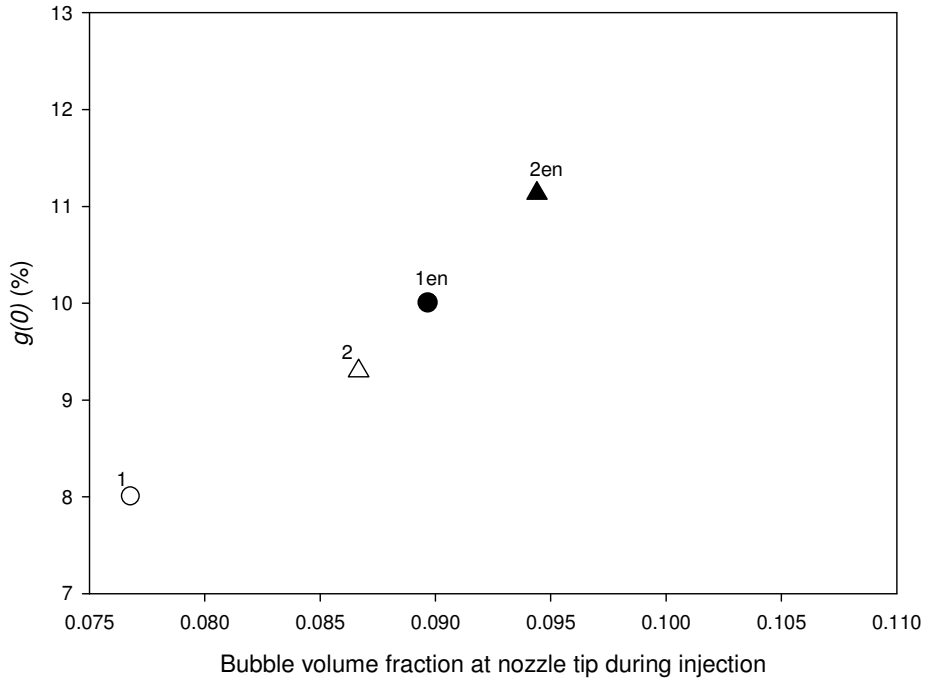

b)

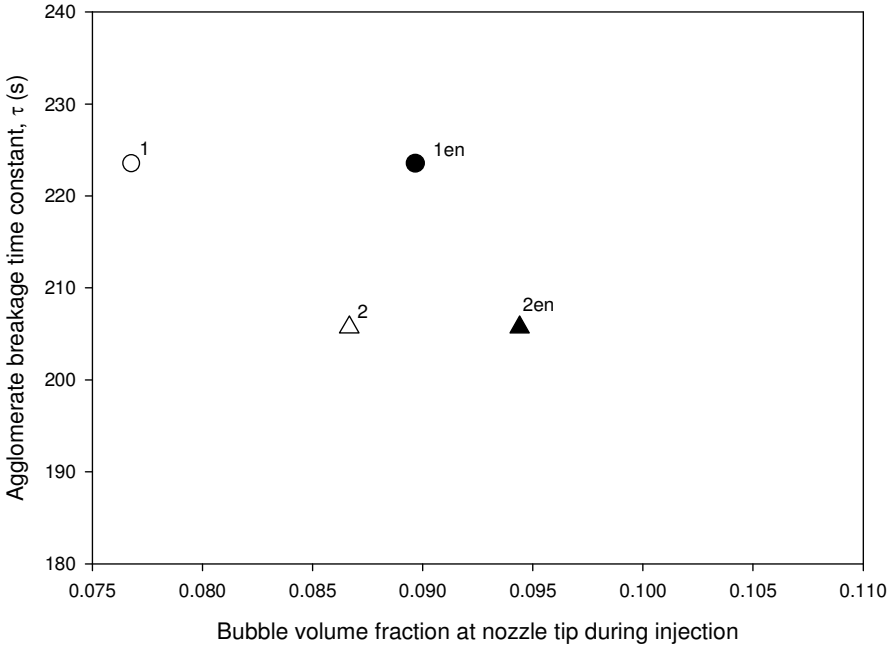

Figure 4.11. a) Percentage of injected liquid which is free liquid right after injection versus bubble volume fraction at tip of horizontal nozzle with and without local addition of extra gas near the nozzle tip (fluidization velocity = 0.2 m/s) (see Table 4.2 for the conditions corresponding to the run numbers indicated on the figure); b) Time constant of agglomerate breakage versus bubble volume fraction at tip of nozzle for horizontal nozzle with and without local addition of extra gas near nozzle tip (fluidization velocity = 0.2 m/s) (see Table 4.2 for the conditions corresponding to the run numbers indicated on the figure)

Figure 4.12a shows the time constant of agglomerate breakage before and after adding extra gas at a specified location to change the bubble volume fraction at the tip of the jet with the same nozzle location. The conditions of each run have been provided in table 3. Local addition of extra gas confirms that increasing the bubble volume fraction at the tip of the jet decreases the time constant of agglomerate breakage. Figure 4.12b shows the percentage of injected liquid which is free liquid immediately after injection (*g(0)*) before and after the local addition of extra gas to change the bubble volume fraction at the tip of the jet. This figure shows adding extra gas near the jet tip does not affect the free liquid just after injection.

a)

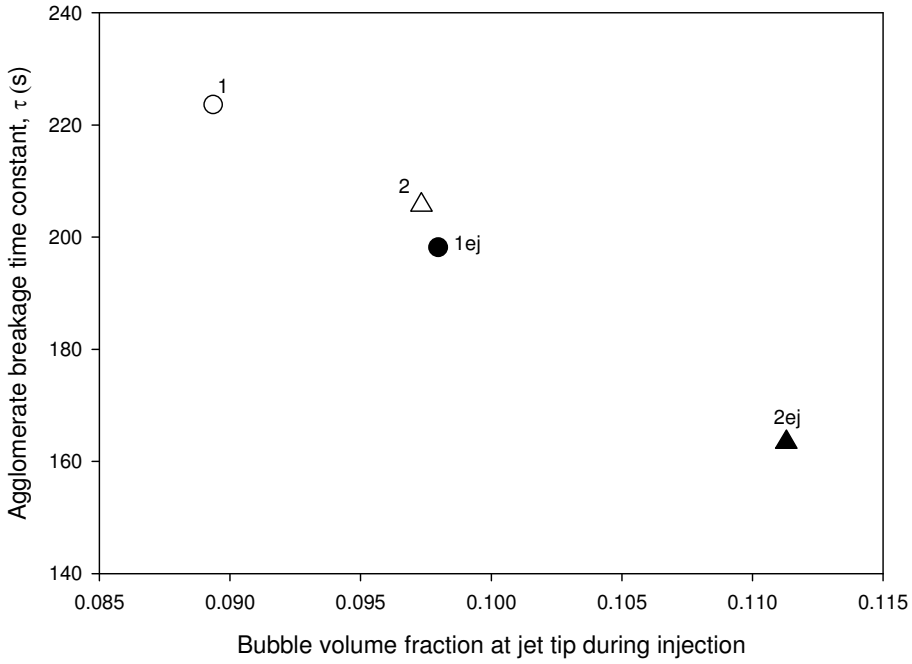

b)

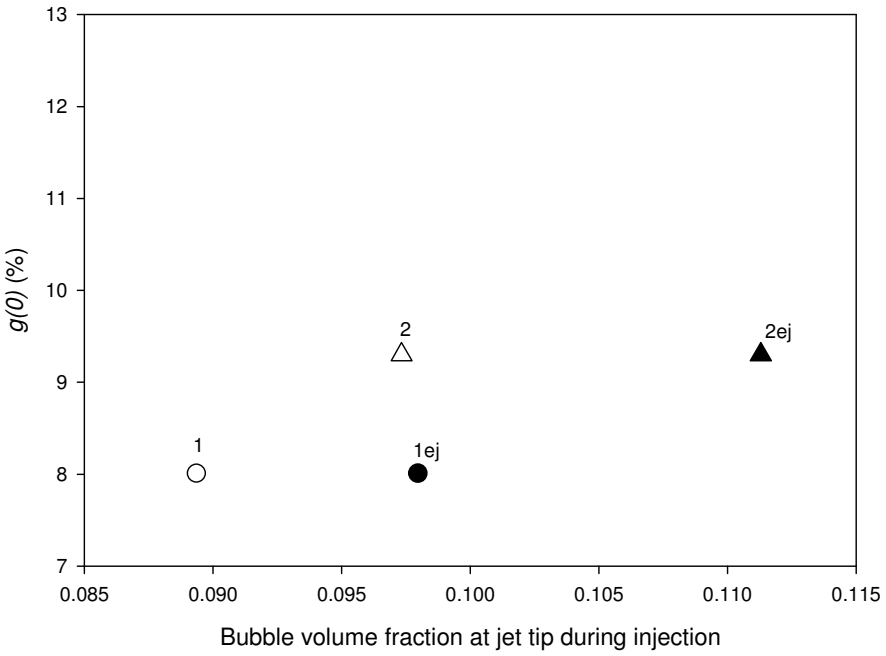

Figure 4.12. a) Time constant of agglomerate breakage versus bubble volume fraction at tip of jet for horizontal nozzle with and without local addition of extra gas near jet tip (fluidization velocity = 0.2 m/s) (see Table 4.3 for the conditions corresponding to the run numbers indicated on the figure); b) Percentage of injected liquid which is free liquid

right after injection versus bubble volume fraction at tip of jet for horizontal nozzle with and without local addition of extra gas near jet tip (fluidization velocity = 0.2 m/s) (see Table 4.3 for the conditions corresponding to the run numbers indicated on the figure)

4.6 Effects of nozzle inclination on liquid-solid contact

4.6.1 Experimental conditions

To investigate the impact of nozzle angle on the jet-bed interactions, some experiments were carried out in the fluidized bed with different nozzle inclinations and the same nozzle port height (item 17 Figure 4.1a) from the distributor plate. The conditions of these experiments were shown in Table 4. Negative and positive angles indicate spraying liquid downward and upward, respectively. For all these experiments, 550 g of Varsol were injected in a bed of about 420 kg of coke particles for 10 s through a scaled-down version of the industrial nozzle illustrated in Figure 4.1b. When modifying the nozzle angle in the nozzle inclination experiments, however, the locations of both the nozzle tip and the jet tip were modified. Some experiments were, thus, performed, with the same nozzle and jet tip location in the bed and different inclinations as shown in Table 4.4. For example for an angle of -30^0, an experiment was performed with an angle of zero degrees for which the jet tip location was the same. Jet penetration calculations were used to find the nozzle height above the distributor and the nozzle penetration depth to have the same jet tip location. The jet penetration was calculated from the standard deviation of the signals collected from the three rows of electrodes (Figure 4.2) during the injection. For the horizontal nozzle arrangement, the standard deviation of the electrodes positioned along the middle window was used, as the height of the electrodes above the distributor was the same as that of the nozzle. However, for the downward nozzle, the standard deviation of the electrodes along the bottom row was utilized, whereas for the upward nozzle, the location of the jet tip was evaluated by comparing the standard deviations of the electrodes along the top row.

Figure 4.13 shows the standard deviation of the capacitance measurements resulting from downward, horizontal and upward sprays. The location corresponding to a significant decrease in the standard deviation of the capacitance signals was considered as the position of the jet tip. The jet penetration depth for the horizontal nozzle was calculated

from a correlation from Ariyapadi et al. (2004), as mentioned in section 4.5.1.1. For the inclined nozzle, the jet penetration was also calculated from a correlation proposed by Hong et al. (2005). This correlation shows there is about 4.5% increase in jet penetration for an angle of $+30^0$ when compared with the horizontal jet, while an angle of -30^0 resulted in a 6% decrease. The capacitance measurements, as shown in Figure 4.13, provide the horizontal penetration of the inclined nozzle and indicate that the jet penetration for an angle of -30^0 is consistent with the correlation and is about 10% lower than predicted by the correlation for an angle of $+30^0$. This slight discrepancy may have resulted from the poor resolution of the capacitance measurements, which had not been originally intended to perform these measurements (for an angle of $+30^0$, the jet tip is between the centers of adjacent electrodes).

Table 4.4. Experimental conditions for inclined nozzle

Run#	Height relative to top of distributor plate (m)			Lateral position relative to inner left-hand side wall (m)		angle (^{0})	GLR (wt%)	Fluidization velocity (m/s)
	Nozzle port	Nozzle tip	Jet tip	Nozzle tip	Jet tip			
1	**0.525**	0.525	0.525	0.06	0.58	0	1.5	0.2
7	**0.525**	0.54	0.667	0.058	0.53	+15	1.5	0.2
8	**0.525**	0.555	0.83	0.052	0.53	+30	1.5	0.2
9	**0.525**	0.51	0.40	0.058	0.475	-15	1.5	0.2
10	**0.525**	0.495	0.25	0.052	0.475	-30	1.5	0.2
11	0.59	**0.59**	0.59	**0.24**	0.76	0	1.5	0.2
12	0.45	**0.59**	0.87	**0.24**	0.72	+30	1.5	0.2
13	0.45	**0.45**	0.45	**0.24**	0.76	0	1.5	0.2
14	0.59	**0.45**	0.21	**0.24**	0.665	-30	1.5	0.2

15	0.175	0.175	**0.175**	0.08	**0.6**	0	1.5	0.2
16	0.525	0.415	**0.175**	0.19	**0.6**	-30	1.5	0.2
17	0.525	0.525	**0.525**	0.08	**0.6**	0	1.5	0.2
18	0.175	0.25	**0.525**	0.13	**0.6**	+30	1.5	0.2

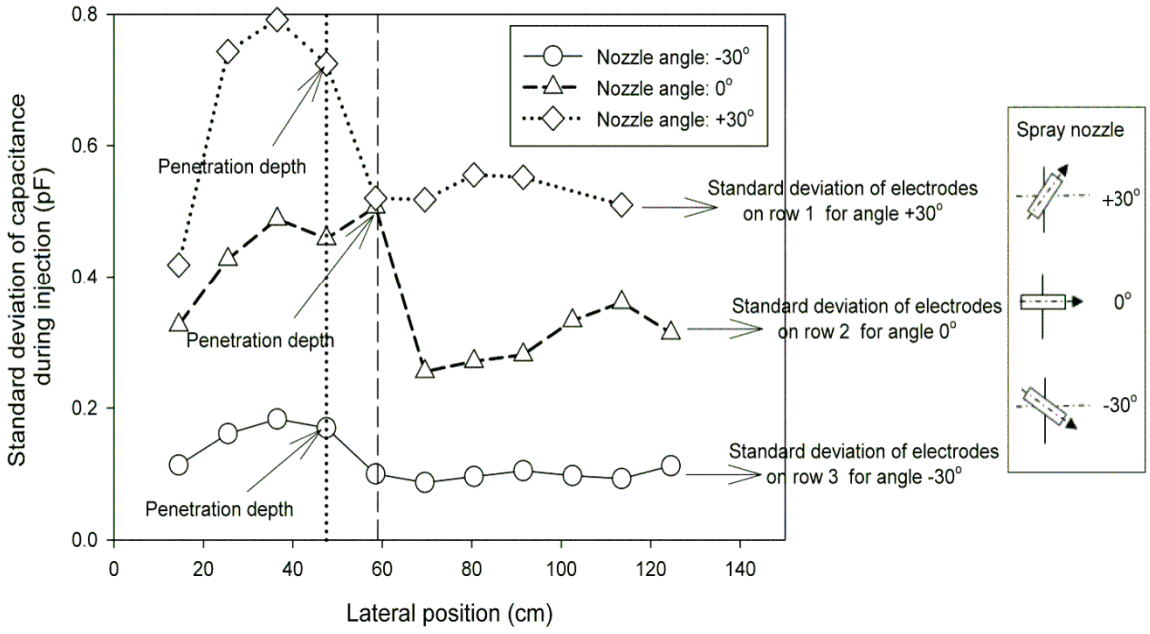

Figure 4.13. Standard deviation of the capacitance during injection versus lateral distance relative to inner left-hand side wall for nozzle inclinations of -30^0 (spraying downward), 0^o (Horizontal) and $+30^0$ (spraying upward), fluidization velocity = 0.2 m/s, GLR = 1.5 wt%, nozzle height = 52.5 cm above the distributor, and nozzle penetration depth = 6 cm

4.6.2 Results and discussion

The initial free liquid after injection was obtained from the calibration curves for each electrode. Figure 4.14 shows the total initial free liquid corresponding to the average of the initial free liquid measured by the thirty-two electrodes. This figure shows that the

initial distribution of liquid on solid particles improves when spraying the liquid downward.

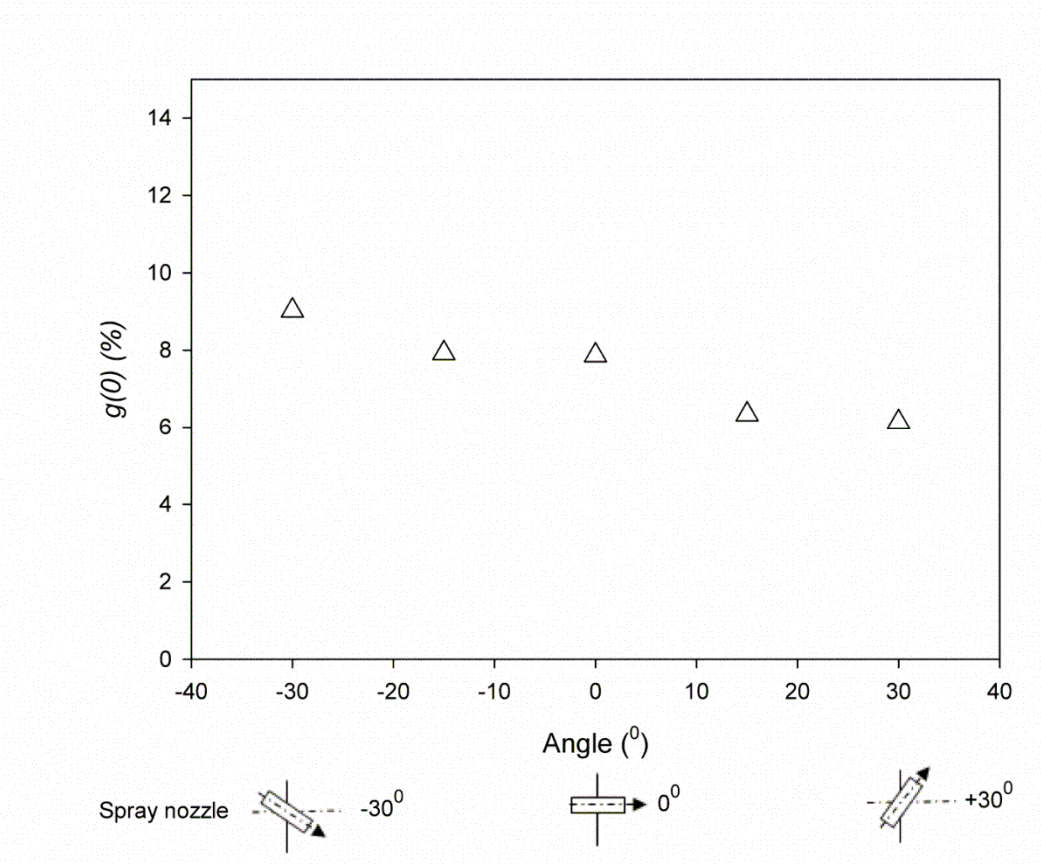

Figure 4.14. Percentage of injected liquid which is free liquid right after injection for different nozzle inclinations (GLR = 1.5 wt%, fluidization velocity = 0.2 m/s, Nozzle height = 52.5 cm and nozzle penetration depth = 6 cm)

Figure 4.15 shows the time constant for agglomerate breakage at different nozzle inclinations. This figure illustrates that injecting downward reduces the time constant of agglomerate breakage.

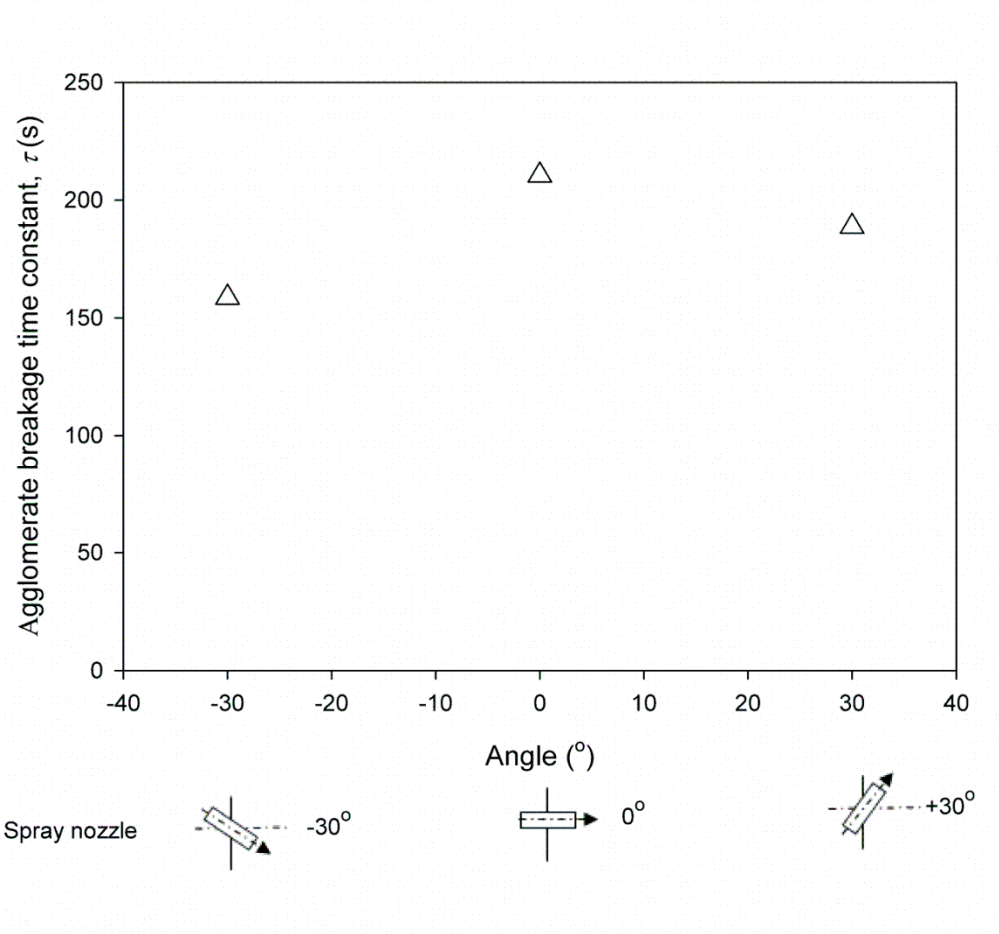

Figure 4.15. Time constant of agglomerate breakage for different nozzle inclinations (GLR = 1.5 wt%, fluidization velocity = 0.2 m/s, Nozzle height = 2.5 cm and nozzle penetration depth = 6 cm)

The experimental results for experiments with different angles and the same nozzle tip location (run # 11 to 14) were shown in Figure 4.16. For each run, the initial free liquid has been shown in this figure. The results of these experiments indicate that nozzles with different inclinations and the same nozzle tip location have almost the same impact on agglomerate formation. The experimental results for experiments with different angles and the same jet tip location (run# 15 to 18) were shown in Figure 4.17. The time constant of agglomerate breakage for each experiment was calculated and the results are illustrated in this figure. The findings show that the strength of the formed agglomerates is a function of jet tip location and nearly independent of nozzle inclination.

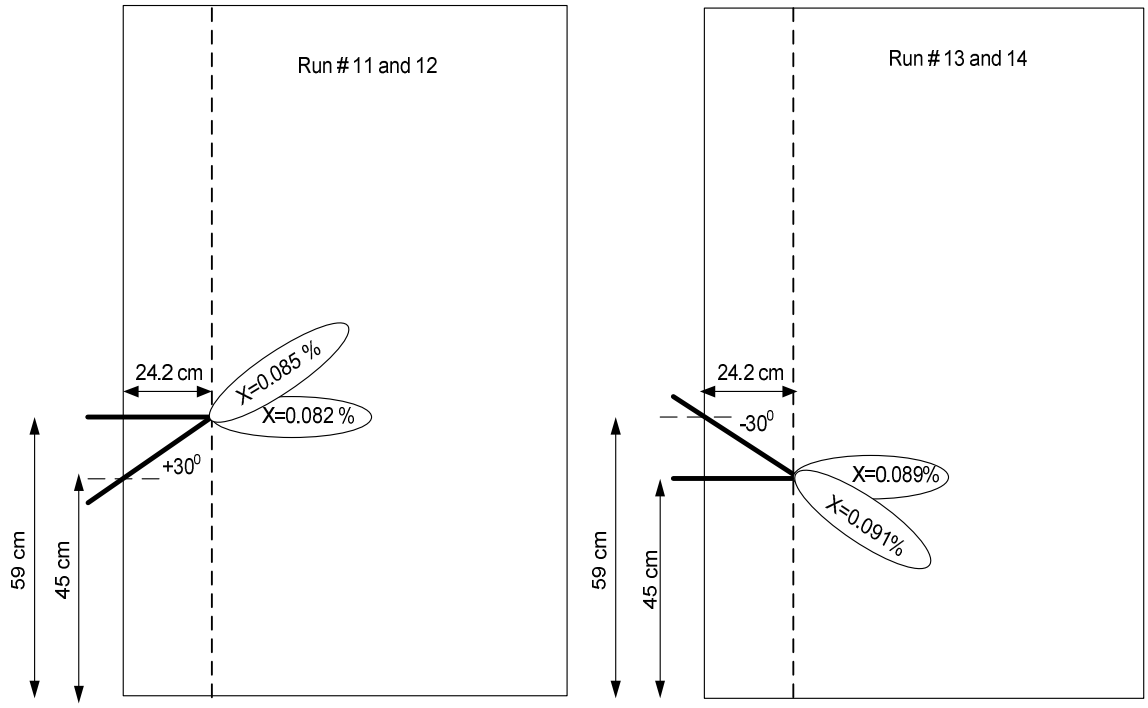

Figure 4.16. Comparison of the percentage of injected liquid which is free liquid immediately after the injection for experiments with the same nozzle tip location and different injection angles (GLR = 1.5 wt% and fluidization velocity = 0.2 m/s)

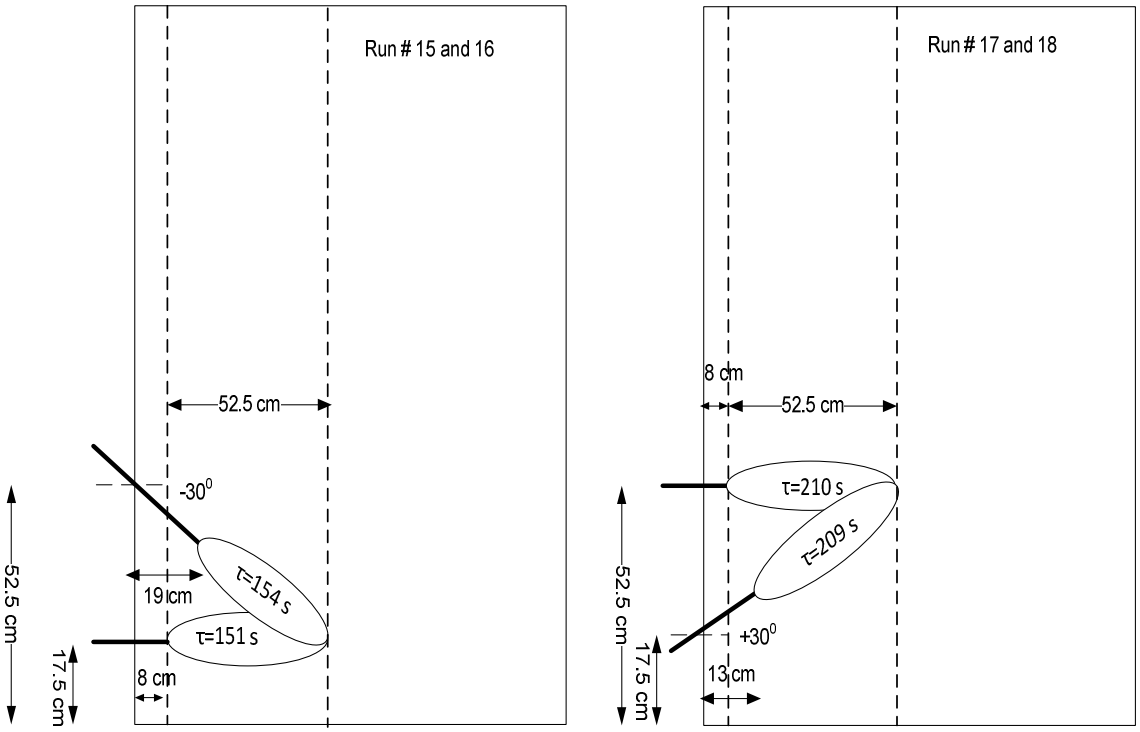

Figure 4.17. Comparison of the time constant of agglomerate breakage for the experiments with the same jet tip location and different nozzle spray angles (GLR = 1.5 wt% and fluidization velocity = 0.2 m/s)

4.7 Conclusions

This study identifies the parameters with predominant effect on agglomerate formation and agglomerate breakage during the injection of liquid feed in a gas-solid fluidized bed:

- The predominant factor for agglomerate formation is the bed bubble volume fraction at the nozzle tip, where gas bubbles promote solids entrainment and mixing within the jet cavity.
- For agglomerate breakage, the predominant factor is the bubble volume fraction at the jet tip, where gas bubbles interact with the freshly formed agglomerates.

The results for various nozzle inclinations verified the dominant effects of bed hydrodynamics at the nozzle and jet tips on the distribution of liquid on solid particles. The nozzle inclination has no measurable effect on agglomerate formation, which is

primarily affected by the hydrodynamics at the tip of the nozzle, and on agglomeration strength, which is mainly influenced by the hydrodynamics at the tip of the jet cavity.

References

"U.S. National Library of Medicine.". (http://www.webwiser.nlm.nih.gov).

Ariyapadi, S., D. Holdsworth, C. Norley, F. Berruti and C. Briens. 2003. "Digital X-Ray Imaging Technique to Study the Horizontal Injection of Gas-Liquid Jets into Fluidized Beds." *International Journal of Chemical Reactor Engineering* 1 (A56).

Ariyapadi, S., F. Berruti, C. Briens, B. Knapper, R. Skwarok and E. Chan. 2005. "Stability of Horizontal Gas-Liquid Sprays in Open-Air and in a Gas-Solid Fluidized Bed." *Powder Technology* 155(3):161-174.

Ariyapadi, S., F. Berruti, C. Briens, J. McMillan and D. Zhou. 2004. "Horizontal Penetration of Gas-Liquid Spray Jets in Gas-Solid Fluidized Beds." *International Journal of Chemical Reactor Engineering* 2.

Base, T., E. Chan, R. Kennett and D. Emberley. 1999. "Nozzle for Atomizing Liquid in Two Phase Flow.".

Briens, C., F. Berruti, V. Felli and E. Chan. 2008. "Solids Entrainment into Gas, Liquid, and Gas-Liquid Spray Jets in Fluidized Beds." *Powder Technology* 184(1):52-57.

Briens, C., M. Dawe and F. Berruti. 2009. "Effect of a Draft Tube on Gas-Liquid Jet Boundaries in a Gas-Solid Fluidized Bed." *Chemical Engineering and Processing: Process Intensification* 48(4):871-877.

Bruhns, S. and J. Werther. 2005. "An Investigation of the Mechanism of Liquid Injection into Fluidized Beds." *AICHE Journal* 51(3):766-775.

Chan, E. W., S. McDougall and B. Knapper. 2004. "Fluid Coking Reactor with Mixing of Bitumens with Steam Carrier Gas and Spray Atomization Nozzle for Coking of Bitumens and Heavy Oils.".

Darabi, P., K. Pougatch, M. Salcudean and D. Grecov. 2010. "Agglomeration of Bitumen-Coated Coke Particles in Fluid Cokers." *International Journal of Chemical Reactor Engineering* 8.

Department of Physics and Astronomy. "*Dielectric Constant at 20 ^{o}C. Department of Physics and Astronomy, Georgia State University*.". (http://hyperphysics.phy-astr.gsu.edu.).

Gogolek, P. 1998. "Mathematicalmodeling of Fluctuations in Fluidized Bed Combustions." Queen's University, Kingston (ON), .

Hong, Ruoyu, Haibing Li, Jianmin Ding and Hongzhong Li. 2005. "A correlation equation for calculating inclined jet penetration length in a gas-solid fluidized bed." *China PARTICUOLOGY* 03(05):279-285 (http://www.worldscientific.com/doi/abs/10.1142/S1672251505000631).

House, P. K., C. L. Briens, F. Berruti and E. Chan. 2008. "Effect of Spray Nozzle Design on Liquid-Solid Contact in Fluidized Beds." *Powder Technology* 186(1):89-98.

Knapper, B. A., M. R. Gray, E. W. Chan and R. Mikula. 2003. "Measurement of Efficiency of Distribution of Liquid Feed in a Gas-Solid Fluidized Bed Reactor." *International Journal of Chemical Reactor Engineering* 1 (A35).

Leach, A., G. Chaplin, C. Briens and F. Berruti. 2009. "Comparison of the Performance of Liquid-Gas Injection Nozzles in a Gas-Solid Fluidized Bed." *Chemical Engineering and Processing: Process Intensification* 48(3):780-788. Retrieved 7 March 2013.

McCracken, T., A. Bennett, K. Jonasson, D. Kirpalani, Z. Tafreshi, T. Base, I. Base, D. Emberley, R. Kennett, D. Bulbuc and E. Chan. 2006. "*Mixing Arrangement for Atomizing Nozzle in Multi-Phase Flow*.".

McMillan, J., D. Zhou, S. Ariyapadi, C. Briens, F. Berruti and E. Chan. 2005. "Characterization of the Contact between Liquid Spray Droplets and Particles in a Fluidized Bed." *Industrial and Engineering Chemistry Research* 44(14):4931-4939.

Mohagheghi, M., M. Hamidi , F. Berruti , C. Briens and J. McMillan. 2013a. "The Effects of Liquid Properties and Bed Hydrodynamics on the Distribution of Liquid on Solid Fluidized Particles in a Cold-Model Fluidized Bed.".

Mohagheghi, M., M. Hamidi, F. Berruti, C. Briens and J. McMillan. 2013b. "Study of the Effect of Local Hydrodynamics on Liquid Distribution in a Gas-Solid Fluidized Bed using a Capacitance Method." *Fuel*.

Portoghese, F., L. Ferrante, F. Berruti, C. Briens and E. Chan. 2010. "Effect of the Injection-Nozzle Geometry on the Interaction between a Gas-Liquid Jet and a Gas-Solid Fluidized Bed." *Chemical Engineering and Processing: Process Intensification* 49(6):605-615.

Pougatch, K., M. Salcudean and J. McMillan. 2012. "Influence of Conical Nozzle Attachments on Horizontal Spray Dispersion in a Fluidized Bed." *Chemical Engineering Research and Design* 90(10):1506-1516.

Vaccaro, S., D. Musmarra and M. Petrecca. 1997. "Evaluation of the Jet Penetration Depth in Gas-Fluidized Beds by Pressure Signal Analysis." *International Journal of Multiphase Flow* 23(4):683-698.

Chapter 5

5. THE EFFECTS OF RELATIVE VELOCITY BETWEEN NOZZLE AND PARTICLES ON THE DISTRIBUTION OF INJECTED LIQUID IN A FLUIDIZED BED

5.1 Abstract

In Fluid Coking™ or Fluid Catalytic Cracking liquid feedstocks are injected into a bed of fluidized particles. In the Fluid Coking process, the fluidized bed includes a central, relatively dilute, core of primarily upward moving particles and an annular denser region where hot coke particles flow mostly downward and in which liquid feed is injected through several sets of nozzles located at different heights. In Fluid Cokers™, the uniform distribution of liquid droplets on solid particles has been shown to result in a higher yield of valuable liquid products and a better reactor operability. In this study, a cold model fluidized bed has been developed to investigate the impact of the velocity of particles, relative to the spray nozzle, on solid-liquid contact. In this cold model, the coke particles are fluidized and liquid is sprayed through a spray nozzle that moves at a specified velocity to provide the desired relative velocity between nozzle and solid particles. This design provided an inexpensive and accessible means to study the impact of bed hydrodynamics on the distribution of liquid on fluidized particles. It also makes it possible to determine the effect of the relative velocity between nozzle and particles independently of other bed hydrodynamic characteristics. The impacts of the fluidization velocity and of the relative velocity between nozzle and particles were, thus, studied independently. Capacitance sensors were used to determine the proportion of the sprayed liquid that was initially trapped in wet agglomerates, and the rate at which the trapped liquid was gradually released through agglomerate breakage.

For short injections of liquid, of less than about 2.5 s, there was no measurable impact of the injection duration on the wet agglomerates. In contrast, for a stationary nozzle, there was a degradation in the liquid distribution with the injection duration, and the agglomerates that were formed took longer to release their trapped liquid. Finally, when

the nozzle passed more than once through the same bed region, there was a degradation in the liquid distribution.

5.2 Introduction

A fluidized bed is the essential part of many processes, such as Fluid Coking™ or Fluid Catalytic Cracking, where liquid feedstocks are injected into a bed of particles. The Fluid Coking™ process is used for upgrading bitumen and residual oils. In the Fluid Coking™ process, bitumen is atomized with steam into a fluidized bed of hot coke particles through several sets of spray nozzles arranged at different heights. Upon contact with the hot particles, the bitumen heats up and thermal cracking occurs. The lighter hydrocarbons cracking products rise up through the coker bed and are removed from the top of the bed and condensed to produce "synthetic crude". The remaining heavy hydrocarbons and the solid by-product from the cracking reactions, which is called coke, remain on the surface of the hot coke particles that flow down to the stripper. In the stripper, interstitial hydrocarbon vapors are removed with steam and then the coke particles are transported to the burner. The burner provides the required energy for re-heating the coke particles by burning a portion of the coke, and the re-heated particles are then sent back to the reactor (Bi et al. 2005; Hammond et al. 2003; Song et al. 2006).

When liquid is sprayed into a fluidized bed with atomization nozzles operating with a practical flow of atomization gas, wet agglomerates are formed (Bruhns and Werther 2005). Heat and mass transfer limitations within such agglomerates reduce the yield of valuable liquid product from Fluid Cokers™ (Hammond et al. 2003; Song et al. 2006) through two mechanisms. First, the slower reaction rate of the liquid increases the yields of undesired solid coke. Secondly, when there are agglomerates with a high liquid content or of a large size, the bed temperature needs to be increased to ensure that most of the liquid is converted to vapors and coke before the agglomerates reach the stripper and, thus, prevent stripper fouling that would lead to a premature shutdown; the higher temperature increases the conversion of hydrocarbon vapors to undesired permanent gases. House (2007) developed a model for Fluid Cokers which predicts the product yield considering heat transfer, mass transfer and chemical kinetics within bitumen-coke agglomerates. Gray et al. (2004) developed a kinetic model for cracking and

devolatization of bitumen residue in Fluid Cokers that considers the reaction kinetics, mass transfer, and vapour-liquid equilibrium.

Various experimental methods have been used in studies dealing with the distribution of liquid on solid particles in a fluidized bed. With evaporative liquids, the local bed temperature provides indirect information on the liquid distribution (Bruhns and Werther 2005; Fan et al. 2001). Bruhns and Werther (2005) found that even when the temperature of the fluidized bed is higher than the boiling point of the injected liquid, not all the injected liquid is instantaneously vaporized due to agglomerate formation. They proposed a model of agglomerate formation based on their experimental results. The processes through which liquid is distributed can be visualized with capacitance tomography or X-rays. Fan et al. (2001) developed electric capacitance tomography for real time imaging of a gas-solid fluidized bed with an evaporative liquid jet, and used this method to study the distribution of bubbles in gas-solid fluidized bed with and without an evaporative liquid jet. Ariyapadi et al. (2003) studied the expansion angle of the gas-liquid jet and its penetration distance into a fluidized bed using an X-ray imaging system.

The concentration of the liquid that is not trapped in agglomerates and, therefore, wetting individual moving particles can be obtained from bed conductivity or capacitance measurements, which are rapid, accurate and non-invasive. Conductivity measurements are restricted to systems with a large difference between liquid and particles conductivities (Ali Zirgachian et al. 2013; Farkhondehkavaki 2012; Leach et al. 2008). Capacitance measurements can be applied not only to systems where water is injected in a bed of sand or coke particles but, also, to systems with hydrocarbon liquids (Mohagheghi et al. 2013; Mohagheghi et al. 2014). By accounting for liquid evaporation, conductivity or capacitance measurements in a fluidized bed after the liquid injection can provide the rate at which liquid is released from agglomerates as they break up (Hadi 2009; Mohagheghi et al. 2013; Mohagheghi et al. 2014).

More sophisticated and time-consuming methods must be used to obtain the size distribution and liquid content of the wet agglomerates. Morales (2013) simulated bitumen in the Fluid Coker^{TM} with a solution of Plexiglas^{TM}, Acetone, and Pentane. The

authors injected this solution in a fluidized bed of silica sand particles at about 60 ^{0}C to simulate the rate of liquid evaporation in Fluid Cokers. The authors measured the amount and size of the resulting, solidified, agglomerates that were recovered by sieving the bed material. The concentration of Plexiglas^{TM} inside the agglomerates was obtained by using a solvent to dissolve the Plexiglas^{TM} trapped within the agglomerates, and measuring the dissolved Plexiglas concentration in the resulting liquid. House (2007) and Farkhondehkavaki (2012) used a similar method with an aqueous sugar solution instead of a Plexiglas^{TM} solution. Both Plexiglas^{TM} and sugar solution methods are time consuming since to get information on the agglomerate size distribution, the whole bed should be emptied and sieved with different mesh sizes.

Some publications addressed the key parameters that affect the liquid - solid contact efficiency in a fluidized bed as:

- spray nozzle design
- atomization gas flowrate of spray nozzle
- superficial fluidization velocity in the bed

Several publications reported on the effect of the spray nozzle design on the distribution of liquid injected into a fluidized bed. House et al. (2008) demonstrated that modifications of the standard spray nozzle design, such as incorporating a shroud, can improve the liquid distribution. McMillan et al. (2005) showed that adding a draft tube just downstream of the nozzle tip, in the fluidized bed, can greatly improve the liquid distribution by enhancing turbulence within the spray jet cavity. Leach et al. (2008) developed a triboelectric technique to assess the liquid-solid contact efficiency in a cold model fluidized bed. The authors used this technique to study the effect of nozzle geometry and the atomization gas flowrate by defining a nozzle performance index to characterize the contact efficiency between atomized liquid and solid particles.

Ali Zirgachian et al. (2013) studied the effect of the atomization gas flowrate on the liquid distribution on solid particles in a large scale cold model, using commercial-scale spray nozzles. The authors found that a higher atomization gas flowrate results in better distribution of liquid on solid particles. Tafreshi et al. (2002) studied the impact of two

phase feed characteristics, such as the atomization gas flowrate, in a commercial scale injector on the efficiency of Fluid Cokers, by measuring the droplet size and spray dispersion. The authors concluded that using more atomization gas results in a more consistent dispersed bubble flow and an increased Coker efficiency.

Local bed hydrodynamics affect the formation of agglomerates in a fluidized bed. Mohagheghi et al. (2014) investigated the impact of superficial fluidization velocity on the distribution of liquid on solid particles in a cold model fluidized bed with a liquid whose properties at room temperature are similar to those of the liquid feed used at high temperature in commercial Fluid Cokers. They found that a higher fluidization velocity results in weaker agglomerates. Saha (2012) studied the impact of interactions between a spray jet cavity and a high velocity attrition gas jet on the agglomerate size distribution. They found that, even with no direct interaction between the attrition jet and the liquid spray jet, there is a reduction in the amount of macro agglomerates as they break to drier micro-agglomerates, which are preferable in Fluid Cokers. Mohagheghi et al. (2014) investigated the impact of local bed hydrodynamics on the agglomerate properties by introducing additional gas locally. They showed that introducing extra gas below the jet tip greatly reduces the strength of the agglomerates.

Bi et al. (2005) studied the impact of bed hydrodynamics in a scaled down cold model Fluid Coker, using pressure fluctuation measurements, and showed that the bed hydrodynamics are mainly affected by the superficial gas velocity and the solid circulation rate. House et al. (2004) investigated the impact of liquid-solid mixing on the liquid yield from Fluid Cokers. They concluded that enhancing liquid-solid mixing can improve the liquid yield by up to 0.6 wt% and decrease the coke yield by up to 2 wt%.

In a Fluid Coker, the fluidized bed includes a central, relatively dilute, core of upward moving particles and an annular denser region where hot coke particles flow downward and in which liquid feed is injected through several sets of nozzles located at different heights. At the top of the Fluid Coker, the bitumen is injected in a region where particles flow with a velocity of about 1 m/s, while at the bottom of the reactor, the bitumen is injected in a region where particles flow at a velocity of about 0.5 m/s (Song et al. 2004).

Figure 5.1 shows a schematic diagram of upward and downward flowing particles in a Fluid Coker. The annular denser region is thicker at the top of the bed than at the bottom of the bed. There is no published work on the effect of the relative velocity between particles and spray nozzle on the liquid-solid contact efficiency in a fluidized bed, although it varies greatly with location in actual Fluid Cokers. This study intends to use a cold model fluidized bed to investigate the effect of the relative velocity between particles and spray nozzle on liquid-solid contact.

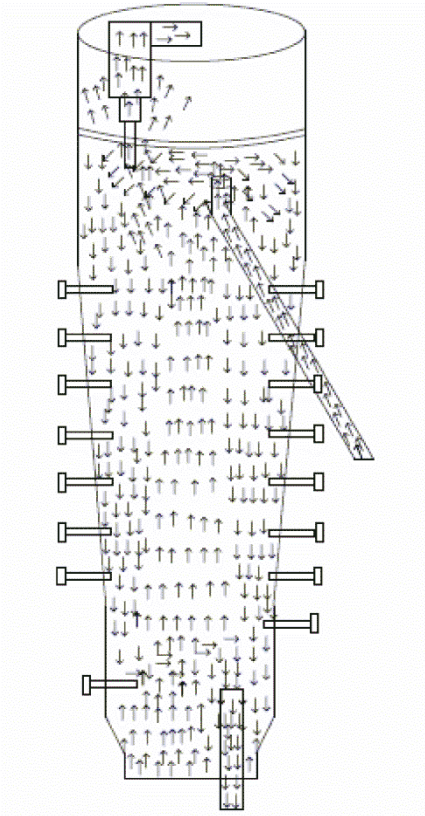

Figure 5.1. Schematic diagram of upward and downward flowing particles in a Fluid Coking reactor (Berruti, 2000)

5.3 Experimental setup

This study used a rectangular cold model fluidized bed with a cross-section of 1.5 by 0.28 m and a height of 2 m equipped with a partitioned windbox to allow the introduction of fluidizing gas at different velocities in each half of the fluidized bed using separate banks

of sonic nozzles. Air and nitrogen were used as the fluidization and atomization gas, respectively. Figure 5.2a shows the experimental setup. Pressure transducers on the bed wall monitored the pressure at different heights, from which the bed pressure drop and the bed height were calculated. Two thermocouples measured the bed and freeboard temperatures.

A convergent-divergent-convergent nozzle with a 2.2 mm diameter, which is a scaled-down version of an industrial nozzle, was used as the spray nozzle, except for calibration experiments. Figure 5.2b shows the schematic diagram of this nozzle (Base et al. 1999). The nozzle was moved vertically inside the bed with a rodless pneumatic cylinder (Figure 5.2c). It included a piston, which moved in an extruded aluminum cylinder containing a slot running the length of cylinder. The maximum length of travel for the piston was 1.2 m, which is acceptable for the total bed height of about 1.15 m at a fluidization velocity of 0.2 m/s. The nozzle was adjusted so that it could travel from a location 12 cm above the distributor plate to the top of the bed. The nozzle velocity was adjusted by varying the air pressure of the rodless cylinder. A PING)))^{TM} Ultrasonic Distance Sensor #28015 was used to measure the nozzle velocity. Figure 2c shows the sketch diagram of the moving nozzle. Two solenoid valves were installed on the atomization gas and liquid line to control the injection and two other solenoid valves were used on the rodless cylinder to control the up and down motion of the nozzle. Two Hall effect sensors were used to control the position of the nozzle. All solenoid valves and sensors were wired to an EATON controller (Easy 500 Intelligent Relays) and programmed to control motion, injection and location of the nozzle.

Varsol^{TM} was used as liquid feed and mixed with atomization gas in a premixer before being injected through a spray nozzle into the fluidized bed of coke particles as shown in Figure 5.2c (McCracken et al. 2006). The flowrate of the atomization gas was set with a calibrated sonic nozzle and a pressure regulator. For all experiments except calibration experiments, the liquid flowrate was 55 g/s.

a)

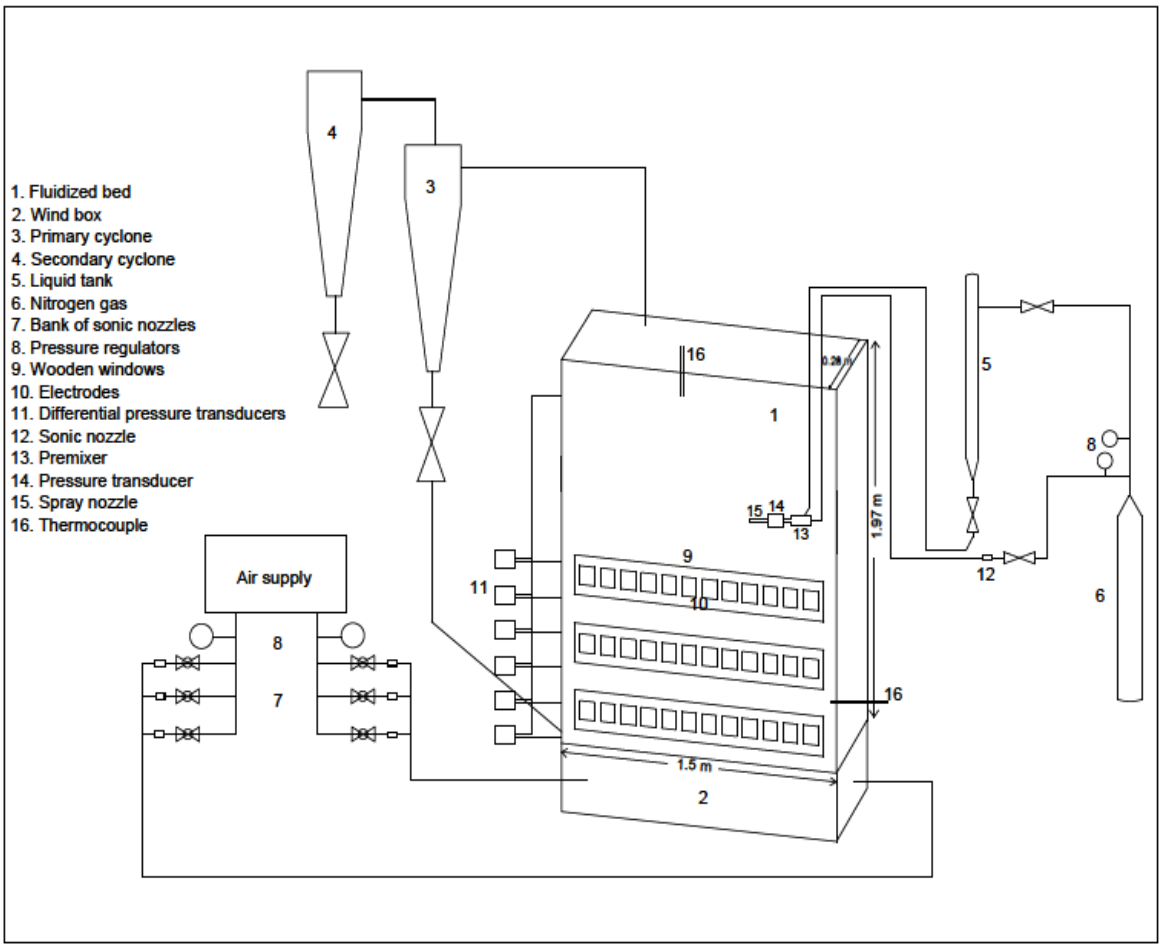
1. Fluidized bed
2. Wind box
3. Primary cyclone
4. Secondary cyclone
5. Liquid tank
6. Nitrogen gas
7. Bank of sonic nozzles
8. Pressure regulators
9. Wooden windows
10. Electrodes
11. Differential pressure transducers
12. Sonic nozzle
13. Premixer
14. Pressure transducer
15. Spray nozzle
16. Thermocouple
Air supply
1.97 m
1.5 m

b)

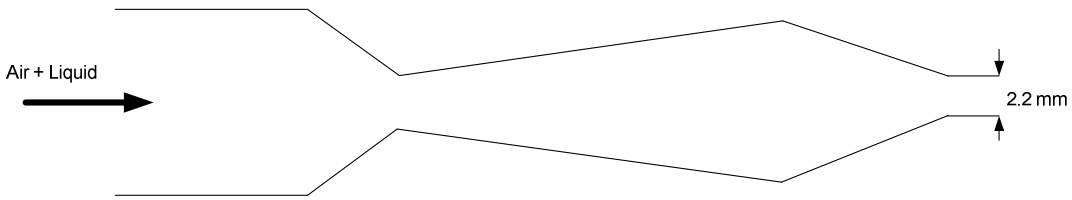
Air + Liquid
2.2 mm

c)

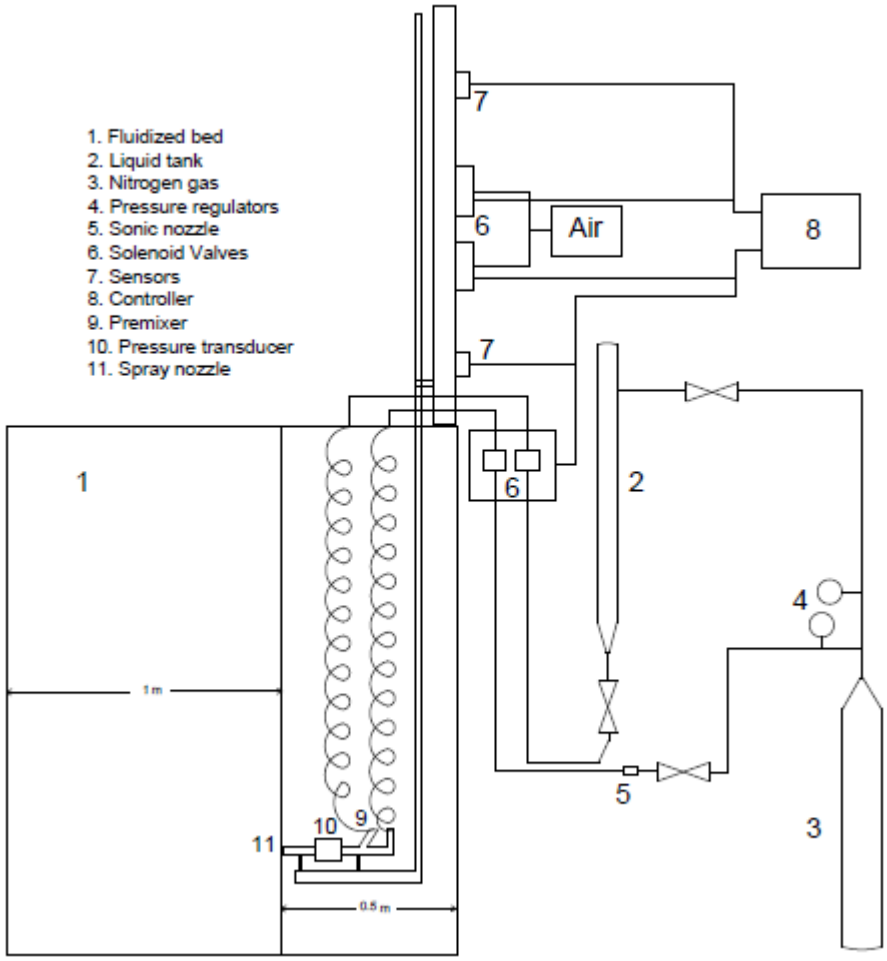

Figure 5.2. a) Schematic diagram of experimental setup; b) Schematic diagram of spray nozzle; c) Schematic diagram of Moving nozzle

5.4 Measuring system

Some of the injected liquid from the spray nozzle is normally trapped within agglomerates formed with the fluidized bed solids, while the remainder is "free liquid", which forms a thin layer on individual particles (Ariyapadi et al. 2003; Bruhns and Werther 2005; Knapper et al. 2003). A capacitance method was used as a measuring system in this study. It determines the relative permittivity of the bed between each set of electrodes. In this study, Varsol™ was used as the liquid with a relative permittivity of 3 (U.S. National Library of Medicine). The relative permittivity of the bulk fluid coke was experimentally determined to be 7 by comparing the capacitance of air and bulk coke

measured in a small box (the relative permittivity of air is 1 (Department of Physics and Astronomy, Georgia State University). Preliminary experiments in the small box have shown that the capacitance of a wet bed is a linear function of the free liquid volume fraction, and liquid trapped within agglomerates had a negligible impact on the measured capacitance (Mohagheghi et al. 2014).

In the fluidized bed, the local capacitance was measured by thirty-two 8 × 10 cm electrodes placed inside one side of the wall, on three wooden windows at different lateral and vertical locations as shown in Figure 3. There were three 135 × 20 cm electrodes on the other side of the wooden windows connected to the signal generator. The capacitance meter used in this study was an AC based circuit with a differential noise cancelling system (Mohagheghi et al. 2014). In the circuit, an amplifier was connected to 32 electrodes through its virtual ground. A multiplexer switched between electrodes every 2.7 ms and a signal from each electrode was converted to DC by a RMS to DC converter. The DC signal was then transmitted to the computer by a microcontroller. Figure 4 shows a schematic diagram of the capacitance meter.

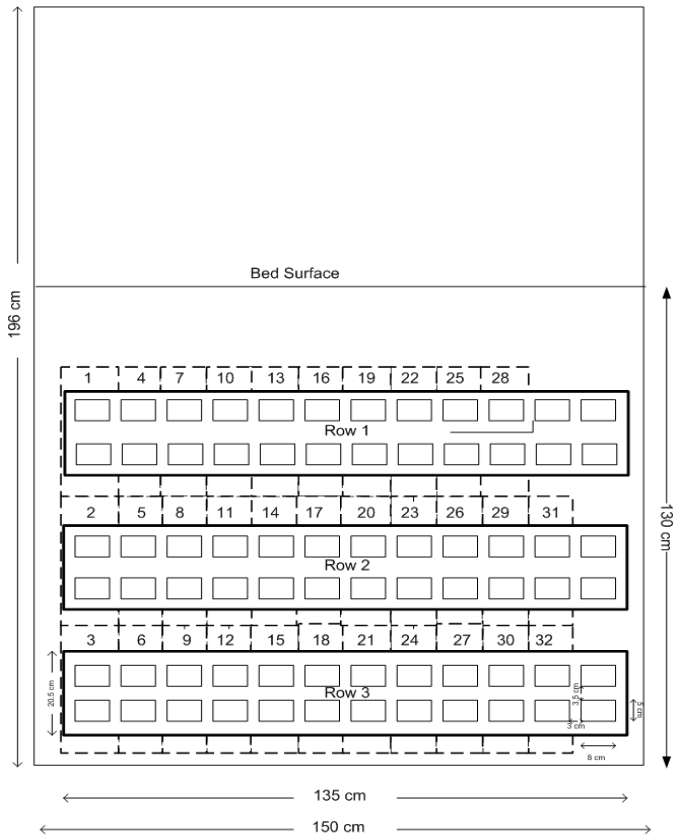

Figure 5.3. Position of electrodes on wooden windows of fluidized bed setup

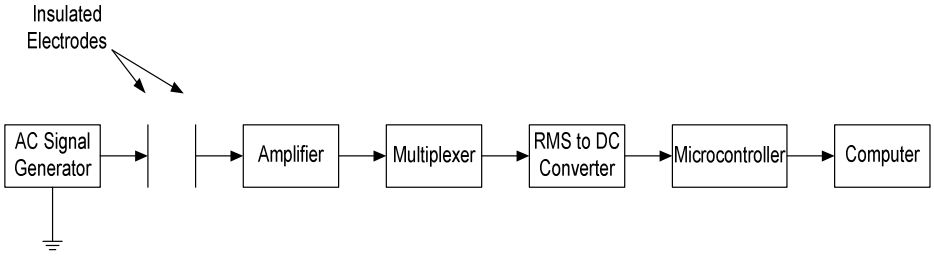

Figure 5.4. Schematic diagram of capacitance meter

5.5 Calibration experiments

An “ideal nozzle”, consisting of a straight cylindrical tube with a 3.6 mm diameter, was used for the calibration experiments. This special nozzle was defined as “ideal” as it ensured almost perfect distribution of liquid on individual solid particles because of its low liquid flow rate of about 1.5-3 g/s and its high atomization gas to liquid flowrate (about 50 wt%). Such a high atomization gas flowrate would be impractical in

commercial applications. With this “ideal nozzle”, all the injected liquid formed free liquid, since no liquid was trapped within agglomerates.

The capacitance was measured for each electrode corresponding to different amounts of free liquid. Then, it was normalized with respect to the value corresponding to dry particles. To obtain the calibration curves, the normalized capacitance for each electrode was plotted versus the amount of free liquid. For instance, Figure 5.5a and 5.5b show the calibration curves for electrodes 15 and 2 (the positions of these electrodes are shown in Figure 5.2).

a)

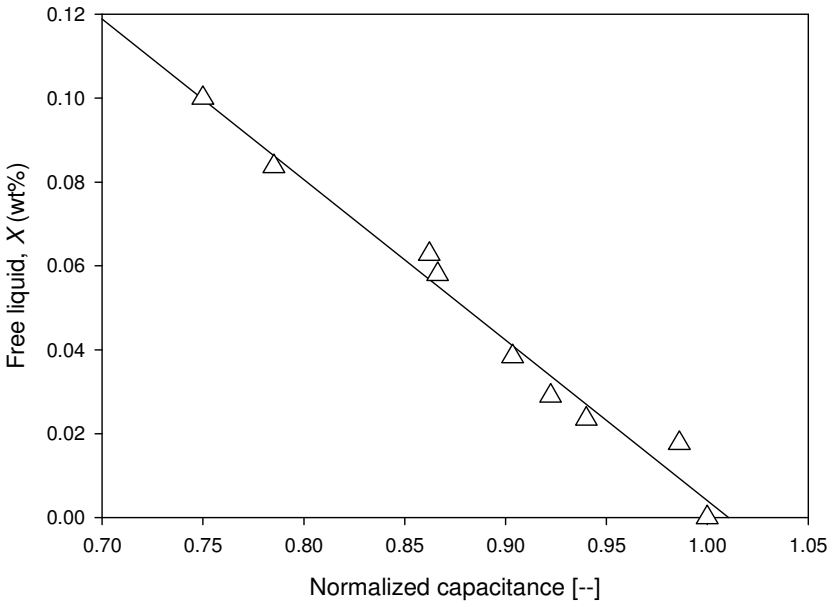

b)

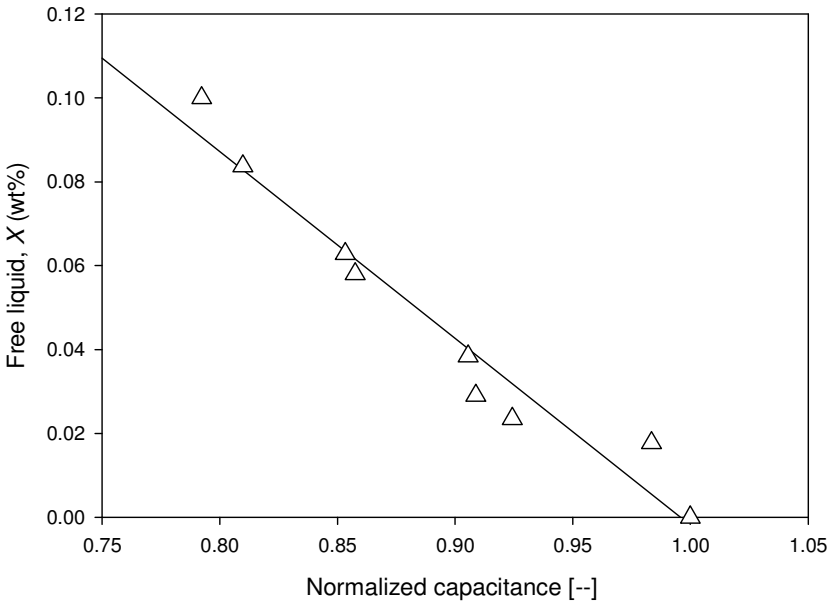

Figure 5.5. a) Calibration curve for electrode 15 (with Varsol^{TM}); b) Calibration curve for electrode 2 (with Varsol^{TM} liquid)

5.6 Experimental method

In this study, to prevent direct interactions between the spray jet and the distributor plate, the nozzle was not allowed to go below a position located 12 cm above the distributor plate, which was calculated from the angle of the jet, reported as 16^0 by Berruti et al. (2009). The positions of the Hall effect sensors were thus set to allow liquid injection between nozzle positions ranging from 12 to 102 cm above the distributor plate. Since the bed height was about 115 cm at a fluidization velocity of 0.2 m/s, no part of the spray jet exited the top surface of the bed. Based on the total length of injection for one pass, corresponding to the nozzle going down or up between 102 cm to 12 cm above the distributor plate, the number of moving passes was calculated for each nozzle velocity to cover a total injection time of 10 s.

5.6.1 Measuring the height of nozzle versus time

The location of the moving nozzle above the distributor plate at a specified velocity was measured as a function of time with a PING)))™ Ultrasonic Distance Sensor (Figure 5.2c), as shown in Figure 5.6. Figure 5.6 also shows the number of passes for four different velocities of the nozzle versus the injection time. The total injection time was kept constant at 10 seconds for all the experiments.

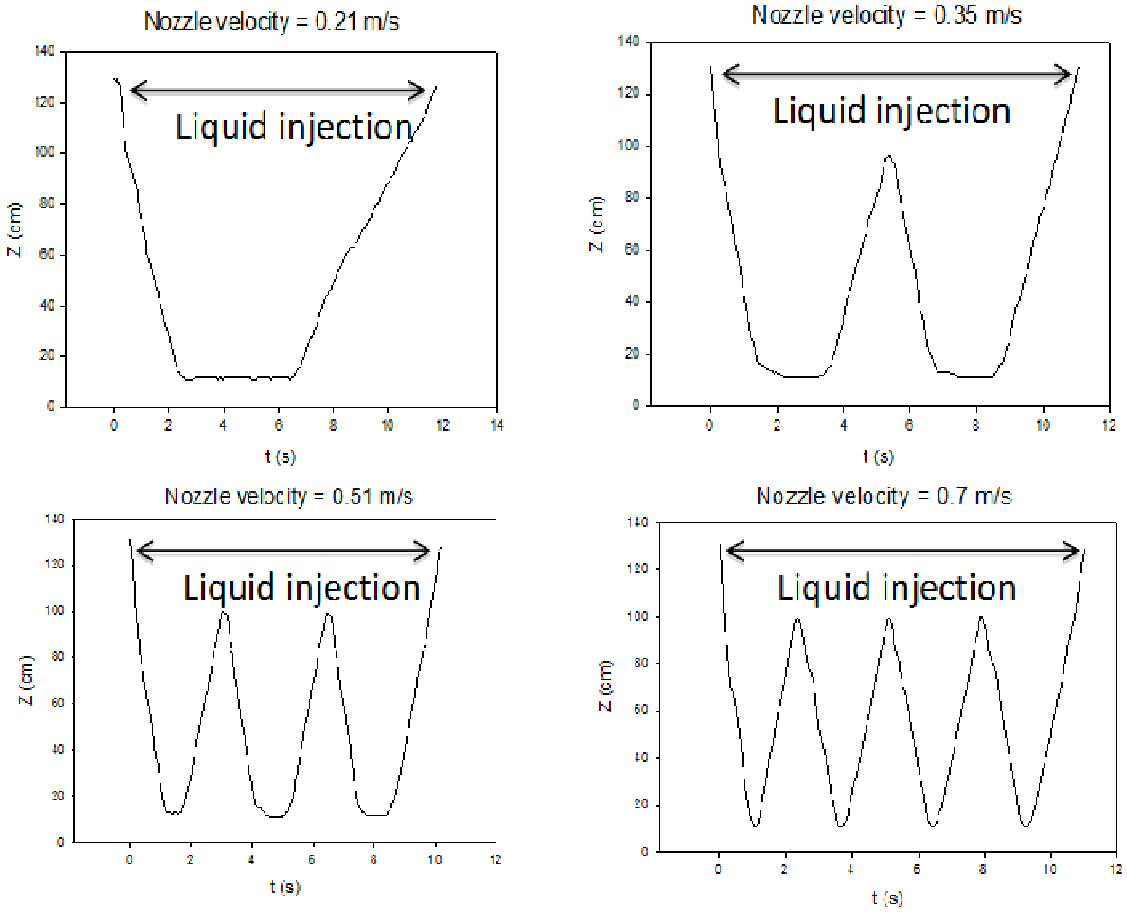

Figure 5.6. Height from distributor plate versus time measured by PING)))™ Ultrasonic Distance Sensor for four different velocities of nozzle

5.6.2 Method to summarize the liquid-solid contact information

To evaluate the interaction between liquid and solid particles, the initial liquid-solid contact and the strength of the resulting wet agglomerates were investigated. The initial distribution of liquid was calculated from the capacitance measured by each electrode. The free liquid right after injection is the average of the free liquid measured with the 32

electrodes, using individual calibration curves. To assess the strength of the agglomerates, the breakage rate of agglomerates was calculated from the total amount of liquid freed from agglomerates using the following procedure.

Two processes occurred simultaneously after injection: agglomerate breakage and liquid evaporation. To calculate the rate at which liquid was freed from agglomerates through agglomerate breakage, the impact of evaporation was removed as shown in Equation 5.1.

$$M_S\left[\frac{dX}{dt}\right]_{br} = M_S\left[\frac{dX}{dt}\right] - M_S\left[\frac{dX}{dt}\right]_e \tag{5.1}$$

The evaporation rate is a function of bed temperature, fluidization gas velocity and free liquid content. It was obtained from preliminary experiments using the same nozzle and conditions as the electrode calibration experiments, where all the liquid was free liquid, without any agglomerates.

The summation of free liquid right after injection and cumulative liquid freed resulting from agglomerate breakage gives the total, cumulative amount of freed liquid in the bed. As a result, *g(t)* is defined as the total percentage of injected liquid that is freed liquid:

$$g(t) = \frac{M_S}{M_L}\left[X|_{t=0} + \int_0^t \left[\left(\frac{dX}{dt}\right) - \left(\frac{dX}{dt}\right)_{cal}\right] dt\right] \tag{5.2}$$

where M_S is total mass of solid and M_L is total mass of liquid in kg.

g(t) was plotted versus time after injection for each experiment. An exponential curve was fitted to *g(t)* and the time constant of agglomerate breakage (τ) was calculated from this curve.

$$g(t) = 1 + (g(0) - 1)e^{-t/\tau} \tag{5.3}$$

where $g(0)$ represents the value of $g(t)$ at the end of injection.

For instance, Figure 5.7 shows the percentage of liquid trapped in agglomerates (1-*g(t)*) versus time for two different nozzle velocities. Equation 5.3 always gave a very good fit of all the experimental data.

The magnitude of the impact of liquid-solid contact on the initial liquid distribution and strength of agglomerates was evaluated by comparing the values of *g(0)* and the time constant τ of agglomerate breakage. Figure 5.8 shows *g(0)* and the time constant of agglomerate breakage, τ, for two different nozzle velocities. The results show that the required time to compensate the difference between values of *g(0)* for nozzle velocities of 0.21 m/s (2 passes) and 0.7 m/s (8 passes) is about 10 seconds, which is negligible when compared to the time constant of agglomerate breakage. It can be concluded that the impact of liquid-solid contact on the strength of the agglomerates is more significant than its impact on g(0). Therefore, this study reports the time constant of agglomerate breakage for all the experiments.

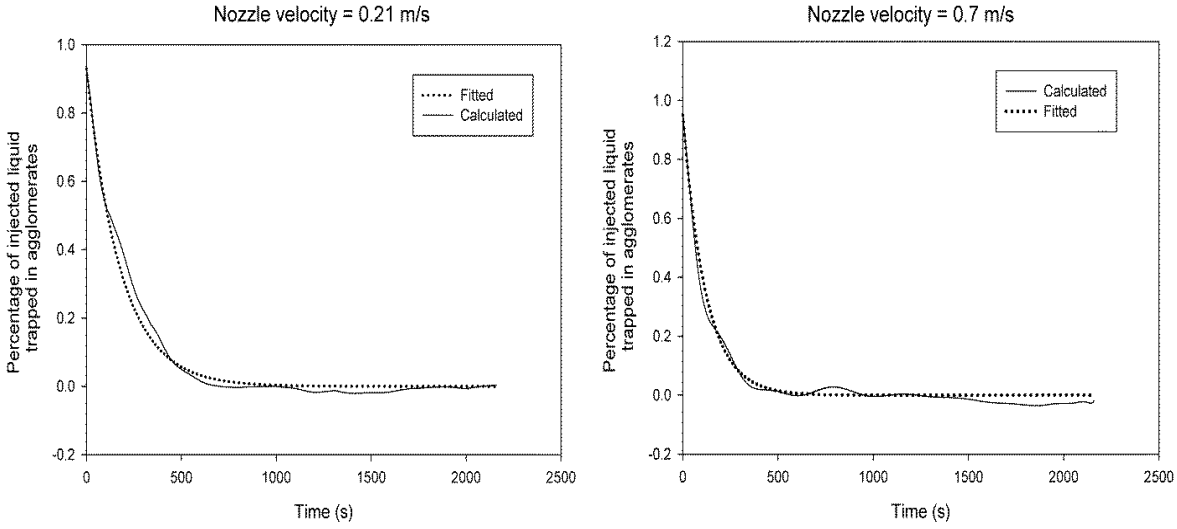

Figure 5.7. Percentage of liquid trapped in agglomerates versus time for two different nozzle velocities (Fitted values were obtained with Equation 5.3)

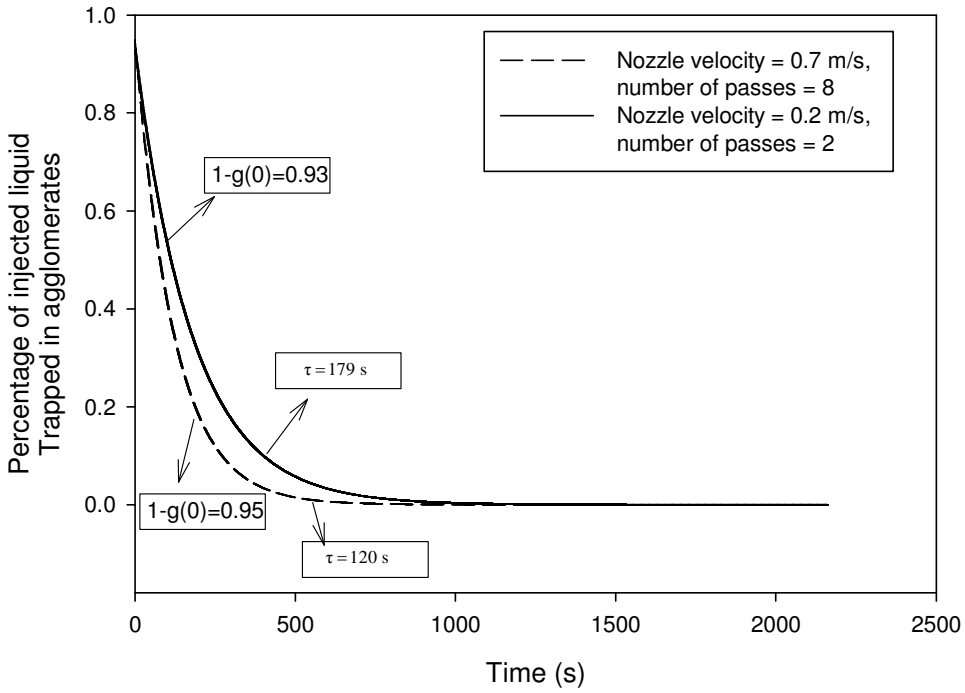

Figure 5.8. Comparing the percentage of injected liquid trapped in agglomerates versus time for two different nozzle velocities and number of passes

5.6.3 Impact of direction of the moving nozzle on liquid-solid contact

In industrial Fluid Cokers, the liquid feed is mostly injected on particles of coke with a relative downward flowing velocity, especially at the top of the beds (Figure 5.1). Therefore, some experiments were performed to study the impact of the direction in which the nozzle is moving relative to the fluidized solids, using the same magnitude of the relative nozzle velocity. The controller was programmed in order to inject liquid either during upward or downward motion of the nozzle. Table 5.1 shows the experimental conditions of these experiments. The liquid flow rate was 55 g/s and total injected liquid in these experiments was 275 g. The experiments were repeated for the same conditions three times.

Figure 5.9 shows that there was a negligible effect of the direction of motion of the nozzle on the time constant of agglomerate breakage. Consequently, it can be concluded that the direction of motion of the nozzle, upward or downward, had negligible impact on

the stability of the agglomerates formed. Based on the results of this part, all the experiments using the moving nozzle were performed when the nozzle was moving both upward and downward, interchangeably.

Table 5.1. Experimental conditions for the moving nozzle with liquid injection when the nozzle is moving upward or downward

Experiment No.	Injection when nozzle moving:	Nozzle velocity (m/s)	Total injected liquid (g)	Liquid mass flow rate (g/s)	Fluidization velocity (m/s)
1	downward	0.325	275	55	0.2
2	upward	0.31	275	55	0.2
3	downward	0.62	275	55	0.2
4	upward	0.63	275	55	0.2

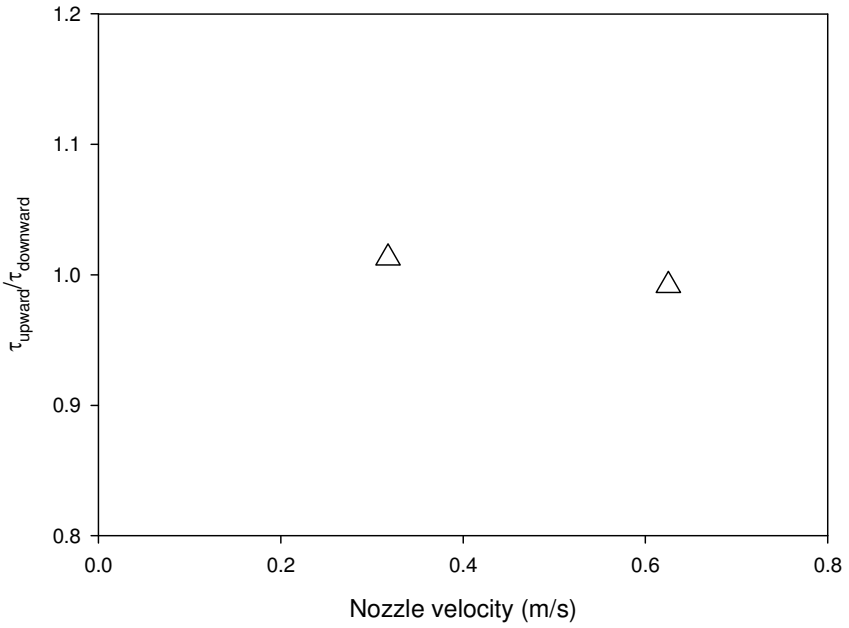

Figure 5.9. Time constant of agglomerate breakage for injecting when nozzle is moving upward or downward (fluidization velocity = 0. 2 m/s, GLR = 1.5 wt%, total liquid = 275 g and liquid flowrate = 55 g/s)

5.7 Results and discussion

5.7.1 Estimate of liquid-solid contact at zero nozzle velocity

In order to compare the results of the moving nozzle with the stationary nozzle, a reference point for a zero nozzle velocity is needed, which corresponds to the average of the results from the stationary nozzle at the various locations from which the moving nozzle sprayed liquid into the fluidized bed. Therefore, some experiments at different nozzle heights, as shown in Table 5.2, were performed for the stationary nozzle with the same lateral position of the nozzle tip as for the moving nozzle, which was 50 cm from the bed wall. The experiments were repeated for the same conditions two times.

Table 5.2. Experimental conditions for stationary nozzle at different nozzle heights

Experiment No.	Height relative to distributor plate (m)	Lateral position relative to inner left-hand side wall (m)	Nozzle velocity (m/s)	Total injected liquid (g)	Liquid mass flow rate (g/s)	Fluidization velocity (m/s)
1	0.20	0.5	0	550	55	0.2
2	0.47	0.5	0	550	55	0.2
3	0.82	0.5	0	550	55	0.2

Figure 5.10a shows the time constant of agglomerate breakage versus height from the distributor plate. This figure illustrates that, with increasing height, the time constant of agglomerate breakage increases, which is consistent with previous results (Mohagheghi et al. 2014). In previous studies (Mohagheghi et al. 2014), it was shown that the bubble volume fraction decreases with height and that a higher bubble volume fraction results in weaker agglomerates, as confirmed by the results of the present study (Figure 5.10b). Equation 4 is the fitted curve of τ versus height from Figure 5.10a and Equation 5 shows the reference, average time constant of agglomerate breakage for the stationary nozzle, over the range of locations from which the moving nozzle sprayed liquid into the fluidized bed. Table 5.3 shows τ_{ref} for each nozzle velocity; it changes slightly due to

small differences in the time spent by the nozzle at each height for different nozzle velocities, as shown in Figure 5.6.

$$\tau = 82.42 + 17.46Z^{0.5} \tag{5.4}$$

$$\tau_{ref} = \frac{1}{T}\int_0^T \tau\big(Z(t)\big)dt \tag{5.5}$$

Table 5.3. Time constant of agglomerate breakage for reference point (nozzle velocity of zero)

Nozzle velocity (m/s):	0.2	0.35	0.51	0.7
τ_{ref} (s)	194.8	199.8	203.4	204.0

a)

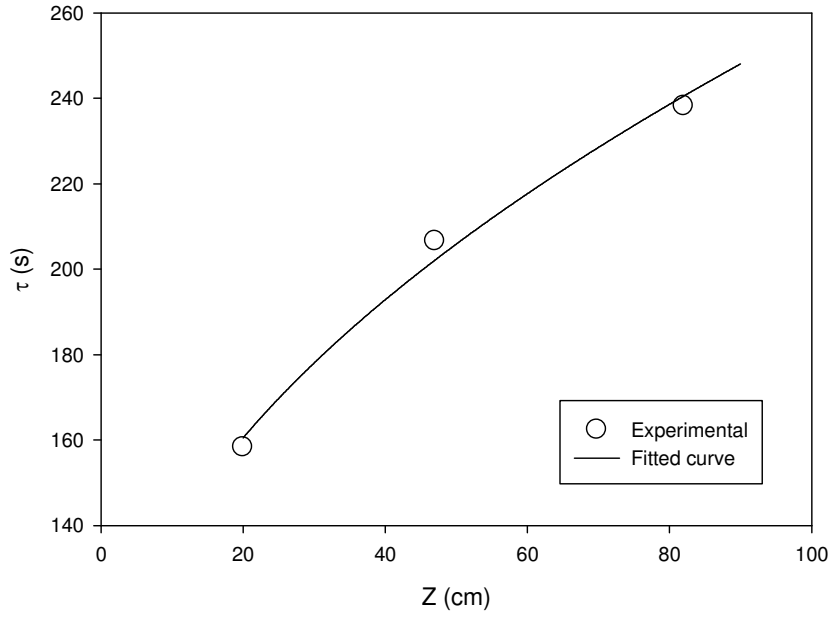

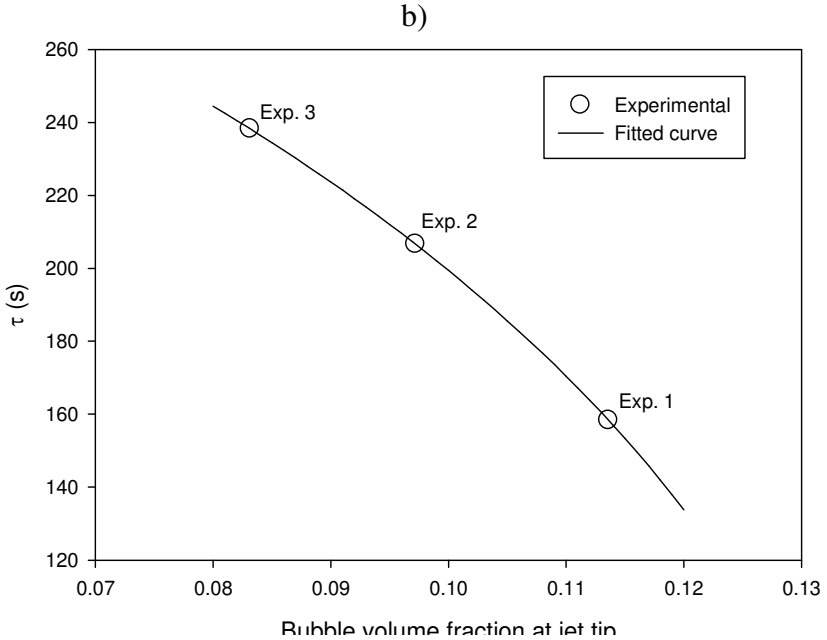

Figure 5.10. a) Time constant of agglomerate breakage versus nozzle height from the distributor for the stationary nozzle (fluidization velocity = 0.2 m/s, GLR = 1.5 wt%, total liquid = 550 g and injection time = 10 s, and lateral position = 50 cm); b) Time constant of agglomerate breakage versus bubble volume fraction near the jet tip (fluidization velocity = 0.2 m/s, GLR = 1.5 wt%, total liquid = 550 g and injection time = 10 s, and lateral position= 50 cm)

5.7.2 Impact of moving nozzle on liquid-solid contact

To investigate the impact of the velocity of solid particles on the jet bed interaction, some experiments were performed at different nozzle velocities. Two cases were considered for these experiments:

- Single nozzle pass (one time moving up or down of the nozzle)
- Multiple nozzle passes

5.7.3 Impact of single nozzle pass on liquid-solid contact

For single nozzle pass experiments, due to limitation of bed height, experiments were performed with either an injection duration of 2.5 s (nozzle velocity of 0.2 m/s) or an injection duration of 5 s (nozzle velocity of 0.4 m/s).

Table 5.4 shows the experimental conditions for experiments that were conducted for a single pass of the moving nozzle and for a stationary nozzle with the same injection

duration. The experiments were repeated for the same conditions two times. The time constant of agglomerate breakage was calculated for these experiments. Since the duration of injection for stationary nozzle experiments in this section is less than 10 s, the time constant of agglomerate breakage was calculated from the described method in section 5.7.1 for the related duration of injection.

Table 5.4. Experimental conditions for a moving nozzle with single pass experiments

Run #	Nozzle velocity (m/s)	Injection time(s)	Fluidization velocity (m/s)	GLR (wt%)
1	0.4	2.5	0.2	1.5
2	0	2.5	0.2	1.5
3	0.2	5	0.2	1.5
4	0	5	0.2	1.5

Figure 5.11 shows how the time constant of agglomerate breakage varied with the injection duration, for both stationary and moving (single pass) nozzles. For a 2.5 s injection, the time constant of agglomerate breakage is almost the same for both stationary and moving nozzles. The time constant of agglomerate breakage does not change with injection duration or nozzle velocity for a single pass moving nozzle, while, for a stationary nozzle, it increases by nearly 60 % when the injection duration is increased from 2.5 s to 5 s. The results demonstrate that for a nozzle velocity higher than 0.2 m/s, a moving nozzle performs about the same as a stationary nozzle for injections of 2.5 s or less, and gives much better results than a stationary nozzle for longer injection durations, as it then forms weaker agglomerates.

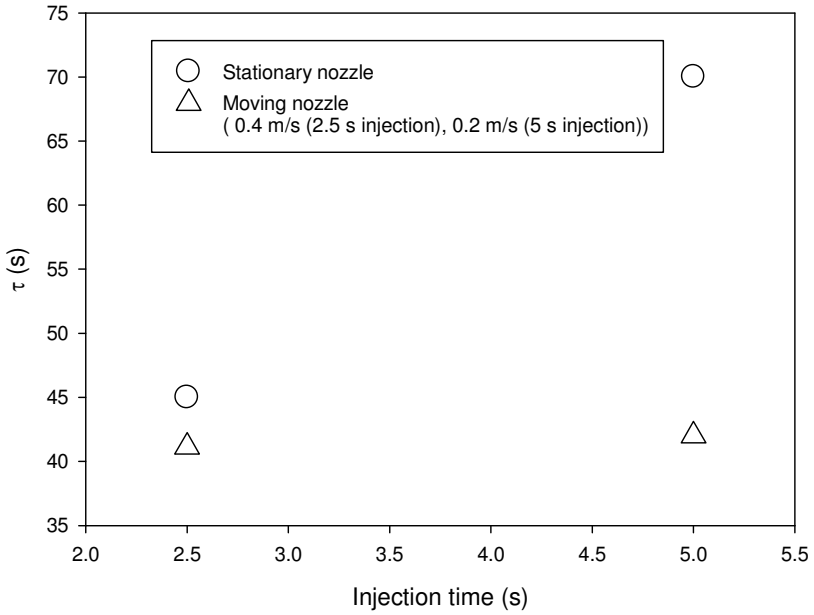

Figure 5.11. Measured time constant of agglomerate breakage versus injection time for both stationary and moving nozzles (single pass) (U_f = 0.2 m/s, GLR = 1.5 wt%, and δin = 0.5 m)

5.7.4 Impact of multiple nozzle passes on liquid-solid contact

Some experiments were performed at different nozzle velocities, a fluidization velocity of 0.2 m/s, and a total injection time of 10 s. The results were compared with the results of a stationary nozzle with the same injection duration as presented in Table 5.3. Table 5.5 shows the experimental conditions of these experiments. As described earlier, all the experiments were performed with both upward and downward injections. The total path length of injection for two passes, i.e. one "return trip" of the spray nozzle, was 1.80 m. To cover the injection time of 10 s, the number of moving nozzle passes was calculated for each nozzle velocity. The experiments were repeated for the same conditions three times.

Figure 5.12 shows the effect of nozzle passes on the time constant of agglomerate breakage. The time constant of agglomerate breakage at first increases sharply when going from a single pass to two nozzle passes. This may be due to the local wetness of the bed solids on the second nozzle pass.

Figure 5.12 shows that when the number of nozzle passes was increased further, past two, the time constant of agglomerate breakage steadily decreased with increasing number of passes. As the liquid flowrate was kept constant and the nozzle velocity was increased to increase the number of passes, this means that less liquid was delivered per pass. As the nozzle moved through the bed, it induced local bed mixing, reducing the local liquid concentration.

Table 5.5. : Experimental conditions for moving nozzle

Experiment No.	Nozzle velocity (m/s)	Number of moving passes	Δt (s)	Total injected liquid (g)	Liquid mass flow rate (g/s)	Fluidization velocity (m/s)
1	0.21	2	0	550	55	0.2
3	0.35	4	0	550	55	0.2
4	0.51	6	0	550	55	0.2
5	0.71	8	0	550	55	0.2

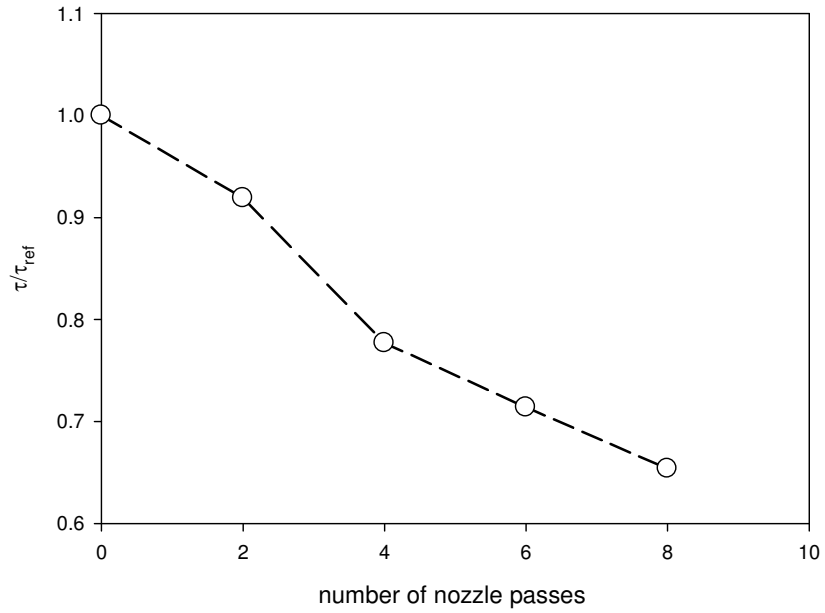

Figure 5.12. Ratio of the time constant of agglomerate breakage to the reference time constant (stationary nozzle) versus nozzle passes for U_f = 0.2 m/s, GLR = 1.5 wt%, total liquid = 550 g and injection time = 10 s (except for the single pass value, taken from Figure 5.11)

5.7.5 Impact of fluidization velocity

Previous studies have shown that, for a stationary nozzle, increasing the fluidization velocity during injection improves the initial distribution of liquid on solid particles and also results in the formation of weaker agglomerates (Mohagheghi et al. 2014). Figure 5.13a shows the ratio of the time constant of agglomerate breakage to the time constant of agglomerate breakage at a fluidization velocity during injection of 0.2 m/s versus the fluidization velocity during injection for a stationary nozzle; note that in all experiments, a fluidization velocity of 0.2 m/s was used after the liquid injection, so that Figure 5.13a shows the effect of fluidization velocity on agglomerate formation. Figure 5.13a confirms that increasing the fluidizing velocity during atomization results in weaker agglomerates that release liquid more quickly.

In this study, the impact of the fluidization velocity during injection on the strength of formed agglomerates was also investigated for a moving nozzle. Figure 5.13b shows the ratio of the time constant of agglomerate breakage to the time constant of agglomerate breakage at a fluidization velocity during injection of 0.2 m/s at two different fluidization

velocities during injection for a nozzle velocity of 0.51 m/s, for 6 nozzle passes; note that in all experiments, a fluidization velocity of 0.2 m/s was used after the liquid injection, so that Figure 5.13b shows the effect of fluidization velocity during injection on agglomerate formation. As with a stationary nozzle (Figure 5.13a), increasing the fluidizing velocity during atomization results in weaker agglomerates that release liquid more quickly.

a)

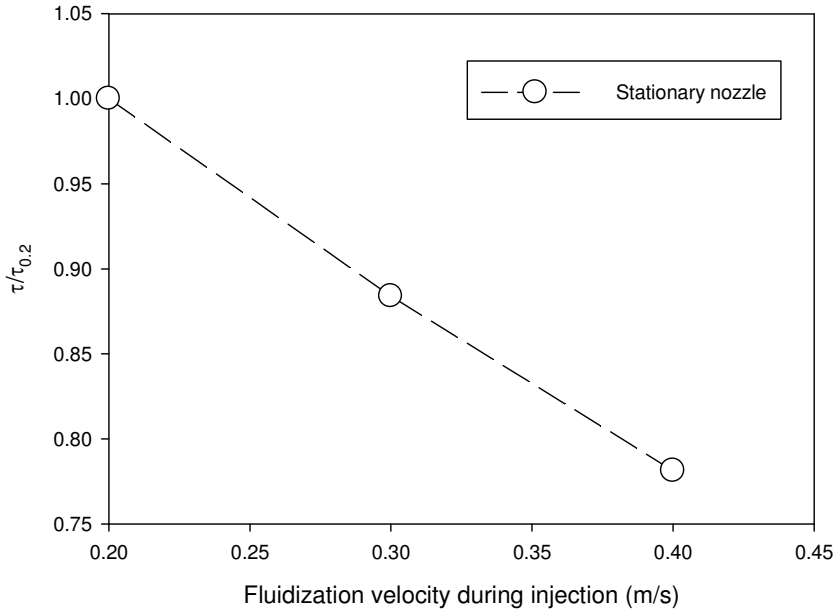

b)

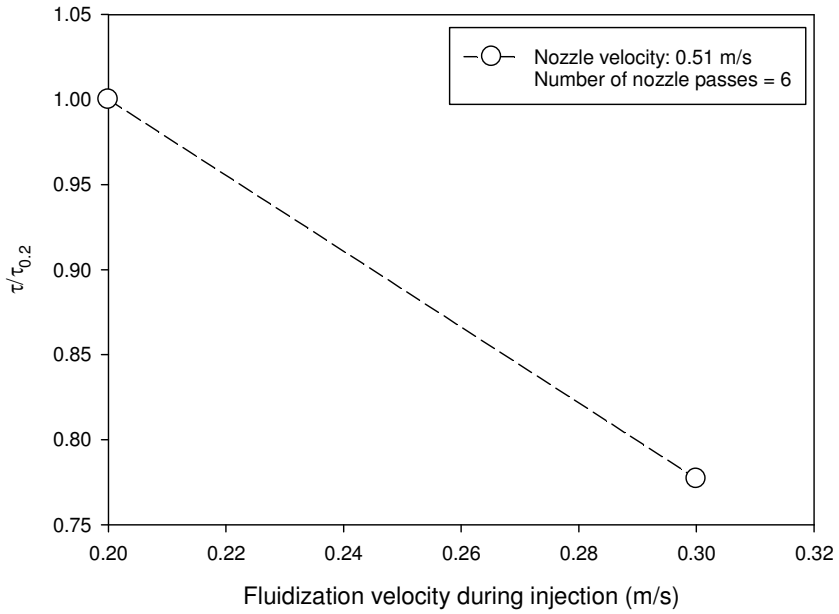

Figure 5.13. a) Ratio of time constant of agglomerate breakage to time constant at a fluidization velocity of 0.2 m/s versus fluidization velocity during injection for a stationary nozzle(GLR = 1.5 wt%, total liquid = 550 g, injection time = 10 s, δin = 8 cm, and fluidization velocity after injection = 0.2 m/s); b) Ratio of time constant of agglomerate breakage to time constant at a fluidization velocity of 0.2 m/s versus fluidization velocity during injection (nozzle velocity = 0.5 m/s, GLR = 1.5 wt%, total liquid = 550 g, injection time = 10 s, δin = 0.5 m, and fluidization velocity after injection = 0.2 m/s)

5.8 Conclusions

For short injections of liquid, of less than about 2.5, there was no measurable impact of the injection duration on the wet agglomerates when using the moving nozzle. In contrast, for a stationary nozzle, there was a degradation in the liquid distribution with the injection duration, and the agglomerates that were formed took longer to release their trapped liquid.

When the nozzle passed more than once through the same bed region, there was a degradation in the liquid distribution.

The results of the experiments in this study also show that a higher fluidization velocity during injection by a spray nozzle results in the formation of weaker agglomerates, which break up more easily, whether the nozzle is moving or not.

References

"U.S. National Library of Medicine.". (http://www.webwiser.nlm.nih.gov).

Ali Zirgachian, M., M. Soleimani, C. Briens and F. Berruti. 2013. "Electric Conductance Method for the Assessment of Liquid-Gas Injection into a Large Gas-Solid Fluidized Bed." *Measurement: Journal of the International Measurement Confederation* 46(2):893-903.

Ariyapadi, S., D. Holdsworth, C. Norley, F. Berruti and C. Briens. 2003. "Digital X-Ray Imaging Technique to Study the Horizontal Injection of Gas-Liquid Jets into Fluidized Beds." *International Journal of Chemical Reactor Engineering* 1 (A56).

Base, T., E. Chan, R. Kennett and D. Emberley. 1999. "Nozzle for Atomizing Liquid in Two Phase Flow.".

Berruti, F., M. Dawe and C. Briens. 2009. "Study of Gas-Liquid Jet Boundaries in a Gas-Solid Fluidized Bed." *Powder Technology* 192(3):250-259.

Berruti, F. 2000. "Coker 2000 Project (video)." *University of Saskatchewan.*

Bi, H. T., J. R. Grace, C. J. Lim, D. Rusnell, D. Bulbuc and C. A. McKnight. 2005. "Hydrodynamics of the Stripper Section of Fluid Cokers." *The Canadian Journal of Chemical Engineering* 83(2):161-168.

Bruhns, S. and J. Werther. 2005. "An Investigation of the Mechanism of Liquid Injection into Fluidized Beds." *AICHE Journal* 51(3):766-775.

Department of Physics and Astronomy. "*Dielectric Constant at 20 ^{o}C. Department of Physics and Astronomy, Georgia State University*.". (http://hyperphysics.phy-astr.gsu.edu.).

Fan, L. -., R. Lau, C. Zhu, K. Vuong, W. Warsito, X. Wang and G. Liu. 2001. "Evaporative Liquid Jets in Gas-Liquid-Solid Flow System." *Chemical Engineering Science* 56(21-22):5871-5891.

Farkhondehkavaki, M. 2012. "Developing Novel Methods to Characterize Liquid Dispersion [Dissertation]." Western University, London (ON), .

Gray, M. R., W. C. McCaffrey, I. Huq and T. Le. 2004. "Kinetics of Cracking and Devolatilization during Coking of Athabasca Residues." *Industrial and Engineering Chemistry Research* 43(18):5438-5445.

Hadi, B. 2009. "Characterization of Multi-Phase Flow in Circulating Fluidized Beds using Electrical Capacitance Tomography " Western University, .

Hammond, D. G., L. F. Lampert, C. J. Mart, S. F. Massenzio, G. E. Phillips, D. L. Sellards and A. C. Woerner. 2003. "Refining: Review of Fluid Bed Coking Technologies." *Petroleum Technology Quarterly* 8(5):27-31, 33.

House, P. K. 2007. "Interaction of Gas-Solid Jets with Gas-Solid Fluidized Beds: Effect on Liquid-Solid Contact and Impact on Fluid Coking Operation " Western University, .

House, P. K., C. L. Briens, F. Berruti and E. Chan. 2008. "Effect of Spray Nozzle Design on Liquid-Solid Contact in Fluidized Beds." *Powder Technology* 186(1):89-98.

House, P. K., M. Saberian, C. L. Briens, F. Berruti and E. Chan. 2004. "Injection of a Liquid Spray into a Fluidized Bed: Particle-Liquid Mixing and Impact on Fluid Coker Yields." *Industrial and Engineering Chemistry Research* 43(18):5663-5669.

Knapper, B. A., M. R. Gray, E. W. Chan and R. Mikula. 2003. "Measurement of Efficiency of Distribution of Liquid Feed in a Gas-Solid Fluidized Bed Reactor." *International Journal of Chemical Reactor Engineering* 1 (A35).

Leach, A., F. Portoghese, C. Briens and F. Berruti. 2008. "A New and Rapid Method for the Evaluation of the Liquid-Solid Contact Resulting from Liquid Injection into a Fluidized Bed." 184(1):44.

McCracken, T., A. Bennett, K. Jonasson, D. Kirpalani, Z. Tafreshi, T. Base, I. Base, D. Emberley, R. Kennett, D. Bulbuc and E. Chan. 2006. "*Mixing Arrangement for Atomizing Nozzle in Multi-Phase Flow*.".

McMillan, J., D. Zhou, S. Ariyapadi, C. Briens, F. Berruti and E. Chan. 2005. "Characterization of the Contact between Liquid Spray Droplets and Particles in a Fluidized Bed." *Industrial and Engineering Chemistry Research* 44(14):4931-4939.

Mohagheghi, M., M. Hamidi, F. Berruti, C. Briens and J. McMillan. 2014. "The Effects of Injection Nozzle Location and Inclination on the Interaction between a Gas-Liquid Jet and a Gas Solid Fluidized Bed.".

Mohagheghi, M., M. Hamidi, F. Berruti, C. Briens and J. McMillan. 2013. "Study of the Effect of Local Hydrodynamics on Liquid Distribution in a Gas-Solid Fluidized Bed using a Capacitance Method." *Fuel*.

Mohagheghi, M., M. Hamidi, C. Briens, F. Berruti and J. McMillan. 2014. "The Effects of Liquid Properties and Bed Hydrodynamics on the Distribution of Liquid on Solid Fluidized Particles in a Cold-Model Fluidized Bed." *Powder Technology* 256:5-12.

Morales M, C. B. 2013. " Development and Application of an Experimental Model for the Fluid Coking™ Process " Western University, .

Saha, M. 2012. "Simultaneous Particle Agglomeration and Attrition in a High Temperature Fluidized Bed." Western University, .

Song, Xuqi, John R. Grace, Hsiaotao Bi, C. J. Lim, Edward Chan, Brian Knapper and Craig McKnight. 2006. "Experimental Simulation of the Reactor Section of Fluid Cokers: Comparison of FCC and Fluid Coke Particles." *The Canadian Journal of Chemical Engineering* 84(2):161-169.

Song, X., H. Bi, C. J. Lim, J. R. Grace, E. Chan, B. Knapper and C. McKnight. 2004. " Hydrodynamics of the Reactor Section in Fluid Cokers." *Powder Technology* 147:126.

Tafreshi, Z. M., D. Kirpalani, A. Bennett and T. W. McCracken. 2002. "Improving the Efficiency of Fluid Cokers by Altering Two-Phase Feed Characteristics." *Powder Technology* 125(2–3):234-241.

Chapter 6

6. MODELLING OF INTERACTIONS BETWEEN LIQUID-GAS SPRAY JET AND FLUIDIZED PARTICLES IN A GAS-SOLID FLUIDIZED BED (PART I: STATIONARY NOZZLE)

6.1 Abstract

In part I of this study, a model for the interactions between sprayed liquid and fluidized particles was developed for the case of a stationary spray nozzle and no net motion of the fluidized solids. The model provides the liquid concentration of the agglomerates that are formed at the tip of the jet cavity. This model was used to investigate the impact of parameters such as fluidization velocity during injection, nozzle atomization gas flowrate, nozzle location, nozzle inclination, and duration of injection on the resulting agglomerates. The model results were compared with experimental results and were found to provide consistent information on the liquid concentration of agglomerates.

6.2 Introduction

Gas-liquid spray jets into a fluidized bed are used in many processes such as Fluid Coking^{TM}, Fluid Catalytic Cracking (FCC), and gas-phase polymerization. In a Fluid Coker liquid feed is injected in a bed of fluidized hot coke particles through a set of steam-assisted nozzles located at different heights. Within a Fluid Coker^{TM} bed, there are significant variations in hydrodynamics in both axial and radial directions. In a Fluid Coker^{TM}, bitumen is injected in a region where particles flow with a velocity of about 1 m/s near the top of the reactor and about 0.5 m/s near the bottom of the reactor bed (Song et al. 2004).

In a Fluid Coker^{TM}, the interaction between the gas-liquid spray jet and solid particles greatly affects the yield of valuable products and operability, as poor contact results in the formation of liquid-solid agglomerates that survive long enough to adversely affect the process. Agglomerates that survive long enough decrease the yield of liquid products due to mass and heat transfer limitations (Hammond et al. 2003; Song et al. 2006). Gray et al. (2004) presented a model which predicts cracking reactions yield of Athabasca vacuum

residue. They developed this model to describe the kinetics of pyrolysis for vacuum residue. House (2007) combined the model from Gray et al. (2004) with heat transfer, mass transfer and chemical kinetics models for bitumen-coke agglomerates, and showed that liquid holdup and agglomerates survival time greatly impact liquid yield and operability. The model also predicted that large wet agglomerates have a high impact on the average liquid yield. Ali Zirgachian et al. (2013) combined experiments and modeling to show that, while heating rate did not affect the coke yield, mass transfer limitations within agglomerates greatly increased the coke yield, when compared to thin bitumen films.

Morales (2013) described how, when bitumen liquid is injected into a Fluid Coker, liquid is distributed onto the fluidized particles through three consecutive stages (Figure 6.1):

> Stage 1: Initial distribution of liquid sprayed in the form of fine droplets among entrained particles in the jet cavity formed by the spray. This initial distribution includes the impact of liquid droplets on the solids at the tip of the jet cavity.
>
> Stage 2: Wetting and spreading of the liquid on the surface of the particles and formation of agglomerates in the jet or at the jet tip. Note that the average liquid concentration of the agglomerates does not change during stage 2, but the manner in which the liquid is spread on the surface of the particles changes, which affects the next stage.
>
> Stage 3: Break-up of agglomerates due to shear forces in the fluidized bed and the destabilization of the wet agglomerates that results from the cracking of the bitumen and devolatilization of its products. In laboratory experiments with cold models, when liquid is injected into a bed at room temperature, with slow evaporation, as in the present study, the break-up mechanisms are different as there is no reaction and the break-up is caused solely by the shear forces in the fluidized bed.

Weber et al. (2009) studied the processes through which agglomerates break up (Stage 3 in Figure 6.1) in a cold model fluidized bed and found that they are controlled by

complex interactions of several parameters. They found that the superficial fluidization gas velocity controls the method of agglomerate destruction: as the superficial gas velocity is increased, the breakup process changes from pure erosion to a combination of erosion and fragmentation. Increasing the fluidization velocity greatly reduces the amount of agglomerates recovered from the fluidized bed, while the number of fragments in the fluidized bed increases. Weber et al. (2009) also showed that the liquid concentration within wet agglomerates has a considerable impact on the time that is required to break them up in a fluidized bed. Parveen et al. (2013) also found that agglomerates with a higher liquid content are more stable in a fluidized bed and that increasing gas superficial velocity increases the probability of breakage.

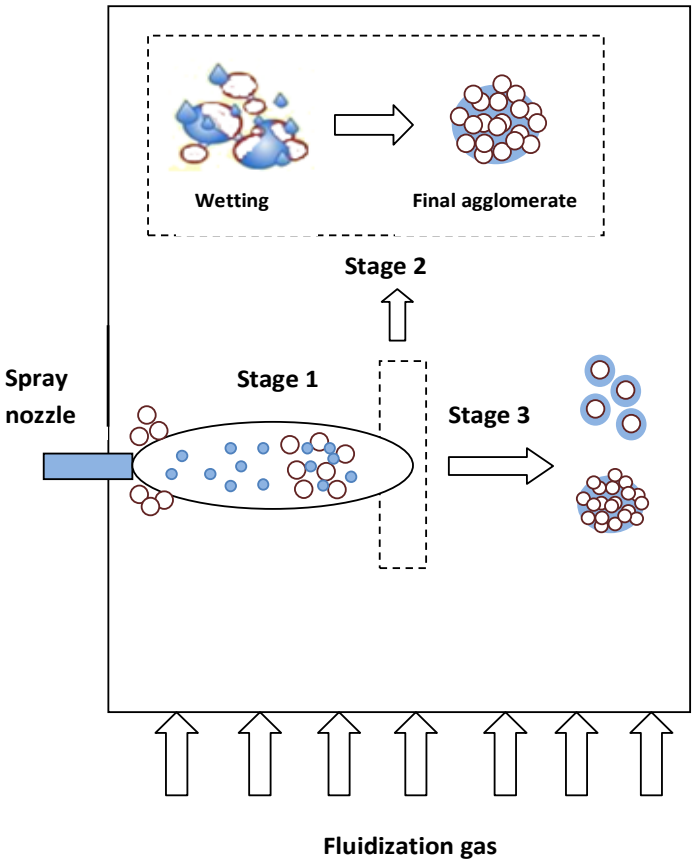

Figure 6.1. Stages of liquid distribution onto the fluidized particles

Various studies modeled gas-liquid spray jets and their interaction with solid particles in a fluidized bed (Stage 1 in Figure 6.1). Some studies focused on hot model fluidized beds. Li et al. (2010) modelled spraying of an evaporative liquid on hot fluidized solids in a riser using an Eulerian multi-fluid model. They focused on the collision mechanism and heat and mass transfer phenomena between hot particles and cold sprayed liquid, and did not focus on the parameters such the mass of particles interacting with droplets during total injection time which are mostly affected by bed and jet hydrodynamics and have considerable impact on the liquid concentration of formed agglomerates.

Some other studies addressed modelling of spray jet and its interaction with solids particles in a cold model fluidized bed. Ariyapadi et al. (2003b) developed a momentum-conservation model for the solid entrainment to the jet cavity. The model results were in good agreement with the experimental measurements (Briens et al. 2008). Ariyapadi et al. (2005) also proposed a model for the prediction of the mixing behaviour between liquid and solid particles within a spray jet using a spray nozzle with a draft tube attachment, located in the fluidized bed downstream of the nozzle tip. Pougatch et al. (2012) developed a model for interaction between jet and fluidized bed using two-fluid Eulerian-Eulerian model. The model was used for the evaluation of the effect of fluidization velocity on the liquid distribution in the fluidized bed. They used the kinetic theory of granular flow for the motion of solid particles and some empirical correlations for droplet-solid particles collisions in order to find the fraction of liquid that sticks to the particles. By modelling droplet-particle interactions, the model proposed by Pougatch et al. (2012) can predict not only the average liquid concentration of the agglomerates, but also the distribution of the liquid concentration in agglomerates. A drawback of this model is that it requires two empirical parameters that must be adjusted with experimental distributions of the liquid concentration in agglomerates (Pougatch et al. 2012). Pougatch et al. (2012) compared their model predictions with the distributions of the liquid concentration in agglomerates measured by McMillan et al. (2005) with and without a draft tube located downstream of the jet tip. The model can predict that the draft tube reduced the liquid concentration of the agglomerates, and they attributed the imperfect quantitative agreement between model predictions and experiments to the model used for droplet-particle interactions and moisture spreading.

There are some studies just on the modeling of agglomerate formation for systems that are naturally agglomerating (Saleh et al. 2003; Terrazas-Velarde et al. 2009), while in Fluid Cokers and also in our experiments, the system is not naturally agglomerating, which means that if the liquid is uniformly sprayed on particles, particles will not agglomerate. Our experiments used the Varsol^{TM} -coke system that is not naturally agglomerating as was described in our earlier study (Mohagheghi et al. 2014) and also based by McDougall et al. (2005). In Fluid Cokers and also in our experiments, with normally operated spray nozzles, agglomerates form during the initial interaction between spray jet and bed particles. These agglomerates are important in Fluid Cokers as the only agglomerates that are present in the Fluid Coker beds originated during this initial interaction and survived.

To the authors' knowledge, no model can accurately predict the impact of bed hydrodynamics or nozzle operating conditions on initial agglomerate properties. The contact between particles and liquid droplets in a gas-solid fluidized bed is affected by parameters such as spray nozzle location, fluidization velocity, atomization gas flowrate, and duration of injection (Ali Zirgachian et al. 2013; Farkhondehkavaki 2012; House et al. 2008; Mohagheghi et al. 2014; Portoghese et al. 2008). The liquid concentration of the agglomerates is the most important agglomerate property since it affects not only how agglomerates break up in the fluidized bed, and hence their size, but also the rate at which reactions proceed within the agglomerates. Thus, a model that could reliably predict the liquid concentration of the initial agglomerates resulting from interaction between sprayed liquid and solids particles would be very valuable. For example, it would allow for the quick and inexpensive exploration of conditions that would reduce the formation of wet, stable agglomerates.

The objective of this study is to develop a model that provides information on the liquid concentration of the initial agglomerates formed from contact between the gas-liquid spray jet and fluidized particles (Stage 1 in Figure 6.1). To avoid using empirical parameters, the model will take advantage of the very large body of knowledge on gas-solid fluidized beds. The impacts of spray quality and bed hydrodynamics such as atomization gas flowrate, fluidization velocity during injection, and nozzle location and

inclination were explored with this model, and related to previous experimental results. Part I of this publication is restricted to the case of a stationary spray nozzle and no net motion of the fluidized solids, as in most previous experimental studies. This will make it possible to use the results of previous experimental studies (Mohagheghi et al. 2013; Mohagheghi et al. 2014; Mohagheghi et al. 2014) to validate this model. Part II will modify the model to the case of a moving spray nozzle, compare its predictions to recent experimental results for moving nozzles and will apply the model to the case of a stationary nozzle and moving solids, as in Fluid Cokers™.

6.3 Review of experimental procedure

6.3.1 Experimental setup

Liquid was sprayed with a scaled-down version of a convergence-divergence-convergence nozzle with an internal throat diameter of 2.2 mm in a cold model fluidized bed of coke particles (Base et al. 1999; Mohagheghi et al. 2013; Mohagheghi et al. 2014). The liquid was mixed with atomization gas in a premixer ahead of the spray nozzle.

The bed particles in this study were fluid coke extracted from an industrial Fluid Coker, which has negligible internal porosity, a Sauter mean diameter of 140 μm (as measured with an HELOS particle size analyzer) and a particle density of 1470 kg/m^3 (as measured with liquid pycnometry). For all the experiments in this study, 430 kg of coke particles were used to give a bed height of approximately 1.2 m at a fluidization superficial velocity of 0.3 m/s. The bed height, mass, and pressure drop were calculated from pressure measurements by transducers installed at different locations on the bed wall.

The fluidized bed has a rectangular cross section area of 1.54 × 0.288 m and height of 1.97 m. There are two banks of sonic orifices and pressure regulators to adjust the fluidization velocity of the bed (Mohagheghi et al. 2013; Mohagheghi et al. 2014).

Liquid was injected for all the experiments in this study via a stationary nozzle and no net motion of fluidized solids. For most of experiments, the injection consisted of a single pulse of 10 seconds, and selected experiments varied the injection duration. Fluidization

velocity during injection was varied, but fluidization after the injection was always with a superficial velocity of 0.2 m/s for all the experiments of this study.

A few experiments were conducted with several successive pulses. In such experiments, the total injection was broken into several periods, interspaced with a time interval that was varied. In these experiments the fluidization superficial gas velocity was kept at 0.2 m/s during injections, between injections and after the final injection.

6.3.2 Measuring system

An AC based capacitance meter with a differential noise cancelling system was used in this study, which is a method based on relative permittivity of materials (Mohagheghi et al. 2013; Mohagheghi et al. 2014). The relative permittivity of air is 1 (U.S. National Library of Medicine). The relative permittivity of Varsol^{TM} and bulk fluid coke, which were used as liquid and solid particles in this study, are 3 and 7, respectively (Department of Physics and Astronomy, Georgia State University). The relative permittivity of bulk coke was calculated based on comparing the measured capacitance of air and a bed of coke in a small box.

There are three wooden windows mounted on the bed wall for measuring capacitance through thirty-two 8 × 10 cm electrodes, which are installed on the inside wall of the wooden windows and are connected to a circuit for capacitance measurements (Mohagheghi et al. 2014; Mohagheghi et al. 2014). On the other side of the wooden windows, there are three 135 × 20 cm electrodes that are connected to the signal generator.

There are two forms of sprayed liquid on particles: a) free liquid, a thin layer of liquid around individual particles and b) liquid trapped within “agglomerates” (Ariyapadi et al. 2003a; Bruhns and Werther 2005; Knapper et al. 2003). Preliminary experiments in a small box have shown that the capacitance of a wet bed is a linear function of the free liquid volume fraction (Mohagheghi et al. 2013; Mohagheghi et al. 2014; Mohagheghi et al. 2014).

6.3.3 Calibration experiments

Calibration experiments were used to find the relation between free liquid and local bed capacitance. For these experiments, an ideal nozzle, which is a straight cylindrical tube with a 3.6 mm diameter, was used. This special nozzle was operated at a very high atomization gas flowrate to liquid flowrate ratio (GLR > 50 wt%) and a low liquid flow rate of about 1.5 - 3 g/s to ensure an almost perfect distribution of liquid on solid particles. This nozzle could not be used in commercial Fluid Cokers due to the very high ratio of atomization gas flowrate to liquid flowrate (GLR) that it would require to perform adequately.

The capacitance was measured for different amounts of free liquid in the bed by changing the amount of injected liquid through the ideal nozzle, as there were no formed agglomerates for this nozzle. The measured capacitance was normalized with its value when the particles were dry. The normalized capacitance for each electrode was plotted versus the free liquid in order to obtain calibration curves (Mohagheghi et al. 2013; Mohagheghi et al. 2014; Mohagheghi et al. 2014).

6.3.4 Experimental method

As shown below, the model can predict the liquid concentration of the agglomerates formed during liquid injection in a fluidized bed. Measuring the liquid concentration of the agglomerates would have been very difficult and, instead, the liquid concentration of the agglomerates was characterized from the rate at which agglomerates break up, since it has been shown that for a given fluidization velocity, this rate is primarily affected by the liquid concentration of the agglomerates (Parveen et al. 2013a; Weber 2009).

The rate at which agglomerates break up was determined from the evolution with time of the concentration in the bed of the free liquid, i.e. the liquid that is not trapped in agglomerates, which can be obtained from the measured bed capacitances (Mohagheghi et al. 2014). As agglomerates formed during liquid injection gradually break up subsequent to the liquid injection, the total percentage of injected liquid which is free liquid, g(t), gradually increases with time and this evolution can be described with the following equation:

$$g(t) = 1 + (g(0) - 1)e^{-t/\tau} \tag{6.1}$$

where $g(0)$ represents the value of $g(t)$ at the end of injection.

The rate at which liquid is freed from agglomerates can, thus, be characterized with the time constant of agglomerate breakage (τ).

g(t) was calculated from the summation of free liquid right after injection and the cumulative liquid freed from agglomerate breakage.

$$g(t) = \frac{M_S}{M_L}\left[X|_{t=0} + \int_0^t \left(\frac{dX}{dt}\right)_{br} dt\right] \tag{6.2}$$

where M_S is total mass of solid, M_L is total mass of injected liquid and X is the mass ratio of free liquid to dry bed solids.

The cumulative mass of liquid freed from agglomerates was calculated from the measured free liquid of the bed, accounting for the impact of evaporation (Mohagheghi et al. 2014). The evaporation rate was obtained from calibration experiments: as there were no agglomerates for these experiments, the free liquid content decreased gradually with time as liquid gradually evaporated from the bed and the rate at which liquid evaporated could, thus, be obtained from $-(dX/dt)_{cal}$. The rate at which liquid evaporated from the bed after regular injections was assumed to be the same as for calibration experiments with the same fluidization velocity, the same temperature and the same free liquid content. Then, the ratio of the total free liquid to the total mass of injected liquid (M_L) can be calculated from:

$$g(t) = \frac{M_S}{M_L}\left[X|_{t=0} + \int_0^t \left[\left(\frac{dX}{dt}\right) - \left(\frac{dX}{dt}\right)_{cal}\right] dt\right] \tag{6.3}$$

6.4 Modelling

6.4.1 Theory

The purpose of this study is to predict the liquid concentration of the initial agglomerates formed from contact between the gas-liquid spray jet and fluidized particles (Stage 1 in Figure 6.1). To find the agglomerate properties, mass conservation was applied around the spray jet cavity. The following assumptions were made to develop the model:

- All the solids entrained from the bed into the jet cavity mix well with the liquid droplets within the jet cavity
- The jet expansion angle is 16 degrees as reported by Berruti et al. (2009)
- Since the duration of liquid injection was always longer than 2 s in this study, and the average time interval between successive bubbles hitting the jet cavity is of the order of 0.1 s (as shown below), the flowrate of solids carried by bubbles to the jet cavity, F_{SB}, may be assumed to be pseudo-continuous.

Figure 6.2 shows a schematic diagram of the jet cavity and its input and output flows. As shown in this diagram, there are four gas, liquid and solids flows entering the jet cavity:

- F_L : flowrate of liquid into the jet from the spray nozzle (kg/s)
- F_a : flowrate of atomization gas into the jet from the spray nozzle (kg/s)
- F_{SE} : solids entrained from the bed into the jet cavity (kg/s)
- F_{SB} : flowrate of solids carried by gas bubbles from the bed into the jet cavity (kg/s)

The flowrate of liquid and gas, F_L and $F_{a,}$ are known for each experiment, while the solids flowrates, F_{SE} and F_{SB}, should be estimated.

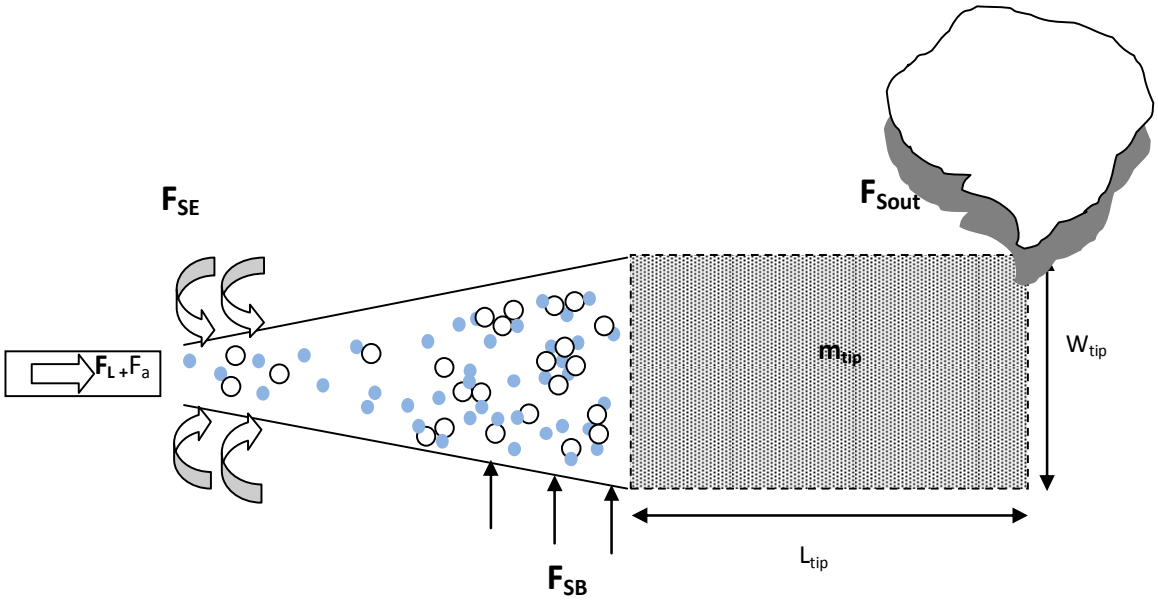

Figure 6.2. Schematic diagram of jet cavity with view from above

6.4.1.1 Flowrate of solids carried by gas bubbles into the control volume (F_{SB})

The following steps were considered to estimate the flowrate of solids carried by bubbles into the control volume:

- Estimate the flux of solids carried by gas bubbles into the jet cavity
- Estimate the horizontal cross-sectional area (A_c) through which gas bubbles can enter the jet cavity
- Calculate the flowrate of solids carried by gas bubbles into the jet cavity (F_{SB})

6.4.1.1.1 Estimate the flux of solids carried by gas bubbles into the jet cavity

To estimate the flux of solids carried by gas bubbles to the jet cavity, the local bubble gas flux must first be calculated. In a previous study with the same equipment and the same range of operating conditions as in this study, the local bubble volume fraction was

obtained from the measured local capacitance (Mohagheghi et al. 2014). Equations are, thus, derived, to estimate the bubble gas flux as a function of local bubble volume fraction.

Equation 6.4 shows how the bubble gas flux can be predicted from the local bubble volume fraction $\varepsilon_{b\,(local)}$ and the local bubble velocity $U_{b\,(local)}$:

$$q_{b\,(local)} = \varepsilon_{b\,(local)} U_{b\,(local)}, \ \left(\frac{m^3}{m^2 s}\right) \tag{6.4}$$

The local bubble velocity was estimated from the local bubble volume fraction. Hamidi (2014) measured the local capacitance of a fluidized bed of the same coke particles as used this study at a high frequency of 500 Hz, and obtained the local bubble volume fraction from pressure measurements. The bubble velocity was calculated from the time delay between capacitance of two vertical electrodes as shown in Equation 6.5 (Hamidi 2014):

$$U_b = \frac{d_r}{t_d} \tag{6.5}$$

where d_r is the distance between the centers of two adjacent electrodes and t_d is the time delay between two local minimums of measured capacitance.

Figure 6.3 shows that there is a linear relationship between the local bubble velocity, normalized with its cross-sectional average, and the local bubble volume fraction, also normalized with its cross-sectional average. Equation 6.6 presents this relationship:

$$\frac{U_b}{\overline{U}_b} = -0.4256\ \frac{\varepsilon_b}{\bar{\varepsilon}_b} + 1.4256 \tag{6.6}$$

where $\overline{U}_b$ is the cross-sectional average of the bubble velocity, $\bar{\varepsilon}_b$ is the cross-sectional average of the bubble volume fraction, U_b is the local bubble velocity, and ε_b is the local bubble volume fraction.

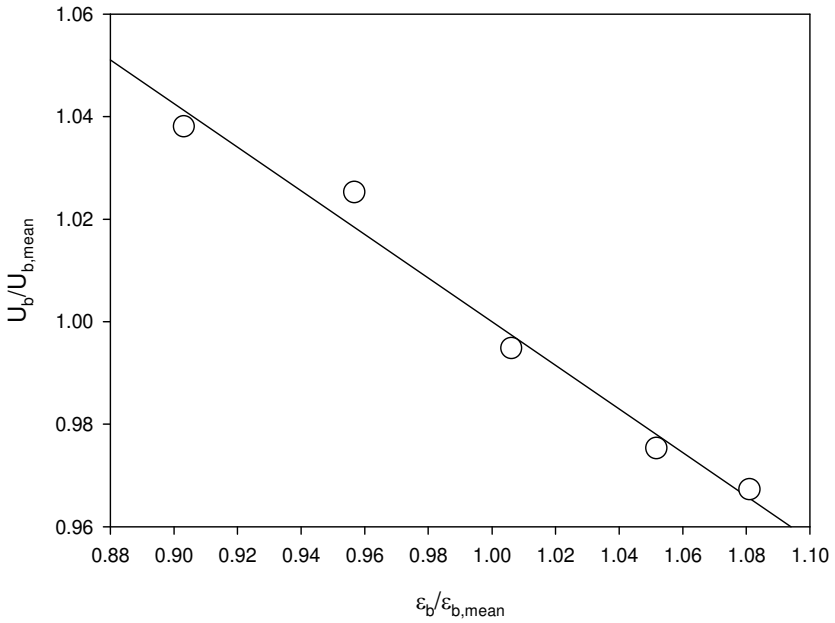

Figure 6.3. The ratio of local bubble velocity to mean bubble velocity versus the ratio of bubble volume fraction to its mean value, using data from Hamidi (2014)

The cross-sectional average of the bubble velocity is required to estimate the local bubble velocity from the bubble volume fraction with Equation 6.6. Equation 6.7 shows the relationship between bubble velocity and the volumetric gas bubble flowrate between lateral coordinates x_{L1} and x_{L2} :

$$Q_b = t_b \int_{x_{L_1}}^{x_{L_2}} U_b \varepsilon_b dx \tag{6.7}$$

Assuming the bubble velocity is approximately the same over the whole cross-section, i.e. $U_b \cong \overline{U}_b$:

$$Q_b = t_b \overline{U}_b \int_0^w \varepsilon_b dx \tag{6.8}$$

where w is the bed width, t_b is the bed thickness, ε_b is the local bubble volume fraction obtained from capacitance measurements (averaged over the bed thickness), and Q_b is the total bubble gas flowrate, which can be predicted from Equation 6.9. In this

equation, Q_g is the total volumetric gas flowrate through the bed and Q_{mf} is the gas flowrate at minimum fluidization:

$$Q_b = Q_g - Q_{mf} \tag{6.9}$$

The cross-sectional average of the bubble velocity obtained from Equation 6.8 is 1.77 m/s for a fluidization velocity of 0.2 m/s, a bed width of 1.54 m, and a bed thickness of 0.288 m, using the local bubble volume fraction from capacitance measurements presented in a previous study (Mohagheghi et al. 2014).

The local bubble velocity can then be calculated with Equation 6.6. Equation 6.4 then provides the local bubble gas flux from the local bubble velocity and the local bubble volume fraction.

Baron et al. (1988) proposed an equation to relate the local flux of solids carried by bubbles to the local bubble gas flux:

$$f_{SB} = k\rho_{mf} q_{b\,(local)}\ ,\ \left(\frac{kg\ solids}{m^2.s}\right) \tag{6.10}$$

Combining with Equation 6.6:

$$f_{SB} = k\rho_{mf}\varepsilon_{bj}\,\overline{U}_b\left(-0.4256\frac{\varepsilon_{bj}}{\bar{\varepsilon}_b} + 1.4256\right),\qquad \left(\frac{kg\ solids}{m^2.s}\right) \tag{6.11}$$

where ρ_{mf} is the bed density at minimum fluidization and k is the ratio of wake volume to bubble volume, which was estimated to be between 0.2 to 0.25 by Baron et al. (1988).

Figure 6.4 shows the flux of solids carried by bubbles into jet (f_{SB}) versus the bubble volume fraction near jet tip region for fluidization velocity 0.2 m/s.

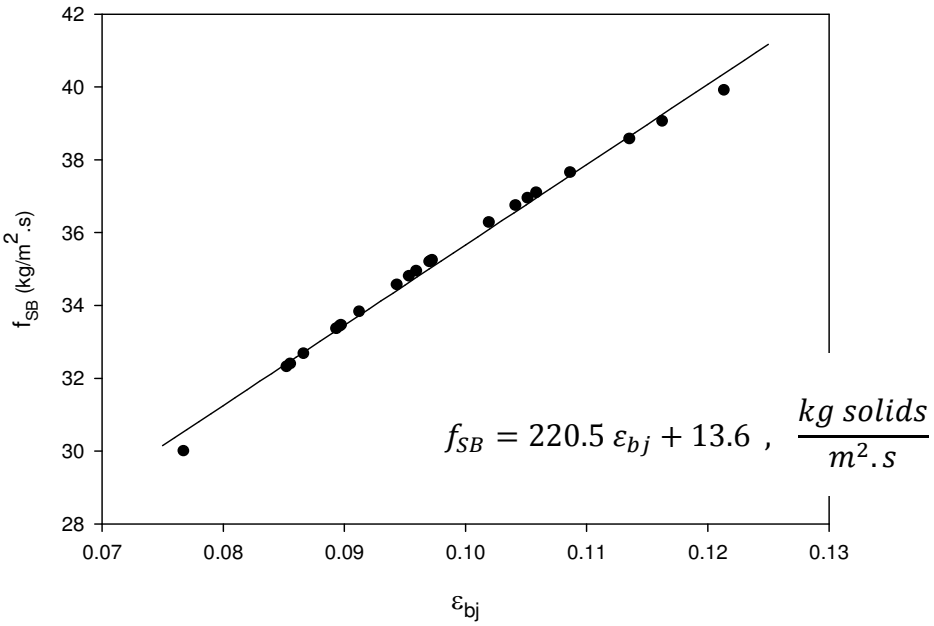

Figure 6.4. Predicted flux of solids carried by bubbles into jet cavity versus a range of bubble volume fraction near jet tip for a fluidization velocity of 0.2 m/s

6.4.1.1.2 Estimate the horizontal cross-sectional area (A_c) through which gas bubbles can enter the jet cavity

Some experiments were carried out in the fluidized bed with the gas-liquid jet to determine the length of the jet which is affected by bubbles. These experiments were performed with a small tube located low enough below the jet cavity (about 20 cm) that gas bubbles from the tube can pick up wake solids before reaching the jet cavity. The tube was moved forward and backward below the jet cavity in order to study the impact of bubbles from the tube at different horizontal locations on the agglomerates resulting from interaction between gas-liquid jet and bed solids. The conditions of these experiments are presented in Table 6.1.

Figure 6.5 shows the time constant of agglomerate breakage for experiments presented in Table 6.1 versus x_L that is the horizontal distance of the small tube tip from the jet tip position. The value of zero for x_L corresponds to the position of the small tube tip exactly below the jet tip location.

The length of the section through which bubbles enter the jet cavity (x_c) was considered the length where the bubbles from the small tube affect the time constant of agglomerate breakage, and was, thus, obtained from the experimental results of Figure 6.5. It was related to the maximum jet penetration length and the mean bubble diameter. The mean bubble diameter was calculated from the mean bubble velocity with the correlation from Hilligardt and Werther (1985). For the mean bubble velocity of 1.77 m/s, the mean bubble size is about 68 mm. Previous studies showed the measured jet penetration (L_{jet}) for a horizontal nozzle with a 2.2 mm diameter is about 520 mm using capacitance measurements (Mohagheghi et al. 2014). The maximum jet penetration length was calculated from the measured penetration length using Equation 6.12 (Xuereb et al. 1991).

$$L_{jet,max} = 1.23 \times L_{jet} \tag{6.12}$$

Table 6.1. Experimental conditions in order to determine the length of the jet which is affected by bubbles

Run #	x_L, horizontal distance of tube tip relative to jet tip position (m)	Fluidization velocity during and after injection (m/s)	GLR (wt%)
1	0.2	0.2	1.5
2	0.1	0.2	1.5
3	0	0.2	1.5
4	-0.1	0.2	1.5
5	-0.2	0.2	1.5
6	-0.3	0.2	1.5

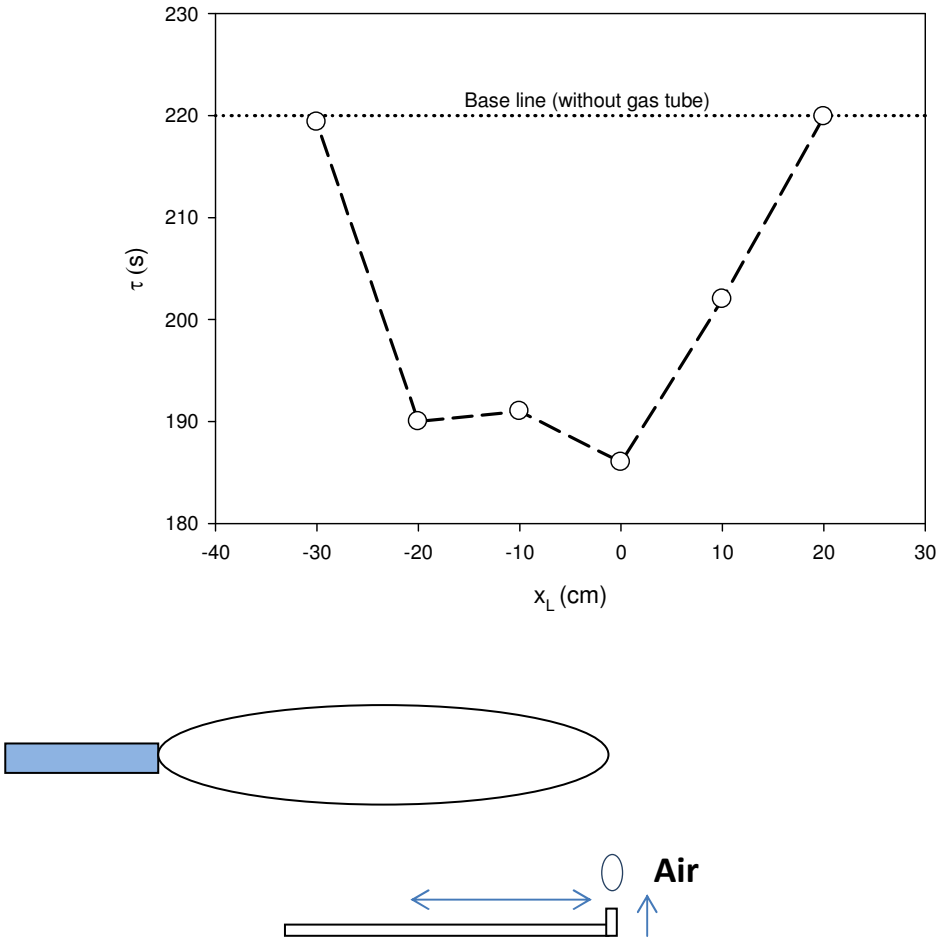

Figure 6.5. Time constant of agglomerate breakage versus horizontal distance of tube tip from jet cavity tip corresponding to the measured jet length (fluidization velocity = 0.2 m/s, GLR = 1.5 wt%, and injection duration = 10 s)

Figure 6.6 shows the relation between x_c, the maximum jet penetration length and the mean bubble diameter. Thus, the length of the section through which bubbles enter the jet cavity (x_c) can be presented as below:

$$x_c = \frac{L_{jet,max}}{2.5} + 1.5\bar{d}_b \tag{6.13}$$

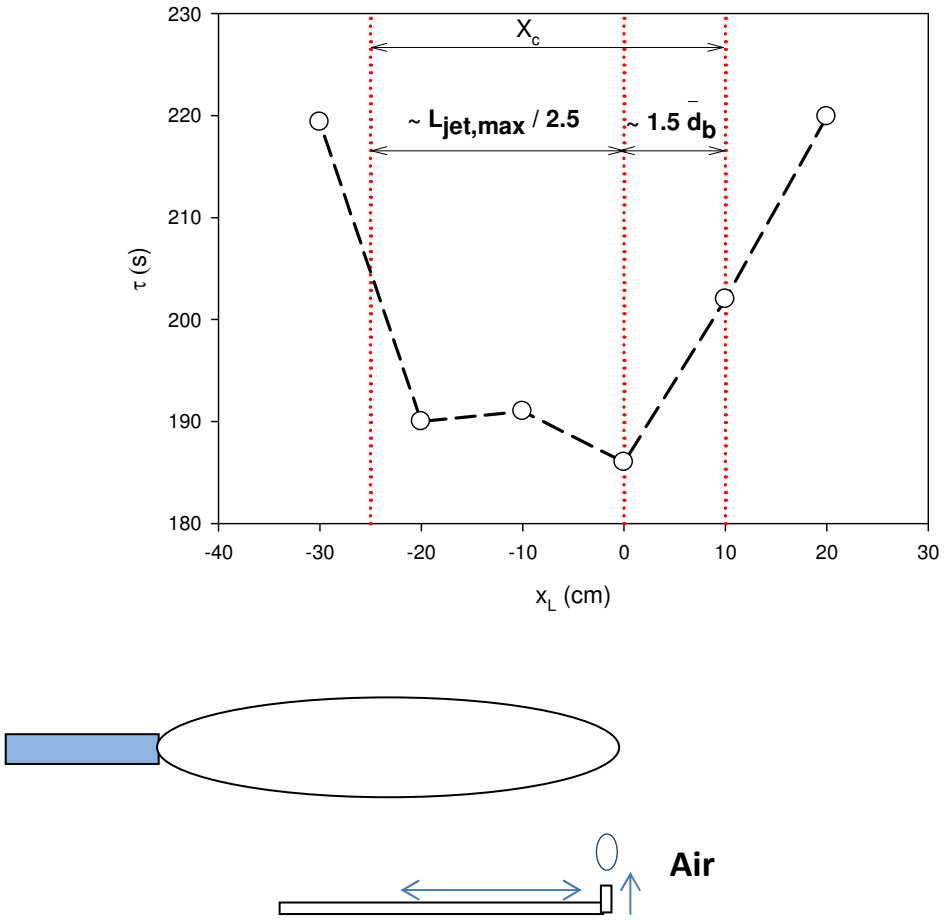

Figure 6.6. The relation of x_c with maximum jet penetration length (L_{jet}) and mean bubble diameter ($\bar{d}_b$) obtained from results for a fluidization velocity of 0.2 m/s, a GLR of 1.5 wt%, and injection duration = 10 s

The shape of the jet along the length of bubble capture area was obtained from Berruti et al. (2009). The horizontal cross-sectional area (A_c) through which gas bubbles can enter the jet cavity can be approximated by a rectangle with a length x_c and a width (W_c) given by Equation 6.14:

$$W_c = \frac{L_{jet,max}}{2.5} tan \frac{\theta_j}{2} \tag{6.14}$$

where $L_{jet,max}$ is the maximum penetration length and θ_j is the jet expansion angle. The jet expansion angle was considered to be 16^0 (Berruti et al. 2009). Equation 6.15 gives the horizontal cross-sectional area (A_c) through which gas bubbles can enter the jet cavity:

$$A_c = x_c W_c = \left(\frac{L_{jet,max}}{2.5} + 1.5\bar{d}_b\right)\frac{L_{jet,max}}{2.5} tan\frac{\theta_j}{2} \tag{6.15}$$

6.4.1.1.3 Estimate the flowrate of solids carried by gas bubbles into the jet cavity

The flowrate of solids carried by gas bubbles into the jet cavity was calculated from the previous sections. Since the horizontal cross-sectional area through which gas bubbles can enter the jet cavity is around the jet tip, the local bubble volume fraction used in the equation is the bubble volume fraction near jet tip location (ε_{bj}). Equation 6.16 shows the flowrate of solids carried by gas bubbles into the jet cavity:

$$F_{SB} = \left(\frac{L_{jet,max}}{2.5} tan\frac{\theta_j}{2}\right)\left(\frac{L_{jet,max}}{2.5} + 1.5\bar{d}_b\right)\left(220.5\varepsilon_{bj} + 13.6\right),\ \frac{kg\ solids}{s} \tag{6.16}$$

Figure 6.7 shows the flowrate of solids carried by gas bubbles into the jet cavity versus the bubble volume fraction near the jet tip for a fluidization velocity of 0.2 m/s, a GLR of 1.5 wt%, a nozzle diameter of 2.2 mm, and a liquid flowrate of 0.055 kg/s. As expected, increasing the bubble volume fraction near the jet tip increases the flowrate of solids carried by bubbles into the jet cavity.

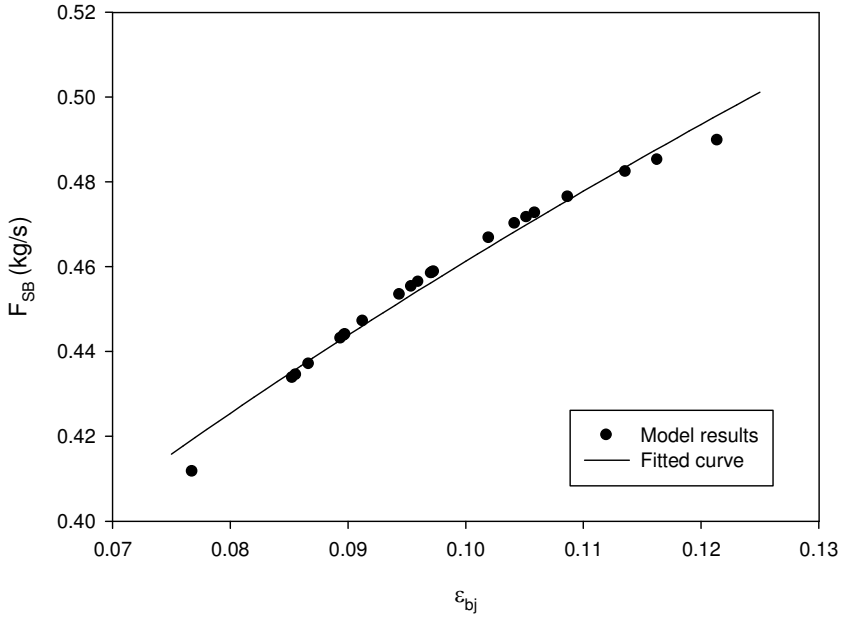

Figure 6.7. The estimated flowrate of solids carried by gas bubbles to the jet cavity versus bubble volume fraction near jet tip region for a fluidization velocity of 0.2 m/s, a GLR of 1.5 wt%, a nozzle diameter of 2.2 mm, and a liquid flowrate of 0.055 kg/s

6.4.1.2 Flowrate of solids entrained to the jet cavity (F_{SE})

Briens et al. (2008) estimated the flowrate of solids entrained to the jet cavity at different fluidization velocities for a nozzle diameter of 1.6 mm. Since the entrained solids flowrate can be assumed to be proportional to the jet penetration length, the correlation from Benjelloun et al. (1995) for jet penetration length is used to estimate the entrained solids flowrate at other nozzle diameters. Equation 6.17 shows the correction factor for the entrained solids flowrate for the nozzle diameter of 2.2 mm that was used in this study:

$$F_{SE} \propto L_{jet} \propto (d_N)^{0.73}$$

$$(F_{SE})_{2.2\,mm} = 1.26(F_{SE})_{1.6\,mm} \tag{6.17}$$

Since the shape and geometry of the reactor used by Briens et al. (2008) is almost the same as for the experimental setup of this study, the local bubble volume fraction (ε_b) from Briens et al. (2008) was assumed the same as the local bubble volume fraction

in the experiments of this study for the same fluidization velocity, U_f. Therefore, for each fluidization velocity, the local bubble volume fraction was estimated from the local capacitance measurements at different fluidization velocities in this study.

The relationship between the flowrate of solids entrained into the jet cavity and the fluidization velocity was obtained from Briens et al. (2008) for a nozzle diameter of 1.6 mm. Equation 6.17 was used to convert this relationship for the 2.2 mm nozzle used in this study. Capacitance measurements were then used to express the flowrate of solids entrained into the jet cavity as a function of the local bubble volume fraction instead of the fluidization velocity. Equation 6.18 shows the flowrate of solids entrained into the jet cavity versus the local bubble volume near nozzle tip (ε_{bN}) for nozzle diameter 2.2 mm (Briens et al. 2008).

$$F_{SE} = 0.44\varepsilon_{bN} + 0.012 \ , \ \frac{kg\ solids}{s} \tag{6.18}$$

Figure 6.8 presents the entrained solids to the jet cavity versus bubble volume fraction near the nozzle tip zone for a fluidization velocity of 0.2 m/s and nozzle diameter of 2.2 mm. This figure shows increasing the bubble volume fraction near the nozzle tip increases the flowrate of solids entrained into the jet cavity.

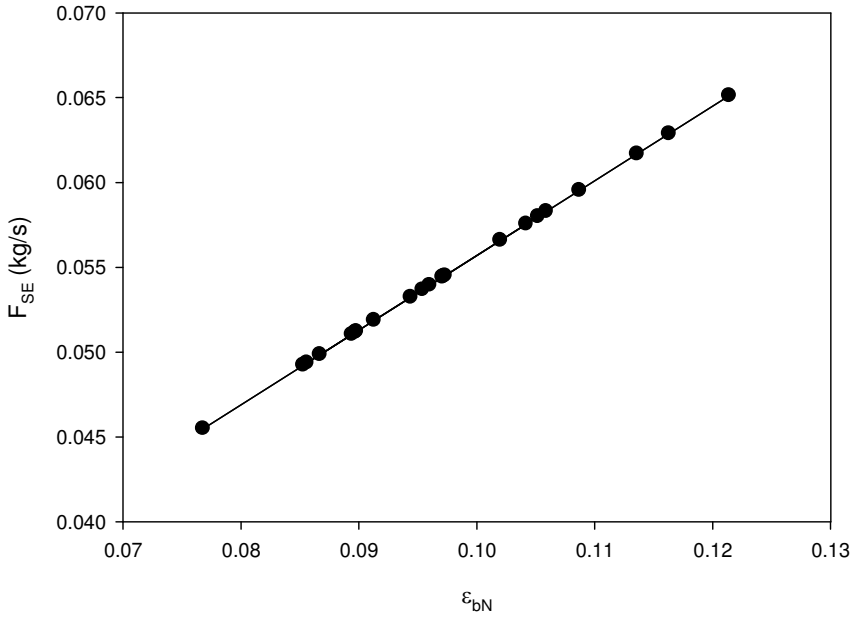

Figure 6.8. The entrained solids to the jet cavity versus bubble volume fraction near nozzle tip zone for a fluidization velocity of 0.2 m/s, a GLR of 1.5 wt%, a nozzle diameter of 2.2 mm, and a liquid flowrate of 0.055 kg/s

6.4.1.3 Estimate the mass of solids at jet tip region (m_{tip})

In order to estimate the mass of solids at jet tip region interacting with gas-liquid jet, the following assumptions were considered:

- Spray jet pushes solids at jet tip to the sides as it expands
- Spray jet expands due to atomization gas and bubbles entering the jet from below
- Jet after expansion eventually releases bubble to the bed
- The diameter of the detached bubbles from the jet is a function of jet length (L_{jet}) as presented in Equation 6.19 (Xuereb et al. 1991):

$$d_d = \frac{L_{jet,max}}{2.88} \tag{6.19}$$

Equation 6.20 shows the volume of the detached bubble which is replaced by bed solids near the jet tip when the jet contracts as the bubble detaches from the jet tip:

$$V_d = V_r = \frac{\pi}{6} {d_d}^3 \tag{6.20}$$

- At the end of each full jet expansion, the total volume of solids at jet tip that interacts with the jet is equal to the volume replaced by the volume of the released bubble from the jet due to jet expansion plus the volume of entrained solids and the volume of solids carried by bubbles into the jet cavity during the full jet expansion time (t_r):

$$V_{tip} = \frac{\pi}{6} {d_d}^3 + (\frac{F_{SB}}{\rho_{mf}} + \frac{F_{SE}}{\rho_{mf}}) t_r \qquad (6.21)$$

Based on the above assumptions to calculate the mass of solids at the jet tip, we need to have the length of the gas-liquid jet and the expansion time (release time of bubble from jet cavity).

The jet length was obtained from capacitance measurements. Then the diameter of the detached bubble was calculated from Equation 6.19.

The time between released bubbles was calculated from the detached bubble volume (Equation 6.20) and summation of atomization gas flowrate (Q_a) and bubble gas flowrate (Q_b) to the jet cavity as shown below:

$$t_r = \frac{V_d}{Q_a + Q_b} \qquad (6.22)$$

The density at minimum fluidization velocity (ρ_{mf}) was considered to be 875 kg/m^3. At the end, the mass of solids at the jet tip region (m_{tip}) is equal to the mass of solids replaced by the jet expansion at the tip of the jet (m_r) and the total mass of solids entrained to the jet cavity during expansion that was calculated from Equation 6.23.

$$m_{tip} = V_{tip}\rho_{mf} \ , \qquad kg\ solids \qquad (6.23)$$

6.4.2 Model

Since all the required parameters for the model were predicted as described in previous sections, we can develop the model with applying the conservation of mass around the jet cavity.

To develop the model the following assumptions were considered:

- The entrained solids and also solids carried to the jet cavity by bubbles were considered to be dry solids
- During each jet expansion from its minimum to maximum penetration length, the model assumes that the liquid from the spray nozzle interacts with the whole volume V_{tip} of solids, which includes the bed solids displaced by the jet expansion, the solids entrained into the jet cavity and the solids carried by gas bubbles into the jet cavity
- At the end of each jet expansion, the bubble released from the jet tip carries solids from the jet tip in its wake to the rest of the bed
- When there are several consecutive jet expansions, the solids at the jet tip that are contacted by the sprayed liquid are dry for the first expansion and wet for subsequent expansions. The liquid concentration of the agglomerates at the jet tip after each expansion is calculated from the liquid concentration at the jet tip at the end of the previous expansion, accounting for the detached bubble wake that transfers part of these solids to the rest of the bed

The injection time (t) was always equal to or larger than the time required for a full jet expansion (t_r). The average liquid concentration (c) of the solids displaced by the jet expansion at the end of the first jet expansion is given by:

$$F_L\, t_r = m_{tip}\, c_1 \tag{6.24}$$

Note that in this study, this average liquid concentration was expressed as the average mass ratio of liquid to dry solids in the solids displaced by the jet.

Some of these solids are carried in the wake of the bubble detaching from the jet tip from the jet tip region to the rest of the bed, and are replaced by an equal volume of dry solids from the rest of the bed. At the end of the second jet expansion, the average liquid concentration of the agglomerates in the jet tip region is, therefore:

$$F_L\, t_r + \left(m_{tip} - m_w\right) c_1 = m_{tip}\, c_2 \tag{6.25}$$

Where the mass m_w of the solids entrained in the wake of the bubble detaching from the jet tip is obtained from the wake volume, which is a fraction k of the total detached bubble volume:

$$m_w = k\, V_r \rho_{mf} \tag{6.26}$$

At the end of n^{th} expansion, the average liquid concentration of the agglomerates in the jet tip region is:

$$F_L\, t_r + \left(m_{tip} - m_w\right) c_{n-1} = m_{tip}\, c_n \tag{6.27}$$

where n is the number of full expansions obtained from the injection time (t) and time required for a full jet expansion (t_r):

$$n = largest\ integer \leq \frac{t}{t_r} \tag{6.28}$$

For a total injection time of t, there would be n full jet expansions and one partial expansion. Therefore, for a total injection time of t, the average liquid concentration of the agglomerates in the jet tip region at the end of injection time (c_{last}) was calculated from Equation 6.29, accounting for partial expansion at the end.

$$F_L(t - nt_r) + \left(m_{tip} - m_w\right) c_n = m_{last}\, c_{last} \tag{6.29}$$

where m_{last} is the total mass of bed solids near the jet tip that are displaced by the full jet expansion (m_r) plus the mass of solids entrained into the jet cavity and the mass of solids carried by bubbles into the jet cavity during the partial jet expansion at the end of total injection time after n full jet expansions:

$$m_{last} = m_r + (F_{SB} + F_{SE})(t - nt_r) \tag{6.30}$$

The mean liquid concentration of agglomerates at the end of injection time in the bed was calculated from the average of liquid concentration of released agglomerates during injection to the bed and liquid concentration at jet tip at the end of injection as shown in

Equation 6.31. The wet solids transferred to the bed in the wake of the first released bubble were assumed to have a negligible impact on the agglomerate strength because of their small liquid concentration. Their impact on the agglomerate breakage time was neglected as they would be very weak and break much more quickly than the subsequent agglomerates (Parveen et al. 2013; Weber 2009).

$$c_{predicted} = c_{mean} = \frac{m_{last}c_{last} + m_w \sum_{i=2}^{n} c_i}{m_{last} + (n-1)m_w} \tag{6.31}$$

6.4.3 Validate the model assumption through successive pulse injection experiments

Before applying the model to the different experimental conditions presented in previous studies, the assumption of rewetting of the solids at the jet tip region for the second and higher expansions of the jet (n>1) for a stationary nozzle, was validated through a set of successive pulse injection experiments.

For successive pulse injection experiments, a pulse injection of 10 s was broken into two periods of 5 s injections. The Fluidized period between injection pulses (Δt) was varied from one experiment to another to study its impact on the time constant of agglomerates breakage. Table 6.2 shows the experimental conditions of these experiments. The time constant of agglomerate breakage was measured for each experiment. Figure 6.9 shows the time constant of agglomerate breakage versus fluidized period between injection pulses (Δt) for 2 successive pulses of 5 s ($5\ s\ injection \rightarrow \Delta t \rightarrow 5\ s\ injection$). As this figure shows for a long enough fluidized period between injection pulses, the agglomerate breakage time is about 70 s which is equal to the agglomerate breakage time after a single pulse of 5 s. The results show that with enough time between pulses, the wet solids will be renewed at tip of jet and the jet will interact with dry solids during the second pulse. Therefore, the assumption of rewetting the solids at the jet tip for a stationary nozzle for several expansions of the jet is correct based on the results of this section.

Table 6.2. Experimental conditions for successive pulse injections of 5 s experiments ($5\ s\ injection \rightarrow \Delta t \rightarrow 5\ s\ injection$)

Run #	Δt (s)	GLR (%)	Fluidization velocity (m/s)
1	2.5	1.5	0.2
2	5	1.5	0.2
3	10	1.5	0.2
4	15	1.5	0.2
5	20	1.5	0.2
6	200	1.5	0.2
7	300	1.5	0.2

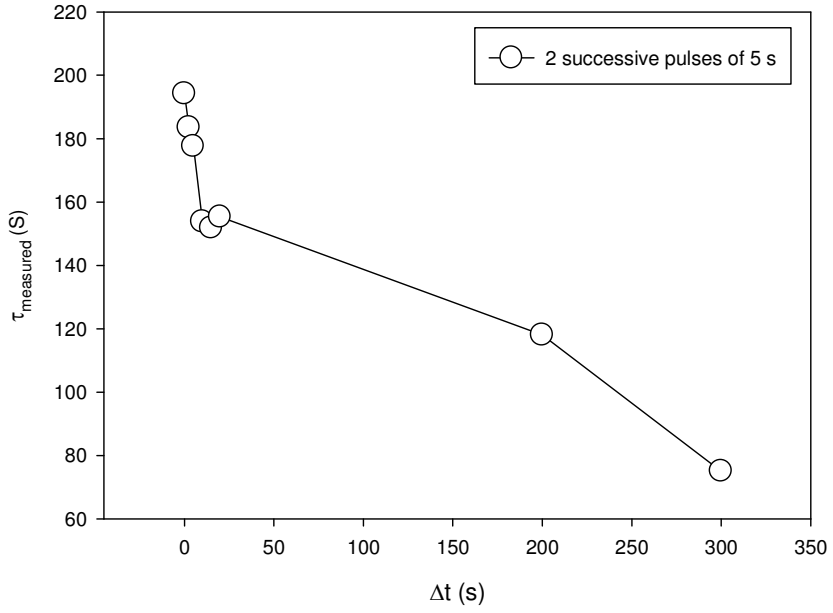

Figure 6.9. Time constant of agglomerate breakage versus fluidized period between injection pulses (Δt) for two successive pulses of 5 seconds (fluidization velocity = 0.2 m/s, GLR = 1.5 wt%)

6.5 Results of the model

The developed model was applied to the experimental conditions presented in previous studies (Mohagheghi et al. 2013; Mohagheghi et al. 2014; Mohagheghi et al. 2014):

- experiments with different nozzle locations in the bed and thus different bed hydrodynamics
- experiments with introducing additional gas at nozzle and jet tip locations to modify the local bed hydrodynamics
- nozzle inclination experiments, where the nozzle inclination was modified
- experiments with different fluidization velocities during injection (the fluidization velocity was always the same subsequent to injection, during agglomerate breakage)
- experiments with different durations of injection
- experiments with different atomization gas flowrates (GLRs)

The model estimates the average liquid concentration (c_{mean}) of the initial agglomerates formed when liquid was sprayed into the fluidized bed, expressed as the mass ratio of liquid to dry solids in the agglomerates. Experimental results provide the time constant of agglomerate breakage (τ). In this chapter, the model results were compared to the experimental results for each experimental condition. If the model provides a good representation, one would expect a good correlation between the predicted mean liquid concentration and the measured time constant of agglomerate breakage.

6.5.1 Model results for nozzle location experiments

Figure 6.10a compares the predicted liquid concentration of the initial agglomerates with the bubble volume fraction near the jet tip for experiments at different nozzle locations. The model predicts that a higher bubble volume fraction near the jet tip results in agglomerates with lower liquid concentration.

Figure 6.10b shows that there is a very good correlation between the measured time constant of agglomerate breakage and the predicted liquid concentration of the initial agglomerates. For all these experiments, the fluidization velocity was 0.2 m/s and the

atomization GLR was 1.5 wt%. As expected (Parveen et al. 2013; Weber 2009), agglomerates with a higher predicted liquid concentration are stronger and their time constant of agglomerate breakage is larger.

a)

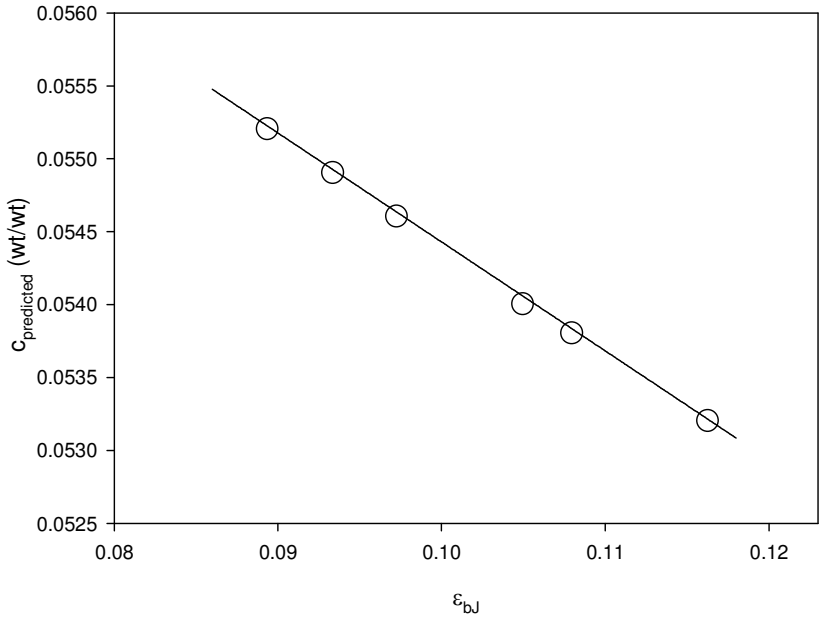

b)

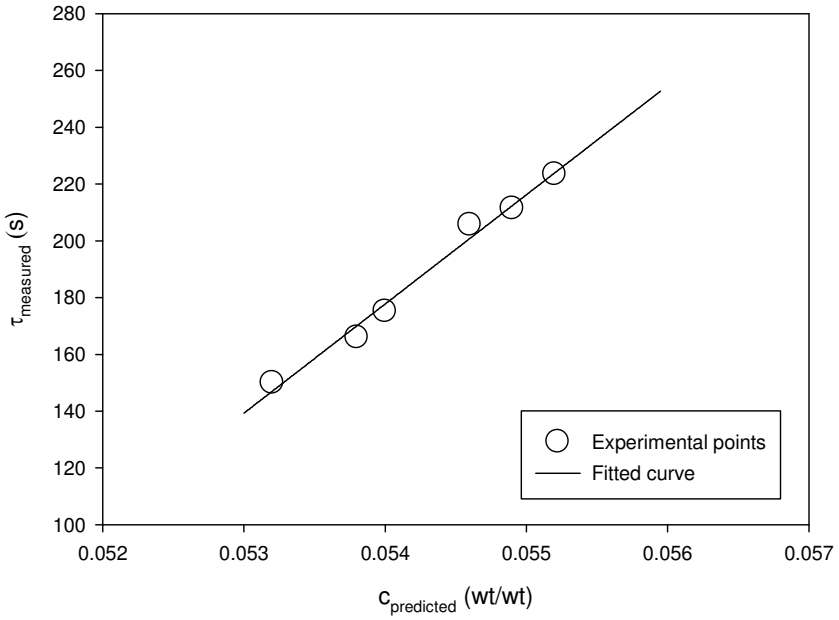

Figure 6.10. a) Liquid concentration of initial agglomerates versus bubble volume fraction near jet tip region for experiments at different locations of nozzle in the bed (fluidization velocity = 0.2 m/s, GLR = 1.5 wt%, and injection duration = 10 s); b) Measured time constant of agglomerate breakage versus predicted liquid concentration of initial agglomerates for U_f = 0.2 m/s, GLR = 1.5 wt%, and injection duration = 10 s

6.5.2 Model results for additional local gas experiments

6.5.2.1 Experiments with introduction of additional gas near the jet tip

Figure 6.11a compares the predicted liquid concentration of initial agglomerates with the bubble volume fraction near the jet tip for experiments with and without adding extra gas near the jet tip with the same nozzle locations. The fluidization velocity for these experiments was 0.2 m/s and the GLR was 1.5 wt%. The model predicts that increasing the local bubble volume fraction near the jet tip results in the formation of agglomerates with a lower liquid concentration.

Experiments showed that adding extra gas near the jet tip region increases the bubble volume fraction near the jet tip and decreases the time constant of agglomerate breakage (Mohagheghi et al. 2014). Figure 6.11b shows a clear correlation between the measured time constant of agglomerate breakage and the predicted liquid concentration of initial agglomerates, for experiments with and without the addition of extra gas near the jet tip, with the same nozzle locations.

a)

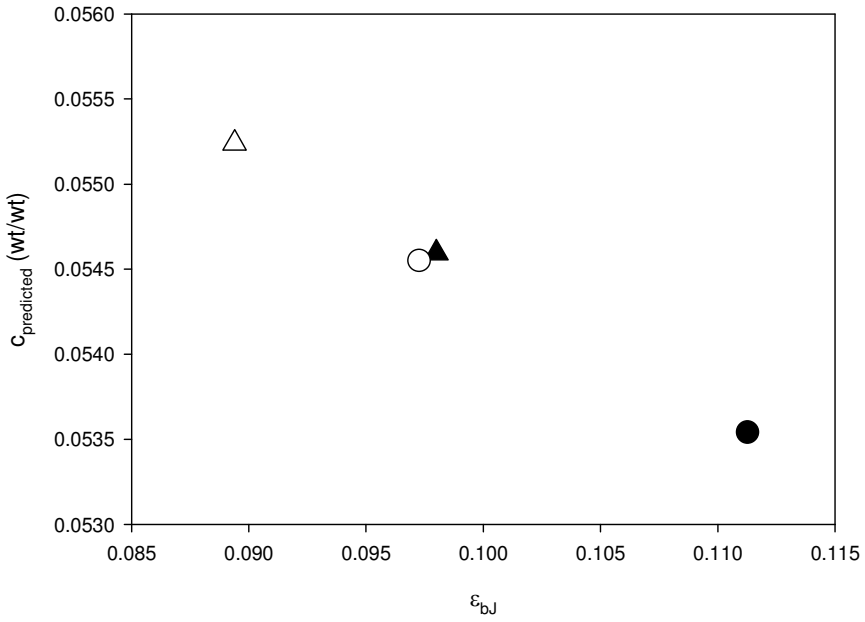

b)

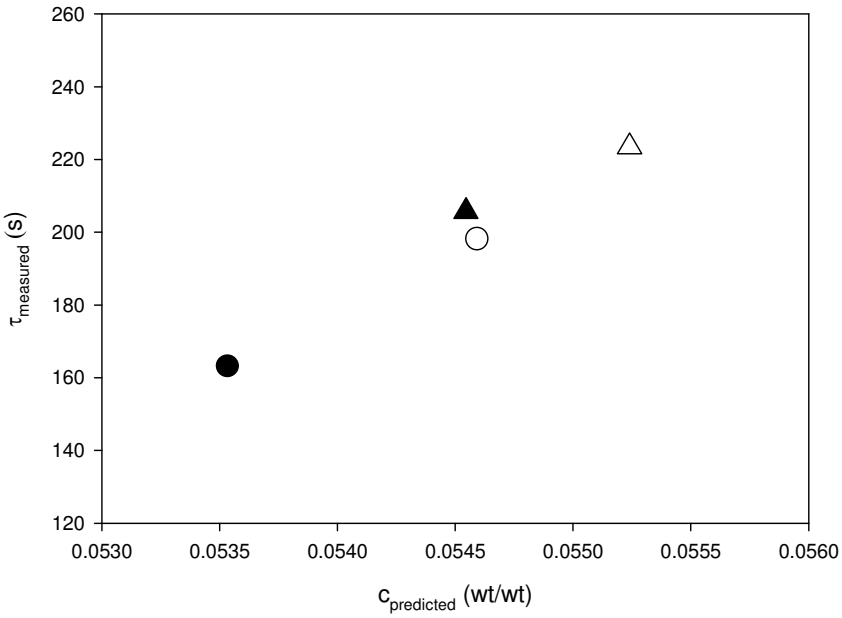

Figure 6.11. a) Predicted liquid concentration of initial agglomerates versus bubble volume fraction near jet tip region for experiments with the same nozzle locations (same symbols) and with local addition of extra gas near jet tip region (closed symbols) (U_f = 0.2 m/s, GLR = 1.5 wt%, and injection duration = 10 s); b) Measured time constant of agglomerate breakage versus predicted liquid concentration of initial agglomerates for experiments with the same nozzle locations (same symbols) and with local addition of extra gas near jet tip region (closed symbols) (U_f = 0.2 m/s, GLR = 1.5 wt%, and injection duration = 10 s)

6.5.2.2 Experiments with introduction of additional gas near the nozzle tip

Figure 6.12a compares the predicted liquid concentration of initial agglomerates with the bubble volume fraction near the nozzle tip for experiments with and without the addition of extra gas near the nozzle tip, at the same nozzle locations. The fluidization velocity for these experiments was 0.2 m/s and the GLR was 1.5 wt%. The model predicts that increasing the local bubble volume fraction near the nozzle tip does not have a considerable impact on the liquid concentration of initial agglomerates.

Experiments with the local addition of extra gas near the nozzle tip show that a higher bubble volume fraction near the nozzle tip does not have a considerable impact on the

time constant of agglomerate breakage (Mohagheghi et al. 2014). Figure 6.12b, however, shows a clear correlation between the measured time constant of agglomerate breakage and the predicted liquid concentration of initial agglomerates, for experiments with and without the addition of extra gas near the nozzle tip, with the same nozzle locations. This confirms that the model can predict the lack of impact of adding additional gas near the nozzle tip.

a)

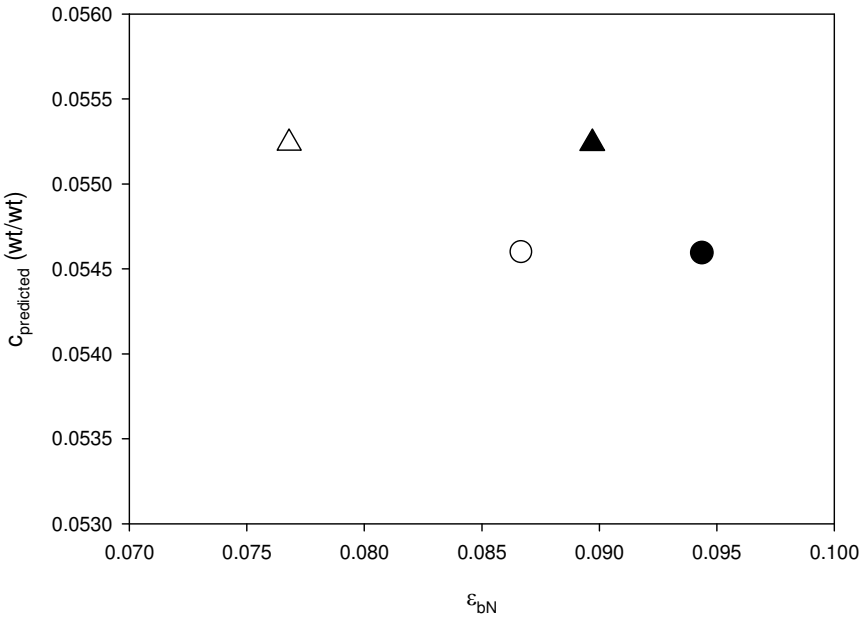

b)

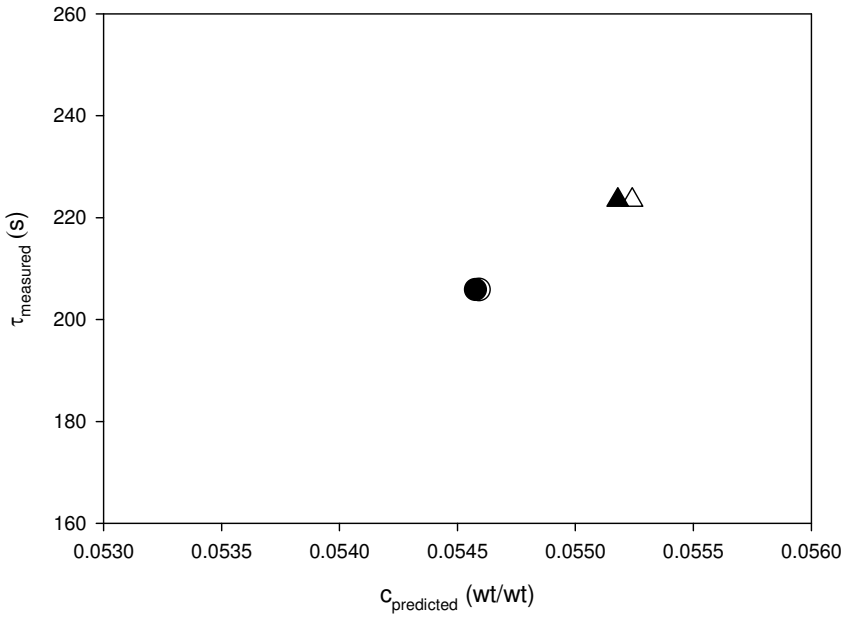

Figure 6.12. a) Predicted liquid concetration of initial agglomerates versus bubble volume fraction near nozzle tip region for experiments with the same nozzle locations (same symbols) and with local addition of extra gas near nozzle tip region (closed symbols) (U_f = 0.2 m/s, GLR = 1.5 wt%, and injection duration = 10 s); b) Measured time constant of agglomerate breakage versus predicted liquid concentration of initial agglomerates for experiments with the same nozzle locations (same symbols) and with local addition of extra gas near nozzle tip region (closed symbols) (U_f = 0.2 m/s, GLR = 1.5 wt%, and injection duration = 10 s)

6.5.3 Model results for nozzle inclination experiments

Figure 6.13 compares the predicted liquid concentration of initial agglomerates with the measured time constant of agglomerate breakage for experiments with the same jet tip locations and different nozzle inclinations. The fluidization velocity for these experiments was 0.2 m/s and the GLR was 1.5 wt%. The model accurately predicts that changing the nozzle inclination, while maintaining the jet tip at the same location, has little effect on the liquid concentration of the agglomerates and, thus, their time constant of breakage.

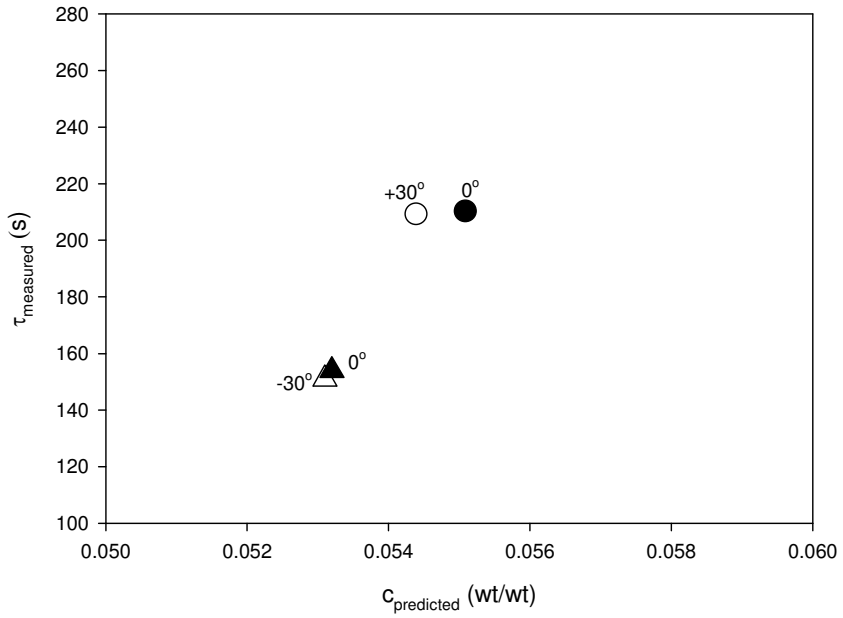

Figure 6.13. Measured time constant of agglomerate breakage versus predicted liquid concentration of initial agglomerates for experiments with the same jet tip locations (same symbols) and different angles of nozzle as shown in the figure (U_f = 0.2 m/s, GLR = 1.5 wt%, and injection duration = 10 s)

6.5.4 Model results for different fluidization velocities during injection experiments

Figure 6.14 compares the predicted liquid concentration of initial agglomerates with the measured time constant of agglomerate breakage for experiments with different fluidization velocities during injection and a GLR of 1.5 wt%. The fluidization velocity after injection for all these experiments is 0.2 m/s. The model predicts that increasing the fluidization velocity during injection decreases the liquid concentration of initial agglomerates. For these experiments, as for the other experiments, there is a clear correlation between the measured time constant of agglomerate breakage and the predicted liquid concentration of initial agglomerates.

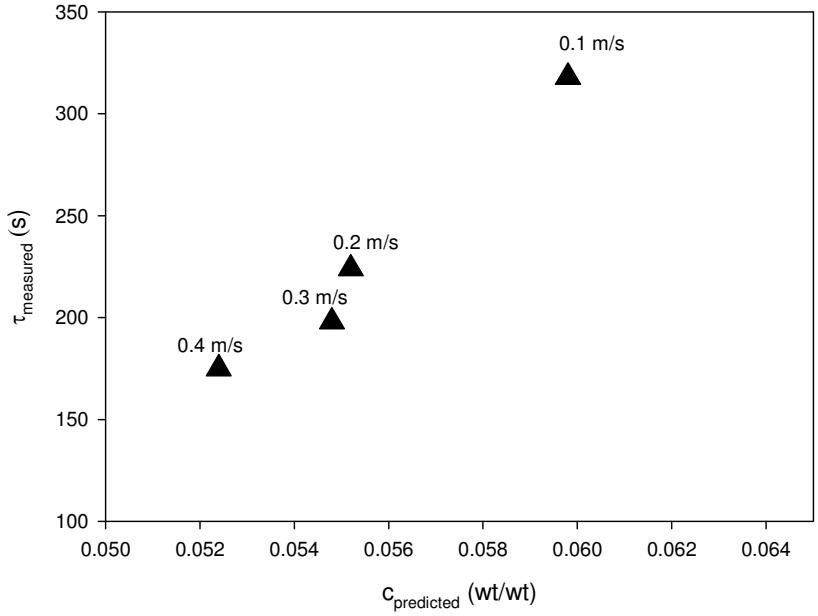

Figure 6.14. Measured time constant of agglomerate breakage versus predicted liquid concentration of initial agglomerates for experiments with different fluidization velocities during injection as shown in the figure (GLR = 1.5 wt%, and injection duration = 10 s)

6.5.5 Model results for different durations of injection experiments

Figure 6.15 compares the predicted liquid concentration of initial agglomerates with the measured time constant of agglomerate breakage for experiments with different durations of injection, a fluidization velocity of 0.2 m/s, and a GLR of 1.5 wt%. The model predicts that a longer injection results in agglomerates with a higher liquid concentration**.** There is a clear correlation between the measured time constant of agglomerate breakage and the predicted liquid concentration of initial agglomerates.

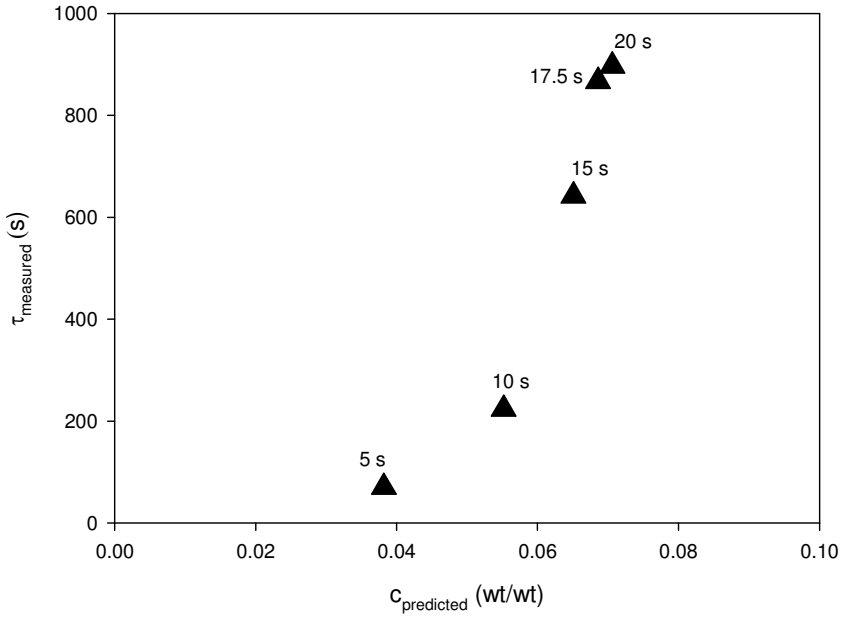

Figure 6.15. Measured time constant of agglomerate breakage versus predicted liquid concentration of initial agglomerates for experiments with different durations of injection as shown in the figure (U_f = 0.2 m/s, GLR = 1.5 wt%)

6.5.6 Model results for different GLRs experiments

Figure 6.16 compares the predicted liquid concentration of initial agglomerates with the measured time constant of agglomerate breakage for experiments with different GLRs (wt %), a fluidization velocity during injection of 0.3 m/s and a fluidization velocity after injection of 0.2 m/s. The model predicts lower GLR causes the formation of stronger agglomerates with a higher liquid concentration. There is a clear correlation between the measured time constant of agglomerate breakage and the predicted liquid concentration of initial agglomerates. The model and experimental results from this study on the impact of GLR are in good agreement with the results of other studies (Ali Zirgachian et al. 2013; Farkhondehkavaki 2012; Portoghese et al. 2008).

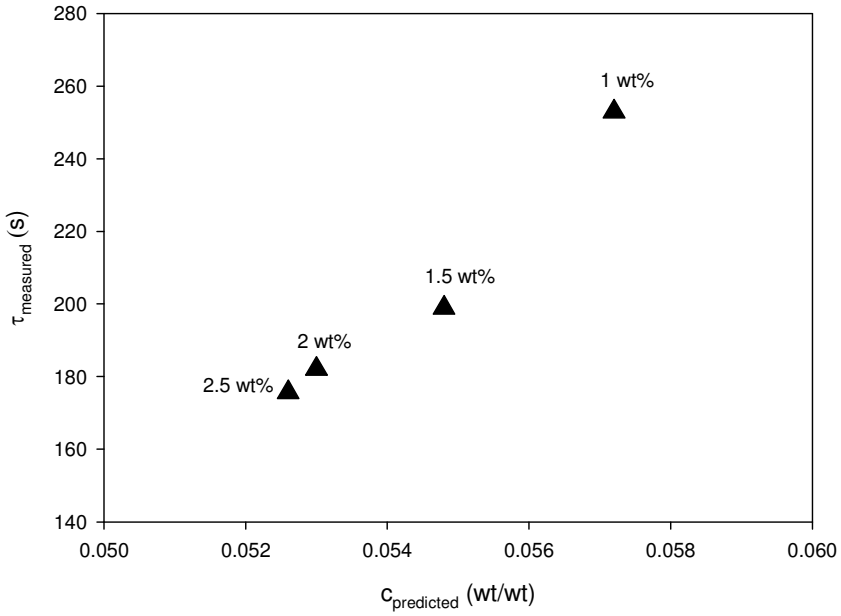

Figure 6.16. Measured time constant of agglomerate breakage versus predicted liquid concentration of initial agglomerates for experiments with different GLRs (wt %) as shown in the figure (fluidization velocity during injection = 0.3 m/s, fluidization velocity after injection = 0.2 m/s, and injection duration = 10 s)

6.6 Discussion

Figure 6.17 shows that there is a very good correlation between the liquid concentration of initial agglomerates predicted by the model and the measured time constant of agglomerate breakage for all the experiments conducted in this study and presented in section 6.5, using different nozzle locations, nozzle inclinations, fluidization velocities during injection, durations of injection, GLRs and the local addition of extra gas. Figure 6.17 also confirms that wetter agglomerates are stronger, as found in other studies (Morales M 2013; Weber 2009). There is also good agreement between the predicted liquid concentration of agglomerates in this study and the reported liquid concentration by House (2007) for a specified condition. They predicted an average agglomerate liquid concentration of about 0.06 wt/wt with a nozzle of a similar size as the nozzle used in this study and a GLR of 1.5 wt%, which is close to what the developed model in this study predicts. There are two different zones in Figure 6.17 which correspond to a different

level of liquid saturation. Newitt and Conway-Jones (1958) and Capes and Sutherland (1967) showed different classification of agglomerates (Pendular, Funicular, and Capillary) based on the fluid content of agglomerates which can be a justification for obtaining two different zones in Figure 6.17.

Other researchers have shown the impact on the initial agglomerate formation and strength of different parameters such as GLR, nozzle geometry and nozzle attachments. This section shows how the model can provide a qualitative interpretation of these earlier studies.

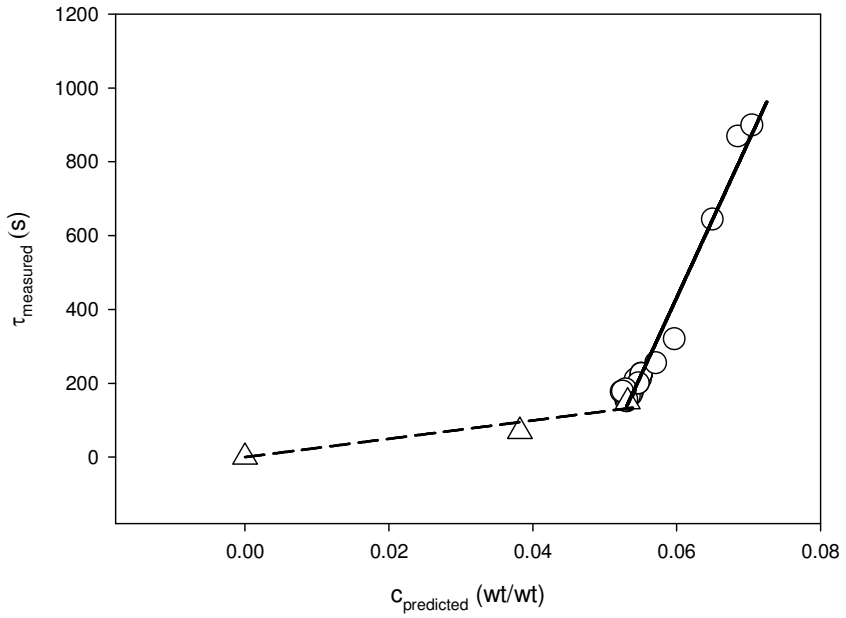

Figure 6.17. Measured time constant of agglomerate breakage versus predicted liquid concentration of initial agglomerates for a fluidization velocity of 0.2 m/s after injection

6.6.1 Effect of nozzle geometry

Prociw (2014) found that increasing the diverging angle of the gas-liquid spray is beneficial. Increasing the diverging angle of the gas-liquid spray increases the horizontal cross-section of the jet cavity and hence, its bubble capture area. According to the model, this increases the bubble gas flowrate and the flowrate of solids carried by bubbles into the jet cavity. This results in a smaller predicted liquid concentration of initial agglomerates when there is higher amounts of solids carried by bubbles to the jet cavity. Therefore, the model predicts that increasing the diverging angle of the gas-liquid spray

reduces the time constant for agglomerate breakage, which is in agreement with Prociw's findings (Prociw 2014).

6.6.2 Effect of GLR

The model predicts that increasing GLR forms agglomerates with a lower liquid concentration, which are weaker and break up more quickly in a fluidized bed. This agrees well with previous studies on the impact of GLR and liquid distribution in fluidized beds (Ali Zirgachian et al. 2013; Farkhondehkavaki 2012; Portoghese et al. 2008).

6.6.3 Effect of High GLR nozzle

As mentioned in the calibration section, a high GLR nozzle is a nozzle with a very high atomization gas and a low liquid flowrate that provides an almost perfect distribution of liquid on solid particles. The model correctly predicts that greatly increasing the flowrate of atomization gas is very effective, causing the spray jet to expand much more quickly, which dilutes the injected liquid with a larger amount of fluidized particles, drastically reducing the liquid concentration of the initial agglomerates.

6.6.4 Effect of interactions with attrition jets

Saha (2012) found that getting an attrition jet to hit the base of the spray jet is more effective than getting an attrition jet to hit the tip of the jet cavity. The model predicts that adding attrition gas to the base of the atomization jet is very effective, akin to greatly increasing the flow of gas bubbles captured by the jet cavity, which means that the spray jet expands much more quickly, which dilutes the injected liquid with a larger amount of fluidized particles. On the other hand, the model predicts that hitting the bed region near the tip of the jet cavity is not very effective, since it does not greatly change the time taken by the jet to expand. The model predictions are, thus, in good agreement with the experimental findings.

6.6.5 Effect of satellite jets

Satellite jets are configurations with a gas shroud, i.e. small satellite jets hitting the base of the jet cavity, just downstream of the nozzle tip. House et al. (2008) found a reduction in liquid concentration in agglomerates when using satellite jets. This reduction was observed even when the atomization gas flowrate was reduced to keep constant the sum of atomization gas flowrate and satellite jets gas flowrate, which would not change the time taken by the jet to expand. There must, therefore, be another effect that could explain the results obtained by House et al. (2008). By disrupting the boundary between the bed and the jet cavity, the satellite jets should enhance the entrainment of the bed solids into the jet cavity; according to the model, this would reduce the liquid concentration of the initial agglomerates. Obtaining reductions of about 20 % observed by House et al. (2008) would require an increase of about 60 % in the flowrate of entrained solids.

6.6.6 Effect of draft tube

Several studies have found that using a draft tube improves the liquid distribution on fluidized bed particles (Ali Zirgachian et al. 2013; Ariyapadi et al. 2005; House et al. 2008; McMillan et al. 2005b). A draft tube is a tube which is coaxial with the nozzle and located in the fluidized bed, downstream of the nozzle tip. For example, House et al. (2008) obtained a 40% reduction in the liquid concentration of the initial agglomerates by using such a draft tube. According to the model, the draft tube should not affect the mean liquid concentration of the initial agglomerates. Ariyapadi et al. (2005) proposed that the draft tube improves liquid distribution by enhancing the turbulence within the jet cavity, ensuring a better distribution of the liquid droplets and entrained particles over the cross-section of the jet cavity, which would result in a more uniform wetting of the bed particles displaced by the expanding jet. Therefore, this should results in agglomerates that all have about the same liquid concentration and reduce the formation of very wet agglomerates, which, according to Figure 6.17, have a disproportionate detrimental impact on the time constant of agglomerate breakage. Unfortunately, the model can only predict the mean liquid concentration of the initial agglomerates. It cannot predict the

distribution of the liquid concentration within the solids displaced by the expanding jet and cannot, therefore, predict the beneficial impact of the draft tube.

6.6.7 Effect of pulsations

Sabouni et al. (2012) and Leach et al. (2013) found that the spray jet pulsation frequencies between about 1 and 10 Hz greatly improved the distribution of liquid on solid particles and they found better distribution for jet frequencies between about 1 and 10 Hz. Because beneficial effects were observed at pulsating frequencies that are about one order of magnitude greater that the frequency of bubble release from the jet cavity, the model predicts that spray jet pulsations should not affect the mean liquid concentration of the initial agglomerates. It is likely, however, that the spray jet pulsations enhance the localized mixing of the liquid droplets with the bed solids displaced by the expanding jet. Unfortunately, the model can only predict the mean liquid concentration of the initial agglomerates and cannot predict the distribution of the liquid concentration within the solids displaced by the expanding jet; the model cannot, therefore, predict the beneficial impact of the spray jet fluctuations.

6.7 Sensitivity analysis

A sensitivity analysis was performed to determine the relative importance of various model parameters. This analysis was performed for the spray nozzles at different locations in the bed. The results show that an increase in the flowrate of solids carried by bubbles to the jet cavity (F_{SB}) that is a result of the increase in the flowrate of bubbles captured by the jet cavity (q_b) (Equation 10) has a large impact on the predicted liquid concentration.

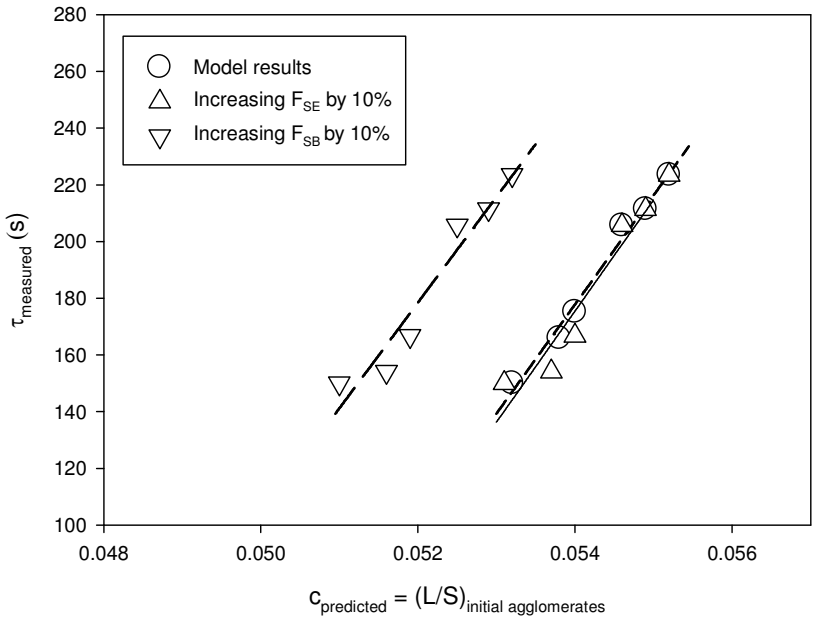

Figure 6.18. Sensitivity analysis of the results of model (predicted liquid concentration of initial agglomerates) by increasing various model inputs by 10% for experiments with a nozzle at different locations of the bed for a fluidization velocity of 0.2 m/s , a GLR of 1.5 wt%, and an injection duration of 10s

6.8 Conclusions

In this study a model was developed which requires no new empirical parameters and provides information on the liquid concentration of agglomerates resulting from the contact between sprayed liquid and solid particles. The results of the model are in good agreement with the experimental results as the liquid concentration of the agglomerates obtained from the model correlates well with the time constant of agglomerate breakage obtained from experiments. The model can also explain most of the published findings on the initial contact between sprayed liquid and fluidized particles.

References

"U.S. National Library of Medicine.". (http://www.webwiser.nlm.nih.gov).

Ali Zirgachian, M., M. Soleimani, C. Briens and F. Berruti. 2013. "Electric Conductance Method for the Assessment of Liquid-Gas Injection into a Large Gas-Solid Fluidized Bed." *Measurement: Journal of the International Measurement Confederation* 46(2):893-903.

Ariyapadi, S., D. Holdsworth, C. Norley, F. Berruti and C. Briens. 2003a. "Digital X-Ray Imaging Technique to Study the Horizontal Injection of Gas-Liquid Jets into Fluidized Beds." *International Journal of Chemical Reactor Engineering* 1 (A56).

Ariyapadi, S., F. Berruti, C. Briens, P. Griffith and C. Hulet. 2003b. "Modeling the Injection of Gas-Liquid Jets into Fluidized Beds of Fine Particles." *Canadian Journal of Chemical Engineering* 81(3-4):891-899.

Ariyapadi, S., J. McMillan, D. Zhou, F. Berruti, C. Briens and E. Chan. 2005. "Modeling the Mixing of a Gas-Liquid Spray Jet Injected in a Gas-Solid Fluidized Bed: The Effect of the Draft Tube." *Chemical Engineering Science* 60(21):5738-5750.

Baron, T., C. L. Briens and M. A. Bergougnou. 1988. "Study of the Transport Disengaging Height." *Canadian Journal of Chemical Engineering* 66(5):749-760.

Base, T., E. Chan, R. Kennett and D. Emberley. 1999. "Nozzle for Atomizing Liquid in Two Phase Flow.".

Benjelloun, F., R. Liegeois and J. Vanderschuren. 1995. "Peneteration Length of Horizontal Gas Jets into Atmospheric Fluidized Beds.":239.

Berruti, F., M. Dawe and C. Briens. 2009. "Study of Gas-Liquid Jet Boundaries in a Gas-Solid Fluidized Bed." *Powder Technology* 192(3):250-259.

Briens, C., F. Berruti, V. Felli and E. Chan. 2008. "Solids Entrainment into Gas, Liquid, and Gas-Liquid Spray Jets in Fluidized Beds." *Powder Technology* 184(1):52-57.

Bruhns, S. and J. Werther. 2005. "An Investigation of the Mechanism of Liquid Injection into Fluidized Beds." *AICHE Journal* 51(3):766-775.

Capes, C. E. and J. P. Sutherland. 1967. "Formation of Spheres from Finely Divided Solids in Liquid Suspension." 6(1):146.

Department of Physics and Astronomy. "*Dielectric Constant at 20 ^{o}C. Department of Physics and Astronomy, Georgia State University*.". (http://hyperphysics.phy-astr.gsu.edu.).

Farkhondehkavaki, M. 2012. "Developing Novel Methods to Characterize Liquid Dispersion [Dissertation]." Western University, London (ON), .

Gray, M. R., W. C. McCaffrey, I. Huq and T. Le. 2004. "Kinetics of Cracking and Devolatilization during Coking of Athabasca Residues." *Industrial and Engineering Chemistry Research* 43(18):5438-5445.

Hamidi, M. 2014. "Development of Advanced Electrical Methods for Fluidized Bed Measurements.".

Hammond, D. G., L. F. Lampert, C. J. Mart, S. F. Massenzio, G. E. Phillips, D. L. Sellards and A. C. Woerner. 2003. "Refining: Review of Fluid Bed Coking Technologies." *Petroleum Technology Quarterly* 8(5):27-31, 33.

Hilligardt, Klaus and Joachim Werther. 1985. "Lokaler Blasengas-Holdup Und Expansionsverhalten Von Gas/Feststoff-Wirbelschichten." *Chemie Ingenieur Technik* 57(7):622-623 (http://resolver.scholarsportal.info/resolve/0009286x/v57i0007/622_lbuevg).

House, P. K. 2007. "Interaction of Gas-Solid Jets with Gas-Solid Fluidized Beds: Effect on Liquid-Solid Contact and Impact on Fluid Coking Operation " Western University, .

House, P. K., C. L. Briens, F. Berruti and E. Chan. 2008. "Effect of Spray Nozzle Design on Liquid-Solid Contact in Fluidized Beds." *Powder Technology* 186(1):89-98.

Knapper, B. A., M. R. Gray, E. W. Chan and R. Mikula. 2003. "Measurement of Efficiency of Distribution of Liquid Feed in a Gas-Solid Fluidized Bed Reactor." *International Journal of Chemical Reactor Engineering* 1 (A35).

Leach, A., R. Sabouni, F. Berruti and C. Briens. 2013. "Use of Pulsations to Enhance the Distribution of Liquid Injected into Fluidized Particles with Commercial-Scale Nozzles." *AICHE Journal* 59(3):719-728.

Li, Tingwen, Konstantin Pougatch, Martha Salcudean and Dana Grecov. 2010. "Numerical Modeling of an Evaporative Spray in a Riser." *Powder Technology* 201(3):213-229.

McDougall, S., M. Saberian, C. Briens, F. Berruti and E. Chan. 2005. "Effect of Liquid Properties on the Agglomerating Tendency of a Wet gas–solid Fluidized Bed." *Powder Technology* 149(2–3):61-67.

McMillan, J., D. Zhou, S. Ariyapadi, C. Briens, F. Berruti and E. Chan. 2005. "Characterization of the Contact between Liquid Spray Droplets and Particles in a Fluidized Bed." *Industrial and Engineering Chemistry Research* 44(14):4931-4939.

Mohagheghi, M., M. Hamidi, F. Berruti, C. Briens and J. McMillan. 2014. "The Effects of Injection Nozzle Location and Inclination on the Interaction between a Gas-Liquid Jet and a Gas Solid Fluidized Bed.".

Mohagheghi, M., M. Hamidi, F. Berruti, C. Briens and J. McMillan. 2013. "Study of the Effect of Local Hydrodynamics on Liquid Distribution in a Gas-Solid Fluidized Bed using a Capacitance Method." *Fuel*.

Mohagheghi, M., M. Hamidi, C. Briens, F. Berruti and J. McMillan. 2014. "The Effects of Liquid Properties and Bed Hydrodynamics on the Distribution of Liquid on Solid Fluidized Particles in a Cold-Model Fluidized Bed." *Powder Technology* 256:5-12.

Morales M, C. B. 2013. " Development and Application of an Experimental Model for the Fluid Coking^{TM} Process " Western University, .

Newitt, D. M. and J. M. Conway-Jones. 1958. "A Contribution to the Theory and Practice of Granulation." 36:142.

Parveen, F., C. Briens, F. Berruti and J. McMillan. 2013. "Effect of Particle Size, Liquid Content and Location on the Stability of Agglomerates in a Fluidized Bed." *Powder Technology* 237:376-385.

Portoghese, F., L. Ferrante, F. Berruti, C. Briens and E. Chan. 2008. "Effect of Injection-Nozzle Operating Parameters on the Interaction between a Gas-Liquid Jet and a Gas-Solid Fluidized Bed." *Powder Technology* 184(1):1-10.

Pougatch, K., M. Salcudean and J. McMillan. 2012. "Three-Dimensional Numerical Modelling of Interactions between a Gas-Liquid Jet and a Fluidized Bed." *Chemical Engineering Science* 68(1):258-277.

Prociw, N. 2014. "Effect of Nozzle Geometry on Jet-Bed Interaction." Western University,.

Sabouni, R., F. Berruti and C. Briens. 2012. "Comparison of the Impact of Flow Pulsations on the Performance of various Liquid-Gas Injectors in a Gas-Solid Fluidised Bed." *Canadian Journal of Chemical Engineering* 90(1):51-60.

Saha, M. 2012. "Simultaneous Particle Agglomeration and Attrition in a High Temperature Fluidized Bed." Western University, .

Saleh, K., D. Steinmetz and M. Hemati. 2003. "Experimental Study and Modeling of Fluidized Bed Coating and Agglomeration." *Powder Technology* 130(1–3):116-123.

Song, Xuqi, John R. Grace, Hsiaotao Bi, C. J. Lim, Edward Chan, Brian Knapper and Craig McKnight. 2006. "Experimental Simulation of the Reactor Section of Fluid Cokers: Comparison of FCC and Fluid Coke Particles." *The Canadian Journal of Chemical Engineering* 84(2):161-169.

Song, X., H. Bi, C. J. Lim, J. R. Grace, E. Chan, B. Knapper and C. McKnight. 2004. " Hydrodynamics of the Reactor Section in Fluid Cokers." *Powder Technology* 147:126.

Terrazas-Velarde, Korina, Mirko Peglow and Evangelos Tsotsas. 2009. "Stochastic Simulation of Agglomerate Formation in Fluidized Bed Spray Drying: A Micro-Scale Approach." *Chemical Engineering Science* 64(11):2631-2643.

Weber, S. C. 2009. "Agglomerate Stability in Fluidized Beds." Western University, .

Weber, S. C., C. Briens, F. Berruti and M. R. Gray. 2009. "Thermal Conductivity of Agglomerate Material for Non-Evaporating and Evaporating Conditions." *8th World Congress of Chemical Engineering: Incorporating the 59th Canadian Chemical Engineering Conference and the 24th Interamerican Congress of Chemical Engineering*.

Xuereb, C., C. Laguérie and T. Baron. 1991. "Etude Du Comportement De Jets Continus Horizontaux Ou Inclinés Introduits Dans Un Lit Fluidisé Par Un Gaz I: Morphologie Des Jets." *Powder Technology* 67(1):43-56.

Chapter 7

7. MODELLING OF INTERACTIONS BETWEEN LIQUID-GAS SPRAY JET AND FLUIDIZED PARTICLES IN A GAS-SOLID FLUIDIZED BED (PART II: MOVING SPRAY NOZZLE)

7.1 Abstract

In Part II of this study, a model was developed for the interactions between sprayed liquid and fluidized particles with a relative velocity between the spray nozzle and particles. In a Fluid Coker™, a set of nozzles located at different heights injects liquid into a fluidized bed of downward flowing particles with a gas superficial velocity ranging from 0.3 to 0.5 m/s and, thus, the model takes into account the relative velocity between the spray nozzle and bed particles. The model predicts the liquid concentration of initial agglomerates resulting from a moving nozzle which is closer to a Fluid Coker unit than a stationary nozzle with a pulse injection. The model provides the liquid concentration of the initial formed agglomerates at the tip of the jet cavity. The model results were compared with experimental results on the strength of agglomerates, when there is a relative velocity between spray nozzle and bed particles.

7.2 Objectives

In Part I of this study a model was developed for the case of a stationary spray nozzle and no net motion of the fluidized solids, as in most previous experimental studies. The model results were compared to the previous experimental studies (Mohagheghi et al. 2013; Mohagheghi et al. 2014; Mohagheghi et al. 2014) and were found to provide consistent information on the strength of wet agglomerates, which was inferred from the rate at which trapped liquid was released from the agglomerates. The objectives of this Part II are to:

1. modify the model to take into account the relative velocity between spray nozzle and bed particles,
2. validate its predictions with experiments conducted with a moving spray nozzle,
3. apply the model to cases relevant to commercial-scale Fluid Cokers™.

7.3 Review of experimental procedure

7.3.1 Experimental setup

The experimental setup for Part II is the same as for Part I, except that in this study, the spray nozzle is moved to provide a relative velocity between sprayed liquid and fluidized particles, as in Fluid Cokers™. The nozzle is moved up or down inside the bed with a rodless pneumatic cylinder. The nozzle velocity is set by changing the air pressure of the rodless cylinder, and measured with a PING)))™ Ultrasonic Distance Sensor #28015. There are two solenoid valves for controlling the injection on the atomization gas and the liquid line. There are also two other solenoid valves on the rodless cylinder to control the up and down motion of the nozzle. Two Hall effect sensors are used to control the position of the nozzle. An EATON controller (Easy 500 Intelligent Relays) is used to control the motion, injection and location of the nozzle. More experimental details may be found in the earlier study.

7.3.2 Experimental methods

The measuring system, calibration experiments and method for calculation of time constant of agglomerate breakage (τ) are as in Part I.

7.4 Modelling

7.4.1 Theory

The model developed in the first part of this study was extended for a moving nozzle. The basic theory and equations are as in Part I.

7.4.2 Model

Since all the required parameters for the model were predicted as described in previous part, the model was modified with applying the conservation of mass around the jet cavity for a moving nozzle.

To develop the model for a moving nozzle, several cases were considered:

1) Single jet expansion (and single pass). The spray forms a jet cavity in the fluidized bed, which fluctuates as it first expands gradually until it reaches its maximum volume, a large bubble escapes from the tip of the jet, reducing the jet volume suddenly, and the jet starts expanding again gradually. Since there were no significant differences in agglomerates formed from downward-moving or upward-moving nozzles, it is assumed that for a spraying time less than or equal to the time for a single jet expansion, the model developed for a stationary nozzle can be applied to a moving nozzle without any modification. Using the model developed in part I, one can obtain the concentration c of liquid in the agglomerates released from the spray jet cavity:

$$F_{L_{in}} = F_{L_{out}} = F_{S_{out}} \times c \tag{7.1}$$

$$F_{S_{out}} = (Q_b + Q_a) \times \rho_{mf} + F_{SB} + F_{SE} \tag{7.2}$$

$$c = \frac{F_L}{(Q_b + Q_a) \times \rho_{mf} + F_{SB} + F_{SE}} \tag{7.3}$$

2) Multiple jet expansions (and single pass). For multiple jet expansions, the model for the stationary nozzle assumed that some of the solids wetted during the first jet expansion would be re-wetted during subsequent jet expansions. For a nozzle moving at a velocity above a critical velocity, it is assumed that no previously wetted solids are re-wetted, which means that Equation 7.3 still applies. This only applies to a single pass, i.e. when the nozzle does not move through bed regions that have been previously exposed to the spray. The critical nozzle velocity is estimated to be about the same as the jet expansion velocity. The jet expansion velocity was calculated from the length of the expansion and the time between consecutive bubbles released from the jet cavity:

$$u_{expansion} = \frac{4V_{tip}}{\pi\, t_r\, {W_{tip}}^2} \sim 0.18 \frac{m}{s} \tag{7.4}$$

$$W_{tip} = 2L_{jet}\, tan\frac{\theta_j}{2} \tag{7.5}$$

where V_{tip} is the volume of the detached bubble from the jet, W_{tip} is the jet width at the tip of the jet, L_{jet} is the measured jet length, θ_j is the jet expansion angle obtained from Berruti et al. (2009) and t_r is the required time for a full jet expansion. In the moving nozzle experiments of this study, the nozzle velocity was always higher than the critical velocity.

3) Multiple passes. The nozzle moves through bed regions that have been previously exposed to the spray. It is then assumed, as shown below, that the wet solids affect the local bed hydrodynamics, reducing the rate at which gas bubbles penetrate the jet cavity.

7.5 Experimental results

An earlier study measured the time constant of agglomerate breakage for a moving nozzle with a single pass. Table 7.1 shows the experimental conditions for these experiments, which were conducted for a single pass of the moving nozzle.

Table 7.1. Experimental conditions for single pass experiments

Run #	Nozzle velocity (m/s)	Injection time(s)	Number of full jet expansions	Fluidization velocity (m/s)	GLR (wt%)
1	0.4	2.5	1	0.2	1.5
2	0	2.5	1	0.2	1.5
3	0.2	5	2	0.2	1.5
4	0	5	2	0.2	1.5

Figure 7.1 shows how the time constant of agglomerate breakage varied with the injection duration, for both stationary and moving (single pass) nozzles. For a 2.5 s injection, the time constant of agglomerate breakage is almost the same for both stationary and moving nozzles. The time constant of agglomerate breakage does not change with injection duration for a moving nozzle, while, for a stationary nozzle, it increases by nearly 60 % when the injection duration is increased from 2.5 s to 5 s.

According to the model presented in part I, a 2.5 s injection is just longer than the time for a single jet expansion. It therefore, appears that a single pass moving nozzle behaves as a stationary nozzle with a single jet expansion.

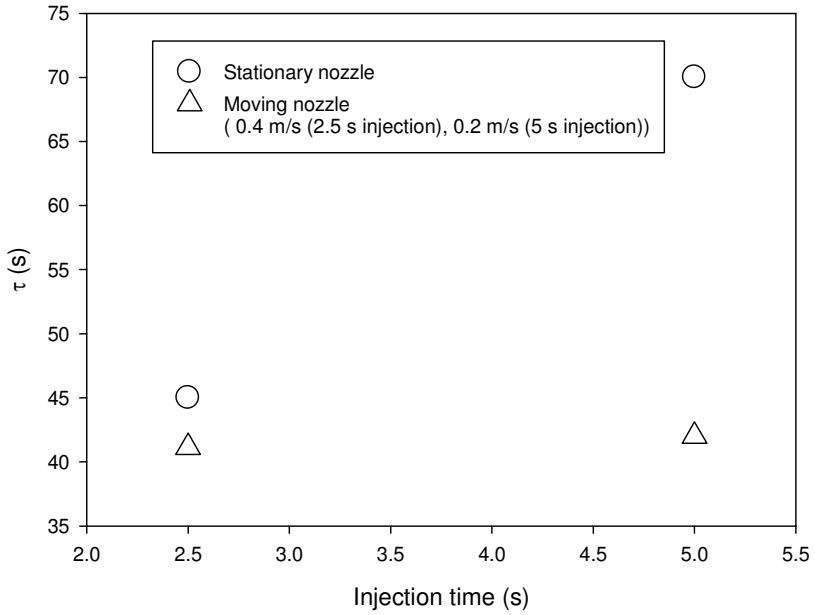

Figure 7.1. Measured time constant of agglomerate breakage versus injection time for both stationary and moving nozzles (single pass) (U_f = 0.2 m/s, GLR = 1.5 wt%, and δin = 0.5 m)

7.6 Results of the model

7.6.1 Results of the model for a single nozzle pass (either moving up or down)

The developed model was applied to the experiments with a single pass (Table 7.1). For these experiments all the entrained solids and also solids at tip of the jet are considered to be dry.

Figure 7.2 shows how the measured time constant of agglomerate breakage (τ) correlates with the liquid concentration of agglomerates as predicted by the model, for both single pass moving nozzle experiments and for a stationary nozzle. Figure 7.2 shows that, for a single pass moving nozzle, the model predicts the agglomerates liquid concentration is not affected by the injection duration or the nozzle velocity (which was larger than the

critical velocity), and this is confirmed by the measurements, which yielded the same time constant of agglomerate breakage. Figure 7.2 also shows that, for a stationary nozzle both the predicted agglomerates liquid concentration and the measured time constant of agglomerate breakage increase with the injection time, as solids wetted during the first jet expansion are re-wetted in subsequent jet expansions.

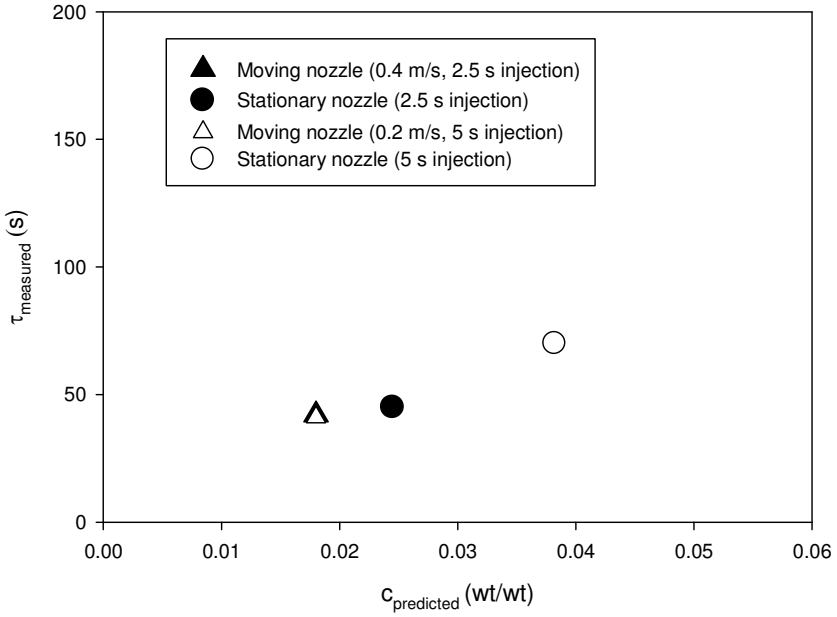

Figure 7.2. Experimental results (τ) versus model predictions (liquid concentration of agglomerates) for moving nozzle experiments with single pass injection and also for a stationary nozzle with the same injection time (GLR = 1.5 wt%, U_f = 0.2 m/s, and δin = 0.5 m)

7.6.2 Model predictions for multiple nozzle passes

An earlier study measured the time constant of agglomerate breakage for a moving nozzle with different nozzle velocities (fluidization velocity of 0.2 m/s, GLR of 1.5 wt% and a lateral position of nozzle tip (δin) of 0.50 m from the bed wall). The injection time was kept constant at 10 s, and the number of passes varied with the nozzle velocity, as the distance traveled for each pass was kept constant. The total path length of injection for one cycle, i.e. one "return trip" of the spray nozzle, was 180 cm. Table 7.2 shows the experimental conditions of these experiments.

Table 7.2. Experimental conditions for moving nozzle experiments

Experiment No.	Nozzle velocity (m/s)	Number of moving cycles	Δt (s)	Total injected liquid (g)	Liquid mass flow rate (g/s)	Fluidization velocity (m/s)
1	0.21	1	0	550	55	0.2
2	0.21	1	5	550	55	0.2
3	0.35	2	0	550	55	0.2
4	0.51	3	0	550	55	0.2
5	0.71	4	0	550	55	0.2

7.6.2.1 Predictions assuming no significant background liquid for multiple passes

The model was applied for a moving nozzle with multiple passes, assuming there is no significant background liquid for the second and higher passes. Figure 7.3 shows that the measured time constant of agglomerate breakage is greater than expected from the correlation between the predicted agglomerates liquid concentration and the time constant of agglomerate breakage obtained from experiments with both the single pass moving nozzle and the stationary nozzle. Therefore, the assumption of no significant background liquid for multiple passes does not appear valid.

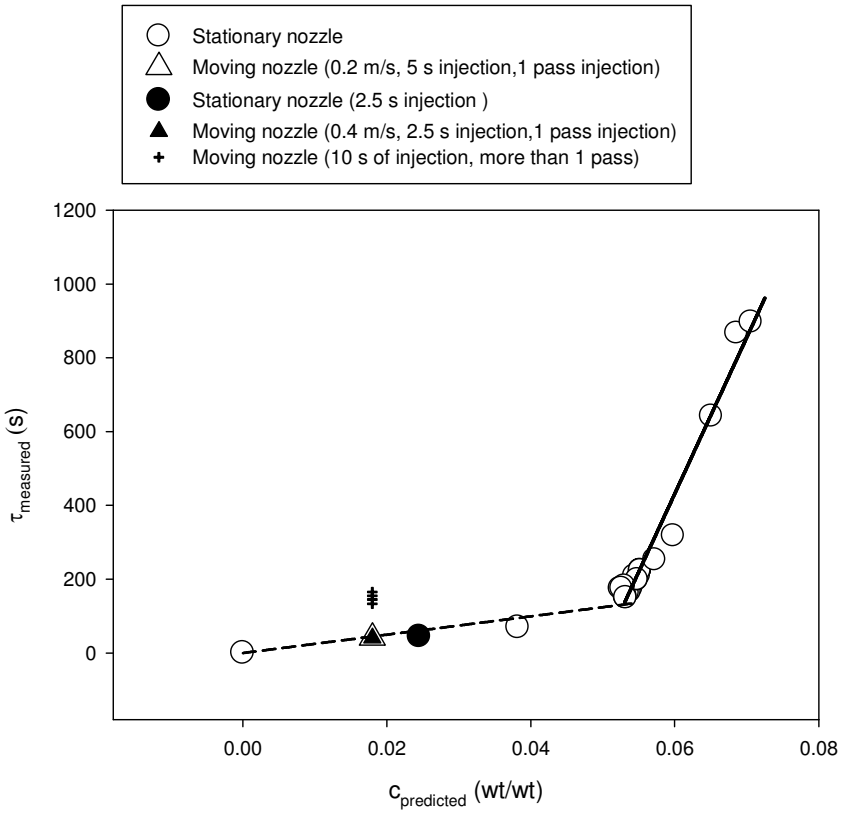

Figure 7.3. Measured time constant of agglomerate breakage versus predicted liquid concentration of agglomerates for a moving nozzle with different nozzle velocities (multiple nozzle passes) along with results for moving nozzle with single pass (GLR = 1.5 wt%, Uf = 0.2 m/s, and δin = 0.5 m) and all the stationary nozzle results from part I

7.6.2.2 Predictions assuming significant background liquid without impact on local hydrodynamics

To check the impact of background liquid for multiple passes, the model accounted for the background liquid for passes larger than one. Liquid from the agglomerates formed in the first pass were assumed to mix with solids from the jet area , i.e. an area with the same length and width as the jet, and a height equal to the height traveled by the nozzle over the whole pass. The model predicts that the background liquid concentration just before the second pass is 0.00417 wt/wt, for the experiments of this study.

Figure 7.4 shows that, although considering the background liquid increases the predicted agglomerate liquid concentration, it is still far from the value that would be expected from the measured time constant of agglomerate breakage. There is therefore, another cause that must increase the agglomerate liquid concentration.

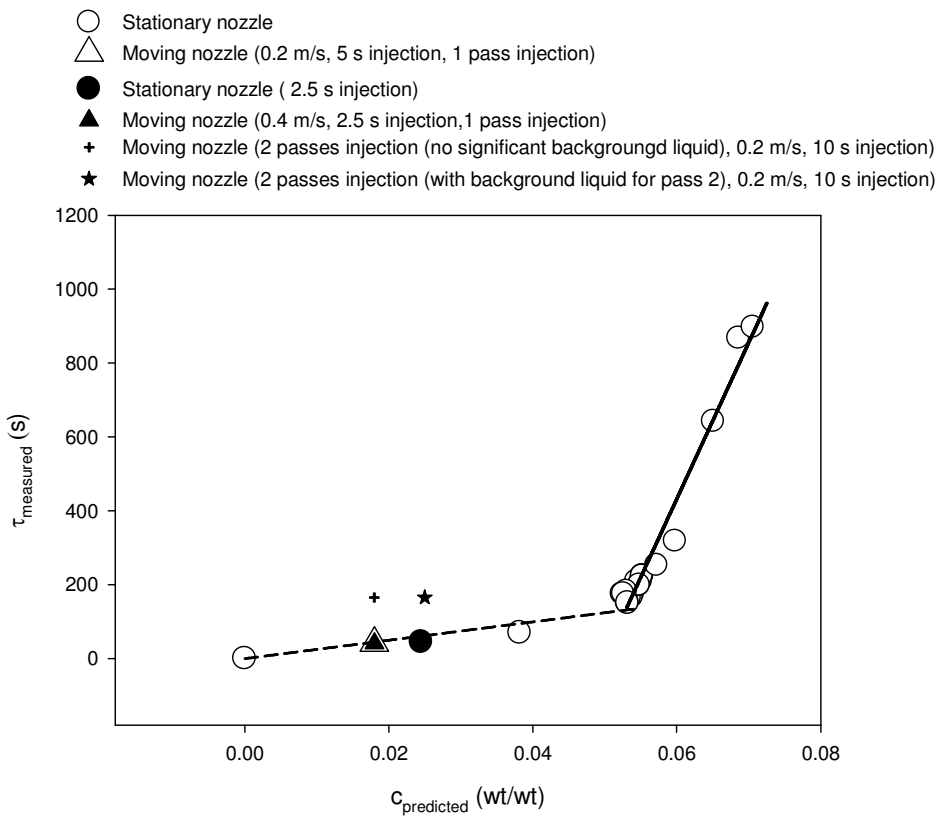

Figure 7.4. Measured time constant of agglomerate breakage versus predicted liquid concentration of agglomerates for a moving nozzle with velocity 0.2 m/s (2 passes), a GLR of 1.5 wt%, U_f = 0.2 m/s , and δin = 0.5 m for two cases: no significant background liquid concentration for second pass and a significant background liquid concentration for second pass along with results for moving nozzle with single pass and all the stationary nozzle results from part I

7.6.2.3 Predictions accounting for the impact of background liquid on local bed hydrodynamics

This section accounts for the impact of the background liquid on the local bed hydrodynamics and, in particular the bubbles motion around the jet cavity. Another study with a similar system (Hamidi 2014) has shown that, as the background liquid concentration increases, the bubbles motion is greatly affected: bubbles tend to bypass regions where the background liquid makes particles cohesive. It was, therefore, assumed that for passes higher than one, the flow of gas bubbles into the jet cavity was reduced. This reduces the amount of solids entering the jet cavity with the bubbles, as well as slowing the jet expansion.

The bubble flowrate into the jet cavity for passes subsequent to the first pass was reduced to an assumed fraction of the bubble flowrate into the jet cavity for the first pass. Figure 7.5 shows that the predicted agglomerate liquid concentration for a moving nozzle with two passes is, then, in agreement with the results obtained with a stationary nozzle.

The experimental results of an earlier study for a moving nozzle shows a nozzle with higher velocity (more passes) forms weaker agglomerates and the time constant of agglomerate breakage for them is lower. For a moving nozzle with higher velocity, it can be assumed that there is more mixing around the jet and the nozzle area, so, there is less decrease in the flow of bubbles into the jet cavity which causes the formation of weaker agglomerates.

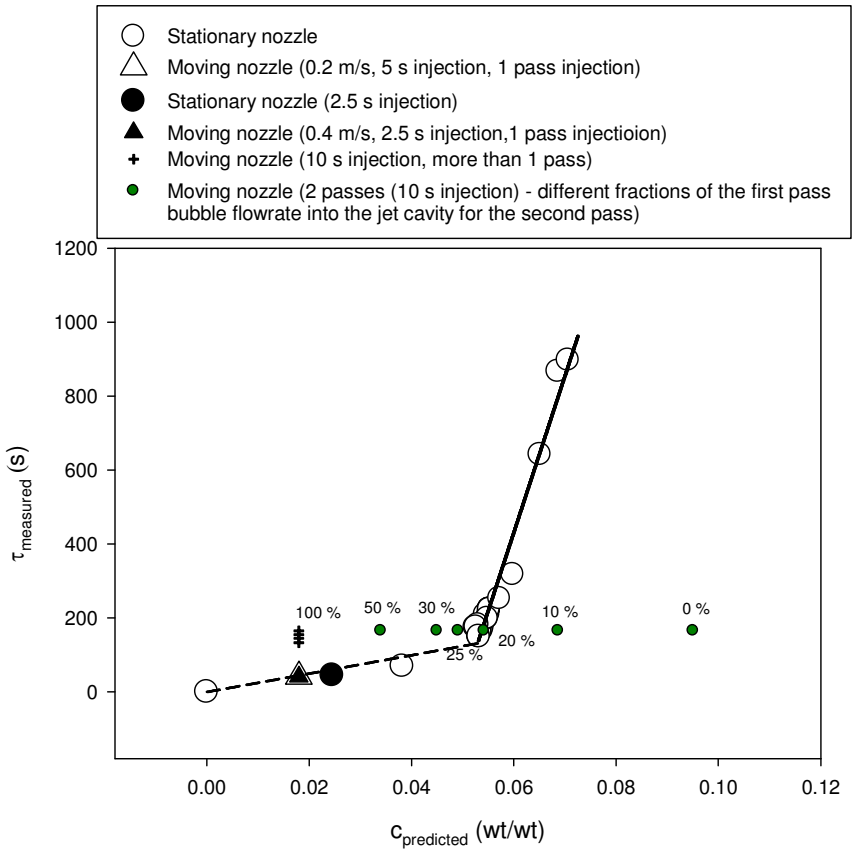

Figure 7.5. Measured time constant of agglomerate breakage versus predicted liquid concentration of agglomerates for moving nozzle with velocity 0.2 m/s (2passes) and different fractions of the first pass bubble flowrate into the jet cavity for bubble flowrate into the jet cavity for passes subsequent to the first pass along with results for moving nozzle with different nozzle velocities (multiple nozzle passes) without considering the impact of background liquid and its impact on the local bed hydrodynamics, moving

nozzle with single pass ((GLR = 1.5 wt%, U_f = 0.2 m/s, and δin = 0.5 m), and all the stationary nozzle results from part I

7.7 Application of the model to cases relevant to commercial Fluid Cokers™

7.7.1 Model predictions for typical Fluid Coker™ conditions with no significant background liquid

In an actual Fluid Coker, there are six feed rings at different heights of the reactor. The radial voidage distribution is different at different heights of a Fluid Coking reactor, because of the vapors and gases generated by the cracking of the feedstock. Song et al. (2004) investigated the voidage distribution in a small scale cold model Fluid Coker, which was a scaled down by a factor of 20 from two industrial Fluid Cokers operated by Syncrude Canada Limited in Fort McMurray, AB, Canada. Figure 7.6 shows the schematic diagram of this small scale Fluid Coker (Song et al. 2004). The radial voidage distribution was obtained at heights of feed ring 1 (top row nozzles), feed ring 2, and feed ring 6 (bottom row nozzles) using Song et al. (2004). The local bubble volume fraction was calculated from the local void fractions using Equation 7.6.

$$\varepsilon_b = \varepsilon - \varepsilon_{mf} \tag{7.6}$$

where ε_b is the bubble volume fraction, ε is the local void fraction and ε_{mf} is the void fraction at minimum fluidization velocity. The void fraction near the wall (r/R = 1) was assumed to be the void fraction at minimum fluidization velocity. Figure 7.7 shows the radial bubble volume fraction at the jet tip as a function of the nozzle tip radial location for three heights in the Fluid Coking reactor (height of feed ring 1, ring 2 and feed ring 6) obtained from the voidage profile provided by Song et al. (2004) and using the jet penetration from Benjelloun's correlation (Benjelloun et al. 1995) for the specified nozzle throat diameter.

The radial position of the nozzle tip for feed ring 1, ring 2, and feed ring 6 in Fluid Coker was also obtained from Song et al. (2004). Table 7.3 shows the operating conditions for both the experimental setup in this study and an actual Fluid Coker™ (Ali Zirgachian et

al. 2013; Farkhondehkavaki 2012; Prociw 2014). Using conditions presented in Table 7.3 and also assuming no background liquid even for lower feed rings, the model was applied for different radial positions of the nozzle tip for feed rings 1, 2, and 6. The average bubble volume fraction for the bubble capture area (estimated in part I of this study as a function of jet length) for different radial locations of the nozzle tip for feed rings 1, 2, and 6 was calculated using Figure 7.

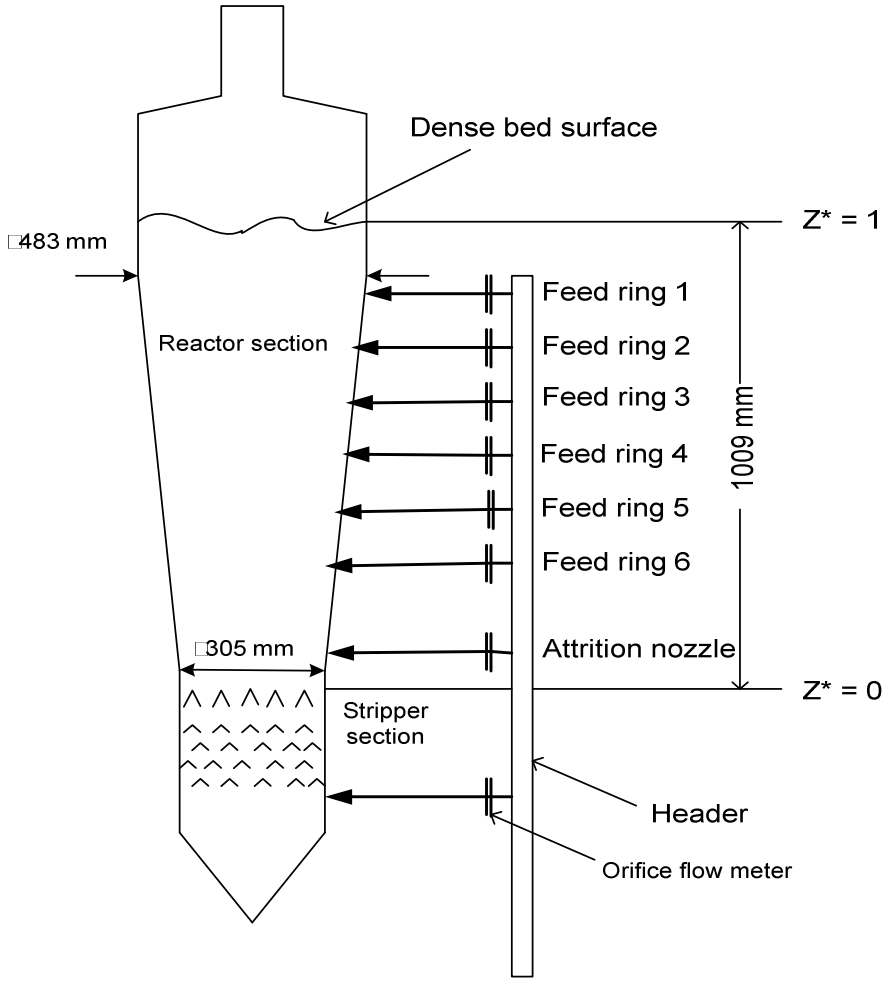

Figure 7.6. Schematic of a scaled down Syncrude Fluid Coker™ by a factor of 20 obtained from Song et al. (2004)

Table 7.3. Operating conditions for the experimental setup used in this study and a Fluid Coker™

Conditions	Experimental Setup in this study	Fluid Coker
Total Liquid flowrate (kg/s)	0.055	3
Nozzle size (mm)	2.2	10-15
Flux of liquid (kg/(m^2.s))	14.5×10^3	17×10^3 - 38×10^3
Gas to Liquid ratio of nozzle (wt%)	1.5	0.8
Atomization gas	Nitrogen	Steam
Feed temperature (^{0}C)	ambient	350
Bed pressure at bottom of the bed (Pa)	130×10^3	2950×10^3
Density of atomization gas at feed temperature and bed pressure (kg/m^3)	1.3	1.1
Average superficial gas velocity (m/s)	0.2	0.3-1
Jet expansion angle (^{0})	18	18

Figure 7.8 shows how the predicted liquid concentration of the initial agglomerates varies with the radial location of the feed nozzle tip for three rings at various dimensionless heights (Z*). Depending on the feed ring height, the optimal nozzle tip location may be near the column wall or far from the column wall. Figure 7.8 presents the results for a nozzle throat diameter of 12.5 mm and a GLR of 0.8 wt%. Since GLR, nozzle throat diameter, and also the spray angle have a considerable impact on the results of the model, their impact on the model predictions were investigated.

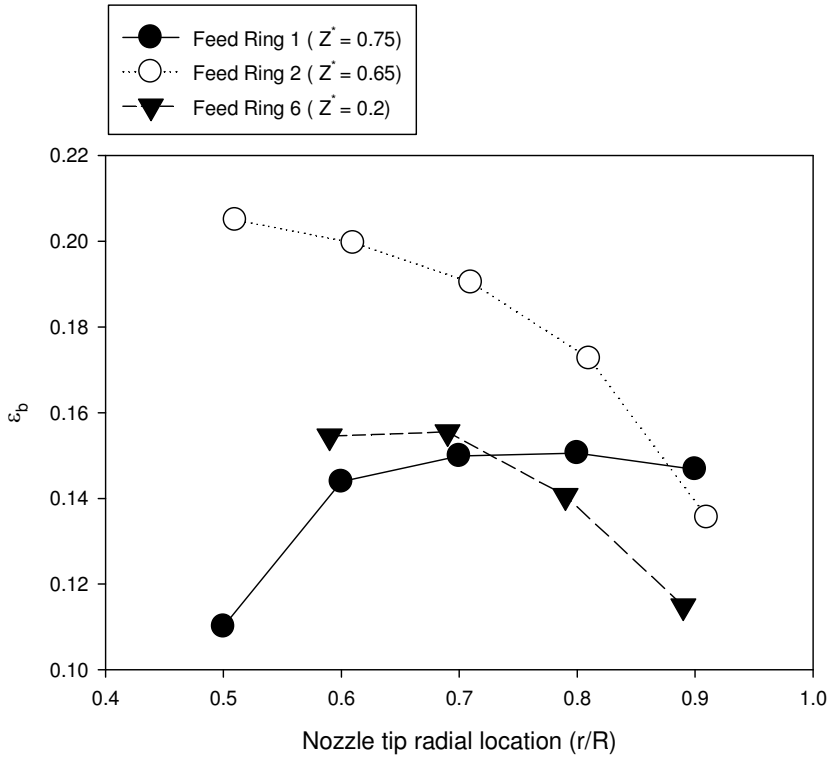

Figure 7.7. Bubble volume fraction near the jet tip versus the radial location of the feed nozzle for three rings at various dimensionless heights (Z*) from (Song et al. 2004)

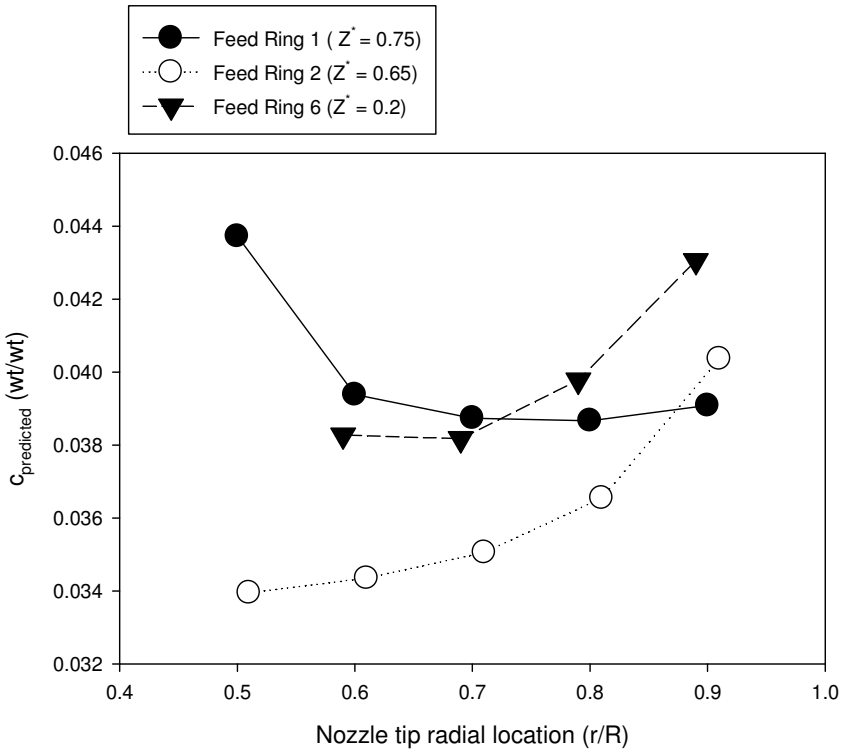

Figure 7.8. Predicted liquid concentration of initial agglomerates for the Fluid Coker conditions (presented in Figure 7.7 and Table 7.3) versus the radial location of the feed nozzle tip for three rings at various dimensionless heights (Z*)

Figure 7.9 shows, that as expected, increasing the GLR reduced the liquid concentration of the initial agglomerates, for Fluid Coker conditions presented in Table 7.3 (feed nozzle throat diameter and the radial location of the feed nozzle tip (r/R) were considered 12.5 mm and 0.9 respectively). This result was valid for all the feed rings.

Figure 7.10 shows that increasing the nozzle throat diameter while keeping the liquid flowrate constant had a detrimental effect, increasing the agglomerates liquid concentration. The predictions used Benjelloun's correlation (Benjelloun et al. 1995) to obtain the jet length for each nozzle throat diameter, the Fluid Coker conditions presented in Table 7.3 and a feed nozzle tip location (r/R) of 0.9. Increasing the feed nozzle throat diameter for the same feed rate decreases the jet length, thus reducing the bubble capture area of the jet cavity. Consequently, fewer solids enter the jet cavity.

Figure 7.11 shows how the predicted liquid concentration of the initial agglomerates varies with the nozzle throat diameter while keeping liquid flux constant for three rings at

various dimensionless heights (Z*). The predictions used a liquid flux of 24.5×10^3 kg/m^2.s, the Fluid Coker conditions presented in Table 7.3 and a feed nozzle tip location (r/R) of 0.9. Figure 7.11 shows that increasing the nozzle throat diameter, while keeping the liquid flux constant, increases the agglomerates liquid concentration and has a stronger detrimental effect than when keeping the liquid flowrate constant (Figure 7.10).

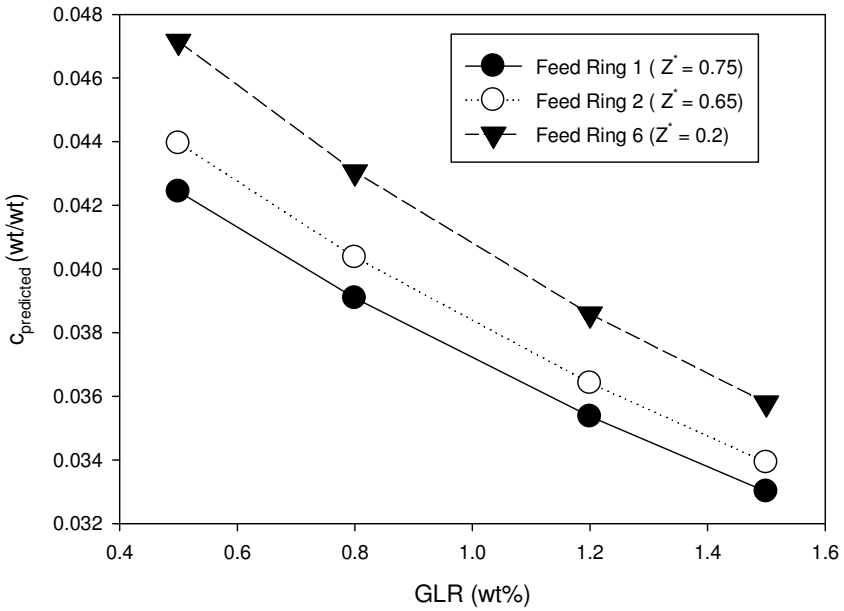

Figure 7.9. Predicted liquid concentration of initial agglomerate for the Fluid Coker conditions (presented in Table 7.3) versus GLR for three rings at various dimensionless heights (Z*) (the radial location of feed nozzle tip (r/R) = 0.9)

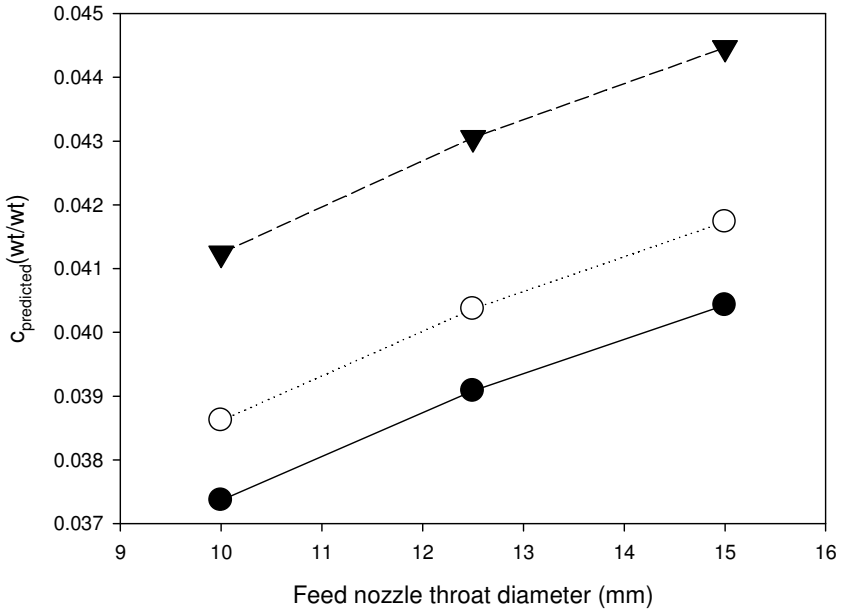

Figure 7.10. Predicted liquid concentration of initial agglomerates obtained from the model while keeping liquid flowrate constant (3 kg/s) for the Fluid Coker conditions (presented in Table 7.3) versus feed nozzle throat diameter for three rings at various dimensionless heights (Z*) (radial location of feed nozzle tip (r/R) = 0.9)

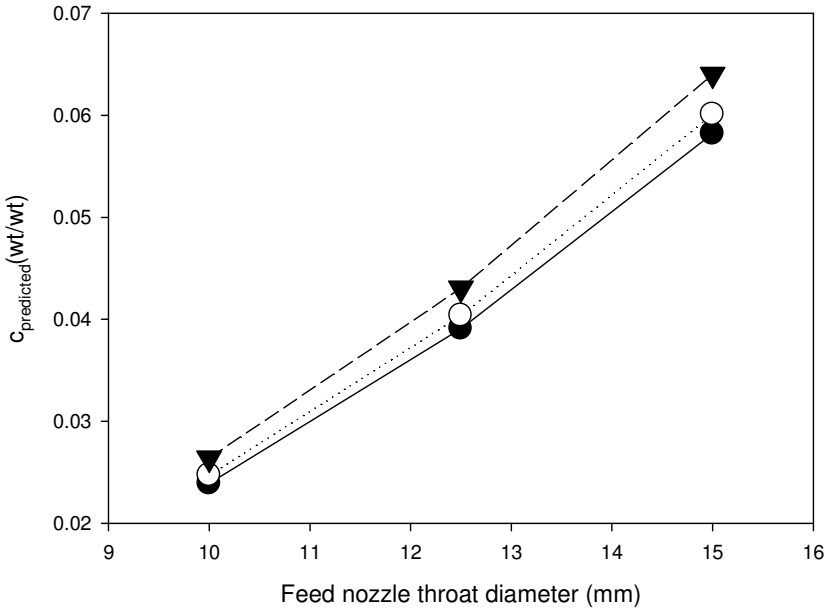

Figure 7.11. Predicted liquid concentration of initial agglomerates obtained from the model while keeping liquid flux constant (24.5×10^3 kg/m^2.s) for the Fluid Coker conditions (presented in Table 7.3) versus feed nozzle throat diameter for three rings at various dimensionless heights (Z*) (radial location of feed nozzle tip (r/R) = 0.9)

Figure 7.12 shows that increasing the spray angle was beneficial, by reducing the liquid concentration of the agglomerates. The predictions of Figure 7.12 are for the Fluid Coker conditions presented in Table 3, a feed nozzle tip location (r/R) of 0.9, and a feed throat diameter of 12.5 mm. The beneficial impact of increasing the spray angle results from an increase of the jet cavity bubble capture area.

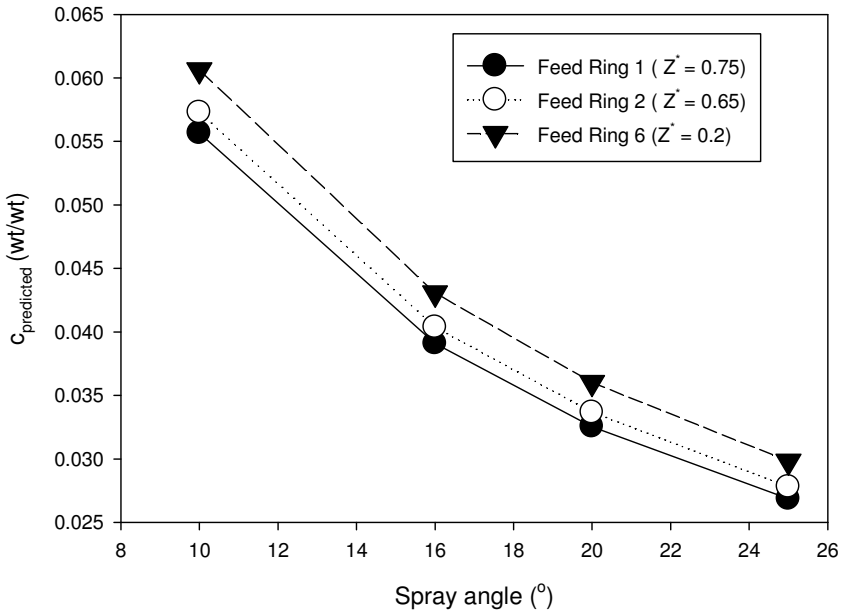

Figure 7.12. Predicted liquid concentration of initial agglomerates for the Fluid Coker conditions (presented in Table 7.3) versus spray angle for three rings at various dimensionless heights (Z*) (the radial location of feed nozzle tip (r/R) = 0.9)

7.7.2 Model predictions for typical Fluid Coker™ conditions accounting for the impact of background liquid on local bed hydrodynamics for lower feed rings

It was assumed for lower feed rings such as feed ring 2, that the solids are not dry as the solids move down the Fluid Cokers and have thus been wetted by the upper rings. Figure 7.13 shows the predicted liquid concentration of agglomerates for two cases:

- Solids at the jet tip area are dry

- Solids are wet enough to modify the local bed hydrodynamics and, for feed ring 2, reduce the bubble flowrate to the jet cavity by 50%

Figure 7.13 shows the strong detrimental impact of the solids liquid concentration reaching the ring 2 level on the liquid concentration of the agglomerates formed at ring 2.

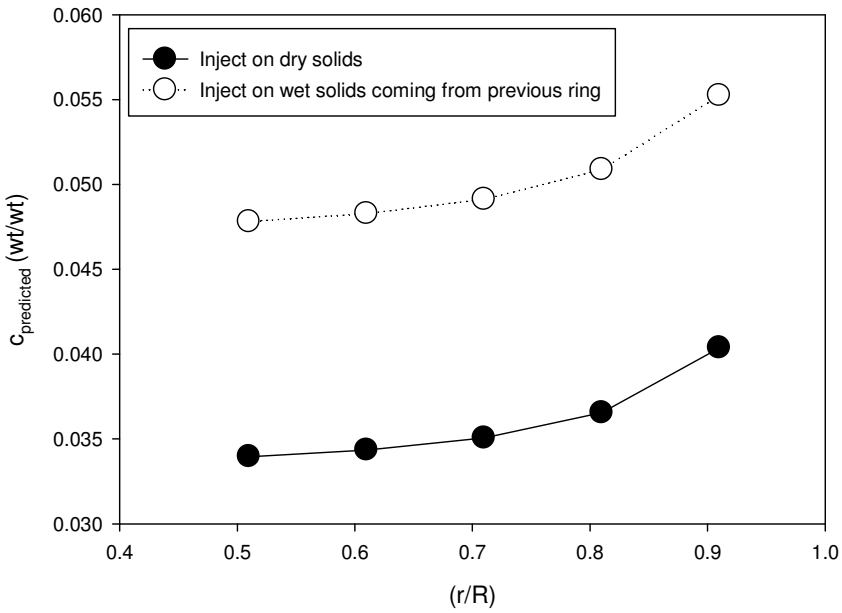

Figure 7.13. Predicted liquid concentration of initial agglomerate breakage for the Fluid Coker conditions (presented in Table 7.3) versus radial location of nozzle tip for feed ring 2 for two cases: 1) solids at the jet tip area are dry, 2) solids are wet enough to modify the local bed hydrodynamics and, for feed ring 2, reduce the bubble flowrate to the jet cavity by 50%

Comparing results of the impact of different parameters presented above shows that the liquid concentration of agglomerates is greatly affected by the spray angle and the wet solids coming from upper rings. The results show by increasing the spray angle by 50 % reduces the agglomerates liquid concentration by about 30 %, while increasing the GLR by 50% only decreases the agglomerates liquid concentration by about 10%. The impact of localized bogging with considering 50% decreasing in bubble flowrate to the jet cavity is about 37% increase in the liquid concentration of agglomerates. The results also show increasing the nozzle throat diameter by just 20% while keeping liquid flux constant increases the liquid concentration of agglomerates by about 49%.

7.8 Conclusions

In this study a model was developed that provides information on the liquid concentration of agglomerates resulting from the contact between fluidized particles and a liquid sprayed from a moving nozzle. The nozzle was moved at relative velocities with the fluidized bed solids that are within the range of velocities expected in a Fluid Coker™, where nozzles are stationary and fluidized solids move downward.

The spray forms a jet cavity in the fluidized bed, which fluctuates as it first expands gradually until it reaches its maximum volume, a large bubble escapes from the tip of the jet, reducing the jet volume suddenly, and the jet starts expanding again gradually. Both model predictions and experimental results show that when the total injection time is shorter than the time for a full expansion, there is no difference between the performances of stationary and moving nozzles.

When the total injection time is longer than the expansion time and for a single moving nozzle pass, both model predictions and experimental results show that the agglomerates liquid concentration is higher for the stationary nozzle, because some of the solids wetted during earlier expansions are rewetted.

When a moving nozzle passes more than once through a given bed region, both model predictions and experimental results show that there is a major increase in agglomerates liquid concentration, because gas bubbles avoid bed regions where solids are wet and cohesive.

The model was applied to a commercial Fluid Coker™. The model predictions show that increasing the atomization gas flowrate or the spray angle is beneficial, while increasing the nozzle throat diameter while keeping the liquid flux constant has a strong detrimental effect on the liquid concentration of the initial agglomerates.

References

Ali Zirgachian, M., M. Soleimani, C. Briens and F. Berruti. 2013. "Electric Conductance Method for the Assessment of Liquid-Gas Injection into a Large Gas-Solid Fluidized Bed." *Measurement: Journal of the International Measurement Confederation* 46(2):893-903.

Benjelloun, F., R. Liegeois and J. Vanderschuren. 1995. "Peneteration Length of Horizontal Gas Jets into Atmospheric Fluidized Beds.":239.

Berruti, F., M. Dawe and C. Briens. 2009. "Study of Gas-Liquid Jet Boundaries in a Gas-Solid Fluidized Bed." *Powder Technology* 192(3):250-259. Farkhondehkavaki, M. 2012. "Developing Novel Methods to Characterize Liquid Dispersion [Dissertation]." Western University, London (ON), .

Hamidi, M. 2014. "Development of Advanced Electrical Methods for Fluidized Bed Measurements." Western University,.

Mohagheghi, M., M. Hamidi, F. Berruti, C. Briens and J. McMillan. 2014. "The Effects of Injection Nozzle Location and Inclination on the Interaction between a Gas-Liquid Jet and a Gas Solid Fluidized Bed.".

Mohagheghi, M., M. Hamidi, F. Berruti, C. Briens and J. McMillan. 2013. "Study of the Effect of Local Hydrodynamics on Liquid Distribution in a Gas-Solid Fluidized Bed using a Capacitance Method." *Fuel*.

Mohagheghi, M., M. Hamidi, C. Briens, F. Berruti and J. McMillan. 2014. "The Effects of Liquid Properties and Bed Hydrodynamics on the Distribution of Liquid on

Solid Fluidized Particles in a Cold-Model Fluidized Bed." *Powder Technology* 256:5-12.

Prociw, N. 2014. "Effect of Nozzle Geometry on Jet-Bed Interaction." Western University,.

Song, X., H. Bi, C. J. Lim, J. R. Grace, E. Chan, B. Knapper and C. McKnight. 2004. " Hydrodynamics of the Reactor Section in Fluid Cokers." 147:126.

Chapter 8

8. CONCLUSIONS AND RECOMMENDATIONS

This chapter summarizes the major findings and contributions from studies conducted in this thesis. The recommendations for future works pertaining to the improvement of current research are also provided.

8.1 Conclusions

This work focused on the effects of the local bed hydrodynamics on the liquid distribution in a gas-solid fluidized bed. The experiments were performed in a cold model gas-solid fluidized bed to study the impact of the bed hydrodynamics such as fluidization velocity, Gas to Liquid ratio of the spray nozzle, nozzle inclination, location of spray nozzle, and relative particle velocities.

A new capacitance method was developed for the evaluation of the distribution of liquid on the solid particles. This non-invasive method measures the "free liquid", i.e. liquid that is not trapped within agglomerates. It was used to measure the rate at which liquid was released from agglomerates, as they progressively broke up. The effects of the local bed hydrodynamics on the initial liquid-solid agglomerate formation during the liquid injection could be separated from the effects on the agglomerate breakup subsequent to the liquid injection.

The capacitance method can be used for a variety of liquid-solid systems. Initial studies indicated that a good simulation of the distribution of liquid in Fluid Cokers^{TM} required the same coke particles as in the commercial unit and a liquid whose viscosity and contact angle on the surface of coke particles are similar to those of the bitumen used in the hot commercial unit. Varsol^{TM} meets the requirements and does not form explosive mixtures with fluidizing air at room temperature.

At this point of the thesis, we were equipped with an accurate, rapid, and non-invasive capacitance meter, an experimental method that could provide valuable information on the initial liquid-solid agglomerate formation during liquid injection and agglomerate

breakup subsequent to the liquid injection, and also a proper liquid-solid system that was varsol^{TM} – coke. Since the distribution of liquid on solid particles has considerable impact on the liquid yield in Fluid Cokers, we focused on the impact of following parameters on the distribution of the injected liquid on the bed particles:

- fluidization velocity and Gas to Liquid ratio of the spray nozzle

The important findings were that improving the distribution of the liquid on solid particles by improving the initial distribution through either increasing the atomization gas flowrate or, preferably, the fluidization velocity near the spray nozzle. It was also found that increasing the rate of agglomerate breakage after injection also improves the distribution of the liquid and that can be achieved by increasing the fluidization velocity in the bed region where the agglomerates move just after being formed in the spray region.

- Spray nozzle location and inclination

The results of the nozzle location experiments show the predominant factor for the initial agglomerate formation is the bed bubble volume fraction at the nozzle tip, where gas bubbles promote solids entrainment and mixing within the jet cavity. For agglomerate breakage the predominant factor is the bubble volume fraction at the jet tip, where gas bubbles interact with the freshly formed agglomerates. The dominant effects of bed hydrodynamics at the nozzle and jet tips on the distribution of liquid on solid particles also verified with the results for various nozzle inclinations experiments. It was found the nozzle inclination has no measurable effect on the agglomerate formation and agglomeration strength.

- velocity of particles, relative to the spray nozzle

To investigate the impact of the velocity of particles, relative to the spray nozzle, on the solid-liquid contact, a moving nozzle was designed since there is a relative velocity range of 0.3 to 1 m/s between particles and the gas-liquid jet in an actual Fluid Coker. This design provided a means to study the effect of the relative velocity between the nozzle and particles independently of other bed hydrodynamic

characteristics. Therefore, the impact of the fluidization velocity and of the relative velocity between nozzle and particles were studied independently. We found the relative velocity mainly has an impact on the strength of formed agglomerates than on the initial amount of the free liquid. It was also found that a relative velocity between nozzle and particles has a beneficial impact compared with a stationary nozzle with the same injection duration and also a higher fluidization velocity during injection by a spray nozzle resulted in the formation of weaker agglomerates, which broke up more easily, whether the nozzle was moving or not.

After gathering all the experimental results, for the rest of thesis, we focused on the modeling and a model was developed for the interaction between the liquid-gas spray jet and fluidized particles in a gas-solid fluidized bed. The model was developed for two cases: a) a stationary spray nozzle with no net motion of the fluidized solids, as in the most experimental studies in chapters 2 to 4 and b) a moving spray nozzle. The results of experimental studies were used to validate the model for both cases. After validating the model, the model was applied to an actual Fluid Coker^{TM} and the impact of parameters such as GLR, feed nozzle throat diameter, and spray angle were studied.

The developed model provided information on the liquid concentration of the initial formed agglomerates resulting from the contact between the sprayed liquid and solid particles. The results of the model are in good agreement with the experimental results as it correlates well with experimental results which is the time constant of agglomerate breakage.

8.2 Recommendations

The following directions are suggested for future research:

1. For the developed model in this study, it was assumed that the liquid is uniformly distributed on the solids with which it interacts. This could be a possible limitation of the model and for checking whether it is a limitation or not, performing some experiments with a hollow cone and a full cone nozzle are recommended. The results of these recommended experiments could also predict

the experimental findings for the effect of the draft tube and pulsations that the current model was not able to predict.

2. For the moving nozzle in this study, all the nozzle velocities were higher than the calculated jet expansion velocity. The equipment should be modified to explore lower nozzle velocities.
3. The ability of using lower nozzle velocities would also allow for single pass measurements with longer injection times. More experiments could, also, be performed with multiple passes to determine the impact of the localized bogging on liquid distribution over a wider range of conditions.
4. In order to decrease the drying time after the injection, installing a heater on the fluidization gas pipe line is recommended. Setting a higher, safe temperature for the fluidization gas would dramatically decrease the drying time.
5. The sampling frequency for the circuit in this study is about 12 Hz which cannot provide accurate information on the bubble velocity and bubble properties. In this study, the goal was to get information on the local liquid distribution with the capacitance method, for which the current sampling frequency is adequate. To get more information on the bubble size and velocity, a capacitance circuit with a higher sampling frequency or other methods such as bubble probes or X-ray are recommended.

APPENDIX A

This appendix shows examples of the reproducibility of the experiments in this thesis. The three examples are:

1) Results of calibration experiments giving the free moisture in the fluidized bed as a function of the measured capacitance, for two typical electrodes.

2) Typical results of the fraction of total injected liquid which is free liquid at the end of the liquid injection.

3) Typical results of the time constant of agglomerate breakage (τ) curves.

For all these examples, the error bars show the range of values obtained with replicate experiments. The number of replicate experiments was three for each of the error bars shown on the following figures.

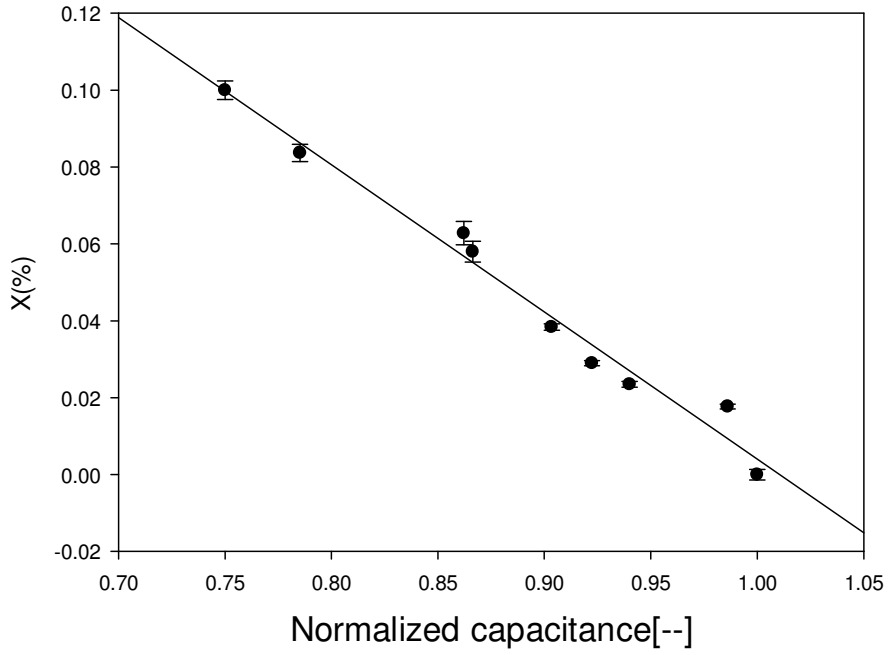

Calibration curve with error bars for electrode 15 (with Varsol^{TM} liquid). The error bars show the range of values obtained with replicate experiments. The number of replicate experiments was three.

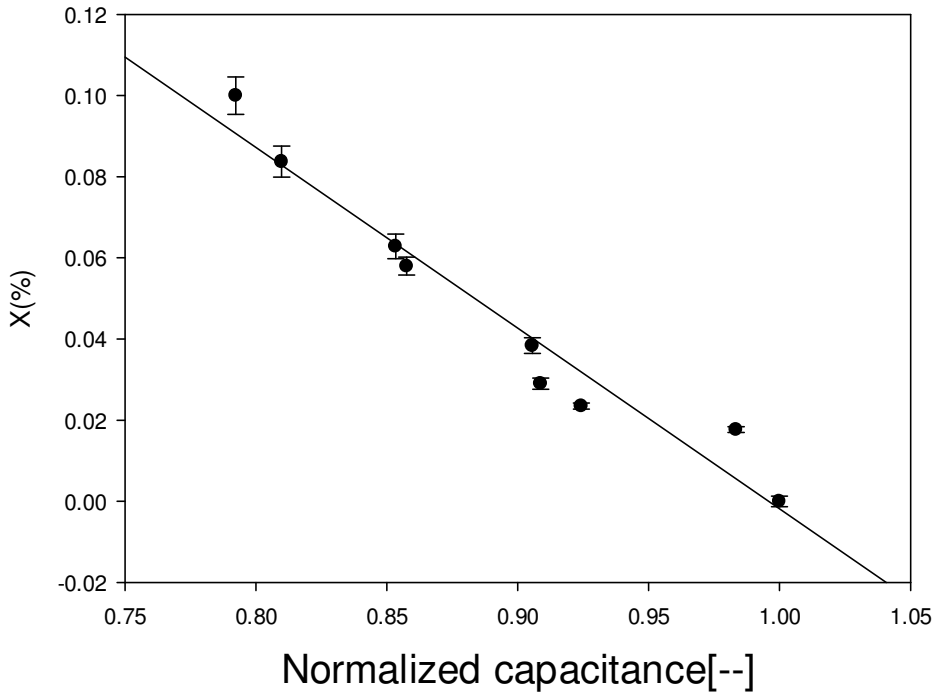

Calibration curve with error bars for electrode 2 (with Varsol^{TM} liquid). The error bars show the range of values obtained with replicate experiments. The number of replicate experiments was three.

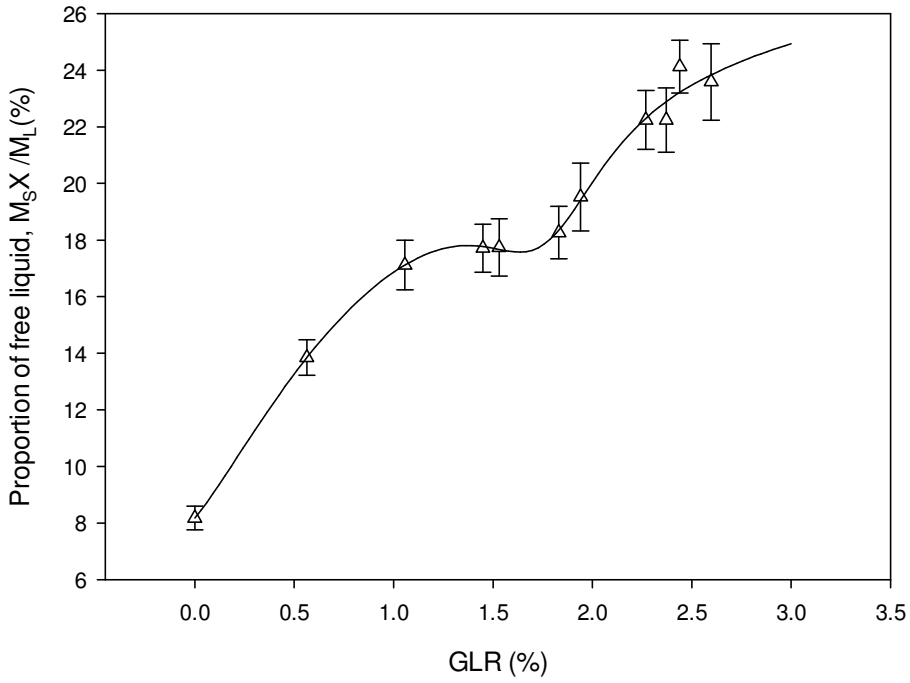

Percentage of total injected liquid which is free liquid at the end of the injection versus GLR with error bars for a fluidization superficial velocity of 0.3 m/s and liquid flowrate of 55 g/s. The error bars show the range of values obtained with replicate experiments. The number of replicate experiments was three.

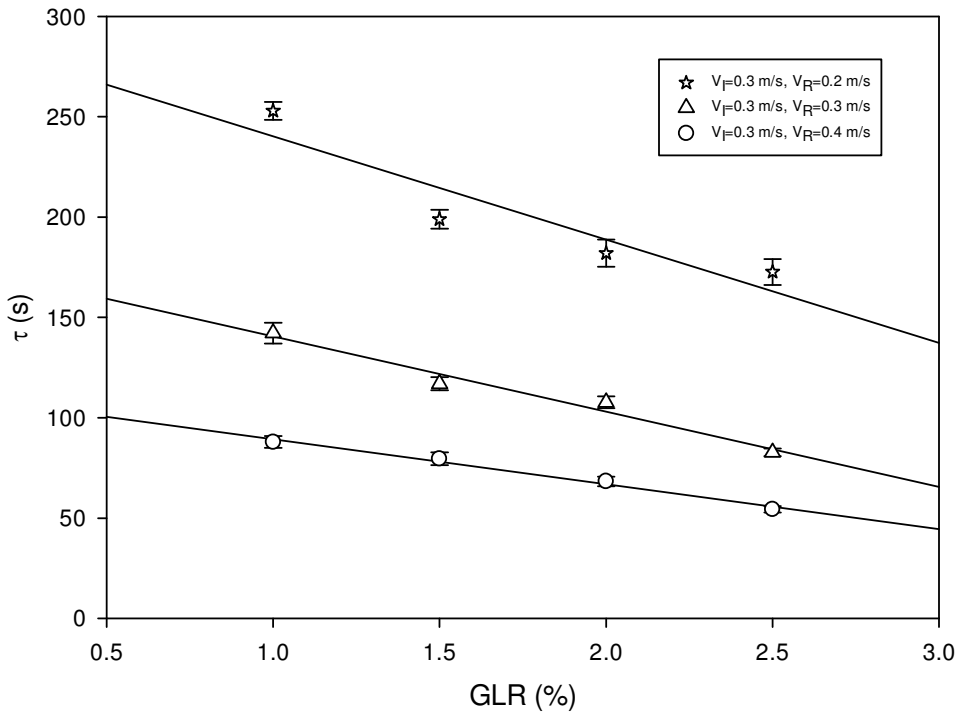

Time constant of agglomerate breakage versus GLR with error bars for three different fluidization velocities after injection. The error bars show the range of values obtained with replicate experiments. The number of replicate experiments was three.

VITAE

Name:	Maryam Mohagheghi Dar Ranji
Post-Secondary Education and Degrees	Western University London, Ontario, Canada 2010-2014 Ph.D., Chemical Engineering Polytechnic (Amirkabir) University of technology Tehran, Iran 2000-2003 M.E.Sc., Chemical Engineering Esfahan University Tehran, Iran 1996—2000 B.Sc., Chemical Engineering
Related Work	Teaching Assistant and Research Assistant Western University, London, Canada 2010-2014 Research Engineer Research & Technology center, National Iranian Petrochemical Company, Tehran, Iran 2002-2009

Publications:

Mohagheghi, M., M. Hamidi, C. Briens, F. Berruti and J. McMillan. 2013. "Study of the Effect of Local Hydrodynamics on Liquid Distribution in a Gas-Solid Fluidized Bed using a Capacitance Method." *Fuel*.

Mohagheghi, M., M. Hamidi, C. Briens, F. Berruti and J. McMillan. 2014. "The Effects of Liquid Properties and Bed Hydrodynamics on the Distribution of Liquid on Solid Fluidized Particles in a Cold-Model Fluidized Bed." *Powder Technology* 256:5-12.

Mohagheghi, M. and Bakeri, Gh. 2008. “Kinetic Studies of Propane Dehydrogenation Over Pt-Sn/Al_2O_3 Catalyst.” XVIII International Conference on Chemical Reactors [CHEMREACTOR-18]

Mohagheghi, M., Bakeri, Gh. and Saeedizad, M. 2007. “Study of the Effects of External and Internal Diffusion on the Propane Dehydrogenation Reaction over Pt-Sn/Al2O3 Catalyst.” Chemical Engineering & Technology 30(12):1721-1725.